SAPIENZA
UNIVERSITÀ DI ROMA

Faculty of Civil and Industrial Engineering

Dottorato di Ricerca in Ingegneria dei Materiali e delle Nanotecnologie (EMNE)

XXXI CICLO

Distortion and faults detection in shipboard AC/DC power distribution system

Tutor:

Prof. Regina Lamedica

Candidate:

Ing. Alessandro Ruvio

Reviewers:

Prof. Massimo Ceraolo
Prof. Giorgio Sulligoi

Summary

Acronyms

AES	*All Electric Ship*
A	*Availability*
AC	*Alternate Current*
AIM	*Asynchronous Machine*
AP	*Power Absorbed*
CODAG	*Combined Diesel And Gas*
CODOG	*Combined Diesel Or Gas*
CSI	*Current Source Inverter*
CV 550	*Cavour Aircraft Carrier*
DC	*Direct Current*
DDGG	*Diesel Generator*
DF	*Distribution Functions*
DOL	*Direct On Line*
e.m.f.	*Electro Motive Force*
EMPAR	*European Multifunction Phased Array Radar*
EPAC	*Electrical Fire Pump*
ESS	*Energy Storage System*
ETO	*Emitter Turn Off*
fco	*Coefficient Of Contemporaneity*
FECs	*Front End Converters*
Gas	*Gate Turn Off Thyristor*
GTO	*Gate Turn Off Thyristors*
HP	*High Pass Filter*
HVAC	*Heating Ventilation And Air Conditioning Systems*
Icm	*A Nominal Short-Circuit Closing Capacity*
Ics	*Nominal Short-Circuit Breaking Capacity*
Icu	*Extreme Short-Circuit Breaking Capacity*
If	*Field Circuit Current*
IGBT	*Insulated Gate Bipolar Transistor*
IGCT	*Integrated Gate Commutated Thyristors*
IGCT	*Hard Driven GTO*
IHD	*Individual Harmonic Distortion*
IM	*Induction Motor*
IPS	*Integrated Electrical System*
JSF	*Joint Strike Fighter*
LV	*Low Voltage*
m.m.f.	*Magnetomotive Force*
MCR	*Maximum Continuous Rating*
MPDCC	*Multi-Port DC/DC Converter*
MTBF	*Mean Time Between Failures (h)*
MTTR	*Mean Time To Repair (h)*
MV	*Medium Voltage*
MVAC	*Medium Voltage – Alternate Current*
MVDC	*Medium Voltage – Direct Current*
NaSG	*Naval Smart Grid*
NP	*Nominal Power*
PDs	*Propulsion Drives*
PF	*Power Factor*
PQ	*Power Quality*
Psc	*Short Circuit Power*
PTO	*Power Take Off*
PWM	*Pulse-Width Modulation*
Q,	*Unavailability*
QM	*Quality Factor*
Rdt	*Repair Downtime*
RMS	*Root Mean Square*
RPM	*Revolution Per Minute*
RV	*Random Variable*
SCR	*Silicon Controlled Rectifier Or Thyristor*
SG	*Shaft Generator*

SM	*Simulink Model*
SSPC	*Solid-State Power Controller*
ST	*Single Tuned Filters*
STANAG	*In NATO A STANdardization AGreement*
STOVL	*Short Take Off & Vertical Landing*
SWBS	*Ship Work Breakdown Systems*
TAG	*Gas Turbine*
Tf	*Total Failures*
THD	*Total Harmonic Distortion*
THDI	*Current Total Harmonic Distortion*
THDV	*Voltage Total Harmonic Distortion*
Tp	*Total Period*
Vd	*Armature Circuit Supplying Voltage*
VSI	*Voltage Source Inverter*
Z(f)	*Network Impedance*
ZEDSs	*Zonal Electrical Distribution Systems*
λ	*Failure Rate (f/h)*
$\phi(If)$	*Excitation Flux*
$\Phi\alpha$	*Armature Magnetic Flux*

Introduction

Nowadays electric propulsion has become a valid alternative to mechanical propulsion for large ships that require high speed.
The electric propulsion advantages are well known and widely documented in the literature: higher dynamic performance of the electric propulsion motors; internal combustion engines separation from shafts; increased flexibility in space/zones subdivision; increased efficiency through the modulation of number of running generators; noise and vibration reduction; increasing in automation, with a consequent crew reduction.
The use of electric propulsion along with the progressive increase, in number and power, in electrical loads used for ship services, led to the development of the All Electric Ship (AES) concept. Over the last years, the All Electric Ships (AESs) concept has begun to be adopted by the most important Navies, principally by the U.S. Navy, giving a boost to the technological research.
An AES is a ship where all onboard electrical loads (including propulsion) are powered by a single electrical system, called Integrated Electrical System (IPS). The IPS requires careful design and management in order to ensure both high Power Quality standard and the continuity of the service.
With the technological progress, the shipboard electrical systems have changed considerably, rising from few MW of installed power to values of the order of hundred MW, both in cruises and military ships.
Especially in military vessels, considering the number of special devices that are present on board (weapon systems, communication equipment, radar, sonar, and missile guidance systems), a performing and reliable electrical systems is required. Moreover, it is necessary to notice that some of the new electrical pulsed loads specific to military applications (e.g. radar, electromagnetic launchers, etc.) together with electric drives for propulsion engines can cause strong disturbances to the system, thus causing the malfunction of other electric utilities that may endanger the continuity of the service. The penetration of power electronics converters is the main issue for the contribution of harmonic distortion in AC grids, which must be limited not to increase system power losses, and to allow the correct operation of system and user devices. Standards dictate the maximum admissible values of the total voltage harmonic distortion and of the individual harmonics amplitudes, as a function of the rated system voltage.
The relatively limited short-circuit power available on board also exposes the IPS to significant voltage sags and flickers caused by switching and/or intermittent loads. In this scenario, DC electrical distribution systems can be very attractive, thanks to their intrinsic immunity to harmonic problems. If DC micro-grids are interfaced to AC networks by means of Front End Converters (FECs), both AC/DC grid decoupling and considerable AC-side harmonic distortion reduction can be achieved. In addition, they simplify the power supply of converter-fed loads and the interfacing of storage systems. The latter can perform several tasks, including ensuring power supply in case of AC grid loss, peak-shaving and levelling pulsating loads further improving both the quality and the continuity of supply to DC islands loads.
In the light of the above, it is evident that the electric power system is of primary importance for a modern ship. Moreover, if high-performance is required, careful analysis of the disturbances in the power system is mandatory. In fact, in order to achieve a reliable and performing power system, together with a high-Power Quality, it is necessary to assess this situation and propose guidelines to be observed for the solution of various problems.
The definition and evaluation of possible IPS architectures should take into account AC/DC protection devices in order to carry out an integrated analysis of the system. Different MVAC/MVDC electrical distribution layouts coupling with all-electric or hybrid propulsion (electric/diesel/gas turbine) needs to be accurately investigated to show its advantages in terms of reliability, safety and quality of power.

The thesis focusses on the Naval Smart Grid (NaSG) research project completed in partnership with the University of Trieste and the Polytechnic University of Milan. The aim of the research is to produce useful results for the design of a new ship, equipped with the following innovative features: modular power system; subsystem flexible integration; efficiency improvement; security improvement; new weapon systems; survivability improvement and high Power Quality standard.
The main focus was the study of methodologies/solutions able to improve and define the onboard Power Quality (PQ). The research project reports Power Quality analysis about aspects of continuity of service, harmonic disturbances, pulsed power loads impact on the system, electromechanical transient evaluation and use of power and energy storage systems.
An exhaustive investigation was carried out on system architectures in frequency domain to identify resonances and non-linear loads to detect disturbance frequencies.
Moreover, the guidelines for the correct coordination of all the elements of the power system design affecting system performance (protections, converters, control systems, energy storage systems, etc.) are reported.
A brief abstract for each Chapter is reported.

Chapter 1 and 2 - Overview of Electrical Naval Systems and Integrated Power System in Military Ships
The chapter reports the complete state of the art on naval electrical system and a brief description of naval classification, showing technological improvements and historical evolution. Details about electric propulsion, electrical generation on board, energy distribution and network layout are carried out. A complete description of the main IPS military ships with their own architecture and features is reported.

Chapter 3 - Methodologies for Harmonic Disturbances Analysis and Power Quality (Service Continuity)
In the field of Power quality (harmonic content, asymmetries, voltage sags, power factor), methodologies applied for the analysis/detection of harmonic disturbances are reported with an overview of electrical systems dependability in order to evaluate the service continuity of the system. Harmonic distortion could affect equipment on shipboard causing its outages, consequently, in an island system, power distribution network should ensure high re-configurability after faults, damage or untimely switch off. However, the increased interest in system's safety and resilience generates, in turn, an increase in design burden necessary to analyze the consequences of faults and demonstrate the system's compliance with the relevant regulations.
The chapter presents the models and calculation code used for simulation activities. A Simulink model for time domain analysis and for time varying non-linear load, as well as a Fortran model for harmonic domain are described.

Chapter 4 and 5 - Characterization of a military aircraft carrier and Aircraft Cavour – Measurement campaign
A measurement campaign onboard the ship Cavour was carried out with the aim to characterize the relevant electric loads on board military vessel and to validate the models of the system's components to be used.
The analysis of data collected, allows to model the behavior of loads in terms of time and frequency domains, thus permitting their use for the required studies. Some specific electrical loads, such as new electrically pulsed loads specific for military applications (e.g. radar, electromagnetic launchers, etc.) with high distorted current absorption were identified. Their characterization was carried out in order to define their contribution to harmonic disturbances and their impact on the network. A model validation based on a measurement campaign is carried out.

Chapter 6 - A New layout for an Integrated Power System Naval Unit-All Electric/Hybrid
Different IPS architectures are defined: a full MVAC (Medium Voltage Alternate Current) power system, a hybrid MVAC plus MVDC/LVDC islands (Medium/Low Voltage Direct Current) and a MVAC 50-60 Hz, with a hybrid (electric/diesel/gas turbine) propulsion. In the architecture of the latter, the power of the installed engines is much lower than the first two cases.

Chapter 7 - Network Equivalents in Harmonic Domain
The needs to easily represent a complex network with high accuracy, lead to the development of a methodology based on aggregation of loads, creating a simplified network to carry out harmonic analysis.
Different equivalent network models have been proposed that show their accuracy, through network impedances, and compare them with the overall representation of the network. The influence of cables was also studied. The best radial equivalent network was identified.

Chapter 8 - Harmonic Analysis
In order to propose appropriate solutions designed to improve power quality, the study of system impedance and power systems in frequency domain were studied. This analysis, carried out on the basis of the schematics and data load obtained in cooperation with the IT Navy, revealed some criticalities in the frequency range for both the systems architectures.
As to full MVAC (Medium Voltage Alternate Current) power system and hybrid MVAC plus MVDC/LVDC islands, the aim was to evaluate whether or not the inclusion of capacitors (on shore, for power factor correction in shore connections) or filters (onboard, to reduce harmonic disturbances produced by propulsion systems) cause special issues, because of the high power of installed propulsion engines. Moreover, the advantages of DC island on electrical distribution in order to ensure high reliability and quality of service, in addition to the need to increase the efficiency of the ships' power systems are highlighted.
For the MVAC 50-60 Hz layout, the goal is to show how the use of hybrid (electric/diesel/gas turbine) propulsion where the power of engines is significantly reduced as compared to previous cases could solve some issues relating to power quality aspects.

Chapter 9 - Reliability Analysis
Preliminary studies about dependability, re-configurability and some top-events relevant for the vessel, were evaluated for all electric MVAC/MVAC "hybrid" models. The analysis of electrical disconnection of load areas due to a fault or an untimely tripping of the switches caused by harmonic disturbances was carried out.

Chapter 10 - Three-Phase Short Circuit Analysis For MVAC 50-60 Hz Layout
Preliminary evaluations were performed by analyzing the system within the perspective of given faults to perform system analysis in both permanent and short-circuit conditions. To highlight possible protection issues, the steady state condition and the three-phase short-circuit faults were studied and simulated under different load conditions for the MVAC architecture plus rotary converters, with hybrid (electric/diesel/gas turbine) propulsion.

Chapter I: Overview of Electrical Maritime Systems

1.1 Electrical Propulsion System in Ships

The concept of electric propulsion was introduced in the naval field since the nineteenth century. The vessels used in Europe were driven by electric motors fed by direct current [1] both in the civil and military field. The electric propulsion developed thanks to this technology, was favoured by the difficulty to create gear reducer systems, necessary to couple the propeller shaft[1] with the high- power steam turbines axis, as they operate at different rotational speeds.
Through the use of specific electric machines[2] it is possible to diversify the speed of both engines and propellers. Once the difficulties related to the development of speed reducers were solved, the mechanical propulsion became the main system adopted in naval applications.
The technological development of electric propulsion was to become a topic of interest after the Second World War, thanks to the evolution of power electronics.
Nowadays, electric propulsion systems are widespread for passenger ships and other types of vessels (ferry boats, icebreakers, tugboats, etc.).
Based on the definition, electric propulsion occurs when the motor that drives the propellers is an electric engine; instead mechanical propulsion is when the main engine is typically a diesel or gas turbine.
The use of a diesel engine to generate the motor torque necessary to provide propulsion, implies a major economic disadvantage: in order to vary the power supplied to the propeller (also called brake power) it is necessary to operate the engine under variable rotation levels, based on sea conditions, ship speed, and – sometimes – on the adjustment of propeller's pitch, when the vessel is equipped with controllable pitch propellers (CPP), rather than fixed pitch propellers (FPP). Adjusting the power by means of rotation speed variation does not allow to maintain the diesel engine at its maximum efficiency, i.e. at a constant RPM. This causes an increase in the specific consumption of fuel that, also because of engines size and hours of navigation, may result in higher operating costs.
When performing power regulation, varying the rotation speed, it is not possible to maintain the diesel engine at the point of maximum efficiency (RPM constant). For this reason, an increase in operating costs is due to higher fuel consumption. Furthermore, it is still necessary to have additional prime movers to generate electricity to supply ship services.
This system is defined as "not integrated", in so far there is a separation between the prime movers used for propulsion systems and those used for electricity generation to supply ship loads. There is no possibility for the two systems to interact.
The evolution of the architecture was developed to share the generators both for electric propulsion systems and for the power supply of ship loads. This system is defined "Integrated", and allows to install fewer prime movers on board and, consequently, fewer auxiliary systems necessary for their operation; it became a flexible system, with a reduction in specific fuel consumption, operating costs, and an increase in plant reliability.
The invasive adoption of electric powered equipment, both for electric propulsion and electric devices, led to the origin of the so-called All Electric Ships (AESs). Such ships are equipped with a power system supplying all shipboard loads, included propulsion, by means of a common set of generators. Because of this, and thanks to its possibility to reroute the power wherever is needed at a specific time, the power system was called Integrated Power System (IPS).

[1] In the mechanical propulsion, it is necessary to develop a shaft that connects the axis of the main motor to the axis line on which the propeller is keyed. This shaft across the entire distance between the engine room and the installation point of the propeller, sometimes reaches considerable lengths.
[2] For example, a coaxial group with an internal combustion engine, a dynamo, a direct current motor, allows to vary the propeller speed keeping the main mover at constant RPM, therefore working at the point of maximum efficiency

An Integrated Power System can be considered equivalent to a land power grid, where generation, distribution, and utilization of the electric power coexists in a limited space (an example is shown in Figure 1). In an All Electric Ship, the Integrated Power System is the core system, being every load electrically powered. Losing power generation (blackout) means losing the ship control, which can lead to harmful consequences for people, things, and the environment.

Nowadays the AES concept is widely applied on large ships: only ships with special requirements, such as high speed or peculiar fuel, still use mechanical propulsion.

Other applications of AES concepts are: ferries, oceanographic ships, gas carriers, cable/pipe laying vessels, oil & gas dedicated vessels and platforms, icebreakers, and mega-yachts.

Different reference should be made for the military area, where mechanical propulsion solutions have so far been the only option considered. This is because of both high speed and reliability requirements of naval vessels, which led designers to focus on well-proven technologies. However, in recent times greater attention was paid to electric propulsion also in the military area. This was clearly demonstrated by the growing number of research projects on this type of propulsion in all the most technologically advanced navies with the construction of new all-electric military ships [2] [3] [4].

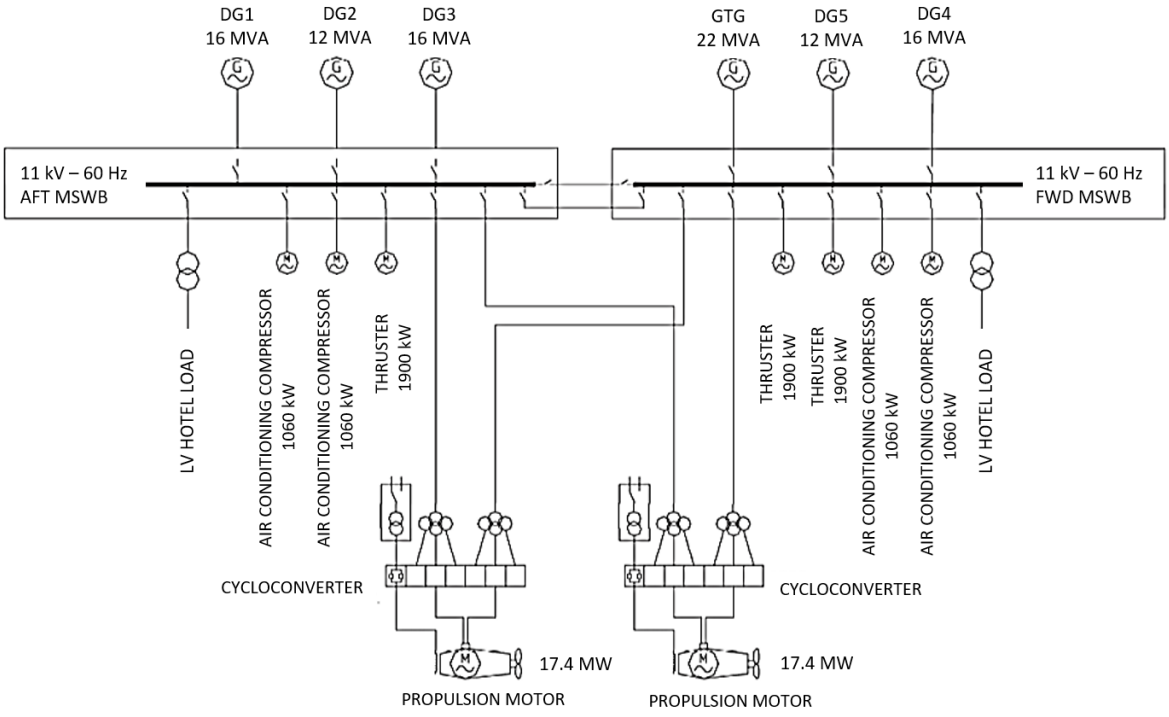

Figure 1 - Typical cruise all electric ship integrated power system [5]

1.2 Electric Propulsion – Historical overview

Figure 2 reports a timeline listing the main milestones in marine vessels power systems [6].
A brief description of famous and historical ships that used electric propulsion in the past is reported.

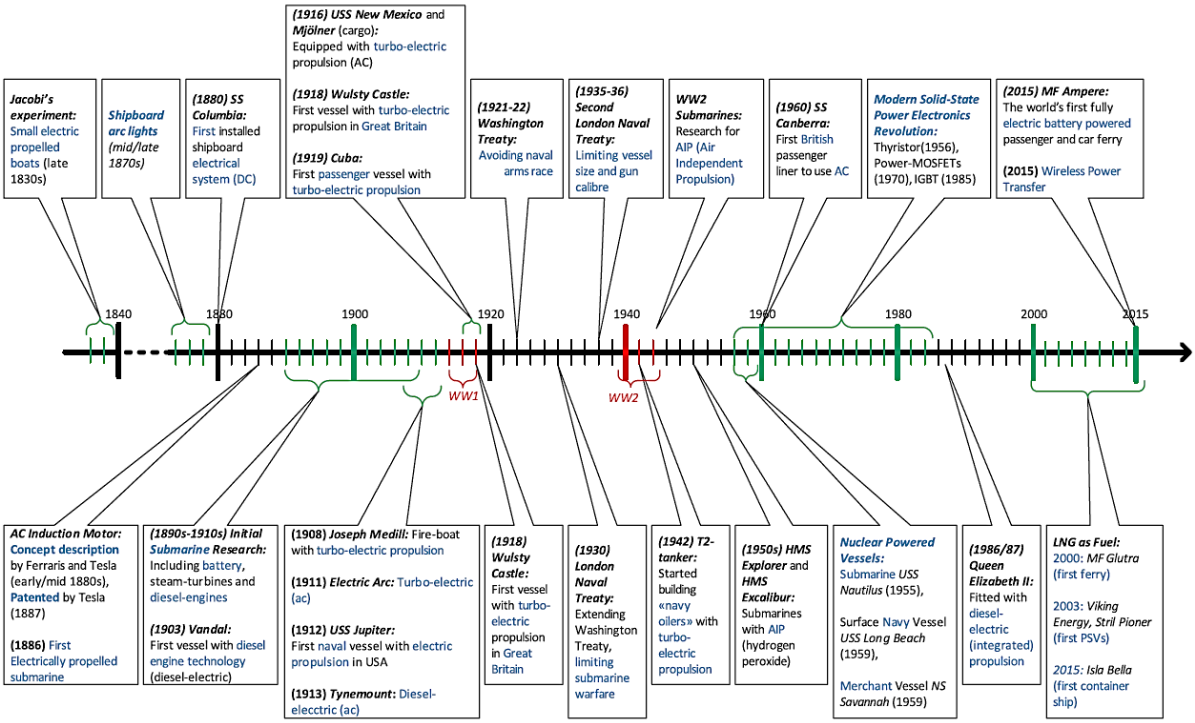

Figure 2 - Historical highlights of the evolution of marine vessels' electrical power systems: timeline.

Amerigo Vespucci - Figure 3

The ship has been in service since 1931, and it is currently employed by the Italian Navy as a school ship of the Naval Academy in Livorno. Built as a sailing ship, over the years it received a lot of upgrades/refitting's and today it is equipped with 2 diesel/dynamo Fiat B-306-ESS groups, and a Marelli electric engine which drives 1 axis with a fixed blade propeller. The total power installed is 1471 kW [7].

Figure 3 - Amerigo Vespucci

Normandie - Figure 4

It was built in France as an ocean liner that connected "Le Havre" to "New York". In service since 1935, it reached a speed of over 30 knots. It was equipped with:

- 29 boilers with naphtha combustion;
- 4 cylindrical auxiliary boilers with smoking pipes, which operated 4 steam turbines connected to alternators.

The generators, which powered 4 synchronous electric motors (each by 30 MW power) coupled to 4 propellers, produced a variable electric system frequency (0 ÷ 81 Hz) for a 120 MW total power.
The advantages were:

- the possibility of rotating the propellers at different speeds from those of steam turbines without mechanical speed reducers;
- steam turbines were installed in the lower areas of the hull, to the advantage of stability, since the generators did not need to be mechanically connected to the electric propulsion engines;
- propeller reversal rotation was obtained without the use of an auxiliary turbine [8].

Figure 4 - Normandie

Queen Elizabeth 2 – Figure 5

Property of Cunard Line from 1969 to 2008, it was used both as a transatlantic and cruise ship (apart from a short period during the Falklands War, when it was used for troops transportation). Originally equipped with three boilers supplying 2 steam turbines, as a consequence of serious reliability issues and operating costs due to fuel consumption, it was upgraded with the replacement of the steam system with a Diesel-Electric system. The new architecture had nine motor-generator groups (10.5 MW) at 10 kV rated voltage. The system powered both the ship services and the two 60Hz synchronous electric motors (44 MW at 144 RPM), which operated two variable pitch propellers. The two propulsion engines were powered by a synchronous inverter, at low speeds up to 72 RPM, and directly from the 60 Hz network for speeds above 18 knots, varying propellers pitch [9].

Figure 5 - Queen Elizabeth 2

1.3 Naval Classification

Nowadays, many ships characterized by different power, dimensions and utilizations, sail the commercial routes in maritime world transport.
Ships are classified based on their field of use and the type of on-board energy generation system.
A general overview of the various types of ships in the world is reported in [1].

1.3.1 Field of use

Ships for passenger transport

It includes cruise ships, transatlantic ships, ferryboats and yachts. This type of boat is characterized by high standards in terms of comfort and hull vibrations, as well as high standards of safety and system reliability.
Private companies rather than public ones own these ships; a common prerogative is to reduce operation costs and increase ship manoeuvrability (a cruise ship is currently able to rotate with millimetric precision).

Figure 6 - From left to right Cruise ship (Costa Diadema), Ocean Liner (Queen Mary 2), Ferryboat (Normandie Express), and Yacht (Fincantieri Mars)

Cargo ships

Cargo ships are both Tankers (oil tankers, chemical tankers, gas tankers or methane tankers), used for fluid or gas carriage and ships the carriage of solid materials (container or bulk carriers). In the first category, common safety standards for the carriage of flammable fluids and gases, or for highly dangerous chemicals are required. The second has a high load capacity with a heavy ship weight. Sophisticated loading/unloading and materials storage systems are required.

Figure 7- From left to right Oil tanker, Gas tanker (Golar Frost), Container ship (Maersk Triple E), and Bulk Carrier (Beluga Nomination)

Ships for the Oil & Gas application

This category includes units for oil and natural gas drilling, extraction and treatment, ships for oil platforms building, transportation and assembly, as well as production support vessels. All the above-mentioned ships meet the same requirements: oil and gas are often located in extreme environments, especially for offshore platforms, and the structures are therefore subject to high mechanical stress within adverse climatic conditions. For these reasons and for the need to operate them in specific locations, all these units are equipped with a "Dynamic Positioning": using GPS technology and radar systems for geolocation.

Figure 8 - From left to right: oil platform (Troll A), Lifting platform (Saipem 7000), Pipelayer (MV Solitaire), and Floating production platform (Maersk Peregrino)

Warships

Warships require maximum performance in terms of speed and autonomy, as well as resistance to damage. Different innovative technologies converge on on-board systems and high reliability standards are required. Warships include a very large number of categories, depending on the mission they perform.

Figure 9 - From left to the right FREMM (F590 Carlo Bergamini), USS Ohio (SSGN 726), USS Nimitz (CVN-68), USS Independence (LCS-2)

Other ships

Other types of ships are listed below:

- icebreakers: ships equipped to sail through frozen areas and open the route to other ships that, otherwise, would be unable to reach some areas of the world. Some of these ships also carry out scientific research activities;
- dredges: ships equipped to underwater excavation of harbours seabed, canals, rivers or lakes. They remove any deposited sediment, dangerous for navigation;
- fishing Ships: cover almost all world seas, engaged in fishing activities preserving also a great variety of fish species;
- semi-submersible ships: units designed for sea transportation of big structures that cannot be transported by land or sea. Moreover, they are suitable for the sea recovery of ships and/or platforms unable to get back to ports because of damages.

Figure 10 - From left to right: Icebreakers (CCGS Amundsen), Dredge (TSHD Cristobal Colon), Fishing ship (Northern eagle), and Semi-submersible ship (Dockwise Vanguard)

1.3.2 On-Board Power

Ships are commonly defined based on the typology of power plant systems installed on board.
In particular, the three typical architectures are the following: not integrated, integrated and hybrid.

Not integrated system

In a non-integrated power system, some engines are dedicated for ship propulsion, while others are destined to feed the engines' auxiliary systems and ship services. These two systems are completely separate and unable to mutually interact. Moreover, there are mechanical propulsion issues, such as the variable RPM engine (maximum efficiency is not reachable), critical speed of the propulsion system[3], and complex manoeuvres for crash stops[4].

Integrated systems

On-board power systems share the electric generators to feed both ship services and electric motors' auxiliary systems as well as the electric propulsion system.

Hybrid systems

All electric systems require the installation of high power and generally very bulky machines.
A hybridization of generation systems is carried out to obtain more space available on board.
In the military field these types of systems are often used, even for the high speeds required.
Possible configurations are reported:

- CODAG (COmbined Diesel And Gas) and CODOG (COmbined Diesel Or Gas): these systems involve the use of diesel engines and gas turbines for propulsion, and they differ for the simultaneous use (CODAG) or the exclusive use (CODOG) of two generation systems. In both cases, diesel engines are used in lower speed ranges, while gas turbines are used to reach maximum speeds.

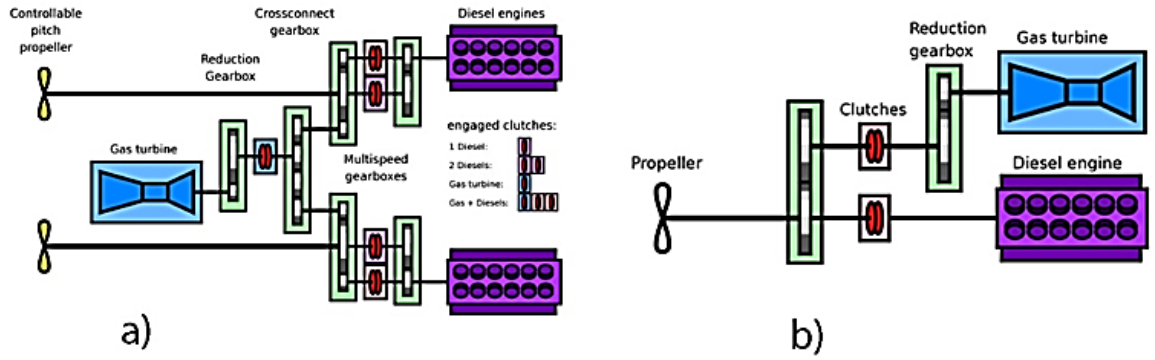

Figure 11 - a) CODAG; b) CODOG

1.4 Electrical Generation On Board

The choice of the system for electrical generation is the main important step of electrical naval design. The choice of generation units selected based on their type, number and size takes into account a great number of aspects and technical-economic requirements.
A difference with a common electrical industrial grid is the surrounding environment of use.

[3] Rotational speeds of the axis-motor in which the vibrations are greater, sometimes even dangerous, as compared to other speed ranges, due to resonance phenomena of the rotating systems.
[4] Operations to perform an emergency stop. A ship sailing at a constant speed, has greater inertia, due to its weight. It moves forward for a few miles if no braking action is carried out.

On board humidity levels and ambient temperature (45° and 55° C, respectively for common zones and electrical panels/machines rooms) may reach high values with possible difficulties for heat dissipation.
Moreover, many standards and regulations affect design decisions related to safety and security, reliability, vulnerability and systems redundancy. First of all, the International Convention for the Safety of Life at Seas imposes fundamental requirements (IMO SOLAS 1974[5] [10]). The first version was written in 1914 in response to the Titanic disaster. The most important concept, upon which the standard is based, is that the ships, engaged on international voyages, must return back to port in whatever condition (damage and malfunctioning) to ensure the safety of the people and equipment on board. The standard reports that the normal operational and habitable condition is a condition under which the ship as a whole, the machinery, services, means and aids ensuring propulsion, ability to steer, safe navigation, fire and flooding safety, internal and external communications and signals, means of escape, and emergency boat winches, as well as the designed comfortable conditions of habitability are in working order and functioning normally. Emergency condition is a condition under which any services needed for normal operational and habitable conditions are not in working order due to failure of the main source of electrical power.
Electrical installations shall be such that: all electrical auxiliary services necessary for maintaining the ship in normal operational and habitable conditions will be ensured without recourse to the emergency source of electrical power, electrical services essential for safety will be ensured under various emergency conditions; and the safety of passengers, crew and ship from electrical hazards will be ensured.
Starting from these simple rules, a common design is the installation of two electric power generation plants located in two different sections of the ship in separate compartments.
As a result of a fire, a flooding or malfunction of one electric generation plant, it is however possible to get back to port with a system performance degradation due to the limited power available from the other generator. The same approach could be applied to propulsion systems. It is possible to increase the ship's reliability by installing propellers with two axis lines and two propulsions motors with two drivers installed in different and separate zones of the ship [11].
In addition, the generating sets shall be such as to ensure that with any one generator or its primary source of power out of operation, the remaining generating sets shall be capable of providing the electrical services necessary to start the main propulsion plant from a dead ship condition. The emergency source of electrical power may be used for the purpose of starting from a dead ship condition if its capability either alone or combined with that of any other source of electrical power is sufficient to provide at the same time those services required to be supplied by regulations.
A total system failure need two failures events at the same time and its probability is the product of the singular failure probability. Therefore, by increasing redundancy of the equipment, the overall reliability will improve.
Inside the power plants, the power is subdivided into two or more groups (DDGG – Diesel Generator) in order to ensure the nominal power also in case of unavailability of one generator (N-1) and manage the navigation operational profile of the electrical system operating the Diesel generator at function point with maximum efficiency (75% for Diesel relating to MCR[6]) as shown in Figure 12.
In power plants design a 10 % more of power is consider to taken into account the increase of electrical loads or new equipment that will be install during the years (Life cycle is 20-30 years).

[5] The present regulations, unless expressly provided otherwise, do not apply to: ships of war and troopships, cargo ships of less than 500 gross tonnage, ships not propelled by mechanical means, wooden ships of primitive build, pleasure yachts not engaged in tradem, Fishing vessels.
[6] Max Continuous Rating: nominal power in continuous service

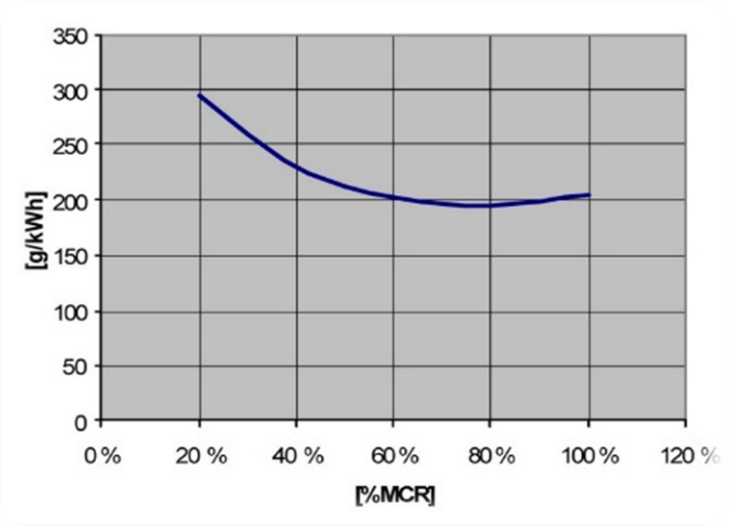

Figure 12 - Specific Fuel Consumption Related To The Percentage Power

Over the years, as regards the electric machines used for electrical generation, the evolution from a synchronous machine with main coaxial exciter (DC current generator) was a synchronous machine with static exciter or a permanent magnets machine with 50 or 60 Hz frequency. The polar pairs ranging between 1 and 8 respectively for high-speed turbo-generator (3000/3600[7] RPM) and generator coupled with a medium speed Diesel engine (375-450[6] RPM).
In naval power network, the short circuit power (P_{sc}) is low[8], especially in operation profile with low power consumption, with one or two operating generation groups.
The break of one generation unit during navigation is more dangerous than in land systems, where the power deficit could be filled by the rotating reserve thanks to the grid interconnection.
Inside the ship the rotating reserve assumes lower values that could pose a critical situation.
Another aspect influencing the stability of the network is that electrical loads with a nominal power comparable with the size of power generators are installed on board.
To manage the insertion of high power loads it is necessary to adopt a *soft starter* strategy or sequential insertion and frequency and voltage regulators having stability dynamic performance.
The frequency and voltage regulator combined with the automation system coordinates generators insertion and detachment, thus reconfiguring the network thanks to generators operation ad faults.
A gas turbine could be coupled with diesel generators reaching 50 MW nominal power.
Gas turbines are lighter and with greater power density; it is possible to install them in areas above the vessel's gravity center without any loss of stability.
For example a Rolls Royce MT7 gas turbine (5 MW) weighs 440 kg and occupies 1 m^3 volume, while a Wartsila 16V26 Diesel Generator of the same electrical power weighs 70 Tons and occupies 96 m^3 volume.
The use of gas turbines is limited to specific applications because the high specific consumption of fuel increases if the turbines operate under 50 % of their nominal power, as show in Figure 13.

[7] Referred to 60 Hz application.
[8] In naval network it is not possible to adopt the short circuit equivalent model adopted for generator with infinite P_{sc}

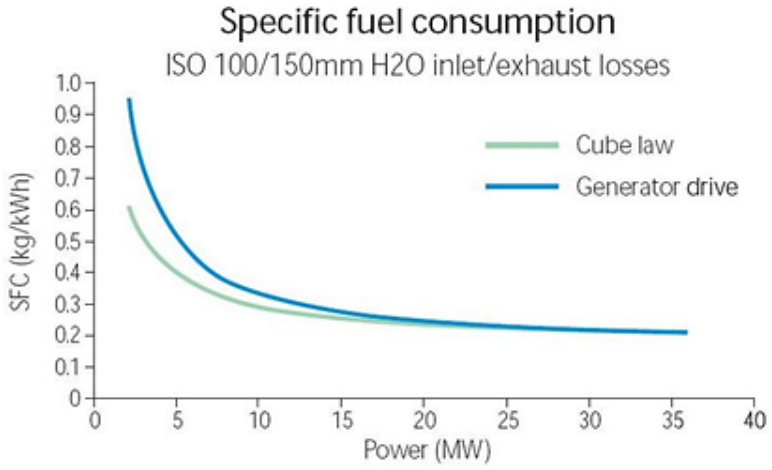

Figure 13- Specific Fuel Consumption Related to the Axis Power Generated

Moreover, an axis gear speed reducer is required to make the turbines speed compatible with the propellers speed or the electric generator. It introduces extra losses that constitute a weakness of the system.
The gas turbines are used to reach high speed (frigates, cruisers, aircraft carrier, etc.).
To improve the overall efficiency of gas turbines it is possible to couple a steam system with thermal energy recover to produce electrical energy and hot water for on board auxiliary system.

1.5 Energy distribution

Energy distribution starts from power stations, where power generation is subdivided and installed in the main electrical panels. The groups[9] are divided into at least two bars (reliability standard), with the possibility of parallel operation by closing a special bar-joint.
The on board power plants supply the entire vessel's loads dislocated into different areas of the ship. For example ambient temperatures in engine rooms reach high value and these rooms are subject to fire and explosion risks; the equipment installed outside the ship is subject to bad weather condition, electrical loads for medical use, indeed, need high safety standard, etc.
Network layouts, voltage levels and neutral operation, generally adopted on board are illustrated in the following chapters [12] [13].

1.5.1 Network layout

The energy distribution system could be defined as radial, double radial, or meshed network.

- radial network (Figure 14a): it is the simplest layout, the main electrical panel has a single section from which all sub-electrical panels are supplied. This layout is the least reliable, because any failure of the main bus-bars can lead to the collapse of the entire electrical system.
- compound Radial network (Figure 14b): it is an evolution of radial network where the main bus-bar is divided into two section with Sub-electrical panel distribution. They divide the power supply to various areas of the ship. Essential load (high continuity requirement) could provide a cross connection supply coming from a separate section, powered by an independent power source. An evolution, adopted by Italian Navy, is the double radial network where each ship zone can be fed from one power station or another.

[9] For example, in power plants only Diesel generators are installed, while in others there are only gas turbines.

- meshed network (Figure 14c): this system has high reliability level, it is possible to reconfigure the system during a fault, by isolating the faulty electrical section. In this type of network, it is possible to adopt directional protections to increase fault selectivity.

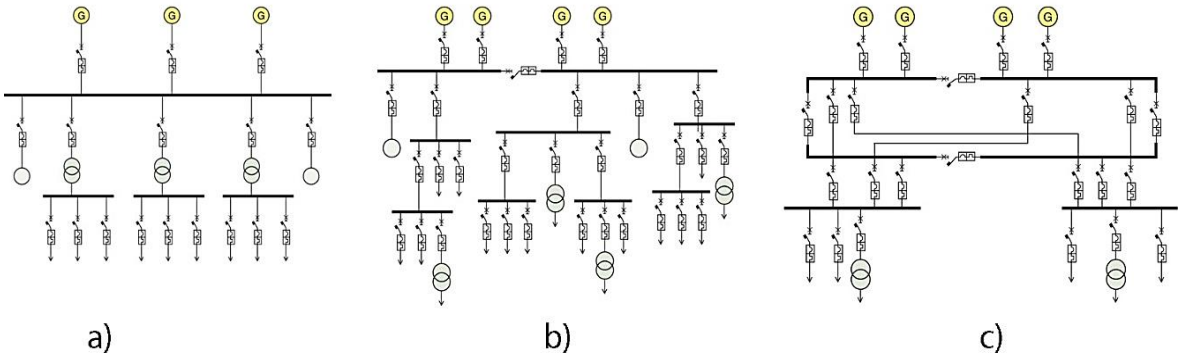

Figure 14- a) Radial b) Compound Radial c) Meshed

1.5.2 Voltage levels

Voltage levels are dictated by power generators and loads installed on board, and classes and insulation distances of the equipment, as well as the type and number of power wires must be sized based on them. Depending on network layout and installed power, more voltage levels are suitable, differentiating into primary, secondary and terminal distribution. In primary distribution voltage levels depend on the total power installed. Medium voltage generation and distribution systems for large ships normally provide 11 kV voltage level for 20 MW generation power plant and engines with power greater than 400 kW, while 6.6 kV distribution voltage is adopted from 10MW to 20MW generation power plants and engines with maximum powers around 300 kW. Other standardized voltage levels (4.16 kV, 3.3 kV, 1 kV) are used according to the geographical area of ship construction, in compliance with the different standards in force. In small boats such as yachts ranging from a few megawatts up to about 12 MW of installed power, voltage generation and distribution level normally occurs with 400 V and 690 V at 50 Hz, 115 V and 440 V at 60 Hz [14], [15]. Figure 15 shows the range of voltage levels relating to the power installed.

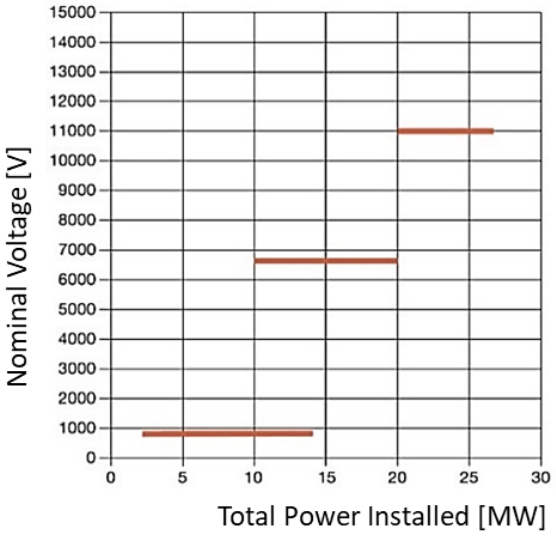

Figure 15 - Nominal Voltage Related to the Power Installed

1.5.3 Neutral operation

In three-phase four-wire networks, the neutral conductor is connected to the neutral point of the transformer or the generator that supplies the network.
In normal operation (symmetrical sinusoidal regime), the neutral conductor is located at ground potential and therefore voltage and current do not change. In perturbed conditions, during short-circuits dissymmetric on the ground, voltage and currents on the ground depend on neutral connection.
The three-phase transmission and distribution networks are designed and operated in such a way that they are as much symmetrical as possible. However, networks can work in a dissymmetric regime when phase to ground or phase to phase short circuits occurs.
The value of the fault current must be evaluated as it depends on the coordination of protections and the damaging effects at the point of failure, as well as the pitch and contact voltages that are generated to the ground. The value of temporary overvoltage must be evaluated for the dimensioning of the equipment insulation, components and users, as well as for the assessment of the risks of electrocution by direct contact.
We can devise two diametrically opposed ways of operating the network neutral:

- Neutral connected directly to the ground;
- Neutral isolated from the ground.

A third mode of neutral operation the ground connection through impedance is also implemented by several network operators, especially in MV networks.
This solution permits to limit the current values and, at the same time, to reduce over-voltage phases not affected by failure. The ground connection impedances of the neutral can be of different types and values; among them, the solutions generally adopted are: resistance, inductive reactance, and inductive reactance in parallel with resistance.
Neutral Grounding via resistor allows to limit single-phase fault currents to ground and permits line protection through simple homo-polar amperometric relays. The use of inductance instead reduces the earth fault current at negligible values. Neutral grounding through inductance in parallel with a resistor compensate the capacitive earth fault current and keeps the current at low values that are detectable by traditional relays. Figure 16 shows, the various neutral layout admissible [16].

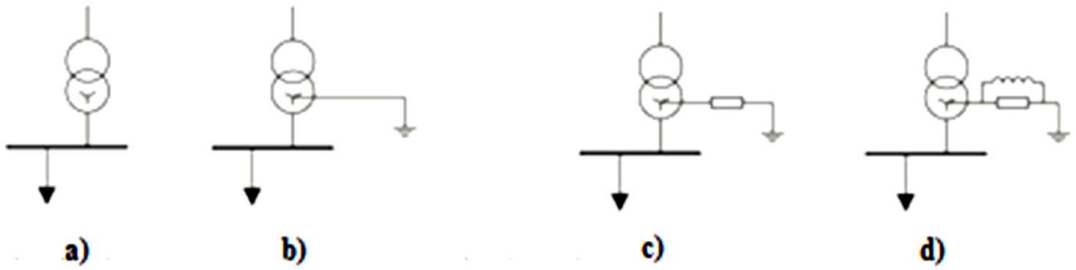

Figure 16 - a) Neutral Isolated b) Neutral Grounded Directly c) Neutral Grounded by Resistance d) Neutral Grounded Via Impedance

Common neutral operation architecture in maritime electrical systems are discussed. In particular, the list below reports the common neutral operation solution for power generators, and for primary and secondary distribution of naval systems [13].

- power generators and primary distribution: it is better to operate generators with neutral isolated from the ground, or connected by impedance. In this case the earth fault currents are reduced to low values (few amps) generally tolerated by the machine windings.

The solution with grounded neutral by high value impedance is a compromise between isolated neutral systems (high over-voltages and low ground fault currents) and systems with neutral directly connected to the ground (high ground fault currents). In both cases, a first fault with relative insulation loss allows to keep the system operating without tripping the protections. Obviously, is necessary to repair the fault to avoid that the first fault evolves into a double ground fault, that is more dangerous in an isolated system. The insulation level is continuously monitored;

- secondary distribution: in the past, when the on-board systems were not very large and with low power generation, the secondary distribution system was a single-phase network with two/three insulated conductors with a medium point of the transformer connected to the ground. Today, due to the increase in power generation, the three-phase system with distributed neutral is, in most cases, not connected to the ground. Therefore, it is possible to arrange the phase-to-phase and phase to ground voltage. The secondary distribution network is generally distributed radially with the possibility of double switchboard power supply via two different lines, implementing the reserve connection.

Table 1 summarizes the distribution systems used on board, differentiated by voltage level and by sector of use.

Table 1 - Neutral Operation for Different Distribution Systems

	Medium Voltage	**Low voltage**
Power Generators	Ground with impedance	isolated
Primary distribution	Ground with impedance	isolated
Secondary distribution/essential load		isolated
Secondary distribution/non essential load		To the ground with differential protection device
Electric propulsion supply	Isolated or to the ground with high value impedance	Isolated or to the ground with high value impedance

1.6 Electric propulsion system

A brief description on common electric propulsion engines is reported; it highlights different characteristic and performance based on their field of use [13].

DC motor: it was the first type of electric machine used for ship propulsion. Nowadays DC engines have been replaced by synchronous or asynchronous alternating current engines because of better performances. DC motors were limited to low power applications, due to the problems related to high currents switching on the machine's collector and the presence of brushes.

Asynchronous AC motor: it is the most widespread and used engine in the world thanks to its low manufacturing costs, robustness and reliability, as a result of the limited number of constituent parts and the absence of sliding contact. Rotation speed depends on frequency of voltage supply and it is characterized by lower starting torques as compared to nominal ones.

As for weight and dimensions, they are similar to synchronous AC motors also in size. For example, a 20 MW asynchronous machine (AIM) occupies about 18 m^3 and weighs about 70 tons, while a synchronous equivalent with permanent magnets (Jeumont axial flow) occupies about 17 m^3 and weighs about 65 tons [17].

The definition of poles number and stator winging phases, as well as a targeted structures design, could reduce the noise produced. This is an important aspect for passenger transport vessels but even more in military vessels, whose safety also depends on their level of detection, so it is essential for them to reduce acoustic emissions.

Synchronous AC motor: it is widely used, on cruise and military ships. These machines are versatile and operate indifferently either as electric motors or as generators, without performance losses. Synchronous machines, in a CODLAG system, operate as electric motors to drive propellers, and also as generators (SG) producing electrical energy when the propulsion is entrusted to the gas turbines that are coupled to the axis lines through speed reducers.
Synchronous machines can be subdivided into two manufacturing types: with rotor winging field and permanent magnets. The first ones regulate the machine excitation both in normal and emergency operation; they have additional losses (Joule losses in the inductor windings).
Adopting a brush and ring system for feeding the rotor circuits, they are globally more cumbersome compared to permanent magnet machines. For these reasons, they are not used as engines for ship propulsion.
Exceptions are synchronous machines with rotating diode excitation, in which a transformer with wound stator and rotor, is used instead of the ring and brush system. The rotor is connected to a rectifier bridge, which feeds DC power supply to the field winding of the synchronous machine. The transformer and the synchronous machine are coaxial, and the transformer's rotor, the diode bridge and the synchronous machine field winding are arranged on the same drive shaft.
Permanent magnet synchronous motors could be adopted in ships. The inductor's magnetic field is not provided by a winding, but by permanent magnets installed inside the rotor. They are extremely compact and need low maintenance, while it is possible to regulate the magnetic field produced by the rotor only with appropriate modulation techniques through electronic drives. The permanent magnet synchronous machines are classified, according to the type of magnetic structure, in axial flow, radial flow and transverse flow. The first ones are characterized by a flat rotor upon which the permanent magnets are mounted, and by a stator (flat) where stator windings are placed.
The magnetic flux spreads in axial direction, parallel to the rotation axis, making the machine extremely compact. Moreover, it is possible to exploit modular structures, through several rotor and stator stages, to increase the nominal power and maintain a high power density in extremely compact spaces. Radial flow machines are the most traditional, they have a mainly axial distribution and are the ones with higher rotation speeds performance, unlike axial flow synchronous machines that display problems due to centrifugal forces. Transverse flow machines are composed of a ring comprising the permanent magnets, which rotates between two rings constituting the stator windings and being coaxial to the rotor ring. The magnetic flux produced by these windings passes through the rotor ring through a series of stator expansions. In addition to the described categories, engines for naval propulsion exploiting the technology of high-temperature superconducting materials are being developed to obtain more compact and higher power density machines.
Figure 17 shows a comparison between a traditional synchronous motor and a synchronous motor with high temperature superconductors.

Figure 17 - Comparison Between A Traditional Synchronous Motor and A Synchronous Motor with High Temperature Superconductors

1.7 Electric propulsion's driver

Widely used power converters for electric propulsion's drivers are:

- AC/DC converters for direct current engines;
- current source inverter (CSI) for AC engines, generally synchronous motors;
- cyclo-converters for AC motors, generally synchronous motors;
- voltage source inverter (VSI), generally for asynchronous motors.

DC Converters for direct current motors

The most commonly used naval propulsion's DC engine had an independent excitation circuit, in which the power supply of the excitation winding was separated from that of the armature winding. A converter manages mechanical parameters, such as the torque and the rotation speed.
In particular:

$$V_d = k \cdot \phi(I_f) \cdot n$$

Where V_d is the Armature circuit supplying voltage, k is a manufacture constant, $\phi(I_f)$ is the excitation flux generated by the field circuit current (I_f) and n is the mechanical rotation speed.
To speed adjustment, armature voltage or magnetic flux excitation control is required, keeping one of the two variables constant and adjusting the second one. Moreover, the supplied torque is proportional to:

$$T = k \cdot I_d \cdot \phi(I_f)$$

Where T is the axis mechanical torque produced and I_d is the current of the armature circuit. Also, in this case, by alternately adjusting one of the two variables it is possible to adjust the mechanical axis torque produced.
A main thyristor bridge is used to supply the armature circuit, while an auxiliary rectifier supplies the excitation circuit power supply. If the engine drives a fixed pitch propeller, it is possible to guarantee the maximum available torque for all the speed range, up to the nominal value, performing speed regulation by controlling the armature voltage.
The V_d is linked to the supply voltage of the AC system:

$$V_d = \frac{3\sqrt{2}}{\pi} \cdot V_{LL} \cdot \cos\alpha \cong V_{d0} \cdot \cos\alpha$$

Where V_{LL} is the nominal rated voltage of AC system, α is the thyristors' triggering angle. By varying the angle α between 0 ° and 180 ° (for stability reasons the variation range is about 15 ° ÷ 150 °) it is possible to supply the dc engine with a voltage ranging between ± V_{d0}.
The disadvantage is that, since the $\cos\alpha \cong \cos\varphi$ relation is valid, the drive absorbs current with a variable power factor between 0° and 180°, and proportional to speed rotation [18].

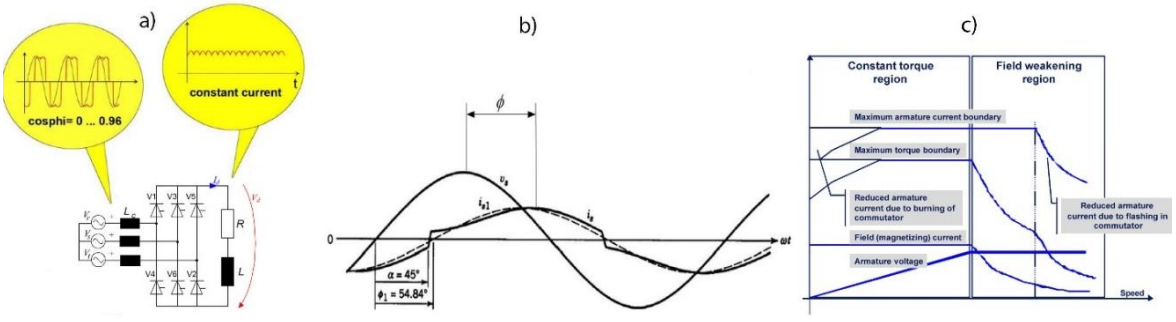

Figure 18 - A) Thyristor Bridge Drive for DC Propulsion Motor B) Grid Side Voltage And Current Absorbed By Converter C) Trend Of The Electrical Parameters According To The Rotation Speed

CSI current source inverter

A current source inverter, also called Synchronous inverter, is characterized by: a thyristor bridge that performs AC/DC conversion, a direct current link with smoothing inductor and a full bridge DC/AC converter that feeds the electric motor. This type of drive is often used to supply synchronous engine but, with some changes, it can also supply asynchronous engines.
The polarization of the thyristors is obtained by means of e.m.f. generated by the synchronous motor in over-excitation, absorbing capacitive reactive power.
The synchronous converter can supply only a synchronous motor. To couple it with an asynchronous motor, it is necessary to insert a capacitor bank between inverter and engine, to supply the reactive power needed and an auxiliary thyristors switching, to manage speeds lower than 60% of nominal speed due to insufficient e.m.f. when the valves are turned off.
With synchronous motor, the stator windings absorb rectangular currents from the inverter, as shown in Figure 19.a, with a high harmonic content [19].

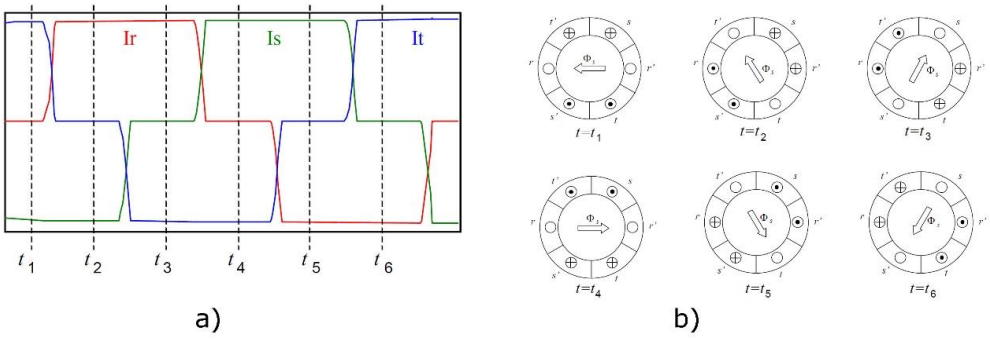

Figure 19 - a) Stator Currents Absorbed By The Synchronous Motor From The Inverter b) Trend of The Magneto-motive Stator Force Within The Period of The Mains Supply Voltage

Figure 19a shows that within a period of the network voltage each thyristor conducts for 60 electric degree. Figure 19b shows that also the magneto-motive force related to the stator phases vary every 1/6 of the period. The trend of the stator magnetomotive force (m.m.f.) is transformed into multiple frequency torque pulses, in so far it is linked to the stator magnetic flow by the following:

$$T_{em} = k \cdot \Phi_e \cdot \Phi_a \cdot \sin\beta$$

Where T_{em} is the air gab electromagnetic torque, k is a manufacture constant, Φ_e and Φ_a are respectively the excitation and armature magnetic flux, β is the electrical angle between Φ_e and $\Phi_a$vectors.
While the excitation magnetic field rotates at a constant speed, the one induced by the stator currents takes on a jerky pattern, from which the high frequency ripple of the driving torque arises.
To mitigate this phenomenon it is possible to adopt double stator windings, to obtain homonymous phases e.m.f. of 30 electric degree offset. The number of positions assumed by the magnetic field passes from 6 to 12, decreasing the torque ripple.
Finally, to reduce the currents harmonic distortion, it is possible to use multiple-pulse reactions, 12, 18 or 24 pulses, significantly reducing the current total harmonic distortion.
Figure 20 shows an electric drive with two synchro-converters supplying a synchronous motor with dodecaphase reaction.

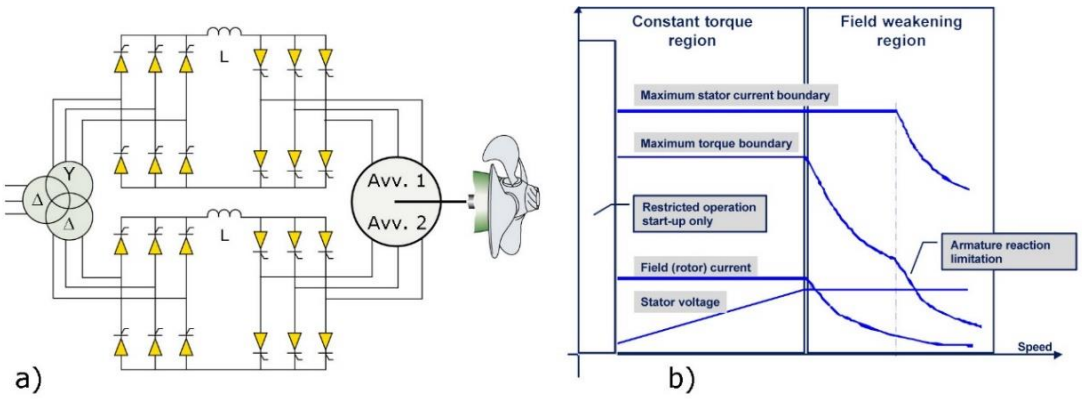

Figure 20 - a) Synchronous Converter for Synchronous Motor b) Trend of The Electrical Parameters Relating Rotations Peed

Cyclonverters

The cycloconverter is a device consisting of two full bridge thyristors connected in antiparallel. It converts an alternating voltage with constant frequency and amplitude into an alternating voltage with variable frequency and amplitude. This conversion occurs in a single stage, without continuous connection (DC link), linearly varying the α trigger angle of the thyristors. A voltage close to the sine wave is obtained.

This drive is mainly used with synchronous motors; with three single-phase cycloconverters it is possible to supply the stator windings of the synchronous machine (Figure 21a).

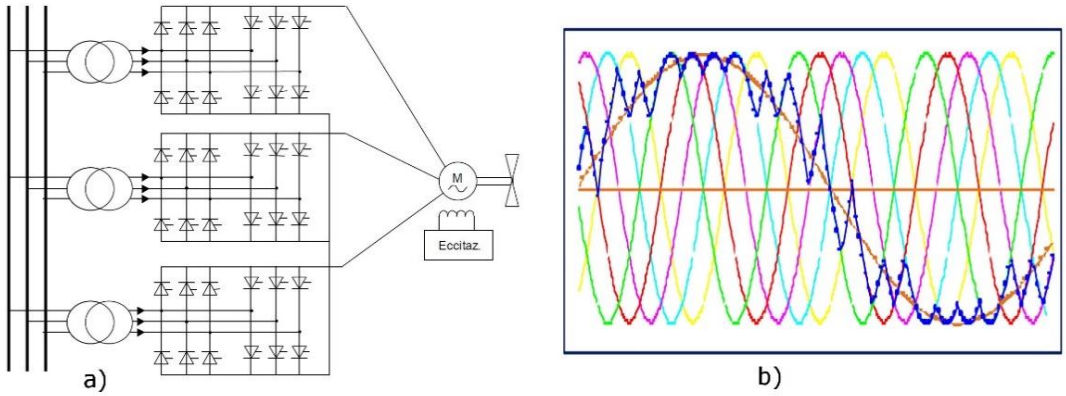

Figure 21- a) Drive with Three-Phase Cycloconverter to Supply a Synchronous Motor b) Motor Supply Voltage Obtained By Selecting Defined Segments Of Network Voltages

Figure 21b shows output voltage waveform obtained by selecting a defined segment of the input waveform. The current harmonic content of the input depends on the ratio between the input/output voltage frequency which cannot decrease below 2.5 (the output frequency can be maximum 40% of the input frequency). The main advantage is the high torque value available at low speed, being therefore suitable for propeller systems of icebreakers, passenger and dynamic positioning ships. The network power factor depends on the engine's voltage and varies with the speed ranging between 0 ÷ 0.75. It is possible to fulfil multi-pulse configurations to limit the current harmonic content absorbed by the network, Figure 22 shows a diagram of a three-phase cycloconverter with dodecaphase configuration.

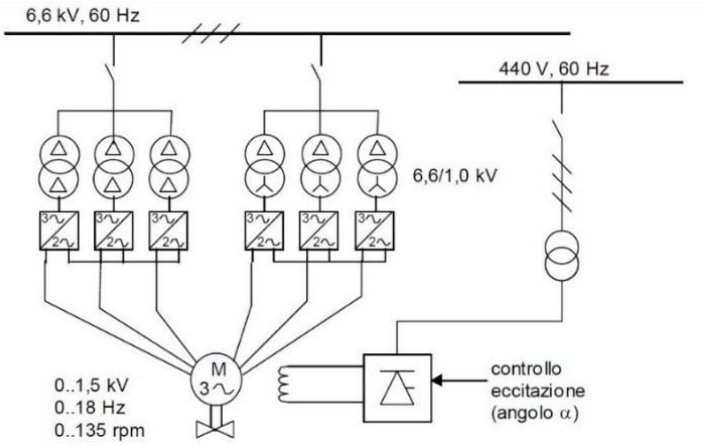

Figure 22– Cycloconverter for Synchronous Motor

VSI voltage source inverter

The most widely used voltage source inverter electronic switches with forced commutation are:

- IGBT (Insulated Gate Bipolar Transistor);
- GTO (Gate Turn Off Thyristors);
- IGCT (Integrated Gate Commutated Thyristors).

The frequency conversion is performed in three stages as reported in Figure 23: a direct current stage (DC link) is obtained from the power supply via rectifier. It is characterized by a constant voltage V_d maintained by a LC filter designed to dampen the voltage ripple limiting the absorption of current harmonics from the network. The DC voltage is transformed into a symmetrical three-phase voltage by an inverter using voltage modulation techniques for feeding the engine windings.
The interdiction of the circuit-breakers is operated through an external control logic circuit. Thanks to this solution it is possible to use this type of converter with asynchronous motors, reaching significant powers, also at low speed.

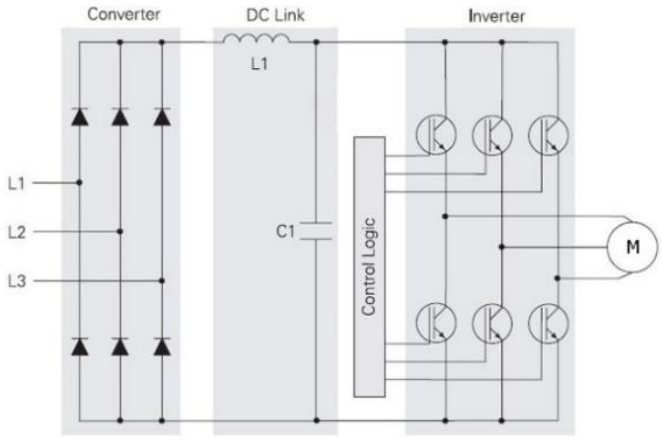

Figure 23 - Driver with Impressed Voltage Inverter

The most common modulation techniques to obtain output voltage are:

- scalar control: it is the simplest control technique based on the stationary electric model of the asynchronous motor. It has a poor dynamic performance, as model parameters strongly depend on frequency, temperature, etc. Furthermore, the output voltage contains high frequency oscillations and widely varying switching losses;

- rotor flux vector control: the method is based on the voltage vector model, flow and motor currents in a rotating coordinates system. It is possible to decouple the machine flux and the torque, and independently control the two parameters. This technique requires coordinates transformation and contains highly variable parameters, especially resistances varying with temperature. A sensor system is therefore necessary for monitoring these parameters;
- direct Torque Control: based on machine flux and torque decoupling, direct Torque Control can be obtained using electrical parameters in a coordinate system that is integral with the stator. Independence from the machine's parametric variations is ensured; on the contrary, it requires a greater calculation capacity than the rotating coordinates. The main advantage is the use of a system without speed sensors, as only power voltages and currents are detected.

For Medium Voltage drives, it is necessary to have appropriately designed electronic switches, which can tolerate higher voltages, currents and frequencies involved.
Multilevel converters can be used, these are converters in which the output voltage takes three or more output values, thus improving the output waveform and its harmonic content.
Figure 24 shows a three-level source voltage-drive diagram (*Integrated Gate Commutated Thyristors*) for a 3.3 kV MV system, and the related output quantities.

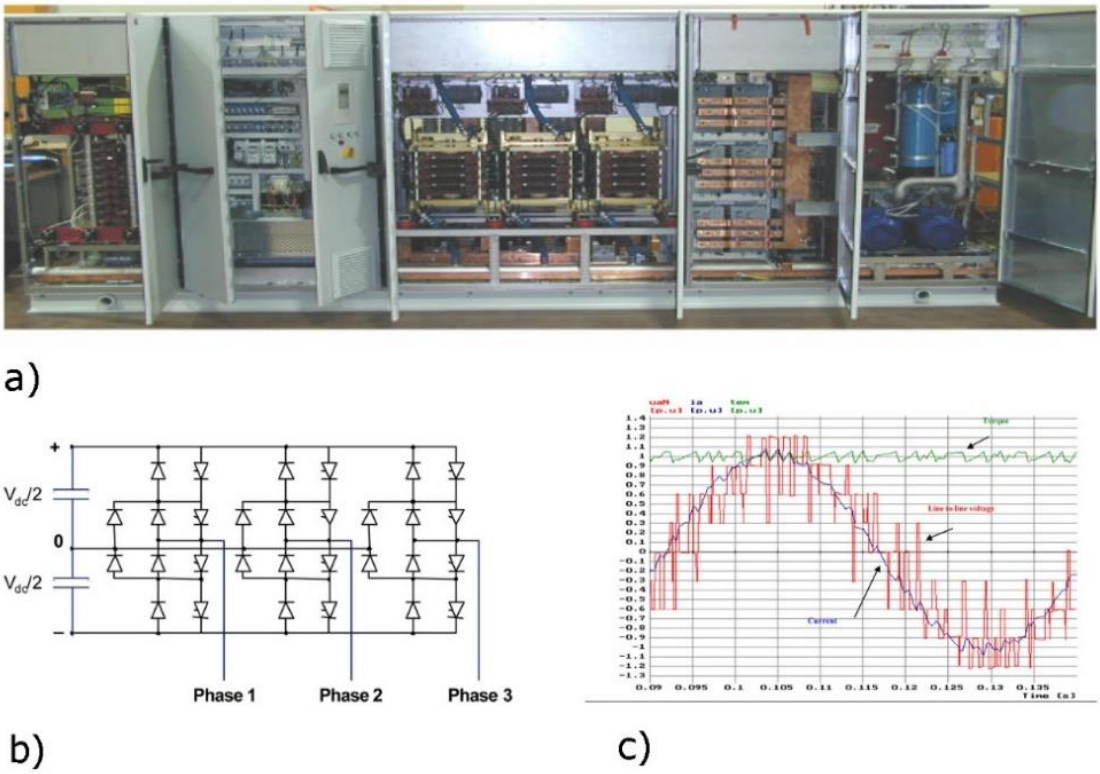

Figure 24- a) 3.3 kV Integrated Gate Commutated Thyristors Drive b) Drive Architecture c) Output Trend

Table 2 summarizes the drivers' characteristics seen previously; the first column reports the characteristics related to the engines' direct insertion into the network.

Table 2- Drive Features

	DOL[10]	SCR DC Motor Drive	cycle converter [11]	CSI[12] (LCI)	VSI[13] DTC
Insertion current	$5 \cdot I_n$	≈ 0	≈ 0	≈ 0	≈ 0
Starting torque	2÷3 x nominal torque	≈ 0	≈ 0	Up to a 50% nominal torque	≈ 0
Power consumption, for low thrust	≈ 15% nominal power	≈ 0	≈ 0	≈ 0	≈ 0
Current, for low thrust	45÷55% della nominale	f (torque)	f (torque)	f (torque)	≈ 0
Power factor, at nominal load	≈ 0.85	> 0.9	> 0.76	> 0.9	> 0.95
Variation of the power factor with the load (cosφ)	0.15 ÷ 0.85 (non linear)	0 ÷ 0.9 (proportional speed)	0 ÷ 0.76 (proportional speed)	0 ÷ 0.9 (proportional speed)	> 0.95 (constant)
Dynamic response (power, torque)	3÷5 sec (propeller pitch control)	<100 ms	<100 ms	lower	<10 ms
Pulsations of torque	nothing	smooth	smooth	pulsating	smooth
Zero push transition	Smooth if negative thrust is allowed	Non continuous	smooth	pulsating	smooth
Full load efficiency	high	low	high	high	high
Harmonic distortion a - low speed / thrust - high speed / thrust	None None	f (torque) f (torque)	f (torque) f (torque)	f (torque) f (torque)	None f (power)
Short circuit contribution	5x nominal power	No	No	No	No
Changes for adaptation to some types of engines	-	Several	Several	Yes	No
Switch presence	No	Yes	No	No	No

1.8 Regulatory requirements and naval registers relating to environmental conditions

The environmental conditions that arise on board the ship are very critical, high humidity and temperatures, mechanical stresses, such as vibrations as a result of the ship's movement or of mechanical origin (engines first), all contribute to creating an extremely heavy and aggressive environment that requires the use of particularly robust electrical equipment.

For ships without navigation restrictions the reference temperature for enclosed spaces varies from + 5° C to + 45° C, for ships with navigation in specific areas (e.g. outside tropical areas) the maximum operating temperature assumed is equal to 40° C. Standard provisions for humidity conditions provide a value of 95% at 55° C.

The required level of vibrations varies in relation to the location of the electrical component. For installations in command and control stations, on exposed bridges or in entertainment spaces of the various rooms on board, the field verification required for the responsiveness to vibrations varies from 2 Hz to 13.2 Hz with a width of 1mm and from 13.2 Hz to 100 Hz with an acceleration of 0.7g (1g = 9.8 m/s^2). Power quality parameters such as voltage variations between +6% and -10%, and +/-5% frequency values are also provided by standards. For the harmonic content of systems without main loads, controlled by power converters through synchronous generators, the total level of harmonic distortion of the voltage must not exceed 5% and the single harmonic must not exceed 3% of the fundamental. In the presence of loads controlled by static converters the single harmonic does not exceed 5% of nominal voltage up to the 15th order of harmonics and the total level of harmonic distortion admitted not must exceed 10%. For the presence of those equipment which allow the

[10] Asynchronous motor coupled with orientable propeller
[11] Synchronous engine
[12] Synchronous engine
[13] Induction asynchronous motor

dissemination or transfer of signals through electromagnetic waves or for radar plants or radio link, registers also prescribe checks for aspects related to phenomena that are generally defined as electromagnetic compatibility and that, for example, include tests for noise immunity caused by conducted and irradiated emissions. The main Naval Register and Standard Parameters are reported in [13].

1.9 Overall reflection about "All electric ship"

The simplest definition of an "All Electric Ship" can be: a vessel equipped with electric propulsion, having all on-board loads electric powered, and with a single power system dedicated to supply both, called Integrated Power System. The main benefits of the AES concept [20] made possible by both the electric propulsion and the integrated power system application, are [2]:

- better dynamic response;
- flexibility in space and weight allocation (propulsion motors and electric generators can be installed in different places, short shafts);
- more degrees of freedom in power system layout design;
- availability of podded-drive solution (removal of shafts and rudders, increased manoeuvrability);
- enhanced control of electric propulsion systems (acceleration and manoeuvring);
- increased overall efficiency (possibility to modulate the number of running generators to reach the optimal operating point, better management of Heating Ventilation and Air Conditioning systems - HVAC);
- noise and vibration attenuation (with consequently increased comfort);
- advanced automation and reduction of the crew;
- increased survivability (generator sets distributed, better ship compartmentation);
- increased maintainability;
- enhanced operating life (less mechanical components, fewer stress on prime movers).

As far as loads are concerned, these are commonly formed by:

Main propulsion system

Used to propel the ship forward and backward, main propulsion systems are the highest power single loads on-board (commonly cruise ships nowadays have $10 \div 20$ MW for each propulsion axis, while other vessels can reach ever-higher power levels [3]. Power electronic converters feed variable speed electric motors directly connected to fixed pitch propellers. Variable pitch propellers can be used in high performance applications, but are not necessary due to the regulation capability of the electric propulsion system. Cycloconverters and synchroconverters coupled with synchronous machines are common on-board, but nowadays high power systems using PWM converters and induction motors are becoming popular.

Manoeuvring propulsion systems (thrusters)

Auxiliary propellers installed on board are used to improve ship manoeuvring during navigation, and to allow side movement (such as in berthing operations). The most common solution is a Direct On Line (DOL) induction motor coupled with a variable pitch propeller. However, PWM supplied motors coupled with fixed pitch propellers may be a future solution, when such systems will be able to achieve the same hydrodynamic performance of conventional ones.

HVAC systems

This set of subsystems keeps the ship in inhabitable conditions, through heating, cooling, and air exchange. Ventilation and heating subsystems are usually scattered throughout the whole ship, and

are electrically powered, while air-cooling is usually achieved through a cold-water closed loop system. Heat exchangers and high power electrical compressors, directly connected to the main switchboard, provide cold water.

Hotel loads

This definition is used to classify loads, such as lighting systems, kitchens, waste management, entertainment, and so on. Hotel load can be a minimum quota of the total ship loads, as it is the case in most merchant and naval vessels, or can be the most relevant load on board (either comparable or higher than main propulsion), in cruise vessels.

Navigation system loads

To keep the ship on the right route, avoiding dangerous collisions at the same time, a set of subsystems are needed. Radar systems, GPS, satellite and radio systems, all of them can be defined as navigation systems. Such loads commonly require high power quality, so they are fed through dedicated power converters.

Other loads

All the loads not included in the above classification are included in this category, such as firefighting pumps, fuel management, etc.

1.10 Electrical system protection devices

The design of the protection of an electrical system is fundamental both to guarantee its correct operation and functionality, and to minimize the problems caused by anomalous service conditions or by faults that may occur.
Protection devices are important to ensure the system's and people's safety, identifying only the area affected by fault.
Any electrical system needs the highest requirements in terms of reliability allowing protection interventions even in case of a malfunctioning device.
However, faults must not only be detected and isolated, but it is always necessary to provide service restoration in the shortest time and with the minimum network perturbations.
IEC or CEI EN 60947-1 and IEC or CEI EN 60947-2 are the standard requirements for protection devices.
It is important to determine the short-circuit currents in different operating conditions. In particular, the maximum short-circuit currents are important for the sizing of the equipment, while the minimum short-circuit currents allow to verify the coordination of the protections.
The reference standards for short-circuit currents calculation in naval applications are [13]:

- IEC 60909-0 2016: Short-circuit currents in three-phase AC systems - Part 0: Calculation of currents;
- IEC 61363-1 1998: Electrical installations of ships and mobile and fixed offshore units - Part 1: procedures for calculating short-circuit currents in the three-phase AC systems.
- IEC 60092-202:2016 Electrical installations in ships - Part 202: System design - Protection

IEC 61363 standard provides a calculation methodology that is well suited to small networks powered by generators as it provides for the calculation of short-circuit currents over time taking into account the time constants of the rotating machines, i.e. motors and generators. In fact, a naval electrical system includes generators, both synchronous and asynchronous motors, and transformers. For calculating the short-circuit current we should consider the maximum number of simultaneously operating generators and the total number of engines that are normally connected to the electricity grid at the same time.

The short-circuit current according to the IEC 61363 standard, provides for the determination of the component I_{ac} (t) which is characterized by the sub-transitory, transitory, and synchronous or regime contribution. The Standard reports the following relation taking into account also the contribution linked to the aperiodic component I_{dc} the component of the current that manifests itself in a circuit immediately after the short circuit:

$$I_p = \sqrt{2} \cdot I_{ac}(t) + I_{dc}(t)$$

This relationship allows to determine the peak value of the short-circuit current depending on preload conditions and typical generator parameters.
All types of circuit breakers used on board the ship will therefore have to be chosen on the basis of the parameters of current and nominal voltage as well as on the basis of the performance in conditions of short circuit according to the following constraints:

- a nominal short-circuit closing capacity, referred to the operating voltage, which must not be lower than the peak calculated according to the requirements of the IEC 61363 Standard at the point of installation of the device itself;
- a rated short-circuit breaking capacity with reference to the operating voltage, which must not be lower than the value calculated for the alternating component I_{ac} (t).

In general, the types of faults that can occur in a three-phase system are:

- three-phase short-circuit;
- two-phase short-circuit;
- two-phase short-circuit on the ground;
- single-phase short-circuit on the ground.

The electrical systems on board are characterized by the presence of high power generators installed in a delimited area. The short-circuit current can also have a high value, reaching higher peak values due to the non-linearity and the time-varying of the impedance of the active components during short circuit and due to the high-section and reduced-length wires deriving from the layout of the plant (reduced distances between generator and the main fault points).
Ship protection devices must be chosen and based on the current and nominal voltage parameters also on the basis of their performance in short-circuit conditions according to the following constraints:

- a nominal short-circuit closing capacity (I_{cm}) referred to the nominal voltage, which must not be lower than the peak of current calculated according to the requirements of IEC 61363 standard at the point of device installation;
- an extreme or nominal short-circuit breaking capacity (I_{cu} or I_{cs}) referred to the nominal voltage, which must not be lower than I_{ac} (t) to T/2;
- a peak value factor at the failure point ensured by circuit breaker nominal performance.

Moreover (back-up protection) between two switches is not allowed.
The naval standard introduces further clarification indicating the type of circuits for which the protection devices must be chosen with reference to its value of I_{cu} or I_{cs}.
For circuits of non-essential load or circuits redundant of essential load the switch can be chosen with reference to I_{cu} value. Protection devices chosen with reference to I_{cs} values are those for generators protection and those for which there is no redundancy supply.
Naval registers provide prescriptions; the main and most important prescriptions to be followed are discussed below. Every power distribution system, (heating or lighting) primary-powered directly from generators or secondary, powered by transformers being isolated must be equipped with a

device capable of continuously monitoring the insulation level on the ground and emit a visible and audible signal in order to indicate isolation values.
In systems directly connected to the ground or through low impedance the circuit affected by failure must be automatically disconnected.
Protection devices must ensure safety against short circuit and overload for each conductor not connected to the ground, while conductors connected to the ground must not be interrupted.
Specific measures must to be adopted for example for auxiliary control circuit or rudders supply systems for which ad-hoc protection against the short circuit must be provided.
Protections must be provided for generators against short circuit with immediate intervention for a current less than the steady state current, and overload for current values from 10 % to 50 % of the nominal current with an intervention time no longer than 2 minutes.
Engine circuit protection must include a thermal protection based on the type of engine starting and magnetic protection must ensure the establishment of high currents during the transient starting phase. The transformers are built to withstand the thermal and mechanical effects following a failure on the secondary circuit without damage and for 2 seconds.
The primary circuit of transformers (normally dry type with air cooling) must be protected by a device with overload protection and short circuit. This device must ensure selectivity towards the circuits fed by the transformer's secondary side.
As for service continuity, the selectivity between the different line arrival and departures switches to other users must be pursued and implemented for the purpose of isolating only the part of the plant concerned with the failure without putting other essential services out of order.
For overcurrent protection, switches, combined switches with fuses or only fuses are generally used; however, it should be noted that the use of the switches is recommended as it avoids the replacement of the melted parts. The medium voltage zones are usually protected with sulfur hexafluoride circuit-breakers, since these are more effective, compact and require less maintenance than those in oil bath or air used in the past. For low voltage, air circuit-breakers are used with wide use of current limiters, i.e. devices able to subdivide the system into parts, thus reducing short-circuit currents.
The overcurrent relays are generally very high settled, about 5-10 times the rated current, while for overload relays this value drops to 1.2-1.5.
For the latters, it is preferable to use relays with mechanical delay on high flow circuits, which have the advantage of being independent from ambient temperature and do not require any waiting time for restarting after the operation. On board, strong cables grouping, limited space, reduced ventilation and high temperature in the various environments determine particularly unfavourable operating conditions and above all high ambient temperatures.
Small and medium circuit-breakers use a bimetallic thermal relay, whose operation occurs after 1-3 minutes with currents of 1.5 times the nominal maximum at 45° C.
Protection devices must guarantee an extremely high level of performance thanks to their overall dimensions, easy installation and an ever-greater safety guarantee for the operator. In addition to protection performance, most switches also include communication systems, particularly suitable for automation, measurements, network analysis and energy savings. In fact, these functions allow the complete monitoring of the load and the generation conditions through the interaction with the ship control systems, depending on the different navigation operational profiles.

AC/DC protection device

Thanks to the well know literature in this field, in this paragraph a brief description on consolidate technology on common switches is reported. A focus on new DC breaker architecture is highlighted. Different various types of AC switches are commonly used in MV systems depending on characteristic type, method used for extinguishing the arc and system voltage. The most representative switches are: oil, sulfur hexafluoride, magnetic deionization air and vacuum switches.

Moreover, for LV systems the circuit breakers can be divided into three types: open, boxed and modular [21] [22] [13] [23].
In DC systems the most representative is the extra-rapid switch used in railway systems but the disadvantages of not having an instantaneous action and not being able to operating repetitively fast, could easily create stability problems in the network. Interruption time, inevitably linked to the operation of complexes mechanical systems, is necessarily long; it is often difficult to interrupt the fault current and at the same time fully meet the needs of the system. Nodaway, due to the increasing of electronic equipment and the development of new dc complex architecture greater attention has been paid on solid state switch.
In the next future, new solid state limiters could provide a very reliable service with little maintenance, limited floor space and many advantages as high interruption speed, limitation of the fault current, possibility of repetitive operation with no arcs generation.
Solid state switches are widely used in DC low voltage systems. An example of application is the "solid-state power controller" (SSPC) in the aircraft system distribution. Solid state power controllers have outputs and logical inputs that allow remote external monitoring so they can be placed close to the load by reducing the complexity of connections. These devices, therefore, simplify the installation, reduce weights and encumbrance and improve the system reliability at the same time.
Limited voltage and current values and the high losses associated with semiconductor power devices, hinder the spread of solid state switches in higher power applications. However, there are some critical applications that require a high rate of power failure, such as in the case of inverters (which require large inductors on the power supply side), switches in the DC drive systems, network protection distribution on board aircraft and ships, where the solid state break would bring considerable advantages [24].
Solid state switches can meet high speed requirements, without arcs, providing a limiting effect and guaranteeing a greater quality and continuity of the power system supply. Solid-state switches could have few hundred microseconds of open time, which is about two orders lower than that of mechanical switches. With the new and emerging power switches equipped with IGCT and ETO, the speed of solid state switches can be further increased: in 2004, for example, a state switch was developed based on IGCT, for medium voltage systems (1800 A / 9000 V c.a.), capable to perform an interruption within 100 μs. In the subsequent years some prototypes have been realized that have successfully passed laboratory tests, tracing a new path for the development of solid state switches. Experimental results indicated that an ultra-rapid interruption of only 5 μs was achieved with a continuous current of 5000 A. An ideal device should have the following features:

- ability to conduct high currents with no voltage drops;
- ability to limit high voltages with no leakage currents;
- no turn-on/turn-off delay;
- current detection capability;
- overcurrent protection and limitation;
- reduced weight and dimensions;
- high reliability;
- low costs.

Currently, no device can guarantee all the features listed; therefore equipment performance is necessarily limited.
At the moment IGBT (Insulated Gate Bipolar Transistor), IGCT (Hard driven GTO) and ETO (Emitter Turn Off) seem to be the most suitable components for the development of solid state switches and limiters, while the SCR (Silicon Controlled Rectifier or Thyristor) does not belong to the category of fully controlled devices, and Gas (Gate Turn Off Thyristor) has now evolved towards a hard-driven type.

Furthermore, latest generation IGBTs are more and more undermining the primacy of Gas in almost all fields of application.
Both mechanical and solid state switches are characterized by positive and negative aspects. The integration of solid state devices with mechanical switches constitute the so-called hybrid technology (Hybrid Switching Technique), where the advantages of one or the other technique are intentionally used to eliminate negative characteristics: for example, the rapidity of intervention of the semiconductors is exploited contextually with lower losses of mechanical contacts.
Generally, a hybrid system includes two different mechanical switches: the main (with a solid-state switch in parallel) and the second isolation switch. The first provides a path for the direct current, while the second allows the dielectric separation of the load after a fault [25].

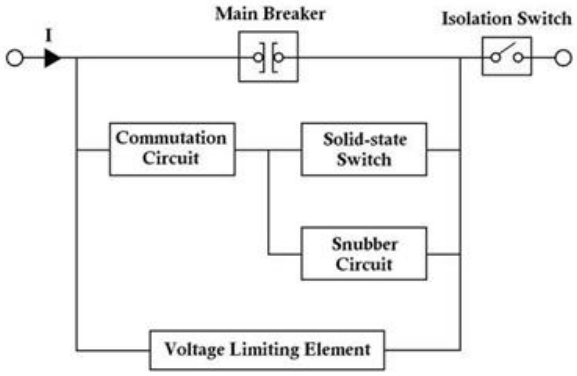

Figure 25 - Hybrid Switch Architecture

Figure 25 shows a hybrid switch architecture. In parallel to the main switch there is a commutation path that includes a transient damper circuit (snubber) and a voltage limiting element (energy absorber). During normal operation, the snubber circuit and the limiter constitute a high-impedance reclosing path. The commutation path is activated by a solid-state switch only during the interruption process. All switches are controlled by electronic circuits; since the reaction times of solid state switches are much shorter than the mechanical ones, the mechanical command of the hybrid switches must be as fast as possible. For higher rated current, the mass of contacts must be greater not getting high speed intervention. Moreover, the main switch must be able to maintain the insulation when the first zero crossing of the current occurs; consequently, a vacuum circuit breaker is very suitable for its excellent insulation properties. The time required for failure, is within the 1-10 ms range.
Figure 26 shows the state of the art in relation to the intervention times and the powers of solid state and hybrid switches that are still undergoing intense analysis, despite many prototypes have already been created and tested.

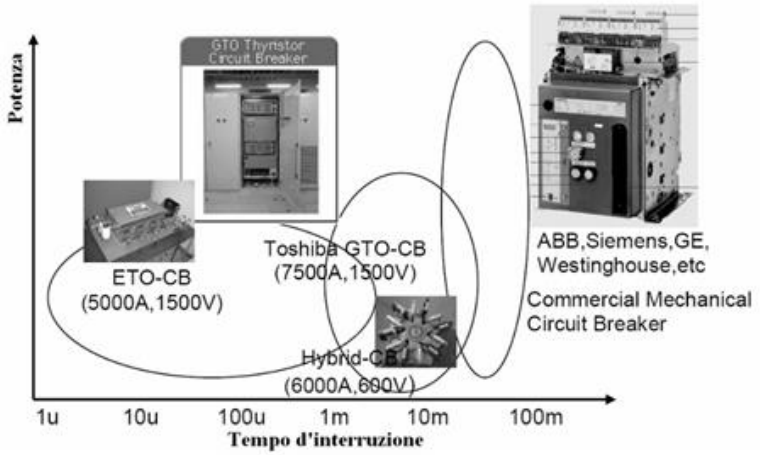

Figure 26 - Solid State and Hybrid Switch State of Art

1.10.1 Selectivity techniques

Different selectivity techniques and their application field are described [16] [26].

Time-current

Generally, the overload protections have a time dependent characteristic. With the increase of the current, the switch tripping time is reduced. Having protections with these characteristics, the selectivity technique used is time-current selectivity. Intervention selectivity is obtained by adjusting the protections so that the downstream protection, for every possible overcurrent value, intervenes more quickly than upstream protection.

Amperometric

It is possible to discriminate the area where the fault occurred by calibrating the instantaneous protections at different current values. Normally it is possible to obtain total selectivity only in specific cases where the fault current is not high and where there is a high impedance component interposed between the two protections (a transformer or a cable of reduced section) and therefore a great difference between the values of the short-circuit current. This type is mainly used in the terminal distribution where there are low nominal current values, low short-circuit current values and high impedance of the connection cables. It is inherently fast, easy to implement and economical. The selectivity is often only partial; furthermore, the setting level of the protections against overcurrent rises rapidly and finally it is not possible to have a redundancy of the protections which guarantees the elimination of the fault in a short time in the event of failure of one of them. It is a type of selectivity that can also be realized between switches of the same size and without protection from the delayed short-circuit.

Chronometric

In addition to the current threshold, an intervention time is also defined. A given current value, in fact, will cause the protections to intervene after a defined period of time, so as to allow any protections placed closer to the fault to operate, excluding the area where the fault occurs. The regulation strategy is therefore to gradually increase the current thresholds and operation time delays as one approaches the power sources by relating the level of setting with the hierarchical level. The delayed thresholds must take into account the tolerances of the two protection devices and of the actual current flows. The difference between the delays set for protections devices in series must take into account the detection and elimination times of the downstream device failure and the inertia time of the upstream device. The operational times and the energy flowing through the protections, especially those near the sources, are high. It is a type of selectivity that can also be realized between switches of the same size, equipped with electronic releases with protection against delayed short-circuit.

Energy

If no time-delayed switches are used, it is not possible to perform time selectivity, but it is possible to extend the selectivity limit, beyond the magnetic threshold of the upstream circuit-breaker. It is necessary to use downstream limit switches. A limiting switch is, according to the IEC 60947-2 standard, "a circuit breaker with a sufficiently short interruption time to prevent the short-circuit current from reaching the peak value that would otherwise reach". In short-circuit conditions, these switches are extremely fast (few milliseconds) and open even with a strong asymmetric component. The energetic selectivity is based on the comparison of the characteristics of specific energy passing through the two series switches of which the downstream one must be a type limiter.

Zone

It is an evolution of the chronometric. In general, zone selectivity is achieved through the communication between the current measuring devices which, once the setting threshold is exceeded, allows to correctly identify and switch off the supply from the fault zone only. It can be realized through measuring devices, which send the information related to the exceeding of the current regulation threshold to a supervision system, thus identifying which protection must intervene.
Another method is that any protection devices sending a blocking signal to the hierarchically superior protection (upstream from the direction of the power flow) through a direct connection or a bus, by checking that, before intervening, a similar blocking signal has not come from the protection downstream. Only through this approach, the protection immediately upstream the fault intervenes.
The delay can be reduced to the time necessary to rule out the presence of a blocking signal coming from the downstream protection. It is suitable for radial networks and in the case of coupling with directional protection also for meshed networks. Compared to a chronometric coordination, the zone selectivity allows to reduce the times to values lower than one hundred milliseconds, reducing both the damage caused by the failure and the perturbations to the power supply system. It is more expensive both in terms of cost and complexity of the plant and requires an auxiliary power supply. This solution is therefore mainly used in systems with high values of the rated current and of the short-circuit current, with mandatory requirements both for safety and continuity of service.

Differential

If the sum of the currents belonging to the same node is different from zero it means that there is a fault. The most popular application is with differential relays (transformer, generator, motor, bus-bar). With this criterion, the protection only detects faults within the component assigned and consequently no selectivity control with other protections of the network is necessary and the intervention can be immediate. This selectivity criterion finds its full application even with high voltage in the regulation of the minimum impedance (or distance measurement) protections that detect faults only in the area of their competence.

Chapter II: Integrated Power System in Military Ships

In this chapter, some Integrated Power Systems of relatively recent military ships are examined [27].

2.1 Frigate Type 23

The frigate type 23 proved to be a very successful design project, were the advantages of electric propulsion are highlighted. Figure 27 shows a simplified architecture of the propulsion and power system.

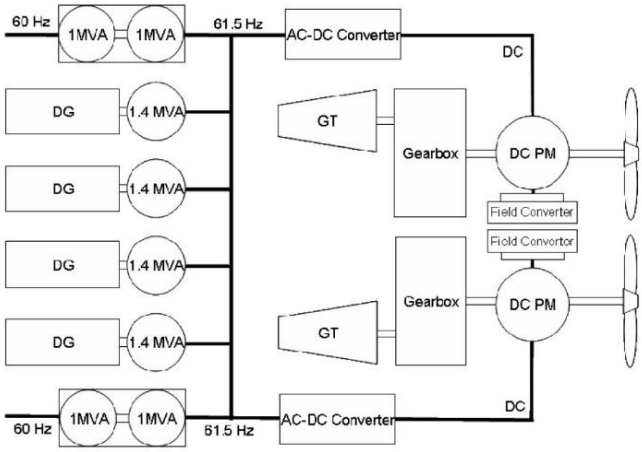

Figure 27 - Frigate Type 23 Architecture

The system was the first installation (the first Type 23 in 1989) of an electric power system with generators operating in parallel in a Royal Navy warship. The system employs a unidirectional semi-controlled AC-DC main converter. The choice of a half-controlled bridge was adopted to reduce thyristors number, very expensive in the years when this plant was developed. A four-quadrant electric propulsion system is able to produce thrust in both directions and absorb the regenerated power (braking phases) in both directions, but with a unidirectional current flow linked to the characteristics of the rectifier bridge.

The field converter was designed with a fully controlled rectifier (number of double thyristors compared to a half-controlled bridge) to allow the converter to invert the current more quickly. This system is characterized by acceptable costs, as the field converter achieves lower current and power values than the main converter of the armature circuit.

To limit the propulsion currents, the propulsion system is designed to operate with an AC voltage set at 600 V RMS, which supplies a continuous 900 V maximum system voltage downstream the main rectifier, so as not to exceed the voltage limit set in LV systems. The propulsion rectifiers have introduced a significant harmonic distortion on the ship's electrical system; to provide high power

quality standard, these subsystems were isolated from the propulsion system through the use of rotary converters, consisting of an electric motor coupled to an electric generator. However, the use of induction motors for rotary converters introduces a difference in frequency between the upstream and downstream voltages, due essentially to the slip of the asynchronous motor. The electricity generation system has been designed to operate at 61.5 Hz, while the supply of the downstream services of the rotary converters is 60 Hz.

2.2 Type 2400 Submarines (Victoria Class)

The propulsion system for the Type 2400 conventional submarine was developed in the same years of the Type 23 frigates system. Figure 28 shows the simplified diagram of the power and propulsion system. The main DC engine has a double armature winding, contained in the same stator tank. For the first time the compensating windings connected in series to the main windings were removed to improve acoustic performance.

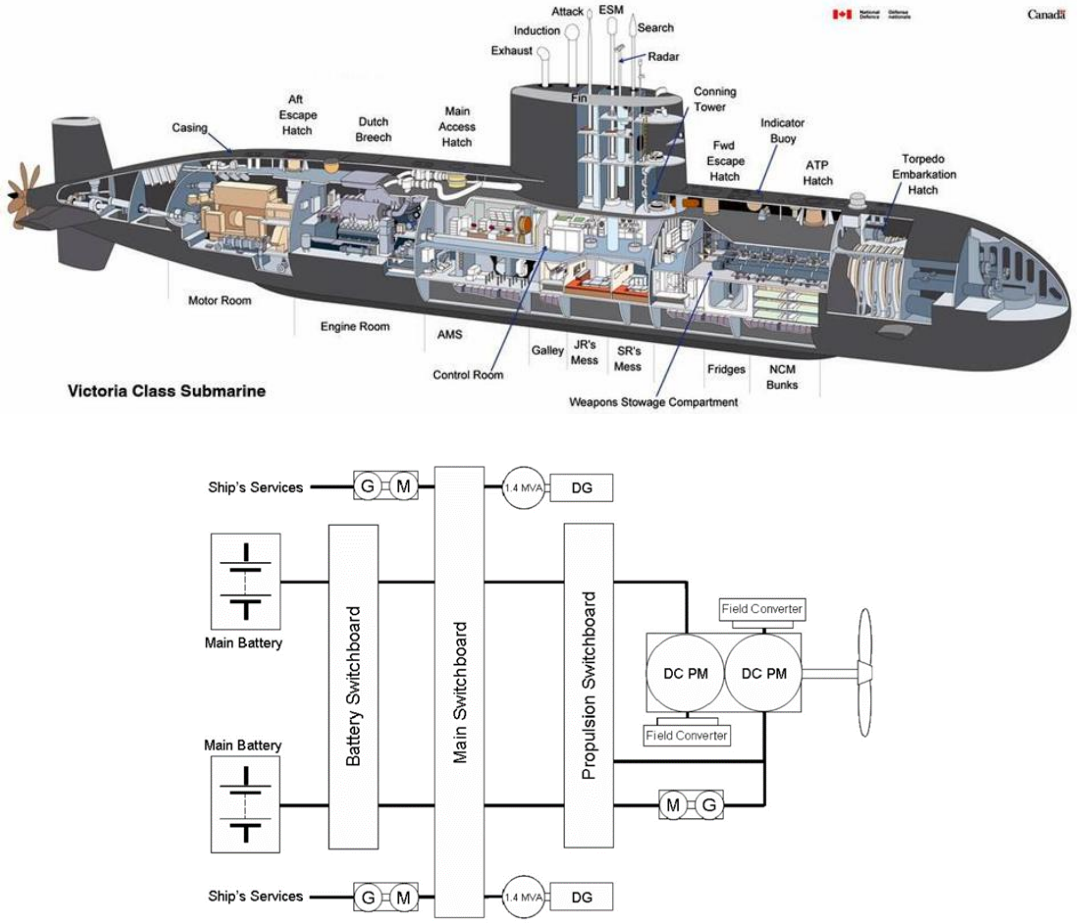

Figure 28 - Type 2400 Submarines (Victoria Class)

Also in this case the available technologies of electronic power converters have been used, except for the drives to controlling the engine armature voltage, due to the high currents. The maximum control of the armature voltage, however, was implemented through series/parallel connection of batteries and electric motors. It was a widely used technique for conventional submarines. This control technique was implemented through an automated system of contactors managed by the electric propulsion panel.

Fine speed regulation within each discrete speed range was achieved using a fully controlled field converter, which was able to reverse the excitation voltage to reverse the engine rotation direction. It was equipped with a single shaft line and there was no possibility of connecting the four reel

windings of the propulsion engine in series, and therefore a dedicated drive train was installed to apply a reduced voltage to one of the two propulsion engine armature windings.

2.3 Type 45 destroyer

The Type 45 destroyer is the first implementation of a main propulsion drive with source voltage converter and PWM modulation in a warship. The PWM modulation, which still entails some disadvantages (high dv/dt that urges the windings and high switching losses), has become a widely used standard in naval applications.
The system implemented in the Type 45 destroyer uses a H-bridge for each single phase of the asynchronous propulsion engine. This configuration requires 15 different H-bridges arranged in 3 balanced groups of pentaphase converters.

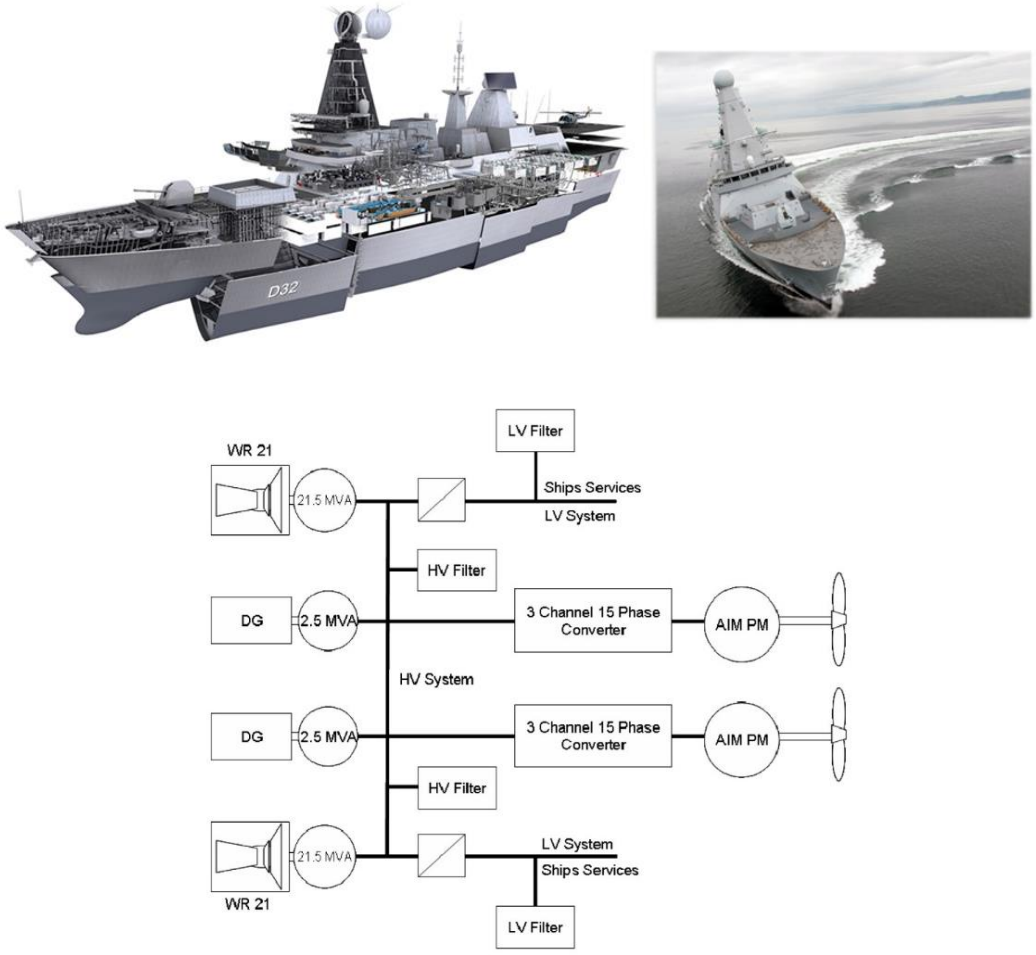

Figure 29 - Type 45 Destroyer Architecture

The power density required was achieved by adopting an advanced air cooling system for the converter by water and dielectric oil. HV and LV filters work in combination to reduce the harmonic distortion caused by the propulsion converter; while the HV filter consists of passive components, the LV filter is an active filter that can also compensate for harmonics generated by the LV system. Both filters are cooled with Midel[14], air and chilled water.

14 Natural and synthetic esters transformer oils

2.4 FREMM

FREMM is the acronym that identifies a new generation of frigates (European Multi-Mission Frigates), named in France “Class Aquitaine” and in Italy “Class Bergamini” (Figure 30 shows the master class F 590 Carlo Bergamini), the result of a joint project between Italy and France. The choice to realize a hybrid CODLAG type integrated power system, rather than an Integrated Full Electric Propulsion system, is a technical-economic compromise, since the system adopted manages to combine the advantages of electric propulsion while maintaining weights, dimensions and costs within acceptable, lower limits compared to an Integrated Full Electric Propulsion system. Figure 30a shows the architecture of the hybrid propulsion system, while Figure 30b shows the distribution system architecture.

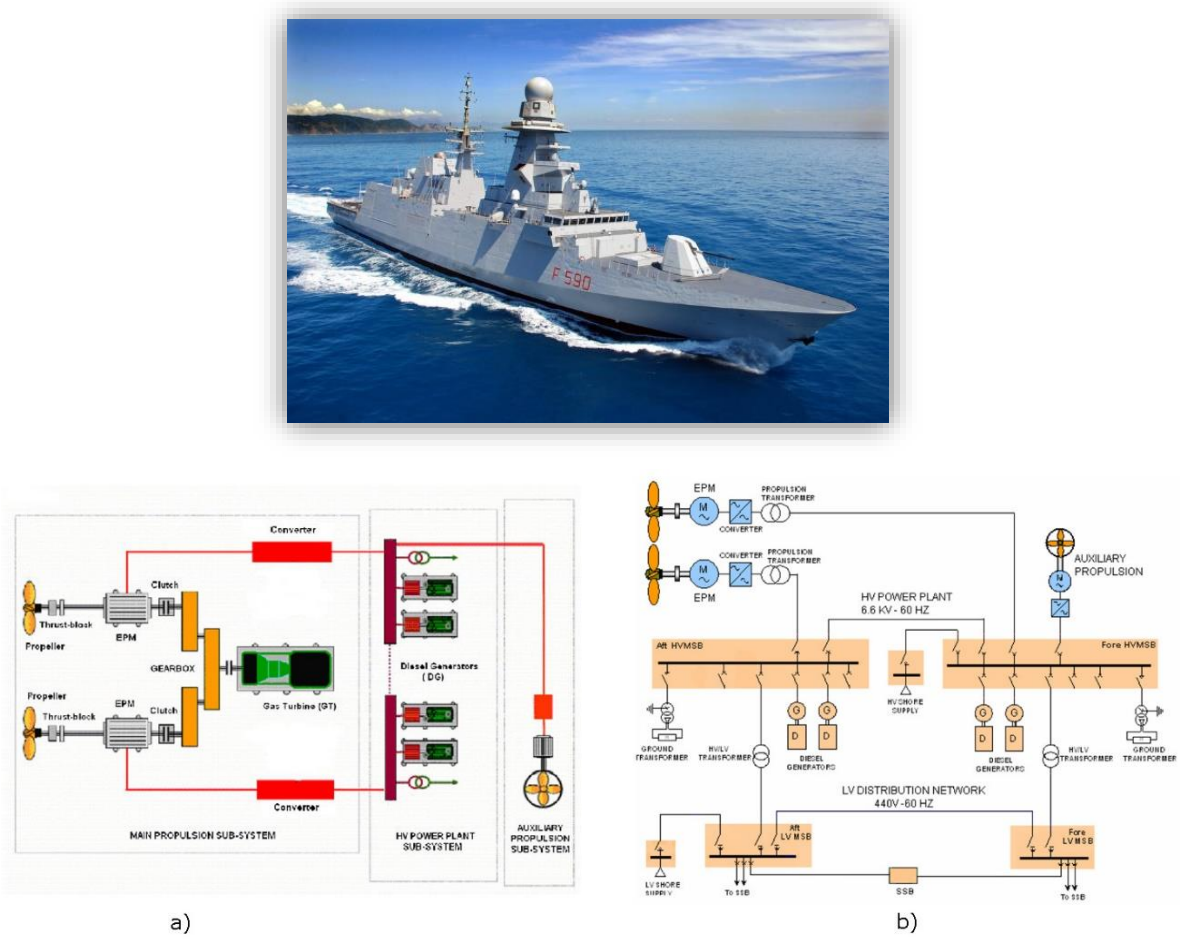

Figure 30 - Frigade F590 Carlo Bergamini a) Hybrid Propulsion System b) Electric architecture of Distribution System

It is equipped with equal diesel generators, 2.15 MW each, respectively installed in the bow and stern main switchboard panel. The distribution system is 6.6 kV at 60 Hz, three-phase with grounded neutral via impedance. The neutral connection adopted is the best compromise for the reduction of fault currents and switching overvoltage. The two main low voltage switchboards are both connected to the medium voltage bus-bars via a 1.8 MVA distribution transformer, connected in parallel to a pre-magnetization transformer to eliminate the insertion currents, which can be dangerous for other electrical devices on board. The three-phase LV distribution system is operated with isolated neutral. The electric propulsion engines are permanent magnet synchronous with four triples of separate stator windings, driven at variable speed by a modular drive with source voltage inverter, supplied by a dedicated propulsion transformers. The rotor is permanent magnet type “NdFeB” mounted on the external rotor surface. The rotor drives the propeller shaft line through an elastic joint connected to it which passes through a hole obtained in the rotor shaft.

The use of one TAG, General Electric - 32 MW AVIO LM 2500 + G4, instead of two turbines with lower power, is motivated by the expected ship operational profile, considering the highest risk of not reaching the maximum speed acceptable due to the unavailability of the TAG. TAG has high level of reliability and low impact in the ship operating profile with high-speed, with the advantage of lower total volumes and weights.
A disadvantage of this solution is the "X" connection that requires the use of a more complicated, cumbersome and noisy cross connection type, with a clutch input for the TAG and two outputs with two clutches for the shafts of the electric engines, installed in three enclosures rigidly connected to each other.
Figure 31 shows the arrangement of the propulsion system and the relative dimensions inside the hull [28].

Figure 31- Arrangement of The Integrated Propulsion And Power System In The Fremms

CODLAG architecture design:

- exclusive use of electric propulsion engines, powered by the electrical distribution system, for 16 knots navigation profile;
- at high speeds ranging from 16 to 26 knots, the propulsion is entrusted exclusively by the Gas turbine. If necessary, it allows the electric propulsion engines to work as a Shaft Generator;
- to reach the maximum speed, all 4 diesel generators with the gas turbine are used simultaneously.

This configuration has some peculiarities allowing an optimal use of the equipment:

- operating electric propulsion engines as axis generators powered by the turbine;
- by rotating pitch propellers, the ship's speed variation is obtained by changing the rotation speed of the propellers adjusting blades' incidence angle, increasing overall efficiency;
- Gas turbine with propeller pitch variation increase speed, accuracy and efficiency during the operation;
- to maneuverer the ship backwards, no reversing electric engines are required. The operation is carried out by adjusting the blades angle orientation. This avoids the temporary and rapid transition from the first to the third quadrant, which would require an accurate energy control strategy by the converters.

2.5 Queen Elizabeth Class aircraft carrier

The Queen Elizabeth class aircraft carrier is the largest and most powerful surface warships ever built for the Royal Navy (in service since 2017, it replaced the HMS Ark Royal R07) disposed of in 2013. This class of aircraft carriers, unlike conventional units, has been designed with twin command centres, separating ship management from flight operations, resulting in greater visibility of flight activities.

The automation level is high to limit the ship operating costs during its entire life; a minimum number of sailors is required.
An example is the ammunition loading system. Missiles and bombs for F-35 fighter jets are taken automatically from the depot and placed in the lower levels of the ship, through mobile platforms and elevators.
The design architecture includes:

- CODLAG system (diesel-electric combined propulsion and TAG);
- two 36 MW Rolls Royce turbines;
- two 11.6 MW Wartsila 16V38 diesel generators and two 8,8 MW Wartsila 12V38 diesel generators, both with a turbocharger to increase performance;
- a 2MW Wartsila 12V200 emergency Diesel generator;
- two drive shafts, each with two 15-phase electric 150-RPM Alstom engines in a compound tandem configuration, with 80 MW total propulsion power.

The aircraft carrier has an Integrated Full Electric Propulsion system consisting of 4 electric engines of 20 MW each, supplied by Converteam UK. These engines are similar to those used on the Royal Navy Type 45 destroyer. The engines are powered by a Converteam VDM 25000 drive, which can operate at variable output frequency allowing the control of the axis line speed in all the operating range, eliminates the speed reducer in the propulsion system.
A summary of the IPS of the QE class aircraft carriers is shown in Figure 32. The distribution system adopted is a 11 kV three-wire at 60 Hz, with neutral point connected to the ground via impedance. The electric propulsion equipped with triple penta-phase stator triplet, each powered by its transformer-converter unit. In order to reduce the harmonic distortion produced by the passive diode front end converters, a 24-pulse network-side reaction was carried out, by suitably shunting the primaries of the propulsion transformers. Passive filters are also provided to attenuate the harmonics produced by the propulsion drive. The 2 Diesel generators Wartsila 16V38 are located in the lower levels of the ship for stability reasons, while the two MT30 turbines are installed in the higher level, adopting a shorter air intake and exhaust system. The 4 propulsion engines are positioned in 3 separate compartments, to guarantee a better survival capacity.

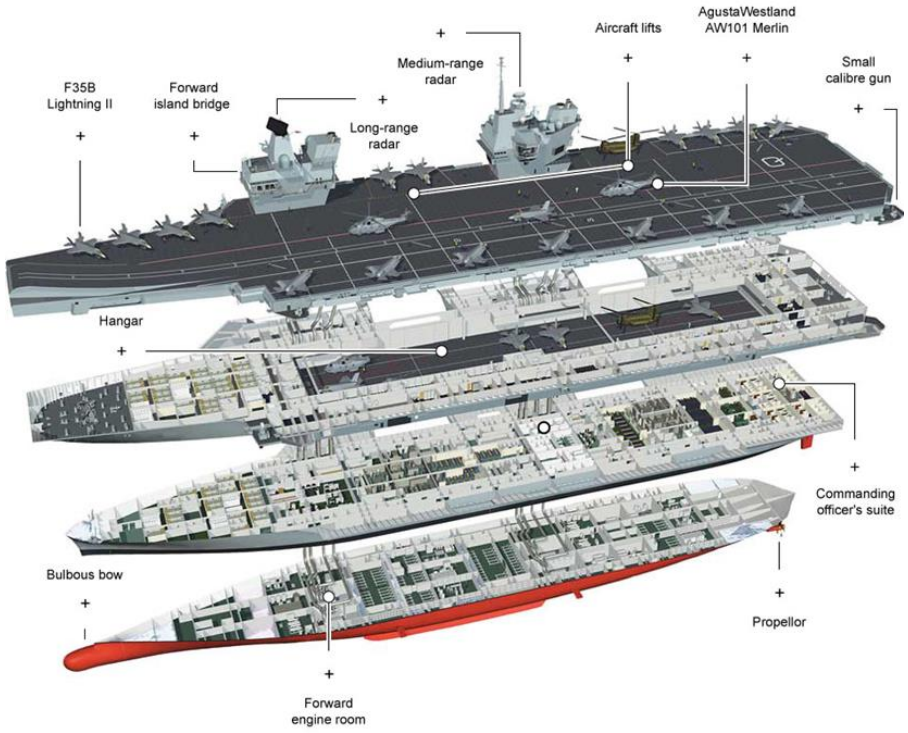

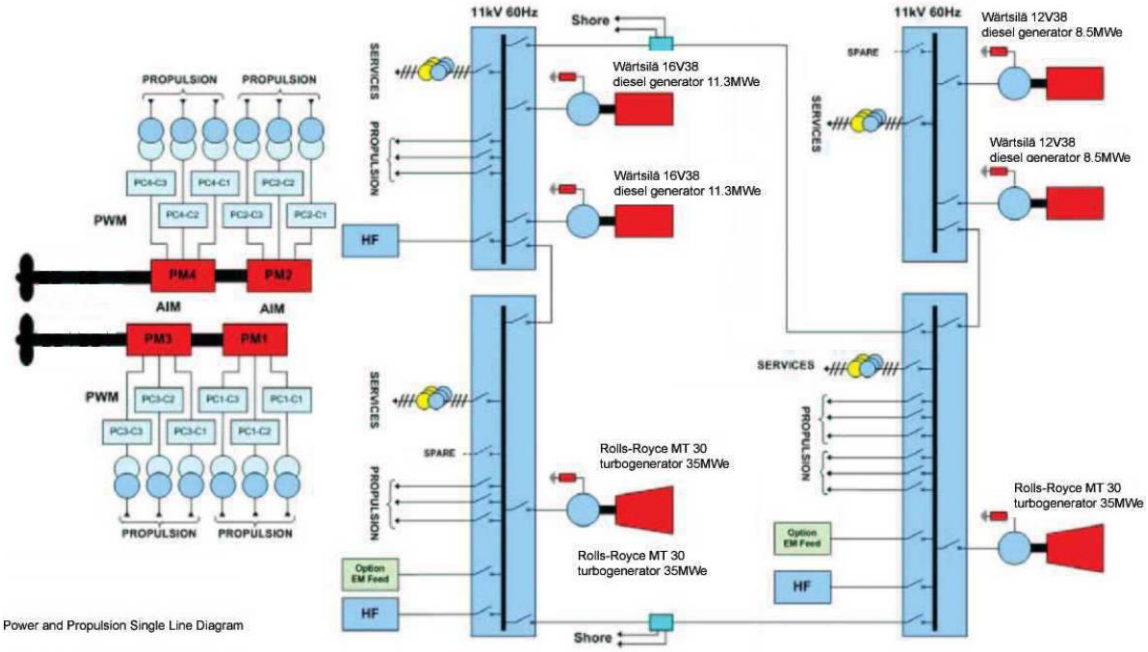

Figure 32 Queen Elizabeth R08, Unit– Integrated Power System

Chapter III: Methodologies for Harmonic Disturbances Analysis and Power Quality (Service Continuity)

3.1 Power Quality – Harmonic discussion

The power quality (PQ) of electric grids was investigated by many researchers and concerned different issues [29]. The waveform deviations (of voltage and current) compared to the sinusoidal trend involved signal processing techniques, classifications and mitigation systems. The International Standards covered different application fields: best practices for PQ monitoring and classification (IEEE 1159), Standards for distribution system voltage characteristics and PQ classification (EN 50160); Standard testing techniques, measurements ad interpretations of PQ in systems at 50-60 Hz (IEC 61000-4-30), Measurements techniques for voltage fluctuations and flicker in AC and their limitations (IEEE 1453). Regarding the general problems caused by high waveform deviations and their identification, many studies were also recently conducted [30] [31] [32] [33] [34] [35]. Many studies were conducted on disturbance detection [36] [37] [38] [39]. Great attention was placed on signal processing techniques in the years ranging from 1990 to 2000 [40] [41] [42] [43] [44] [45] [46] and more recently [47] [48] [49], focused on the use of Fourier Transform, Wavelet Transform [50] [51] [52], Stockwell Transform, Kalman Filter, etc.. As for mitigation systems, many studies focused on the use of filters (passive, active, hybrid) [53] [54] [55], FACTS (flexible AC transmission systems - switches, power converters, storage systems) [56] [57] [58], DG (distribution generation [59] [60] [61]).

Some studies concerned non-sinusoidal waveform with frequency different from fundamental, integer harmonics, inter harmonics (with frequency greater than the fundamental and not multiple of fundamental), and sub harmonics [30] [62] [63] [64].

Most of the studies were based on the modelling and simulation of electrical systems components and required a detailed knowledge of non-linear loads harmonic spectra [65] [66] [67]. It is well known that voltage and current harmonics are usually time-variant by effect of variations of system configurations and load demand [68] [69]; these variations have a non-deterministic nature and give origin to stochastic processes [70] [71]. Furthermore, harmonic sources produce different harmonic currents as a function of different loading levels and changes of harmonic voltages at the point of point of common coupling [72]. The phenomenon is time-varying, and therefore it is very difficult to model and to predetermine the magnitudes and phase angles of harmonic currents at each moment in the time [73]. More recently, harmonic and inter-harmonic estimation methods for stationary and time-varying signals have been proposed [74] [75] [76]. The scenarios are further changing with the introduction of new equipment, such as led lamps [77], and the dissemination of renewable energy sources, such as wind and photovoltaic systems [78] [79]. Therefore, the harmonic disturbances introduced into the grid may change and need new models and procedures for a correct evaluation [80] [81]. Authors discussed about some failures of protection relays badly affected by non-sinusoidal current or voltage waveforms [82]. Thus, the predetermination of harmonic distortions remains a goal to be further investigated.

In the last twenty years, there has been an increase in the number and variety of electric propulsion ships being built around the world with everything from cruise liners to amphibious assault ships (Chapter 1 and 2). This revolution occurred due to power electronic drive technology which is used for the electric propulsion system. The drive adjusts the propeller speed by varying the motor frequency. This was accomplished by the development of high power solid state switching devices.

Nowadays the increase of electronically controlled loads and pulsed loads added to shipboard power systems led to an increase of harmonic distortions [83] [84] . Moreover, due to the increase of the harmonic disturbances the possibility of incurring untimely tripping of the switches with a consequent disconnection of load areas is an issue to be taken into account.

So, the need to be properly evaluated from a standard of harmonic limitation perspective is mandatory.

When limiting harmonics, several aspects need to be considered besides the total harmonic distortion (THD). The time dependence nature of the distortions and the type of equipment need to be taken into account in order to provide an effective way to control any damaging or disturbing effect of harmonic pollution [85]. Moreover, the network component parameter uncertainty and/or the network, supply and load configuration changing may cause significant variations in the amplitude and phase of the nodal equivalent impedances. In particular, the effect of supply or load changing is relevant mainly when resonances are present [80].

3.2 Software and models

Software and models developed both in time and frequency domain are reported. In particular, simulation models for the disturbances analysis caused by the injection of harmonic currents in the three-phase power system, models for time-varying waveform distortion analysis and network impedance calculation, are discussed.

3.2.1 Generators, cable and loads

The generators were represented by the Behn Eschemburg model [86] with their synchronous reactance and stator resistance. They must be defined with the following parameters:

- V_N = *Nominal voltage;*
- f_N = *Nominal frequency;*
- ω_N = *Revolutions per minute [RPM];*
- p = *Poles;*
- S_N = *Power [kVA];*
- *Cos* ϕ_N = *Power Factor;*
- R_S = *Stator resistance [p.u.];*
- X_S = *Stator reactance [p.u.].*

The electrical cables parameters used in the simulations are taken from [87]. The model used to represent the LV cables is the Pai model, in order to reduce the number of nodes in the network and take into account the capacities derived to earth. The model is shown in Figure 33.

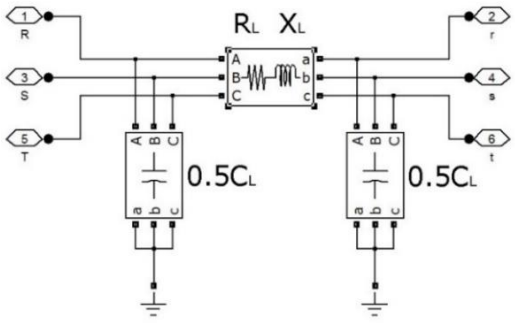

Figure 33 - Cable Equivalent Pi Model

Electrical parameters are obtained through the following formulas:

$$R_L = R_{20°}{}' \cdot [1 + \alpha \cdot (T_{amb} - 20°C)] \cdot SKF \cdot L \quad (1)$$

$$X_L = 2\pi f_N \cdot L_L{}' \cdot L \quad (2)$$

$$C_L = \frac{B_C{}' \cdot L}{2\pi f_N} \quad (3)$$

where:

- *R20 ° C is the electrical resistance of copper conductors per length unit referred to 20° C, expressed in [Ω/km];*
- *α is copper temperature coefficient, equal to 0.004° C^{-1};*
- *T_{amb} is the ambient temperature of the area where the cable is installed. If it crosses areas with different room temperatures, the highest T_{amb} is considered [°C]. SKF = dimensionless incremental coefficient linked to the skin effect of the conductors. Calculated by: $SKF = \left[1 + \frac{1}{48}\left(\frac{R}{a}\right)^4\right]$ with R radius of the conductor in mm, and at the penetration depth of the electric current at 50 Hz equal to 9.3 mm;*
- *L = line length [km];*
- *f_N = 50 Hz nominal frequency;*
- *L_L '= service inductance for single-core cables [mH/km];*
- *B_C '= capacitive service susceptibility for single-core cables [μS/km].*

The cables feeding the three aggregate loads categories (equivalent loads) were obtained using the equivalent electric moment method [87], having deduced the equivalent distance from the electrical panel of the sum of the loads concentrated in a single load. The formula used is as follows:

$$L_{eq} = \frac{\sum_{i=1}^{N} L_i \cdot P_{Ni}}{\sum_{i=1}^{N} P_{Ni}}$$

L_{eq} being the equivalent length, P_{Ni} and L_i the nominal power and the length of the cable relative to the i-th load, and N the total number of the considered loads. For each equivalent load three categories have been found to represent and define the loads behavior: static, converter and rotating (they will be described in Chapter 4). According to IEC 60092-352 [10] and Italian Standard [88] the sections and the cables ampacity have been chosen.
Further hypotheses have been made: for the circuits supplying the transformers from which the main and secondary distribution panels are derived, in the absence of data provided by the datasheets, the value of the power factor is assigned to 0.85.
The rotary converters, consisting of the coupling of an electric motor and a synchronous machine running from a generator, have been assigned the power factor related to an electric machine with rated power equal to the power absorbed by the converter, as this value is not provided by the datasheet.
The models used to represent the static and rotating loads are three-phase RL series loads, triangle connected, with the R and L parameters obtained respectively from the active and reactive powers, resulting from the electrical balance with the application of the global coefficients.
In order to represent the complete model when the exact list of equipment in operation is unavailable, nor is their absorbed power and the arrangement inside the ship, global coefficients to obtain values of powers compatible with the real absorption are defined. This coefficient contains both the coefficient of use and contemporaneity, and it is obtained starting from Table 7 that reports an example of electric balance sheet of the vessel in a specific operational profile).
The global factor applied to the electrical loads belonging to the network included in the equivalent model is given by:

$$K_G = \frac{P_A}{P_{TOT}} \qquad (4)$$

Where N, P_A and P_{TOT} are obtained respectively from:

N = number of active devices referred to the total number installed

$$P_{TOT} = N \cdot power\ absorbed \qquad (5)$$

$$P_A = N \cdot Power\ absorbed \cdot contemporaneity\ factor \qquad (6)$$

As far as the converters are concerned, their equivalent model consists of two sections:

- in the first converter there is a three-phase R-L series load, which takes into account the active and reactive power absorbed by the distorting devices;
- in the second there are current-controlled generators, to represent the harmonic absorption of the converters. Starting from the value of the rated current at 50 Hz absorbed, the single harmonic components were calculated using the disturbance table and added in phase to the fundamental. The possibility that the totality of harmonics are in phase among themselves is remote, but through this choice one gets in worse conditions.

The model to represent the harmonic content of non-linear load will be extended and improved with a dedicated software illustrated in 3.2.3.
Figure 34 shows the first simple model to represent the converter and in general a non-linear load.

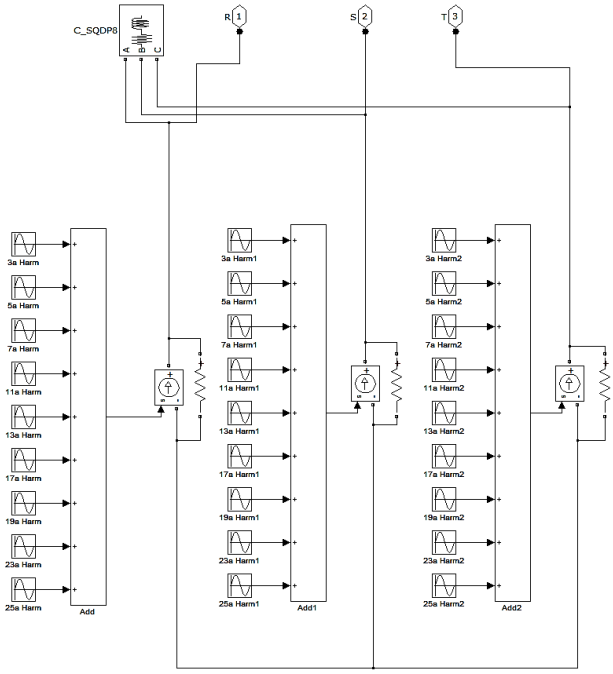

Figure 34- First Simple Electrical Model of Converter

The network model presents obvious simplifications, but is however valid.

3.2.2 Fortran Software: model for harmonic analysis

Simulation models for the disturbances analysis caused by the injection of harmonic currents in the three-phase power system are discussed for instance in [89]. The network impedances at harmonic frequencies and harmonic distortion were evaluated by means of dedicated software "HARMAN", whose outputs include the equivalent network impedance as a function of frequency, harmonic disturbances on node voltages, series and shunt current flows. "HARMAN" also provides the composition of the elementary harmonics contributions. Lastly, comprehensive assessment indices of the harmonics effects on the electrical network are calculated.
Lines are represented by pi circuits calculated at each frequency of interest. Transformers' series impedances use constant inductances and a frequency dependent resistance defined as:

$$R_f = \left(1 + \alpha \cdot \left(\frac{f}{f_0}\right)^{1.8}\right) \cdot R_{f0} \qquad (7)$$

where:

- $\alpha = 0.1$;
- f= generic frequency;

- f_0= *power frequency;*
- Rf_o= *resistances at power frequency;*
- *Rf= resistances at generic frequency.*

The transformer equivalent model is reported in Figure 35.

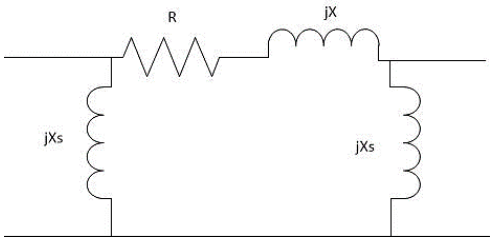

Figure 35 - Transformer Equivalent Model

The shunt magnetizing inductance is assumed to be constant; all winding capacitances are neglected because the frequencies of interest do not exceed 2 kHz (i.e. 40th harmonics of a 50 Hz power frequency). Sub-transient inductances are used in positive and negative phase sequence generators models. For represent generators, direct and homopolar sequences assume a model with constant inductances obtained from those supplied as input at the fundamental frequency. The approximate expression is assumed in the reverse sequence:

$$X_{if} = X_{df} \qquad (8)$$

The LV static plus rotating load model [90] in Figure 36 is defined by the following equations, where subscripts "s" and "a" stand for "stating" and "rotating" respectively. Equations (2), (3), (4) and (5) describe the model of the LV static-rotating load.

$$R_s = \frac{V^2}{P \cdot (1-p)} \qquad (9)$$

$$X_s = 0.05 \cdot h \cdot R_s \qquad (10)$$

$$R_a = R_m \cdot \left[1 + k \cdot \left(h \cdot f_0\right)^{0.5}\right] \qquad (11)$$

$$X_a = \frac{V^2}{P \cdot p} \cdot X_{lr} \cdot h \cdot 2 \cdot \left(h \cdot f_0\right)^{\beta} \qquad (12)$$

where:

- *P, Q are active and reactive load power;*
- *V is 50 Hz nominal voltage;*
- *P is rotating load as a fraction of the total, at power frequency (p.u.);*
- X_{LR} *is locked rotor reactance (p.u.);*
- R_m *is equivalent motor series resistance;*
- f_0 *is power frequency.*

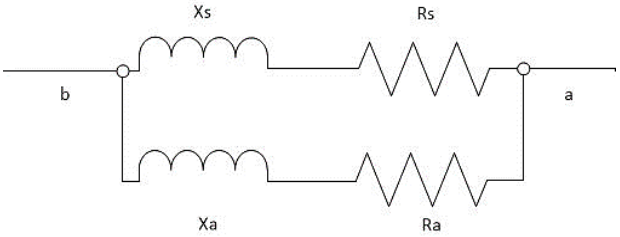

Figure 36 - LV Stating and Rotating Equivalent Circuit Model

X_{lr}, R_m, k and β typically assume different values depending on load (LV or MV). For LV induction motors k is in the (0.15 ÷ 0.75) range, with β ranging between 0.12 and - 0.17 [90].

3.2.3 Simulink model for time varying non-linear load

The Simulink Model (SM) developed for modelling time varying non-linear load uncertainties in power systems is useful to evaluate the harmonic distortion when the behaviour of each load (time-varying) is unknown. The procedure takes into account known and unknown aspects. The first ones are the maximum and minimum values of active power, power factor and of each single order of current harmonic percentage. The second ones derive from the typical uncertainties of an electric system mainly caused by simultaneously active loads according to the work cycles. At the end, the voltage total harmonic distortion at the point of common couple and its spectra are obtained.
In the probabilistic phase, the system parameters relevant to power consumption of each load and harmonic spectra, are extracted to represent all the possible electric scenarios. Therefore, in digital simulation, the introduction of the contribution of random variable to simulate the effect of non-deterministic events is a good approach.
These contributions can generally be represented by:

- changes in temperature, current, humidity, wind speed and so on;
- non-predictable or chaotic effects;
- effects that cannot be described deterministically.

A random variable (RV) can be described by a distribution function. The distribution functions (DF) are divided into continuous and discrete and, can regulate the behaviour of RV [91].
Some of the best-known DF are the Uniform, the Normal, the Binomial, and the Poissonian DF.
Normal distribution is used to describe many chaotic phenomena addressed at the same time; the uniform function applies when a phenomenon is related to a single event (i.e. a dice throw).
The Uniform and Normal distributions have been selected and implemented in the SM because, if on the one hand, it seemed obvious that the non-deterministic factors of the phenomenon experimentally analysed are regulated by many uncontrollable events (the 'normal' nature of the model), on the other hand a comparison of this hypothesis with another distribution appeared worthwhile. For this purpose, a comparison between two distributions was considered: a uniform and normal distribution. Figure 37a shows the SM input, Figure 37b highlights the selection phase correlated to the fundamental current calculation, necessary to define the harmonics spectra of each load, and the harmonic, voltage profile and waveforms output values.

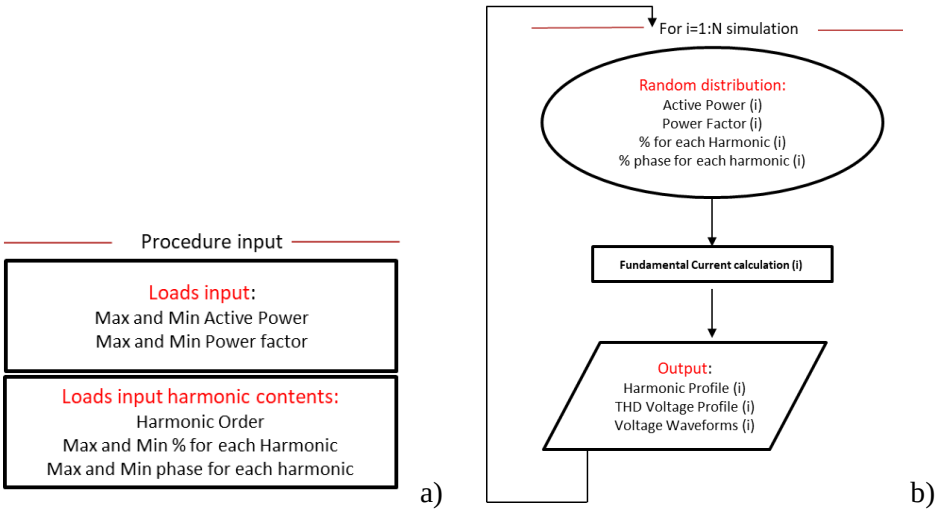

Figure 37 - a) SM Input; b) SM Procedure

Using common Simulink block, two sub-models were developed to compose SM in order to represent the electrical system.

The main sub-models are:

- harmonic generator;
- distortion load.

Harmonic Generator sub-model

This sub-model permits to simulate the injection of harmonic currents for each load into a three-phase power system. It can accept any harmonic spectrum related to a particular load as input. In Figure 38 the sub-model to generate harmonic disturbances is represented. In the "wave generator" block a function calculating the instantaneous value of a sinusoidal function was implemented by using:

- the clock of simulation;
- the peak value of the fundamental component;
- the vector containing the harmonic components of the wave;
- the vector containing the harmonic (in percent) for the respective harmonics;
- the vector containing the harmonic shift angle for the harmonic components.

Figure 39 shows the detail of "current fonts" block, in particular, a three-current controlled source was implemented.

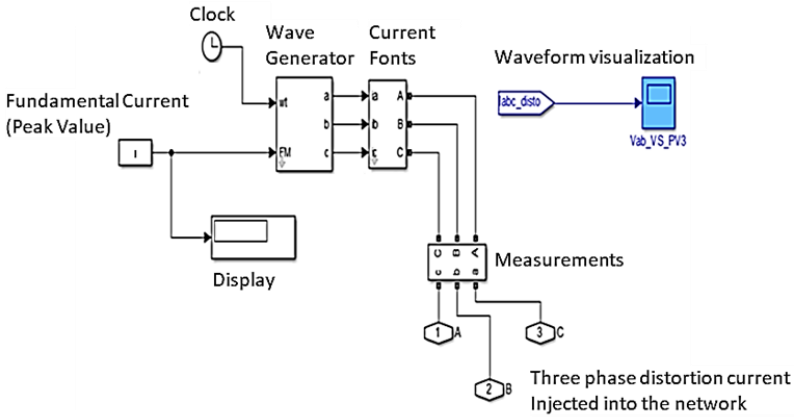

Figure 38 - Harmonic Generator Sub-Model

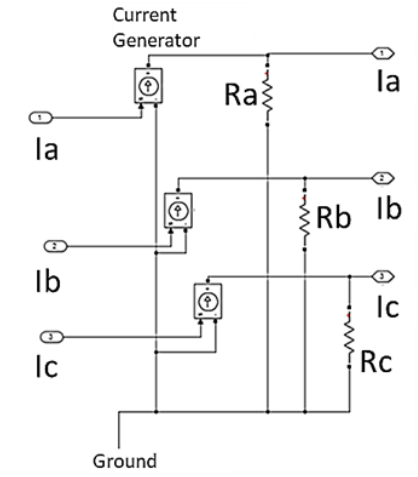

Figure 39 - Three-Current Controlled Block

The following steps describe in an example, the code implemented to generate variable harmonic spectrum using the model described in Figure 38, starting from vectors of parameter set. By way of

example, the code reported in the following is referred to uniform random distribution. The values reported in the following code are only to example, to explain the data input.

Harmonic input

Harmonic Order = [1 3 5 7 9 11], *(13)*
Max % each harmonic = [1 0.01 0.018 0.007 0.007 0.007], *(14)*
Min % each harmonic = [1 0.007 0.003 0.001 0.001 0.001], *(15)*
Max Phase each harmonic = (pi/180)*[0 20 20 20 20 20], *(16)*
Min Phase each harmonic = (pi/180)*[0 -20 -20 -20 -20 -20], *(17)*

Uniform distribution random values for each harmonic

for i = 1:length(Harmonic Order), *(18)*
Real %(i) = Min % each harmonic (i) + (Max % each harmonic(i) - Min % each harmonic (i)) * rand, *(19)*
Real phase(i) = Min Phase each harmonic (i) + (Max Phase each harmonic (i) - Min Phase each harmonic (i)) * rand, *(20)*
End *(21)*

Input values for three phase current source

for i = 2: length (Harmonic Order), *(22)*
Ia = fundamental current * Real%(i) * sin ((2 * π * 50 * t) * Harmonic Order(i)+ Real phase(i)), *(23)*
Ib = fundamental current * Real%(i) * sin ((2 *π *50 * t) *Harmonic Order(i)+ Real phase(i) - 120 * π / 180), *(24)*
Ic = fundamental current * Real%(i) * sin ((2 *π *50 * t) * Harmonic Order(i)+ Real phase(i) + 120 * π / 180), *(25)*
End, *(26)*

Distortion load sub-model

Figure 40 represents a generic variable load with its active and reactive power and its harmonic disturbances related to fundamental peak current absorbed by the loads.
Trough an example, the following steps describe the code implemented to generate active and reactive power for each random simulation, starting from a range of maximum and minimum active power and the power factor set by the user.

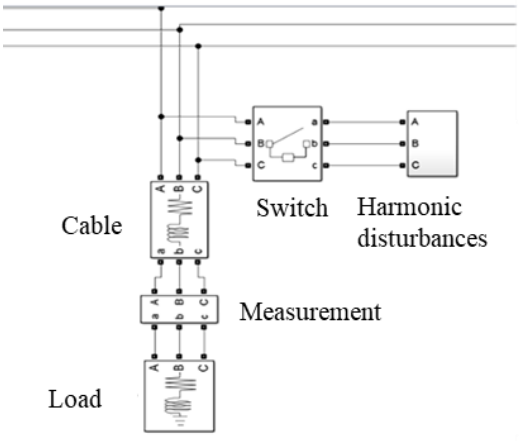

Figure 40 - Model of Load with Harmonic Disturbances

Active power and Power factor input

Active Power max = P_{max} [kW], *(27)*
Power Factor Max = PF_{max} [kW], *(28)*
Power factor Min = PF_{min} [kW], *(29)*

Uniform distribution random values for P and Q

Real power factor = Power factor Min + (Power Factor Max - Power factor Min) * rand, *(30)*
Real Active Power = Active Power min + (Active Power max - Active Power min) * rand, *(31)*
Real Reactive = sqrt ((Real Active Power / Real power factor) * (Real Active Power / Real power factor) - (Real Active Power * Real Active Power)), *(32)*
Peak current = 1.4 * [Real Active Power / (Real Power Factor * Nominal voltage * 1.7)], *(33)*

3.3 Electrical System Dependability [2]

A power distribution network should guarantee a high reconfigurability after faults, damage or untimely switch off.
In this context, the innovative approach given by the dependability theory can be the tool which can provide and analyse the consequences of faults and demonstrate the system's compliancy with the relevant regulations [92].
The key concepts of the Dependability theory are threats, attributes and enforcing techniques [93].
Figure 41 shows a conceptual map of these key concepts highlighting their interconnections and their further decomposition.

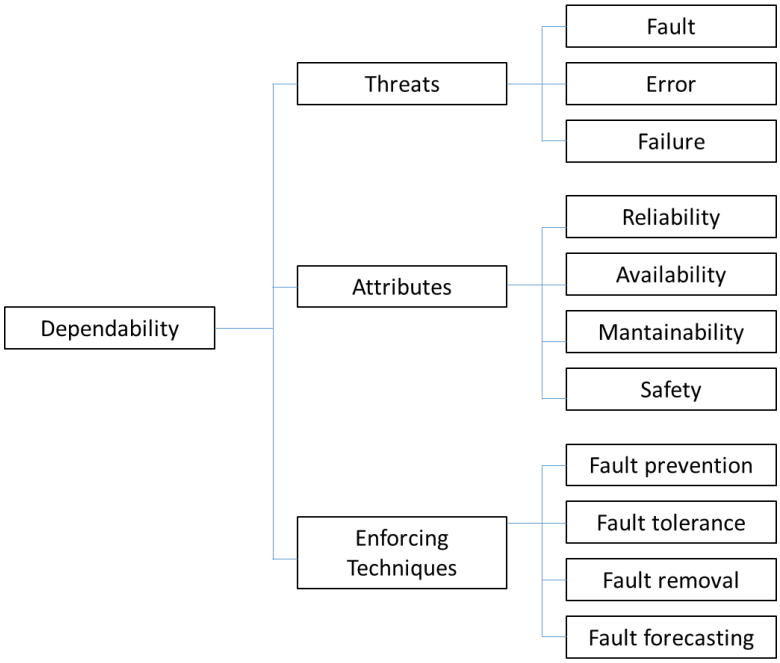

Figure 41 - Dependability Key Concepts, Conceptual Map

The basic definitions and concepts of the Dependability Theory are:

System: a set of components grouped together into a single entity with the purpose of delivering a service.
Service: the set of operations performed by a system in favour of its user(s). To achieve this, the system executes a number of operations. If the system activity meets the user expectations/requirements, the service is correct. Otherwise, the service is not correct and this is due to a fail in executing one (or more) operations.
Dependability: the capability of a system to deliver the correct service with an acceptable trust.

Two different mechanism could lead to a system failure: *generation* and *propagation*.
Generation: the mechanism inherent in the passage of harmful events from one layer to the other. Failure is generated by errors, and errors are generated by faults.
Propagation: the mechanism inherent in the passage of harmful events in the same layer. Faults, errors, and failures can be caused by other faults, errors, and failures respectively (propagation within the same layer). The relations between threats and failure mechanisms are depicted in Figure 42.

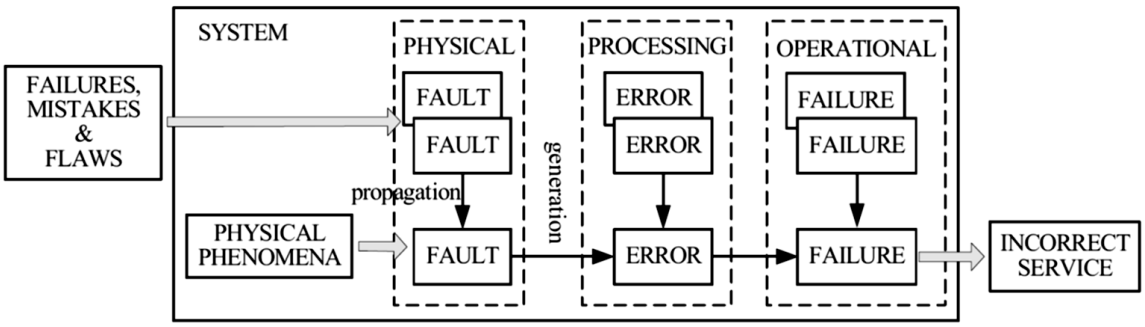

Figure 42- Failure Mechanisms

Table 3 and Table 4 report the main Mathematical relations between dependability indices and Dependability Enforcing Techniques.

Table 3 - Mathematical Relations Between Dependability Indices

Calculated data	Formula for calculation
A, availability	A=MTBF/(MTBF+MTTR)
Q, unavailability	Q=1-A=MTTR/(MTTR+MTTF)
λ, failure rate (f/h)	λ=Tf/Tp
λ, failure rate (f/y)	λ=Tf/(Tp/8760)
MTBF, mean time between failures (h)	MTBF=Tp/Tf
MTTR, mean time to repair (h)	MTTR=r=Rdt/Tf
R(t), reliability at time t	$R(t)=e^{-\lambda t}$

where:

- *repair downtime (Rdt)* is the total downtime for unscheduled maintenance (excluding logistics time) for a given *Tp* (hours).
- *total failures (Tf)*: the total number of failures during the *Tp*.
- *total period (Tp)*: the calendar time over which data for the item was collected (hours).

Table 4 - Dependability Enforcing Techniques.

Enforcing Technique	Action
Fault-prevention	Aimed at avoiding the occurrence of a fault. Applied during system design, development and test stages.
Fault-tolerance	Aimed at coping with a fault. Applied during system operation (common implementation: redundancy).
Fault-removal	Aimed at finding and eradicating a fault, at verifying system's compliance with requirements. Applied during both system design and operation.
Fault-forecasting	Aimed at evaluating dependability attributes. Applied during both system design and operation.

A peculiar case of fail-operational level is the fail-degraded operation, which implies the delivery of a degraded, but still acceptable, service. Fail-safe requirements are commonly applied to subsystems whose incorrect service is acceptable, provided that it is safe. Fail-silent requirements are needed when the delivered service is not critical, so the user prefers to have any service instead of having an incorrect one. Fault-tolerance techniques exploit the concept of *redundancy*, which is the installation of one or more extra subsystems within a system to cope with a fault detected in one or more systems.

Some examples of different potential implementations of the redundancy concept on the same system are offered in [94]. Fault-tolerance may be applied through two different strategies:

- *system reconfiguration*, implying the detection of the fault, its location, and the recovery of the correct service through system reconfiguration (thus removing the fault element from the system operations);
- *fault masking*, implying a ride through the fault using redundant systems, thus avoiding modifications at operational level.

Fault-removal techniques: techniques aimed at assessing system compliance with the requirements (namely *verification*), include those related to dependability. These techniques applied both during system design development and system use, become part of the design procedure in the former, and belong to evaluation (tests and trials) in the latter. Verification during system design development does not require a running system, and it is performed through inspections, reviews, walk-throughs and model checking. Verification during system use is carried out by means of tests (on the real system or a prototype) and simulations (on a virtual replica). If verification process highlights differences between expected and actual performance, corrective procedures have to be adopted.
Fault-forecasting techniques: such techniques aim at assessing system *failure modes* and dependability attributes for a system. The techniques lying in this category can be separated in *qualitative* and *quantitative*, depending on the results given. Qualitative techniques are aimed at identifying, locating, and classifying the faults, and the interactions between components that may fail, that can cause a failure (failure modes). Quantitative techniques are aimed at assessing, in terms of probabilistic indices, the dependability attributes for the system.

Chapter IV: Characterization of A Military Aircraft Carrier

Cavour aircraft carrier (CV 550) is taken as a reference ship in order to define the impact of the relevant and particular electric loads, finalizing its behaviour in the power system. Moreover, thanks to the measurement campaign carried out on board, models, new network proposals, survey methodologies and analysis technique have been proposed and validated.

4.1 System description

The Cavour (shown in Figure 43) is an aircraft carrier produced by Fincantieri launched in 2008. The ship, in STOVL configuration (Short Take Off & Vertical Landing), is a multirole ship that incorporates 4 different functions in a single unit: aircraft carrier, logistics and amphibious platform, a command station unit and a hospital. The ship is able to embark and operate with all types of aircraft supplied to the Navy: Helicopters (AB 212, EH 101, NH 90), aircraft AV-8B (Harrier), as well as, in the future, JSF type aircraft (Joint Strike Fighter pe F35B).
Record numbers for the Italian Navy:

- displacement: 27100 tons at full load;
- overall length: 244 m;
- 544 permanent military crew units + 641 seats to accommodate mobile flight components, Marina San Marco Brigade, health personnel, civilian personnel;
- 4 AVM / GE LM2500 gas turbines of 22 MW each;
- 2 variable pitch propellers Fincantieri C.P.;
- 6 generation groups Wärtsilä CW 12V200, 2.200 kW each;
- 2 axis generators, 2200 kW each;
- main voltage 660V-50Hz through passive distribution ring;
- 2 rudders;
- HVAC in all areas (accommodation and work);
- 6 inverted osmosis desalination plants;
- 2 active stabilizer pairs;
- operating bow and stern thruster;
- 2 aircraft lifts (at the bow and stern straight side).

The propulsion system allows the ship to reach 29 knots with 85% of Maximum Continuous Rating (MCR) of engine and 7000 miles of autonomy at 16 knots [7] [95]. The electrical system, built with technologies available at the end of the 90 s, is unique: the generation and primary distribution is via a 660 V and 50 Hz meshed network, with a three-phase system and non-distributed neutral conductor, the same is applied to the 380 V secondary distribution system. The use of a nominal voltage of 660 V inevitably leads to the use of numerous cables with a high cross-section with particular room requirements inside the ship's premises and related problems. Figure 44 shows the generation ring at 660 V.

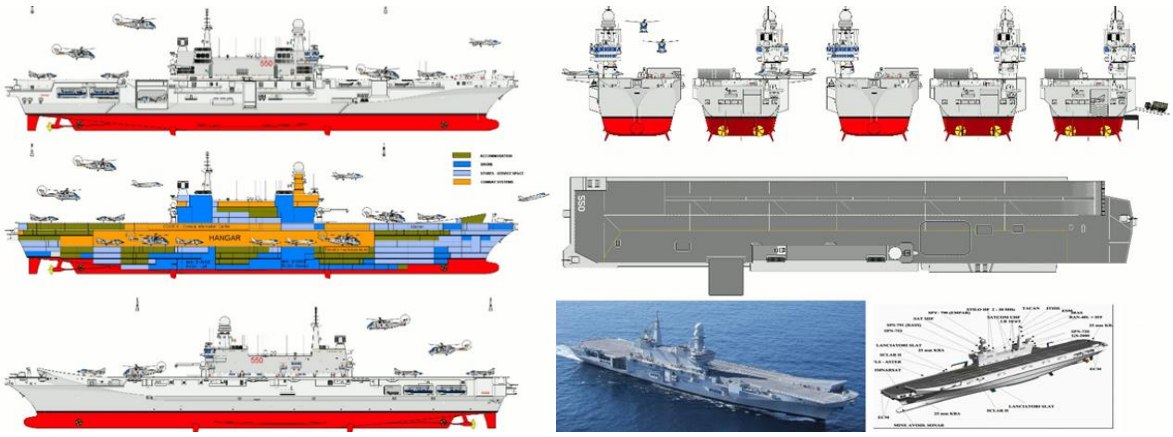

Figure 43 - Aircraft Carrier Cavour

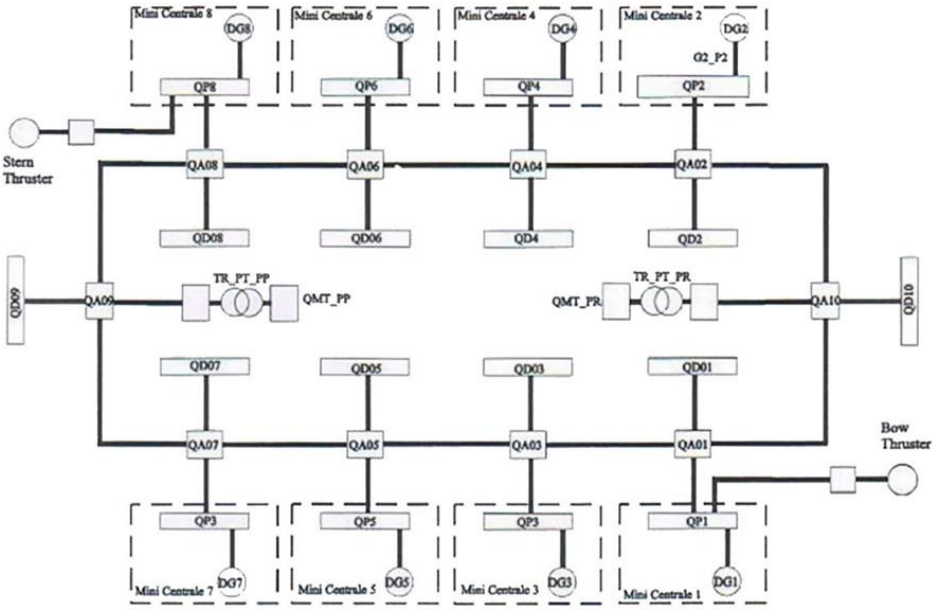

Figure 44 – Cavour Network Layout

The presence of 8 generation groups makes the system very modular and partial, depending on the operating roles required by the ship, and increases the system reliability having 8 independent sources (5 operating simultaneously and 3 generators readily in standby). Moreover, with this type of generation, the power splitting diesel generators operate at their maximum efficiency in each operation role.

The disadvantage is represented by installation costs (purchase and installation of the groups, maintenance, and number of bus-bars on board due to the high safety standards required).

The presence of 8 power plants coupled with the use of directional protection installed in the meshed electrical panels, allows to limit the disservices and the number of users involved.

The presence of a primary distribution mesh network allows the ship to be directly powered via the shore connection without the need to set up a special distribution network only requiring the installation of appropriate electrical panels for this function. Finally, the Cavour employs two axis generators.

The synchronous machine can be used as a generator when the axis line is driven by the gas turbines, transferring energy to the network allowing to put some diesel generators on standby.

To interface with the constant frequency network, axis generators require a converter consisting of two rectifiers, each connected to a stator winding of the machine feeding the DC stage. Subsequently,

four IGBT inverters power the AC network at a constant frequency, delivering 2750 kVA between 80 and 140 RPM and providing reactive energy, thanks to the type of converter used. Figure 45 shows the drive architecture.

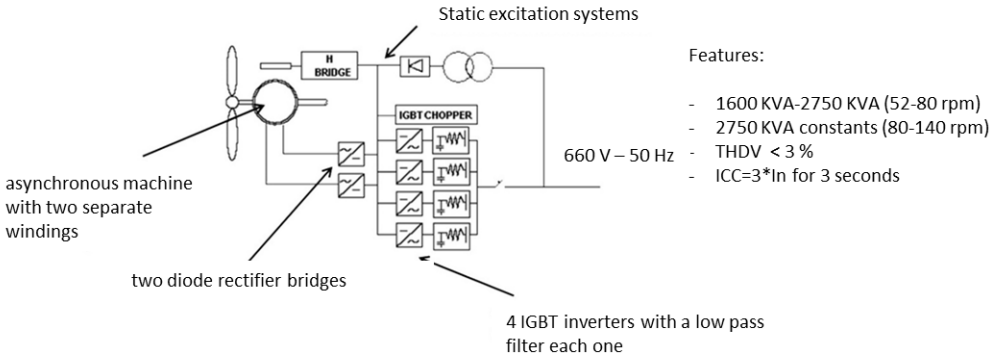

Figure 45 - Drive Architecture of Axis Generator

4.2 On-board electrical loads characterization

A military ship is characterized by a great variety of loads, in number and power, essential and non-essential, and performing different functions. In this chapter, a description of different classes of loads with their characteristic is carried out. Moreover, different operation roles defining the power consumption of each group of loads is highlighted.

4.2.1 SWBS groups

The starting point is the classification of the various loads present on board the aircraft carrier. In general, a ship contains a large number of electrical devices, ranging from the various pumps and engines of the air cooling system, to auxiliary systems for generators and propulsion, to indoor/outdoor lighting systems and navigation lights, as well as the whole electronic network for audio/visual communication, data transmission, automation system and weapon systems.
The SWBS (Ship Work Breakdown Systems) groups reported in
Table 5 shows a general classification according to which the various electric loads have been grouped in the ship's electrical balances provided by the manufacturer. A complete listing of the various SWBS is provided in Annex H of IEEE Standard 45 "A guide to electrical installations" [96].

Table 5 - SWBS (Ship Work Breakdown Systems) Groups

SWBS	**Description**
200	Propulsion system
300	Electrical system
400÷446	Command & Supervision 1
450÷492	Command & Supervision 2
500÷517	Extraction/Ventilation - HVAC
520÷569	Auxiliary Systems 1
570÷593	Auxiliary Systems 2
600	Mounting
700	Armament

Table 6 - SWBS Groups Electric Loads

Application	Description of Electric Loads
Propulsion system	Fan cooling turbines, generators, fuel cleaner, washing module turbine blades, etc.
Electrical system	Local Lighting, 24V battery charger, auxiliary alternator shaft, winch cable recovery, rotary converter 400 Hz, and so on.
Command & Supervision	Navigation and weather system, internal communications, radar, magnetic compensation system, surveillance systems and so on.
HVAC	Air conditioners, fans, local, chillers, boilers, fan coils, and so on.
Auxiliary system	Electrical fire pump, water maker, kerosene purifier, air rudder, thruster, cranes, elevators, lifts, side ramp, and so on
Mounting	Food, health area, laundry room, compactor, workshop
Arming	Machine gun, short-range defense system, rocket launchers and so on.

4.2.2 Operating role

Depending on the ship operating role, the power consumption of various electrical loads can undergo significant variations, passing for example from the less energizing stages of parking and manoeuvring in port, up to special roles that require maximum electrical requirements as in combats. In order to define the electrical scenario it is necessary to identify the operational role adopted by the ship to identify the total and specific needs of each SWBS group.
A table defines the consumption of each SWBS group power for each specific operating role, defining some parameters as show in Figure 46.

Group 200 - Propulsion System											
N	SWBS	Service	N	Power			Power Factor	Absorbed kW	Port Normal		
				Nominal kW	Efficiency	Absorbed kW			N	Contemp. Factor	Power request kW

Figure 46- Caption of Real Table That Define A SWBS Consumption in a Operation Role

The first line indicates the SWBS group and in the second row the first three columns are descriptive of the reported electrical equipment. From the fourth column onwards, we have:

- N: total number of installed devices;
- nominal: rated power in kW;
- nominal efficiency;
- absorption: power absorbed in kW considering nominal efficiency;
- power factor;
- real consumption: indicates the total power absorbed by the grid, taking into account the efficiency and power factor.

The following columns contain data relating to the various operating roles, in this case “in port”:

- N: number of active devices referred to the total number installed;
- contemporaneity factor: indicates the ratio between the absorbed power at the same time and the total power of the active devices;
- power request: is the total power value requested by the load, obtained by multiplying the total power absorbed by the factor of contemporaneity and by the number of active devices.

4.2.3 On-board loads - Macro categories definition

The electrical loads for each electrical panel have been grouped into three macro categories, based on the type of electric load and the harmonic behaviour. The three groupings are:

- static loads;
- non-linear loads - converters;
- rotating loads.

This subdivision will be useful in simulations and system modelling in order to consider those loads that cause harmonic disturbances, or those loads contain a significant percentage of rotating load, consisting of heterogeneous electric motors.

Chapter V: Cavour Aircraft Carrier– Measurement campaign [97]

5.1 Measurement campaign organization

A measurement campaign was carried out on board aircraft carrier Cavour, in order to determine the power quality of the power system (harmonic content, asymmetries, voltage sags, power factor) and the impact of the relevant electric loads. The analysis of the data records, allows to model the loads behaviour in time and frequency domains, thus permitting their use for the required studies.
Measurements have been carried out in port, with shore disconnected connection, and with a reduced number of electrical loads. The results have been subdivided and evaluated in relation to: electrical system areas, electrical load measured, loads working cycle, network behaviour in time domain, voltage and current harmonic distortion. In order to properly assess the data needed for the models realization, different measures have been taken. A first measurement has been made with the entire distribution network connected and energized, with the aim of checking the network status in steady state. Then, for each load considered, the area of the network interested by the measure was restricted to the minimum. This was achieved thanks to the high reconfiguration capabilities of the Cavour distribution system, feeding the loads with a subset of the distribution network (comprising at least one generator) isolated from the rest of the ship. Some specific electrical loads presenting high distorted current absorption have been identified. Their characterization was considered particularly relevant, and has been carried out in order to define their contribution to harmonic disturbance and their impact on the network.
The instrument used for measurements is the Chauvin Arnoux CA 8335 network analyser. It measures four voltages and four currents, thus calculating all the relevant power quality parameters. Thanks to that, it was possible to record voltages, currents and power values for every measure, and to perform harmonic disturbance analysis. The features of the measuring instrument are reported in Annex A. The presence of large-diameter cables bundles (up to 16 conductors of 240 mm^2 each) in some cases forced to the installation of current probes to only a part of the cables of a bundle, being the total beam diameter greater than the current probes. Therefore, a uniform current distribution in the cable bundle was assumed (a condition favoured by the cables' transposition every 15 m). By doing that, the entire cable current was obtained as a product of the measured current by the ratio between the total number of the cables in the bundle and the probed cables (maximum single-core cables cross-section: 185 mm^2) [98].
Cavour's power system presents different configurations, depending on the operational role.
The electrical power absorbed during the operative configurations can be found in the electrical balance, the most common are described in Table 7.

Table 7 – Electrical Balance in Different Operational Profiles

SWBS	Service	Port [kW]	Low speeds [kW]	Training operating [kW]	Battle operating [kW]	Emergency [kW]
200	Propulsion system	49.3	497.5	457.3	645.3	0.0
300	Electrical system	469.6	616.6	859.5	1158.5	79.0
400÷446	Command/ Supervision 1	72.7	74.0	260.9	398.5	249.4
450÷492	Command/Supervision 2	3.5	210.3	452.8	535.4	7.0
500÷517	Extraction/Ventilation HVAC	1807.7	2326.4	2478.8	2488.4	0.0
520÷569	Auxiliary Systems 1	181.5	2456.1	435.4	1181.6	374.9
570÷593	Auxiliary Systems 2	249.8	388.1	202.8	269.56	1.7
600	Mounting	629.7	574.9	574.9	225.9	0.0
700	Armament	54.5	0.0	159.7	166.1	491.2
		3518	7145	5882	7069	1202

5.2 Measurement campaign results

The measurement campaign was carried out at port, with the ship detached from the shore connection. Accordingly, onboard generators supplied the power system. A preliminary study of the plant layout identified the most relevant loads to be analyzed through the measurement campaign. A simplified diagram of the Cavour power grid is shown in Figure 47, where the electrical loads monitored are marked in red. The results have been analyzed paying attention to: power system configuration; characteristics of the electrical load monitored; load work cycle during measurement; network behavior in the time domain; voltage and current harmonic distortion.

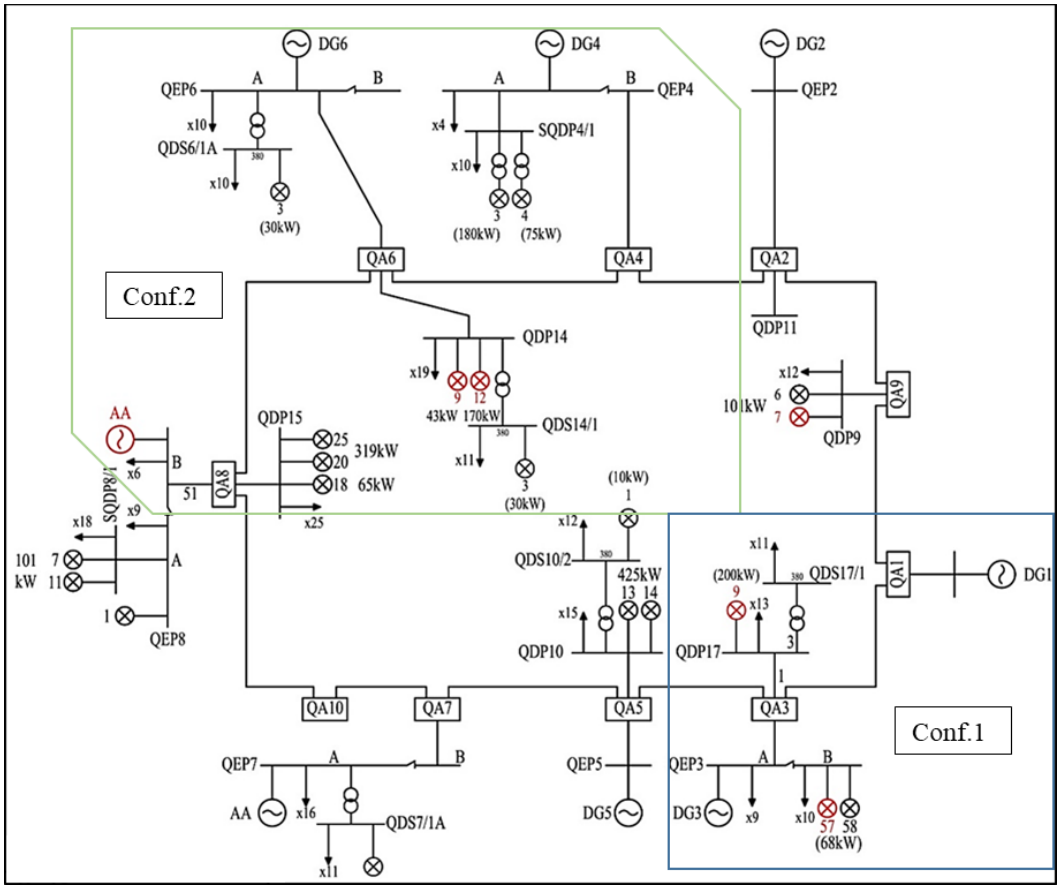

Figure 47 - Electrical Network Diagram of Cavour Used for Electrical Loads Measurements

The measurement campaign was conducted applying the instruments to the main electric panels: QEP3, QEP8, QA3, QA6, and QA9 (referring to Figure 47). Since the ship was in use, and in particular was under ordinary maintenance, it was necessary to limit disturbances produced by the measured loads, by isolating the feeders of the individual loads. This was done thanks to the reconfiguration options given by the ring distribution layout: the monitored network areas were disconnected from the rest of the ship, taking most generators and loads off service. The monitored loads are:

- Side ramp (hangar access from shore) (in QEP3);
- Shaft generator (in QEP8);
- Radar EMPAR (in QDP17);
- 15 Tons elevator (in QDP9);
- 15 Tons crane and electrical fire pump (in QDP14).

A first measurement was conducted connecting the instrument to the electrical panel QA9, with the network in closed loop configuration, and active diesel generators 1 and 4. The goal of the measurement was to acquire the standard network status for the ship during port operation, i.e. total energy demand, current, voltage, and frequency values. Then the ship network was reconfigured for the single loads measurement, sectioning the ring bus into two separated islands (shown in Figure 47). In particular, the two sections were defined as follows:
Configuration 1 - section comprising QA1 and QA3, with diesel generator 1active;
Configuration 2 - section comprising QA8, QA6 and QA4, with diesel generator 4 active. Shaft generator (AA in Figure 47) active only for his single measurement.

5.2.1 Time domain

Standard network status, measured on QA9

The preliminary test (aimed at assessing the standard network status), showed a very stable RMS value for the phase-phase voltage, with variations lower than 0.5%. The frequency was constant, equal to 49.95 Hz. The recorder current was almost constant, not less than 75 A and with two visible steps due to the insertion of small intermittent loads (such as compressors or pumps, widely used on board). Total power consumption was 90 kVA, with a power factor equal to 0.5. This value, despite being rather low, can be justified by the low load applied to the power system. In fact, at port the electric load is mainly constituted by HVAC system's induction motors, whose power factor on light loads is low.

Side ramp measurement, powered by QEP3

The monitoring of the side ramp was performed with the network in Configuration 1. The working cycle of the ramp was the following: starting from the resting position 2 meters lifting, then complete descent, complete lifting and full descent. The measurement was made on electrical panel QEP3 and the test time was about 7 minutes. The voltage remained stable, with negligible changes, during ramp maneuvers. The frequency was constant, at about 49.95 Hz. Figure 48 shows the current and voltage RMS values. Figure 49 reports power consumption and power factor profile. It can be noted that the average value of current is 15 A, with some steps due to the work cycle accomplished, and it reaches 30 A as maximum values during steady state operation. The inrush current is about 90 A, with a current crest factor of five (at starting). The characteristic values, recorded on one of the three phases of the power system, are reported in Table 8. The average active power is approximately 15 kW, with low value steps during ramps maneuvering; conversely, reactive power is not affected by the load cycle, remaining constant at 14 kVAr. The power factor changes from 0.8 at the start, to 0.4 when the current has its minimum values.

Table 8 - Characteristic Values for Side Ramp Measure

Vmin [V]	Vmax [V]	V avg [V]
657	665	658
Imin [A]	**Imax [A]**	**I avg [A]**
0.0	87.4	17.4
Ptot min [kW]	**Ptot max [kW]**	**Ptot avg [kW]**
0.0	27.9	14.3
Power factor min	**Power factor max**	**Power factor avg**
0.35	0.86	0.62

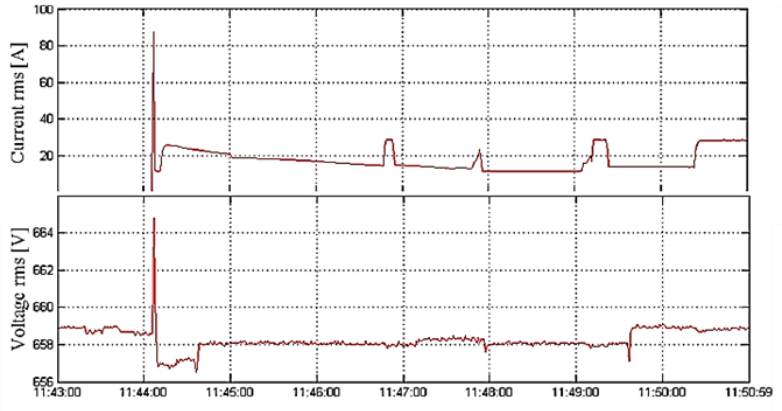

Figure 48 - Current and Voltage Measured During Side Ramp Operation

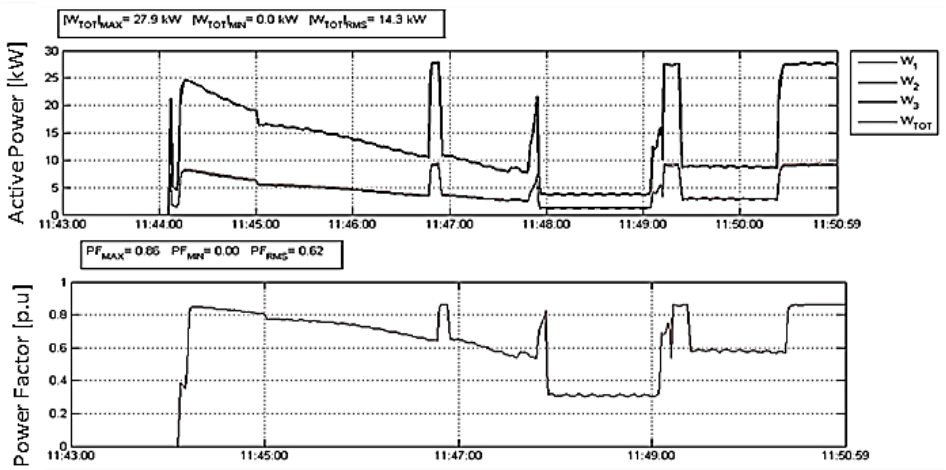

Figure 49 – Active Power and Power Factor During Side Ramp Operation

EMPAR measurement, powered by QDP17

EMPAR stands for "European Multifunction Phased Array Radar": a latest generation multifunctional radar that can simultaneously perform the following tasks: medium-range air surveillance, three-dimensional tracking of multiple targets, and anti-aircraft missiles guidance. The measurement was conducted on the QDP17 electric panel with network in Configuration 1. The EMPAR work cycle was: starting of antenna rotation, radar emission activation and subsequent deactivation. Voltage and frequency remained stable throughout the test. The current (Figure 50) switched from 25 A (EMPAR in stand-by) to 40 A, and remained steady during the operation. The power absorption changed from 24 kW to 40 kW, following the current variations, with a relatively high power factor, equal to 0.9.

Table 9 shows the most relevant values recorded in one of the three phases during measurement.

Table 9 - Characteristic Values for Empar Measure

Vmin [V]	**Vmax [V]**	**V avg [V]**
659	662	661
Imin [A]	**Imax [A]**	**I avg[A]**
23.7	40.1	34.2
Ptot min [kW]	**Ptot max [kW]**	**Ptot avg [kW]**
22.5	41.2	34.4
Power factor min	**Power factor max**	**Power factor avg**
0.80	0.89	0.86

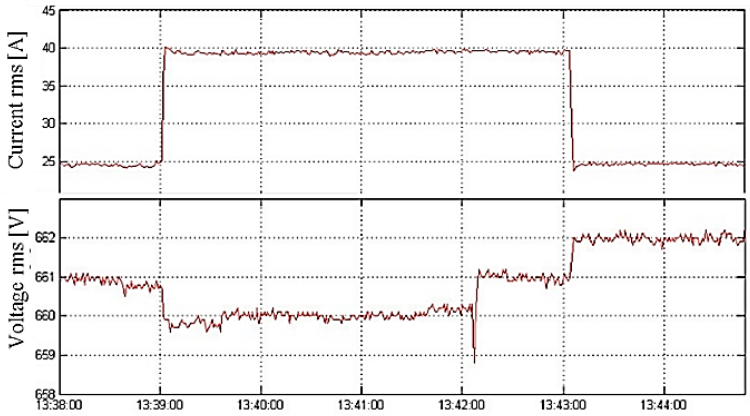

Figure 50 - Current and Voltage Measured During EMPAR Operation.

Shaft Generator measurement, on QEP8

The shaft generator measurement was conducted with the Configuration 2 network: an island composed by QA8, QA6 and QA4 and their related distribution panels. The power supply of this section of the network was achieved by only using a Diesel generator 4 until the start of the shaft generator. The latter can supply his full power only at full speed, so it was impossible to test it in the full load condition. Indeed, when the ship is moored propellers speed rotation has to be kept at low RPM, with 0° of propeller pitch, so as not to produce any thrust on the hull. For this reasons, during measurements the shaft generator worked only at a reduced power, as compared to the nominal value. During the measurement some shaft power variations were recorded. They can be attributable to the interactions between the shaft generator and the Diesel generator 4 (load sharing transients and electromechanical oscillations), and to variations in the resistant torque applied to propellers (caused by the water turbulent conditions).

The measurement was conducted on the main feeder that connects the shaft generator to the QEP8. The feeder consisted in a three-phase cable bundle, each phase constituted by 12 single core 240 mm^2 cables. In order to apply some load variations to the generator during the test, one aircraft elevator (powered by QDP15, distribution panel derived from QA8) was moved. The observation time was 21 minutes. The measured voltage was stable and the frequency was kept at 50 Hz with only small oscillations, due both to load sharing dynamics and loads' activation. A first ramp, of about one minute length, is a consequence of the gradual load sharing between the shaft and Diesel generators. During this first transient power oscillations between the two generators can be easily observed. During the test the current varied from 400 to 600 A with some peaks during loads' activation.

Figure 51 shows current and voltage RMS values. Figure 52 reports active power and power factor during Shaft Generator operation.

Table 10 shows the characteristic values recorded in one of the three supply phases. The power factor was about 0.7, with some fluctuations both at start and in the last minutes of the measurement (0.13 ÷ 0.97).

Table 10 - Characteristic Values for Shaft Generator Measurement

Vmin [V]	**Vmax [V]**	**V avg [V]**
651	657	654
Imin [A]	**Imax [A]**	**I avg [A]**
109.2	627	452.6
Ptot min [kW]	**Ptot max [kW]**	**Ptot avg [kW]**
22.2	527.6	343.5
Power factor min	**Power factor max**	**Power factor avg**
0.13	0.97	0.70

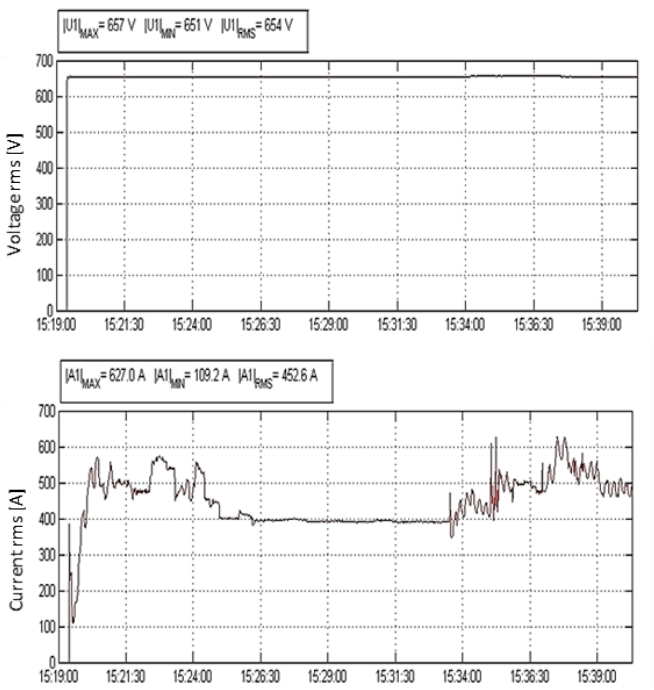

Figure 51 - Current and Voltage Measured During Shaft Generator Operation.

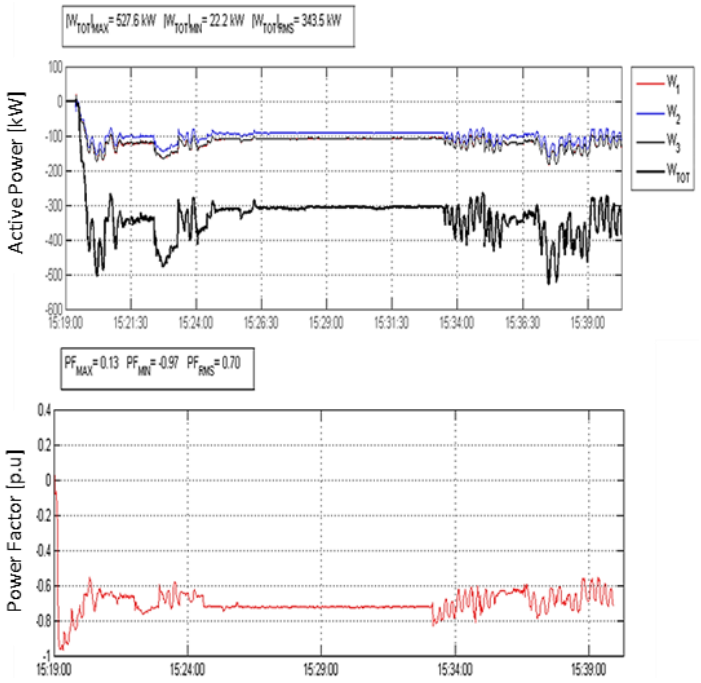

Figure 52 - Active Power and Power Factor During Shaft Generator Operation

15 ton elevator measure, powered by QDP9

This measurement was conducted with the network in Configuration 2. Being the elevator connected to QDP9, and through it to QA9, the network covered by the measurement was complementary to Configuration 2, thus comprising the following electrical panels: QA2-QA9-QA1-QA3-QA5-QA7-QA10. During measurement, in order to limit disturbances, most of the loads powered by QDP9 were not enabled. A first measurement was made to assess the network state, and registered 80 kVA power consumption with a 0.5 power factor. Subsequently, one of the two 15 ton bow munitions elevators was activated. The work cycle consisted in a lifting followed by a complete descent, with some weights on the elevator platform. In this case, the measurement was conducted in QA9, on the QDP9 main feeder. Being the three-phase wiring realized with three bundles cables, each of 6 unipolar 240 mm2 cables, current probes were placed only around two cables of the bundle. Therefore, for this test, the current correction factor is equal to 3 (measured current has to be multiplied by the correction factor to obtain the real feeder current). Voltage reported negligible variations during the test, with some disturbances only during elevator start. The frequency remained stable too, in the range between 50 and 49.9 Hz. The current profile, shown in Figure 53, varies during the elevator movement from a 65 A base value.
Figure 54 shows active power and power factor during 15-Ton elevator operation. Table 11 shows the relevant recorded values for one of the three supply phases. The elevators drive is of hydraulic type, with an oil pump that remains activated during the entire test. Therefore, the elevator system absorbs a constant 35 A current, excluding starting operation. During lifting operations the system absorbs an additional current of 45 A (from 16:27:20 to 16:28:10). The same happens during descent (from 16:29:00 to 16:29:50) with a 15 A absorption. This is due to the security systems embedded into the hydraulic actuators, which prevent the gravity descend of the elevator, so also the descent operation must be done by the pressurized oil of the electric pump (thus consuming additional power and reducing the overall system efficiency).

Table 11 - Characteristic Values for Elevator 15 Ton Measure

Vmin [V]	**Vmax [V]**	**V avg [V]**
657	663	658
Imin [A]	**Imax [A]**	**I avg [A]**
66	215	90.5
Ptot min [kW]	**Ptot max [kW]**	**Ptot avg [kW]**
29.8	129.2	50.9
Power factor min	**Power factor max**	**Power factor avg**
0.30	0.72	0.46

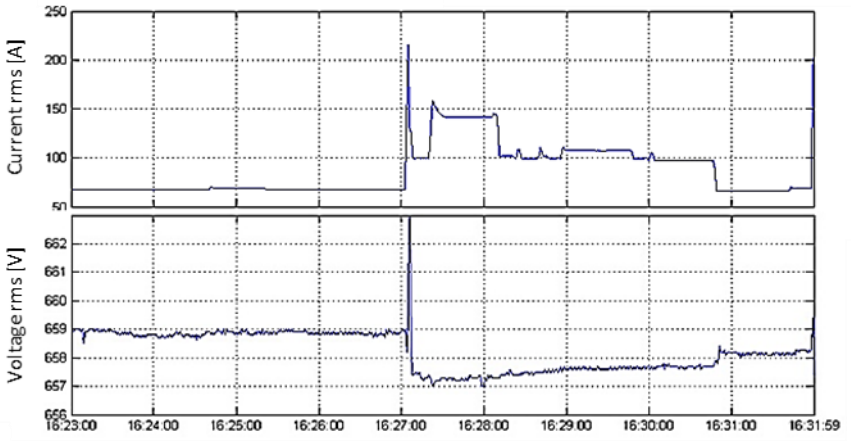

Figure 53 - Current and Voltage Measured During 15 Ton Elevator Operation

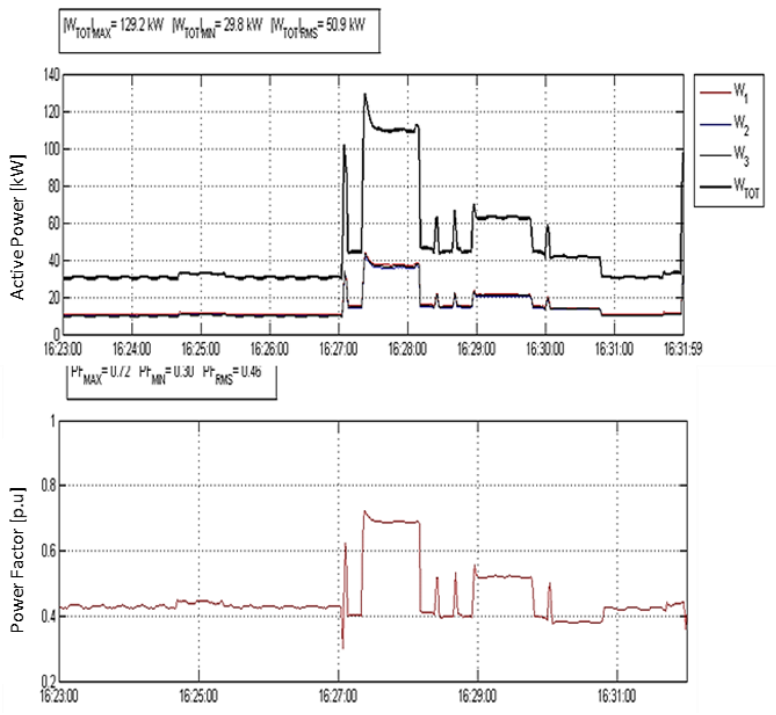

Figure 54 - Active Power and Power Factor During 15 Ton Elevator Operation

15T crane and electrical fire pump measure, powered by QDP14

The measurements were carried out with the network in Configuration 2. Monitored loads are two: a 15 Ton crane and an electrical fire pump (namely "EPAC"). From an initial measure performed on the QDP14 feeder, the steady state power consumption was equal to about 200 kVA, with a 0.65 power factor, because there were other loads in the monitored area. Voltage and frequency were constant and stable. The devices were then operated individually, starting with the crane. Its work cycle consists in lifting and moving some weights. During crane operation, voltage remained stable, with only little variations. The frequency was also stable at 50 Hz, while current values changed from 90 A before start to 110 A with the crane in operation. The crane inrush current was about 180 A (Figure 55). Table 12 shows some characteristic values recorded. The crane's drive (Figure 56) absorbed about 20 kVA, with a 0.6 power factor.

As regards the EPAC, it was loaded at 37% of his rated power during the tests. The measurements show a significant voltage drop at the load insertion, equal to 2.3% of the nominal voltage (rated 660 V). The current absorption is 50 A, obtained as the difference between the currents recorded before and after pump start. The inrush current is 6 times the rated current, as shown in Figure 57. Table 13 shows the characteristic values recorded on one of the three supply phases. The EPAC (Figure 58) absorbs about 60 kVA, with a 0.7 power factor.

Table 12 - Characteristic Values for 15 Ton Crane Measures

Vmin [V]	**Vmax [V]**	**V avg [V]**
656	660	656
Imin [A]	**Imax [A]**	**I avg [A]**
89.7	180.6	108.3
Ptot min [kVA]	**Ptot max [kVA]**	**Ptot avg [kVA]**
99.3	200.8	120.5
Power factor min	**Power factor max**	**Power factor avg**
0.46	0.70	0.62

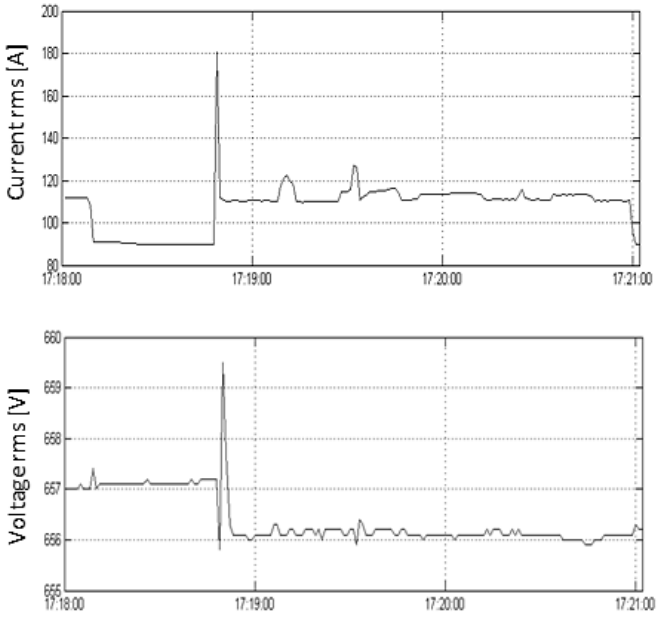

Figure 55 - Current and Voltage Measured During Crane 15 Ton Operation

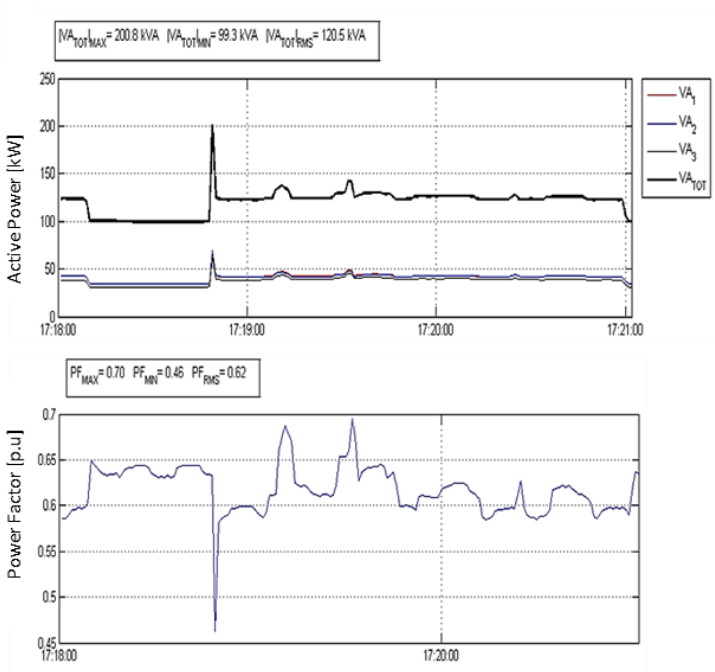

Figure 56- Active Power and Power Factor During Crane 15 Ton Operation

Table 13 - Characteristic Values for EPAC Measure

Vmin [V]	Vmax [V]	V avg [V]
645	658	656
Imin [A]	**Imax [A]**	**I avg [A]**
83.1	393.9	136.0
Ptot min [kVA]	**Ptot max [kVA]**	**Ptot avg [kVA]**
99.8	461.2	167.7
Power factor min	**Power factor max**	**Power factor avg**
0.32	0.76	0.69

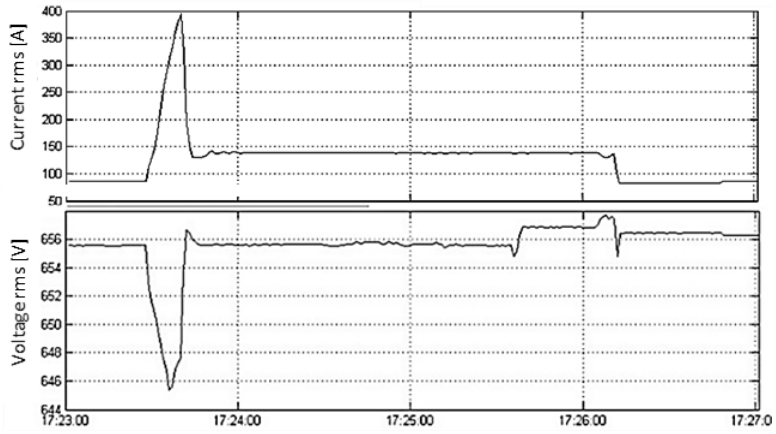

Figure 57 - Current and Voltage Measured During EPAC Operation

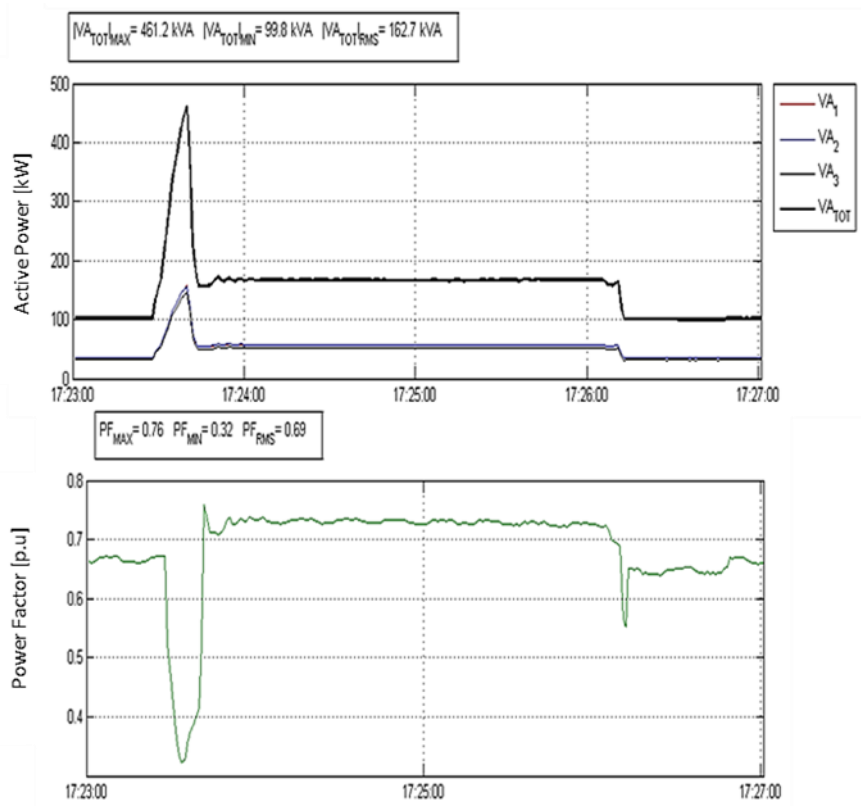

Figure 58 - Active Power and Power Factor During EPAC Operation

5.2.2 Frequency domain

Using the data obtained from the measurements, a frequency analysis on the single electrical devices monitored was carried out. This was done in order to assess the possibility of significant distortion levels in voltage and current waveforms.

Standard network status, measured on QA9

The preliminary measurement performed on the QA9 electrical panel, carried out to assess the standard network status in closed ring configuration, showed that supply voltages had a limited harmonic content (Figure 59). The largest voltage harmonics were the 5th and 7th, respectively equal to 2.5 % and 2%, while the 11th harmonic was less than 1%. The three phase voltages did not show any asymmetries, and the THD_V % was 4.2%. The current presented a significant 5th harmonic, equal to 5% (on a fundamental component of 78 A), and a negligible 7th harmonic. The 11th harmonic was equal to 1% of the fundamental. Finally, there were a negligible 3th harmonic, except in phase 1 where it assumed a value (2%) that was more than double as compared to the values of the remaining phases. Except for the specific case of the 3th harmonic, all the harmonic components were homogeneous on the three phases, and the THD_I % was 6.5%.

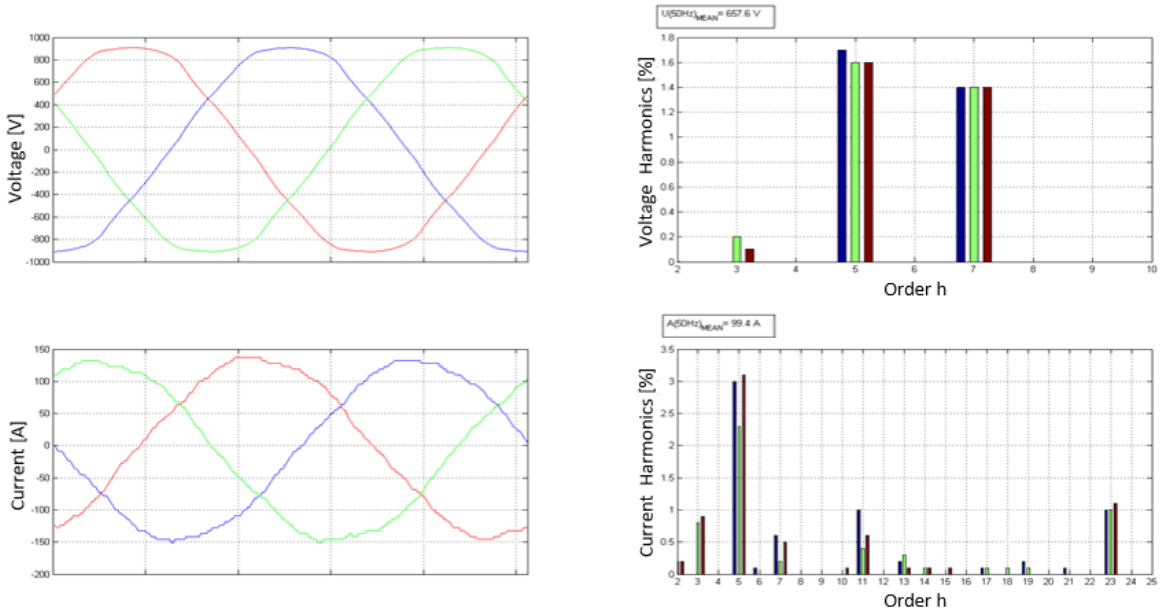

Figure 59 - Network Status: Voltage and Current Harmonic Content

Individual loads

As far as the analysis of individual loads is concerned, the ramp operation showed no critical point (Figure 60). Conversely, the EMPAR harmonic content showed that the current absorbed by the load (25 A at 50 Hz) was strongly distorted, presenting a waveform typical for a three-phase six-pulse bridge rectifier (Figure 61). The harmonic spectrum components showed values greater than 1% up to the 20th harmonic. As it can be expected from the waveform visual analysis, the current showed high values for the 6k ± 1 order harmonic components, with the 5th harmonic equal to 60% of the fundamental. The THD_I current changes from values between 55% and 65%, with EMPAR turned off, to 45% with the device in operation. The harmonic content of the shaft generator shows high frequency components, in particular for voltage the 36th and 38th harmonics were present despite their values were less than 1%. The current harmonics with order 13, 17, 19, 25, 36, 38, 42, and 44 had values comprised between 1% and 2% (Figure 62). As regards the 15 ton crane, the THD_I changed from 3% with the crane in standby to 1.5% during crane operation (Figure 63). The same applies for the electrical fire pump, where the THD_I % remained at 3%, except for the start-up and shut down transients, where the peaks reached 20% (Figure 64). In the case of the 15 T elevator the voltage harmonics were exclusively the 5th and 7th equal to 1.5%, with a THD_V % of 2.4%. The current, with a component of 100 A RMS, showed the 3th, the 5th harmonics, respectively 1% and 3%, and a 23th equal to 1% as relevant harmonics. The 7th, 11th and 13th harmonics are negligible (Figure 65).

The THD_I % varied from values under 10% with the elevator in standby, to 4% with the elevator in operation. Table 14 and Table 15 show the rates of individual and total voltage and current harmonic distortion for each load considered.

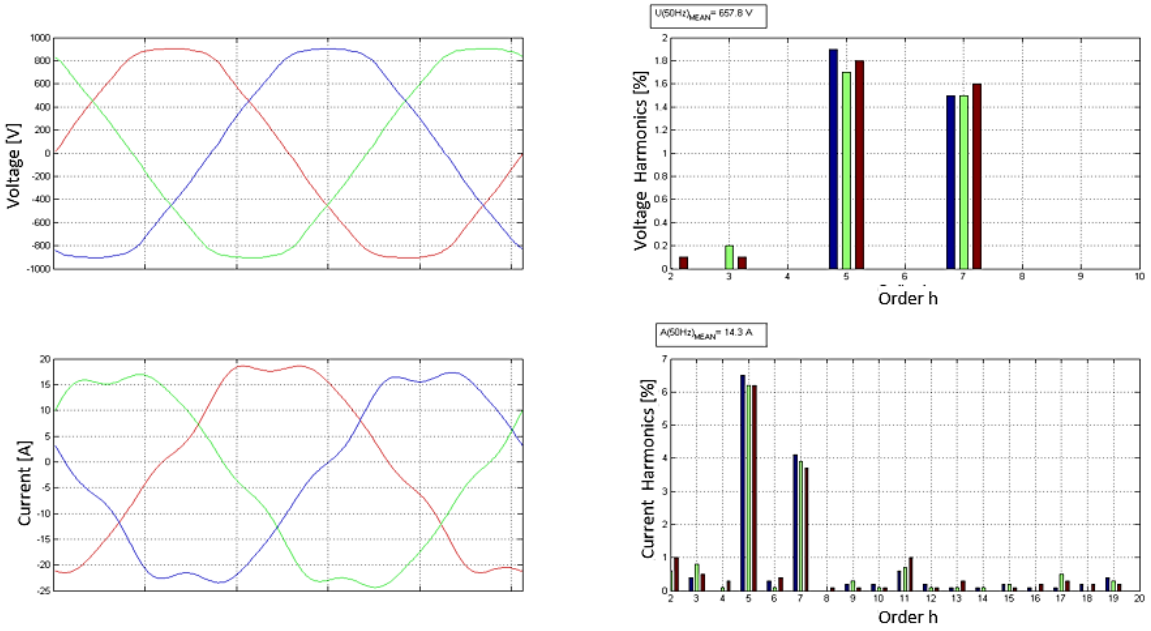

Figure 60 – Ramp: Current and Voltage Harmonic Content

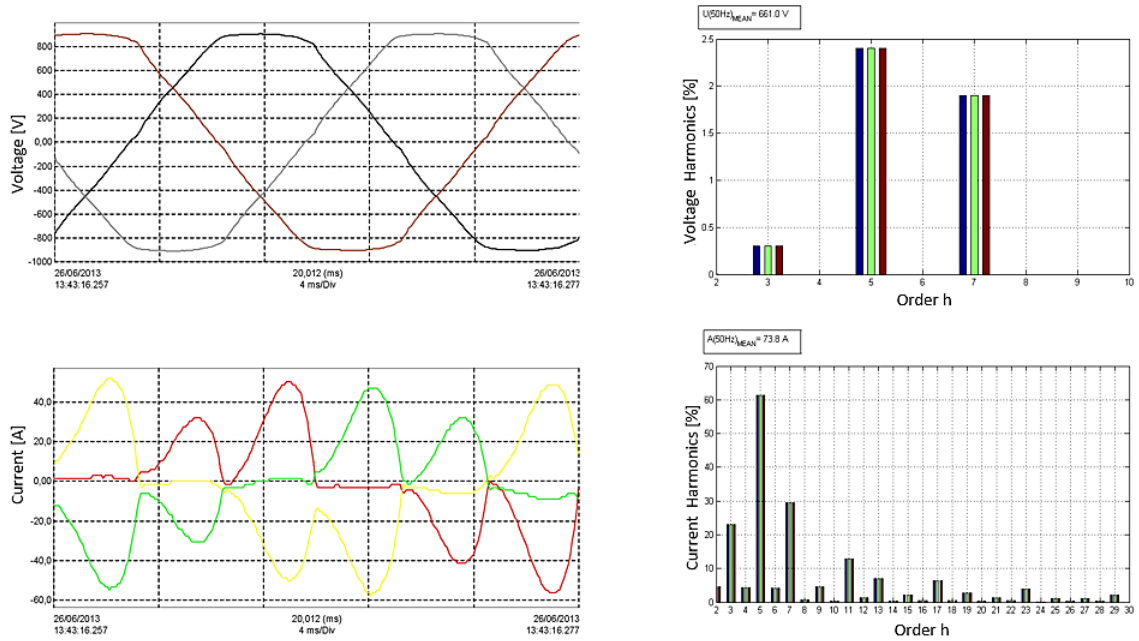

Figure 61 – Empar: Current and Voltage Harmonic Content

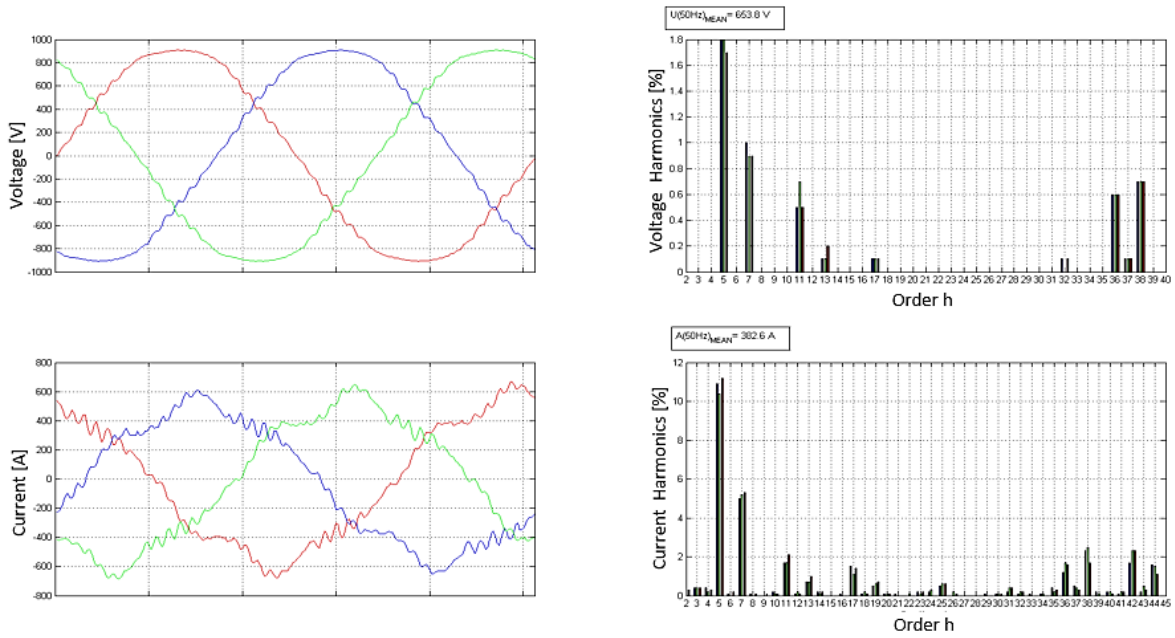

Figure 62 – Shaft Generator: Current and Voltage Harmonic Content

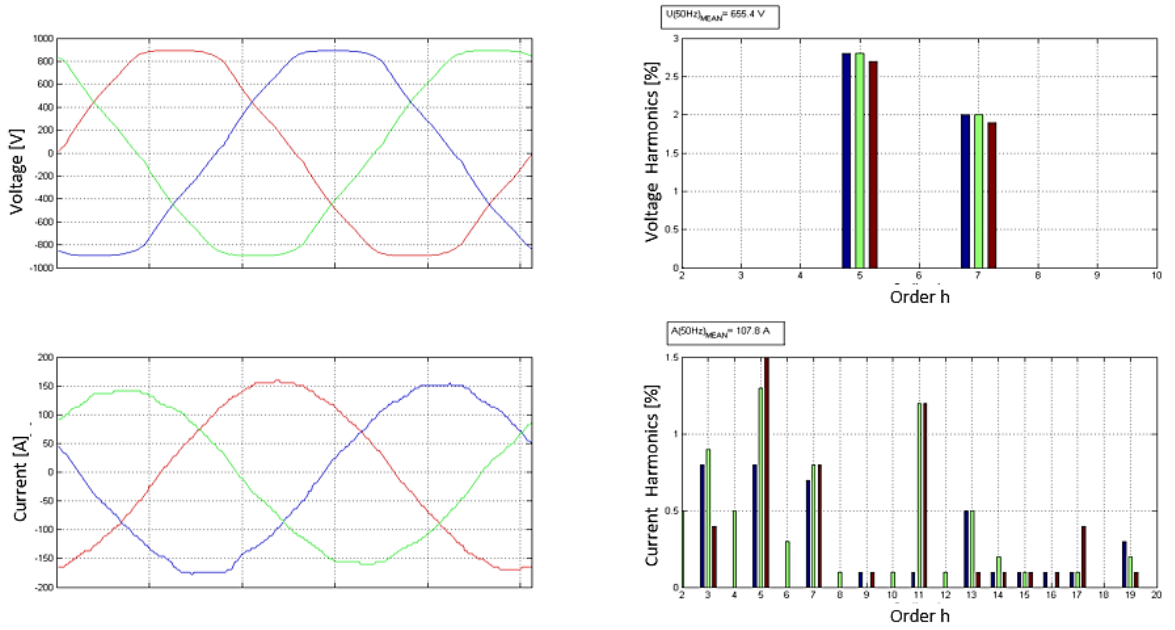

Figure 63 - 15 Ton Crane: Current and Voltage Harmonic Content

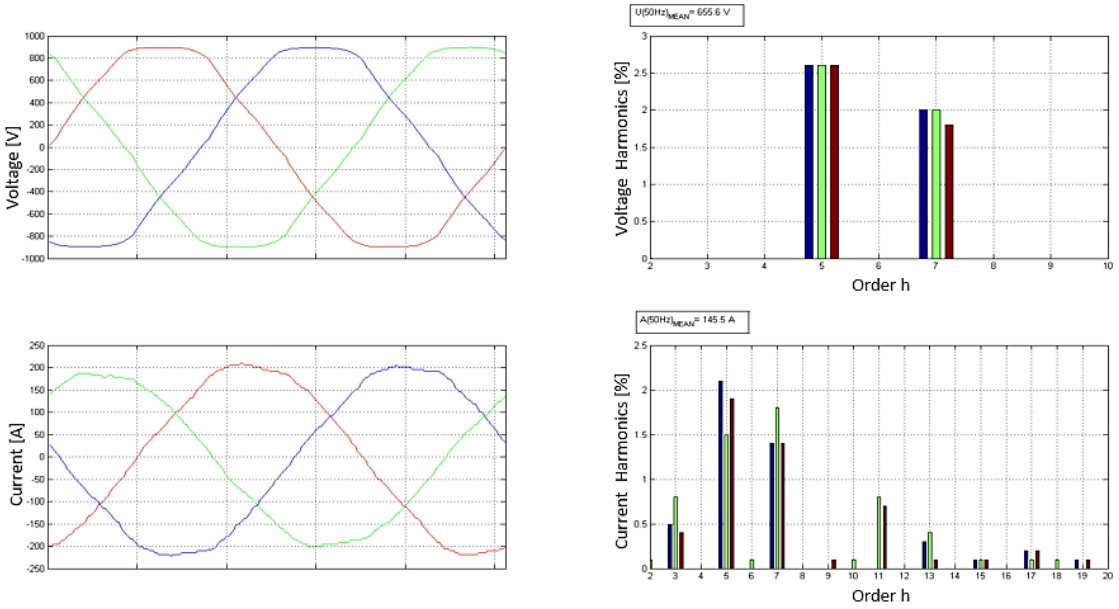

Figure 64 – EPAC: Current and Voltage Harmonic Content

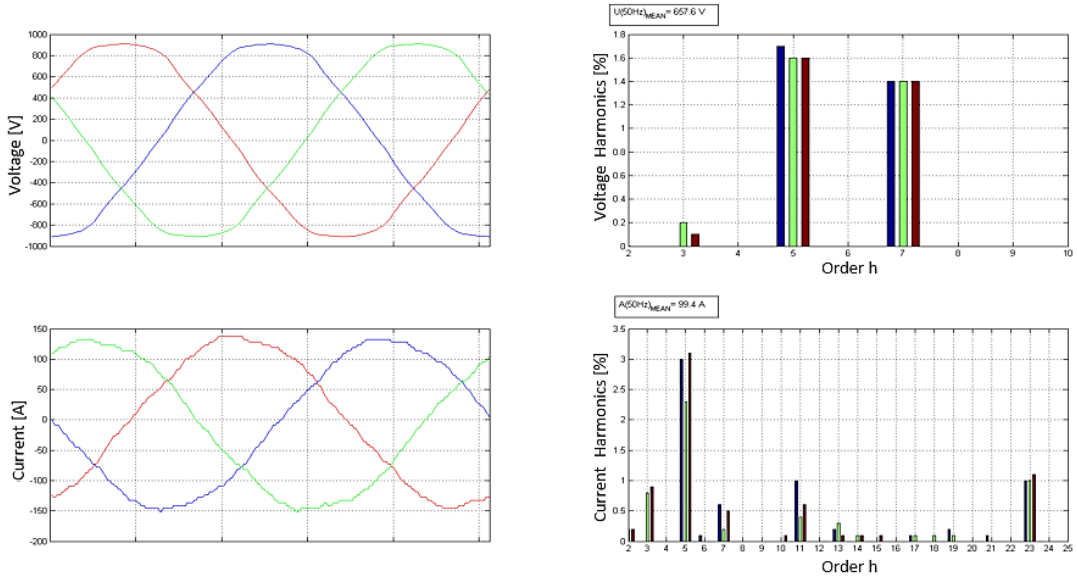

Figure 65 – Elevator 15 Ton: Current and Voltage Harmonic Content

Table 14 - Voltage Harmonic Distortion

Load	THD_v %	V_3 %	V_5 %	V_7 %	V_9 %	V_{11} %
Ramp	2.4	0.2	2.0	2.0	-	-
EMPAR	3.5	0.4	2.4	2.0	-	1.0
Shaft generator	2.4	-	1.8	1.0	-	0.7
Crane	3.6	-	3.0	2.0	-	-
Fire Pump	3.6	-	2.6	2.0	-	-

Table 15 - Current Harmonic Distortion

Load	THD_I %	I_3 %	I_5 %	I_7 %	I_9 %	I_{11} %
Ramp	6.0	1.0	6.0	4.0	0.1	1.0
EMPAR	45-65	23.0	60.0	30.0	5.0	12.0
Shaft generator	11.0	0.2	11.0	5.0	0.1	2.0
Crane	1.5-3.0	1.0	1.5	0.8	0.1	1.2
Fire Pump	3-20	0.7	2.0	1.7	0.1	0.8

From the measurement campaign carried out, it can be inferred that the ring distribution system of the Cavour does not present harmonic distortion issues in standard conditions: the THD_V % value is limited (4%). The side ramp operation showed no critical points, causing no disturbances to the supply voltage. Conversely, the EMPAR operation showed harmonic distortion problems due to strongly distorted current absorption by the load, with a THD_I % equal to 50% during operation. This value increased further when the drive worked at reduced load. The shaft generator did not produce a strong voltage distortion, although there were some high frequency harmonic components (36^{th} and 38^{th} harmonic). On the contrary the current harmonics were significant, especially considering their amplitude (tens amperes order) and distribution (high harmonic spectrum). The 15 ton crane and EPAC operations presented very stable and not distorted voltages. The only relevant issue was the voltage drop occurred at the start-up of the EPAC, which reached 2.4%. This is a significant value, considering that the pump was working at 37.5% of the rated load. Assuming a voltage drop proportional to the applied load, it can be inferred that in correspondence of the nominal load the voltage drop could reach 6.5%.

5.3 Software and model validation

The need to validate software and models starting from the measurement campaign carried out, allows to conduct new investigations proposing alternative solutions. The first step to use and develop a model is calibration; this approach makes it possible to identify critical issues by defining the best solutions for network modeling.
The measurement campaign carried out on the Cavour Aircraft was used to validate and calibrate the software presented in chapter III and that will be used for future investigations on new architectures.

5.3.1 Load Flow

The load flow carried out with Simulink was obtained starting from some hypotheses set in the software. These hypotheses are:

- the only generator in operation was set up as a swing source, which is a balance node. In this mode, the DG supplies exactly the active and reactive power required by the users in "port" operational profile, and the power necessary to compensate for the loss of joule in the cables and the self-consumption of reactors in the network, prevalent on the capacitive elements;
- during the test on the crane supplied by the QDP14, according to the ship automation system data provided at the end of the measurements, the diesel generator number 4 provided an active power equal to 627 kW, a value very close to that obtained in the simulation;
- the loads were considered to be constant active and reactive power absorption;
- the voltage setpoint in the bars of the main electrical panels, where the diesel generators are installed, was set at 1 p.u.

5.3.2 Network impedance analysis – Z(f)

As previously mentioned, the Harman program is able to calculate the equivalent network impedance at the electrical nodes of the system analysed. This calculation is particularly indicated on a weak network, with limited short-circuit power, since any harmonic components can introduce strong distortions on the power supply voltages, causing disturbances also to other loads connected in the network. Moreover, it is possible to find, also for limited distortion currents, high harmonic distortion values on system voltages: this is due to the potential presence of electrical resonances in the network, due to the interaction of inductive components (longitudinal impedance cables, transformers, etc.) with capacitive elements (capacitance of cables to ground, presence of passive filters or banks of re-phasing capacitors) that can amplify certain harmonic components.
To verify possible resonance present in the analysed portion of the network, the equivalent impedances were calculated for each node, in the main electrical panels. The calculation program is

set up to calculate the network impedance module at each node up to the 40th harmonic (2 kHz), the latter being the validity limit of the low frequency models for three-phase AC networks. The calculation step was set at 5 Hz, so as to detect resonances even at frequencies corresponding to inter-harmonic and subharmonic. The Network impedances calculated by software are reported in Figure 66.

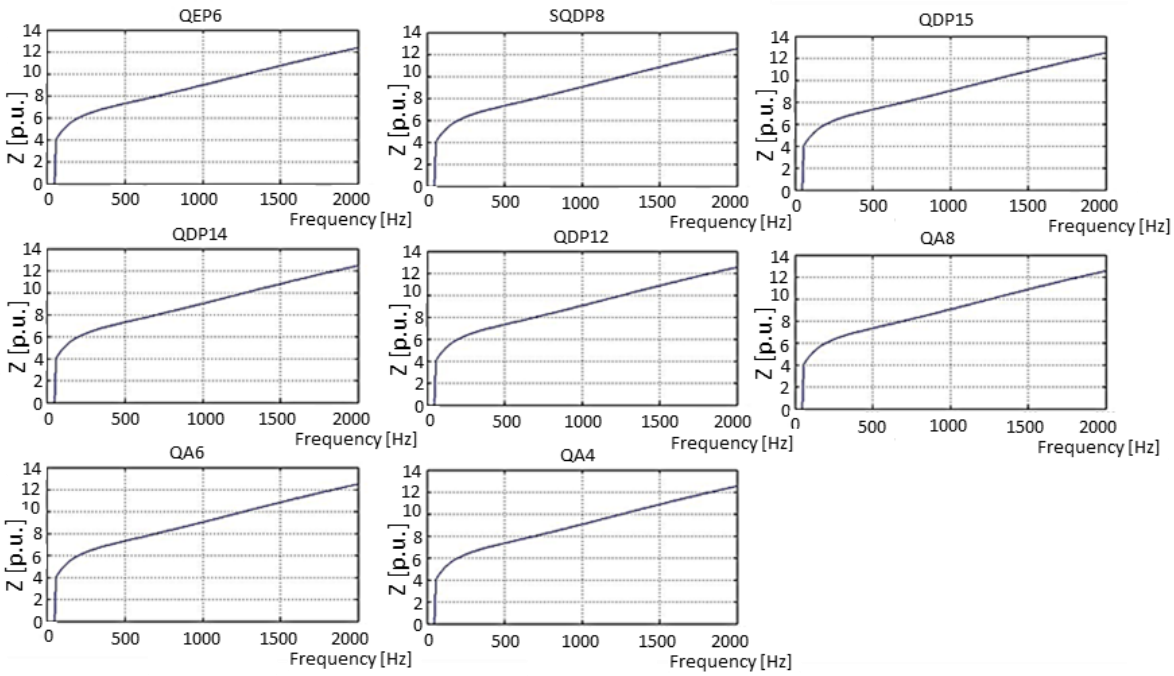

Figure 66 – Network Impedance at Main Electrical Nodes Under Study

Network impedance module is reported in p.u. (per unit) in vertical axis; the value of base impedance is:

$$Z_B = \frac{V^2}{P_B} \quad (34)$$

Where V is the nominal value of the phase-to-phase voltage, and PB is the base power (choice equal to the diesel generators size of 2750 kVA). Figure 66 shows that in the system there are no resonances in the frequency range analysed; an increasing monotonic trend with the frequency caused by the inductive part of the network impedance is shown. There are no harmonic filters or banks of capacitors; these elements could interact with the inductances present in the network and give rise to possible resonances. The only capacitive elements present in the model are the small service capacities of the cables, which have values of nF order, given the low unit capacity and the reduced lengths of the connections.

Figure 67 shows the graph of Z (f) calculated in the SQDP4 electrical panel in a frequency range between 0 and 100 kHz, where it is possible to observe peaks in the value of the network impedance at 3 kHz 80 kHz and 90 kHz frequencies.

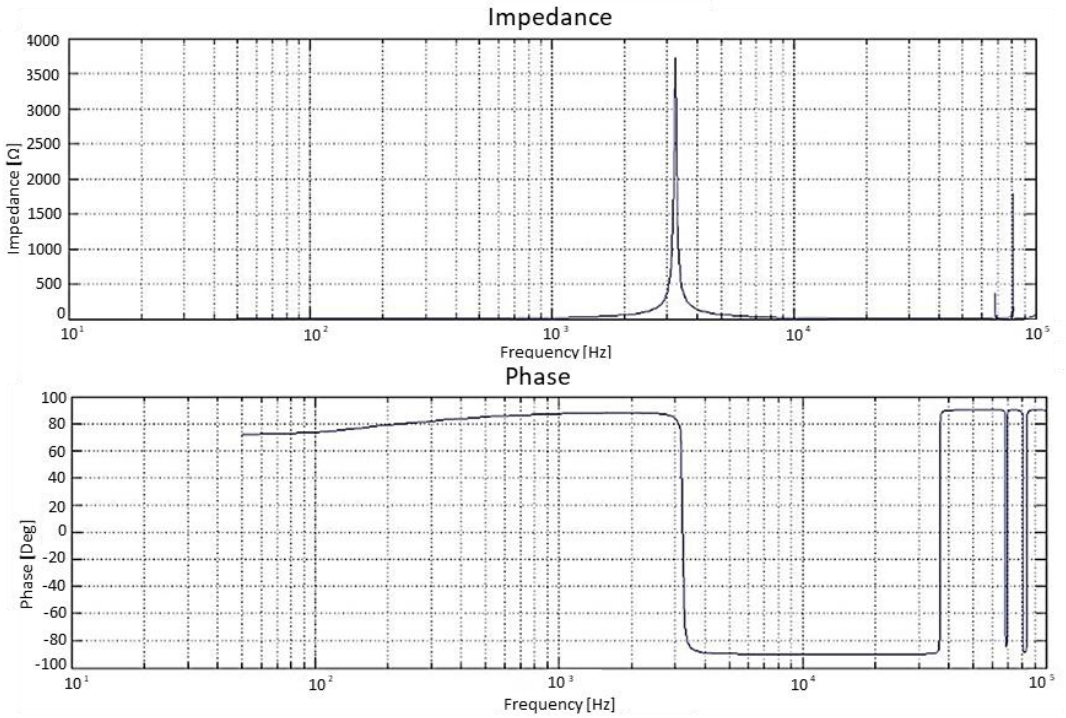

Figure 67 - Z(f) At SQDP4 Electrical Network Node

5.3.3 Total Harmonic Distortion evaluation

In the analysed network, converters have been considered with passive front ends with diodes, contain harmonic current components of 6k ± 1 order, with k = 0 ...N. This assumption is theoretically valid, since the converters, supplied with a voltage that is not perfectly sinusoidal (easily found in a naval system) and because of the constructive imperfections of the components, can introduce sub-harmonics and inter-harmonic components in addition to the harmonics characteristics.
In the simulation phase, it was decided to implement an absorption by the converters next to a theoretical disturbance table of a diode hexaphase rectifier. The disturbance table associated with these loads is shown in Table 16.

Table 16- Converter Harmonic Disturbances

h	**1**	**5**	**7**	**11**	**13**	**17**	**19**	**23**	**25**
% I_N	100	17.5	11.1	4.5	2.9	2.0	1.0	0.9	0.8

Therefore, simulations for total harmonic distortion (THD) calculation in the network were carried out, using converters characterized by the harmonic absorption reported in Table 16.
Figure 68 reports the data-file used in the simulation using Measurements data carried out during “port" operational profile. The network has 29 nodes, one of which is a generation node, and 28 power lines. Figure 69 reports all the output values in which THD are shown (respectively unfiltered, vectorial and correlated) and IHD for each electrical panel (node) and the source of the maximum individual harmonic contribution.

```
porto.dat - Blocco note
File  Modifica  Formato  Visualizza  ?
Rete di competenza LaSapienza zone 4,6,8
01010 40  0
2.75          50.  1.0 25.      61
0.66 0.38
 1.  1.   1.   1.   1.   1.   1.
QEP8    1              0.9984 -0.036  0.     0.    3        D                 B
R-QEP8  1              0.998  -0.0455 0.019  0.011 1        D  99             B
QEP6    1              0.9985 -0.0337 0.     0.    4        D               * B
S-QEP6  1              0.9985 -0.0346 0.039  0.021 1        D   0             B
C-QEP6  1  0.009 0.004 0.9959  0.0306              1        D      ES         B
R-QEP6  1              0.9974 -0.0496 0.190  0.114 1        D  99             B
QEP4    1             G1.0000  0.0000 0.     0.    3        D                 B
QEP4    172.                 2.75 0.66                                        G
R-QEP4  1              1.0000  0.0000 0.     0.    1        D  99             B
SQDP8   1              0.9982 -0.0421              4        D               * B
S-SQDP8 1              0.9981 -0.0434 0.061 0.038  1        D   0             B
C-SQDP8 1  0.009 0.004 0.9951  0.0336              1        D      ES         B
R-SQDP8 1              0.9981 -0.0445 0.017 0.008  1        D  99             B
SQDP4   1              0.9999 -0.0028              3        D                 B
S-SQDP4 1              0.9998 -0.0033 0.052 0.032  1        D   0             B
R-SQDP4 1              0.9996 -0.0049 0.015 0.009  1        D  99             B
QDP15   1  0.012 0.009 0.9985 -0.0345              3        D      ES       * B
S-QDP15 1              0.9985 -0.0349 0.076 0.048  1        D   0             B
R-QDP15 1              0.998  -0.0484 0.019 0.009  1        D  99             B
QDP14   1              0.9987 -0.0308              4        D               * B
S-QDP14 1              0.9986 -0.0308 0.024 0.015  1        D   0             B
C-QDP14 1  0.007 0.001 0.9985 -0.0347              1        D      ES         B
R-QDP14 1              0.9983 -0.0364 0.033 0.019  1        D  99             B
QDP12   1              0.9992 -0.0197              4        D               * B
S-QDP12 1              0.9991 -0.0216 0.038 0.017  1        D   0             B
C-QDP12 1  0.010 0.005 0.9991 -0.0201              1        D      ES         B
R-QDP12 1              0.9991 -0.0207 0.004 0.003  1        D  99             B
QA8     1              0.9986 -0.0333              3        D               * B
QA6     1              0.9987 -0.0290              4        D               * B
QA4     1              0.9992 -0.0186              3        D               * B
LR-QEP8 QEP8    R-QEP8  10.02810.0301   1948.1                         0.200  L
LQE8QA8 QEP8    QA8     10.00560.0060   9740.3                         0.049  L
LQE8SQ8 QEP8    SQDP8   10.00840.0090   6493.5                         0.090  L
LS-SQ8  SQDP8   S-SQDP8 10.01410.0150   3896.1                         0.018  L
LC-SQ8  SQDP8   C-SQDP8 13.38580.1350    249.9                         0.043  L
LR-SQ8  SQDP8   R-SQDP8 10.02110.0225   2597.4                         0.063  L
LQA8QD15QA8     QDP15   10.00650.0069   8441.6                         0.019  L
LS-QD15 QDP15   S-QDP15 10.01330.0113   5194.8                         0.008  L
LR-QD15 QDP15   R-QDP15 10.02710.0301   1948.1                         0.242  L
LQA8QA6 QA8     QA6     10.00530.0056  10390.                          0.029  L
LS-QEP6 QEP6    S-QEP6  10.02210.0182   3246.8                         0.019  L
LC-QEP6 QEP6    C-QEP6  13.38580.1351    249.9                         0.037  L
LR-QEP6 QEP6    R-QEP6  10.02210.0182   3246.8                         0.074  L
LQE6QA6 QEP6    QA6     10.007 0.0075   7792.2                         0.030  L
LQA6QD14QA6     QDP14   10.00940.0100   5844.2                         0.030  L
LS-QD14 QDP14   S-QDP14 10.02040.0225   2597.4                         0.019  L
LC-QD14 QDP14   C-QDP14 10.165 0.0936    639.8                         0.048  L
LR-QD14 QDP14   R-QDP14 10.02670.0227   2597.4                         0.112  L
LQA6QA4 QA6     QA4     10.00530.0056  10390.                          0.042  L
LQE4QA4 QEP4    QA4     10.007 0.0075   7792.2                         0.050  L
LR-QEP4 QEP4    R-QEP4  10.04220.0451   1298.7                         0.165  L
LQE4SQ4 QEP4    SQDP4   10.00940.0100   5844.2                         0.050  L
LS-SQ4  SQDP4   S-SQDP4 10.01410.0150   3896.1                         0.008  L
LR-SQ4  SQDP4   R-SQDP4 10.06950.0465   1279.6                         0.081  L
LQA4QD12QA4     QDP12   10.01690.0180   3246.8                         0.012  L
LS-QD12 QDP12   S-QDP12 10.02670.0227   2597.4                         0.024  L
LC-QD12 QDP12   C-QDP12 10.104 0.0476   1139.5                         0.038  L
LR-QD12 QDP12   R-QDP12 10.05340.0454   1298.7                         0.081  L
ES   1 1 100.   0 520.0   0 714.2   011  9.1  013 7.7   017 5.9   019  5.3  0  D
ES   123    4.3 025 4.0   0                                                  D
C8   1 1 100.   0 518.9   0 711.    011  5.9  013 4.7   017 3.4   019  3.   0  D
C8   123    2.3 025 2.1   0                                                  D
E9   1 1 100.   0 517.5   0 711.1   011  4.5  013 2.9   017 2.    019  1.   0  D
E9   123    0.9 025 0.8   0                                                  D
                                                                             E
```

Figure 68 - Data-File Used in The Simulation (Network Representation)

```
* H A R M A N  PROGRAM (V84:1)

CASE: Rete di competenza LaSapienza zone 4,6,8

TAB A2    OVERALL EFFECT ON SYSTEM  BUS  VOLTAGES   FOR
          HARMONIC CURRENTS INJECTED AT BUSSES:   #   5 C-QEP6      #  11 C-SQDP8     #  16 QDP15      #  21 C-QDP14
          #  25 C-QDP12                               ,  #
```

INFLUENCED BUS DATA		TELEPHONE INTERFERENCE FACTOR (UNREL.)	(VECTOR)	(CORREL)	TOTAL HARMONIC DISTORTION (UNREL.)	(VECTOR)	(CORREL)	M.H.D. (VECTOR)	MAX INDIV. HARMONIC VOLTAGE P.U.	HAR #	MAX HARMONIC CONTRIBUTION VOLTAGE P.U.	DUE TO BUS	HAR #
QEP6	R	22.51	48.88	48.88	.01423	.03091	.03091	.572E-01	.02314	5	.00655	QDP15	5
3	S	22.51	48.88	48.88	.01423	.03091	.03091	.652E-01	.02314	5	.00655	QDP15	5
.7KV	T	22.51	48.88	48.88	.01423	.03091	.03091	.491E-01	.02314	5	.00655	QDP15	5
	AVG	22.51	48.88	48.88	.01423	.03091	.03091	.572E-01					
SQDP8	R	22.48	48.81	48.82	.01421	.03088	.03088	.571E-01	.02312	5	.00655	QDP15	5
9	S	22.48	48.81	48.82	.01421	.03088	.03088	.651E-01	.02312	5	.00655	QDP15	5
.7KV	T	22.48	48.81	48.82	.01421	.03088	.03088	.490E-01	.02312	5	.00655	QDP15	5
	AVG	22.48	48.81	48.82	.01421	.03088	.03088	.571E-01					
QDP15	R	22.47	48.82	48.82	.01421	.03088	.03088	.571E-01	.02312	5	.00654	QDP15	5
16	S	22.47	48.82	48.82	.01421	.03088	.03088	.651E-01	.02312	5	.00654	QDP15	5
.7KV	T	22.47	48.82	48.82	.01421	.03088	.03088	.490E-01	.02312	5	.00654	QDP15	5
	AVG	22.47	48.82	48.82	.01421	.03088	.03088	.571E-01					
QDP14	R	22.49	48.83	48.83	.01422	.03089	.03089	.571E-01	.02313	5	.00655	QDP15	5
19	S	22.49	48.83	48.83	.01422	.03089	.03089	.652E-01	.02313	5	.00655	QDP15	5
.7KV	T	22.49	48.83	48.83	.01422	.03089	.03089	.491E-01	.02313	5	.00655	QDP15	5
	AVG	22.49	48.83	48.83	.01422	.03089	.03089	.571E-01					
QDP12	R	22.46	48.77	48.78	.01420	.03085	.03085	.571E-01	.02310	5	.00654	QDP15	5
23	S	22.46	48.77	48.78	.01420	.03085	.03085	.651E-01	.02310	5	.00654	QDP15	5
.7KV	T	22.46	48.77	48.78	.01420	.03085	.03085	.490E-01	.02310	5	.00654	QDP15	5
	AVG	22.46	48.77	48.78	.01420	.03085	.03085	.570E-01					
QA8	R	22.48	48.83	48.83	.01421	.03088	.03088	.571E-01	.02312	5	.00654	QDP15	5
27	S	22.48	48.83	48.83	.01421	.03088	.03088	.651E-01	.02312	5	.00654	QDP15	5
.7KV	T	22.48	48.83	48.83	.01421	.03088	.03088	.490E-01	.02312	5	.00654	QDP15	5
	AVG	22.48	48.83	48.83	.01421	.03088	.03088	.571E-01					
QA6	R	22.49	48.83	48.83	.01421	.03089	.03089	.571E-01	.02312	5	.00654	QDP15	5
28	S	22.49	48.83	48.83	.01421	.03089	.03089	.652E-01	.02312	5	.00654	QDP15	5
.7KV	T	22.49	48.83	48.83	.01421	.03089	.03089	.490E-01	.02312	5	.00654	QDP15	5
	AVG	22.49	48.83	48.83	.01421	.03089	.03089	.571E-01					
QA4	R	22.47	48.79	48.79	.01420	.03086	.03086	.571E-01	.02310	5	.00654	QDP15	5
29	S	22.47	48.79	48.79	.01420	.03086	.03086	.651E-01	.02310	5	.00654	QDP15	5
.7KV	T	22.47	48.79	48.79	.01420	.03086	.03086	.490E-01	.02310	5	.00654	QDP15	5
	AVG	22.47	48.79	48.79	.01420	.03086	.03086	.571E-01					

Figure 69 – THD and IHD Output Values

By analysing Figure 69 it is possible to highlight that:

- THD_V found in the network is between the uncorrelated and vector values (between 1.4% and 3.1%). In the crane measurement carried out on the QDP14 electrical panel, a THD_V of approximately 3.5% was found, a value in line with which calculated in the simulations;
- The IHD_V is in correspondence with the 5^{th} harmonic and is 2.3%. In the absence of resonances, it is logical to expect that the harmonic that causes the greatest disturbance is the highest in module. In the converters, the harmonic content table, i.e. the amplitude of the single harmonics decreases with the h order as 1/h, the highest component is the 5^{th} harmonic, equal to 20% of the fundamental. In all the analysed nodes, the source that makes the greatest harmonic contribution is the distorting load on the QDP15 electrical panel, which contributes with 0.6% on the 5^{th} voltage harmonic. Specifically, the converters present on the QDP15 absorb 2.5 A of the 5^{th} harmonic, such values are much higher than the other harmonic sources.

5.3.4 Simulink model for time varying non-linear load

To validate and test the Simulink Model, developed for time varying non-linear load simulation, it was not possible to use the measurement campaign carried out on the Cavour Aircraft Carrier, because the measurement was conducted at a certain power consumption (port operational profile). In order to validate the model, that allows to evaluate the harmonic distortion when a non-perfect knowledge of the loads, at any time of the day occurs, a seven day measurement campaign on an industrial plant was considered. In particular, an industrial plant with several load consumption variations a day was chosen. The validation is reported in ANNEX B.

Chapter VI: A New layout for an Integrated Power System Naval Unit-All Electric/Hybrid

6.1 Aims of the chapter [99]

The use of full-electric or hybrid diesel-gas turbines-electric systems on-board marine vessels is nowadays common [100]. Most cruise ships are all-electric, which means that they only use electrical propulsion drives with no mechanical coupling between the on-board generators and the propulsion drives. Some marine vessels, conversely, use diesel-gas turbines-electric propulsion systems. These vessels have both mechanical propulsion drives, which are used during long-range, constant-speed operations and electrical propulsion drives that are used for low-speed and manoeuvring operations. At present, marine vessels primarily run on an AC distribution system. However, there was an increasing interest in a shift towards a DC distribution system. The latter is driven by a potential improvement in efficiency, fuel saving, power quality and reduction in weight and volume of the electrical equipment [101]. The main reasons of interest are the evolutionary development in power electronic technology and the emergence of high-performance energy storage devices. In this context, DC power distribution technologies are a comeback; however, they are considered increasingly interesting for the research field and industrial applications. Maritime power systems can be traced back to the 1880s, starting with the earliest record of a DC-based on-board power system on the SS *Columbia*, where Edison's DC lighting system was first installed. In the last century, maritime power systems were greatly developed along with the increasing demand for on-board electrical loads. During this evolution, shipboard power transformed from a DC power system into an AC power system, as the use of electricity extended from the initial lighting to almost every aspect aboard a vessel where it was necessary to build upon the advances in the ac distribution infrastructure. In recent years, government regulation on emissions has become increasingly strict, while customers' fuel-efficiency requirements have risen. In recent studies, the current integrated power system research trend is turning to DC power distribution systems. This has resulted in advanced research outcomes in the DC microgrid field, especially in its advanced control, management' and optimization methods, all of which can be attributed to a wide body of all electric ship research. It is becoming clear that the DC power system has several major advantages over the AC system, and even some newly recognized advantages, such as:

- replacing bulky ferromagnetic transformers with compact power electronic converters;
- easier parallel connection or disconnection for DC power sources;
- use of variable speed diesel generators with fuel savings achievement;
- elimination of harmonic and imbalance problems;
- elimination of synchronization problems;
- elimination of reactive power flow.

The chapter aims to outline and evaluate new integrated power system architectures with the aim of defining their advantages and disadvantages. The analysis of new architectures will allow us to evaluate their performance in terms of reliability, power quality and technologically innovative solutions. The objective of the analysis will be the identification of solutions aimed at giving the on-board electrical system superior performance than those of the electrical systems previously implemented both civil and military ships. In detail, innovative solutions will be studied to obtain a high level of quality of the electricity supplied to users.
Three electrical system architectures have been proposed, elaborated according to the requirements for the new naval unit.

1. All electric MVAC - alternating current MV system;
2. All electric MVAC "hybrid" - MV system with alternating current with "islands" / electrical areas in direct current, MV and/or LV;
3. Hybrid Propulsion (Electric/Diesel/Gas Turbines) - MVAC alternating current MV system 50-60 Hz

Table 17 reports the main features and difference of three architectures proposed.

Table 17 – Main characteristic of the three architectures proposed

<table>
<tr><th>Architecture</th><th>Generators</th><th colspan="3">Propulsion</th><th>Voltage levels</th></tr>
<tr><td>1 – MVAC
(All electric)</td><td>4 Diesel + 2 Gas
turbines

121 MW</td><td colspan="3">All electric

90 MW
25 knot max speed

2 MW
manoeuvring thruster</td><td>11 kV
0.69 kV
0.44 kV
0.23 kV</td></tr>
<tr><td>2 – MVAC hybrid
with DC island
(All electric)</td><td>4 Diesel + 2 Gas
turbines

121 MW</td><td colspan="3">All electric

90 MW
25 knot max speed

2 MW
Manoeuvring thruster</td><td>11 kV
0.69 kV
0.44 kV
0.23 kV

5 DC island</td></tr>
<tr><td rowspan="2">3 – MVAC 50-60 HZ
Hybrid Propulsion
(Electric/Diesel/Gas
Turbines)</td><td rowspan="2">4 Diesel

26 MW</td><td colspan="3">Hybrid</td><td rowspan="2">6 kV
0.69 kV
0.40 kV
0.23 kV

2 x 50/60 Hz rotating
converters
0.44 kV
0.115 kV</td></tr>
<tr><td>Electric
5 MW
0-10 knot</td><td>Diesel
22 MW
10-18
knot</td><td>Gas
Turbines
74 MW
18-25 knot</td></tr>
<tr><td colspan="4">3.6 MW
Manoeuvring thruster</td></tr>
</table>

The integrated power system proposed must meet redundancy, power availability and reconfigurability requirements. An example of such kind of requirements is to supply still half of the propulsion power and ship services even in case of two flooded compartments. Another requirement is the maintenance of an adequate quality of on board energy supplied by the network to the loads, above all in the case of "sensitive loads". The aim is to combine the typical needs of a combat unit with the desire to make the management of IPS simple and intuitive, while at the same time ensuring a sufficiently low impact on the ship (in terms of dimensions and weights).

6.2 MV All electric ship

The choice of the type, number and size of generators is a key aspect of the shipboard power system design, involving many technical/economical requirements and variables. In turn, shipboard electric distribution networks can have a purely radial, “composite” radial, or ring structure. The 50 Hz IPS under investigation is based on 6 generators (four diesel generators and two gas turbines) with a 121 MW aggregate capacity:

- Nr. 2 Diesel Generators (Wartsila, 9L38, 6.3 MW rated power, 600 RPM);
- Nr. 2 Diesel Generators (Wartsila, 16V38, 11.2 MW rated power, 600 RPM);
- Nr. 2 Gas Turbines (GE, LM6000-PF, 43 MW rated power).

Table 18 shows the generated power for different ship operation profiles.

Table 18 - Total Power Demand as Function of Operation Profiles

Operation profile	Power [MW]	Generators (x2)	Load factor [%]
Manoeuvring thrusters	9.6	9L38	76
Navigation 8 kns, combat role	10.3	9L38	82
Navigation 16 kns, operational training role	33.7	16V38 9L38	96
Navigation 25 kns, operational training role	102.7	LM6000 16V38	95
Navigation 25 kns, combat role	103.0	LM6000 16V38	95
Maximum navigation, gait operational role	104.9	LM6000 16V38	97
Maximum navigation, gait combat role	105.2	LM6000 16V38	97
Amphibious operations	9.6	9L38	76

The structure of the two IPS proposals is fundamentally radial as regards the medium voltage section, and it is common to both architectures (All electric MVAC and MVAC "hybrid"). The 50 Hz radial distribution system has three voltage levels: 11 kV for primary distribution and propulsion, 0.69 kV for secondary distribution and supply of individual loads over 50 kW, and 0.44 kV for terminal circuits. The hypothesys is that the electrical devices deployed in the ship services are distributed similarly to those on the Cavour Aircraft Carrier.
Figure 70 shows the preliminary architecture of MV all electric ship.

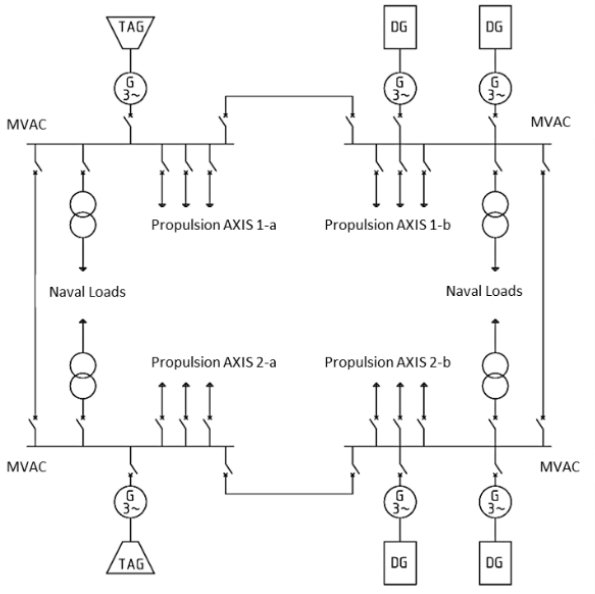

Figure 70 – Basic Architecture of MV All Electric Ship

The two proposals MVAC and MVAC "hybrid" layout differ in the electrical distribution to the ship services: in the first case, the secondary distribution is totally in alternating voltage, while for the second case there is a mixed alternating-continuous or even totally continuous distribution.
Figure 70 highlights the presence of the four separate power plants, with the arrangement of individual generators. These plants are also equipped with connection links. The architecture has a structure similar to a mesh, however the system cannot be used with all the connections closed.
Therefore, in every plant configuration is necessary to ensure at least one open junction switch. This is done in order to eliminate all design problems caused by the ring architecture (e.g. directional protection).

Propulsion Drive

The 90 MW, two-shaft propulsion system in Figure 71 is based on two 22 MW induction motors (IMs) per shaft. The propulsion system includes also two 1 MW manoeuvring thrusters. Each IM is fed by three separate Propulsion Drives (PDs), as shown in Figure 72. In order to ensure reliability in case of failures and combat damages each PD is interfaced to the 11 kV AC busbar via a transformer and a three-phase, 6-pulse diode rectifier. DC/AC conversion is performed by a five-phase PWM controlled voltage-source inverter.

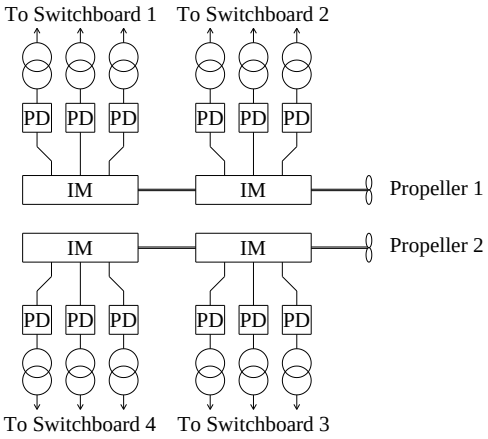

Figure 71 - Propulsion Architecture.

Transformer connections are chosen to ensure 24-pulse operation with all IMs in service. In case of loss of an IM on each shaft (propulsion power reduced to 50 %), a 12-pulse operation is ensured. It should be pointed out, however, that PDs are redundant and moreover the motors' multi-phase construction gives advantages, should one or more phases be lost. Appropriate control strategies allow the motor to operate at reduced power, with constant losses. It is also possible to keep the output torque at the pre-fault level but with an increase in losses of the propulsion system [102].

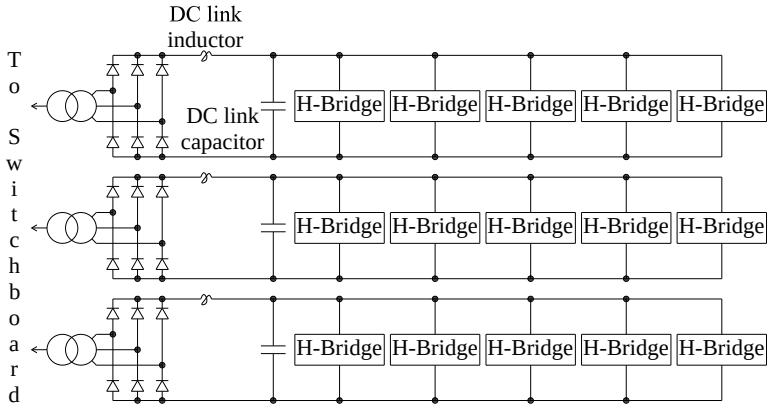

Figure 72 - Converter Topology of The Single Motor Drive

On the basis of preliminary studies the power required for electric propulsion motors as a function of ship speed is reported in Table 19 and Figure 73. This power was then increased by 10% to take into account weather and sea conditions as well as the dirt of the hull and propellers. Finally, the power absorbed at the busbars was obtained assuming a yield of the "electric chain" (efficiency of motor + drive) of 90%. Finally, Figure 74 shows the expected operating profile for the new vessel, which indicates the estimated percentage of the operating life based on which the ship navigates at a generic speed between 0 knots (ship moored in port) and speed maximum (25 knots).

Table 19- Power Required For Electric Propulsion Motors as a Function Of Vessel Speed

Ship speed [Knot]	Axis rotation speed [RPM]	Power [kW]	Power +10 % of Margin [kW]	Power Absorbed Bus-bar [kW]
6	62	2789	3068	3409
7	65	3696	4065	4517
8	68	4800	5280	5867
9	73	6129	6742	7492
10	78	7711	8482	9424
11	84	9571	10528	11698
12	90	11737	12911	14346
13	98	14236	15660	17400
14	106	17095	18805	20894
15	115	20341	22375	24861
16	125	24000	26400	29333
17	135	28100	30910	34345
18	145	32668	35935	39927
19	156	37730	41503	46115
20	166	43314	47645	52939
21	176	49446	54391	60434
22	186	56154	61770	68633
23	194	63465	69811	77568
24	200	71404	78545	97272
25	204	8001	88001	97778

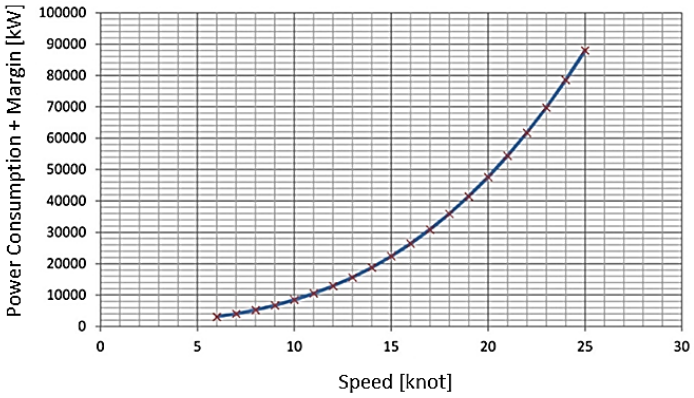

Figure 73 – Trend of Power Required For Electric Propulsion Motors as a Function of Vessel Speed

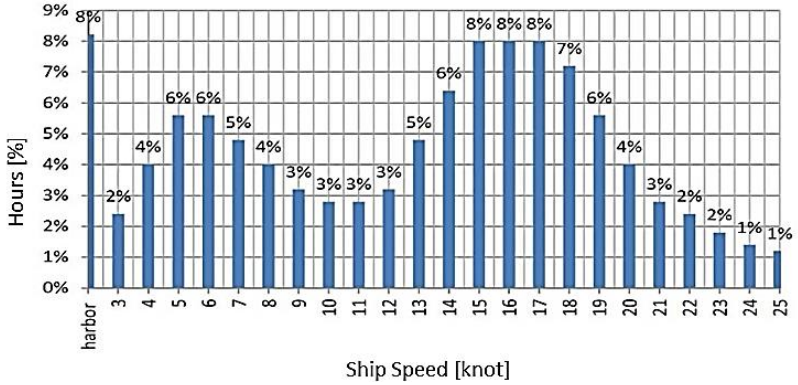

Figure 74 – Operating Profile Estimated For New Naval Unit (2500 Hours in Navigation and 720 Hours In Port)

As a requirement the Italian Navy is taking into account different filter configurations, that could be adopted for the generation of MV busbars [83], [103]. There is little literature on the design of passive filters applied to maritime power harmonics applications. The literature mainly covers the design of passive filters for ship propulsion drives [103], [104], [105], [106] and passive filter placement [107], [108], [109].

The filter types used in different network configurations are:

- High pass filter, with 12th harmonic cut-off frequency (HP);
- 11th and 13th harmonics single tuned filters (ST), plus high pass filter with a 24th harmonic cut-off frequency (HP+ST).

Figure 75 shows the basic configuration of filter configuration.

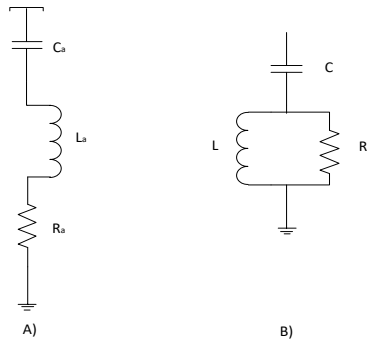

Figure 75 - A) Single Tuned Filter B) High Pass Filter

Filters sizing was obtained by means of the expressions shown in Table 20. Filtering around the 12th harmonics is meant to cope with the loss of half the propulsion power, entailing 12-pulse operation of front end converters.

Table 20 - Filter Sizing

ST FILTER	**HP FILTER**
$C=\frac{Q_i\cdot(h^2-1)}{\omega_0\cdot h^2\cdot V^2}$	$C=\frac{Q_i}{\omega_0\cdot V^2}$
$L=[(\omega_0\cdot h_0)^2\cdot C]^{-1}$	$L=[(\omega_0\cdot h_0)^2\cdot C]^{-1}$
$R=X/Q_M \qquad Q_M=20$	$R=Q_M\cdot X \qquad Q_M=2$
$PassBand=\omega_0/Q_M$	$PassBand=\omega_0/Q_M$

Q_M : quality factor	ω_0 : angular pulsation at frequency network
V : line voltage	Q_i : reactive power of single filter
C: capacitance	h_0 : tuned harmonic order
L: inductance	X : reactance at tuning frequency
R: resistance	

The QM factors of the filters have been chosen considering minimum joule losses, since the values of the damping resistors depend on this parameter. On the other hand, the filter bandwidth is inversely proportional to the QM factor, i.e. the frequency range centred on f_N whose frequency are a threshold value for which filter reactance is equal to resistance (impedance is $\sqrt{R}e^{\pm j\pi/4}$). Much higher is the QM factor and the more selective is the filter.
The sizing reactive power (Q_i) of each filter is computed as a part of the total reactive power (Q_c) required to increase the power factor (PF) of the overall system. In combat role, Q_c must be equal to 12.39 MVAr to improve PF from 0.8 to 0.85. The following configuration was taken into account during simulations:

- HP filters only: each of the four filter capacitors is sized for $Q_c/4$;
- Combined filters: reactive output equally subdivided between HP and ST filters (HP, $Q_c/8$ each; ST, $Q_c/16$ each).

Reactive power thus has been split on the four 11 kV generation busbars.

6.3 All electric MVAC - alternating current MV system

The first proposed layout, called "MVAC", is shown in figure VII.8.

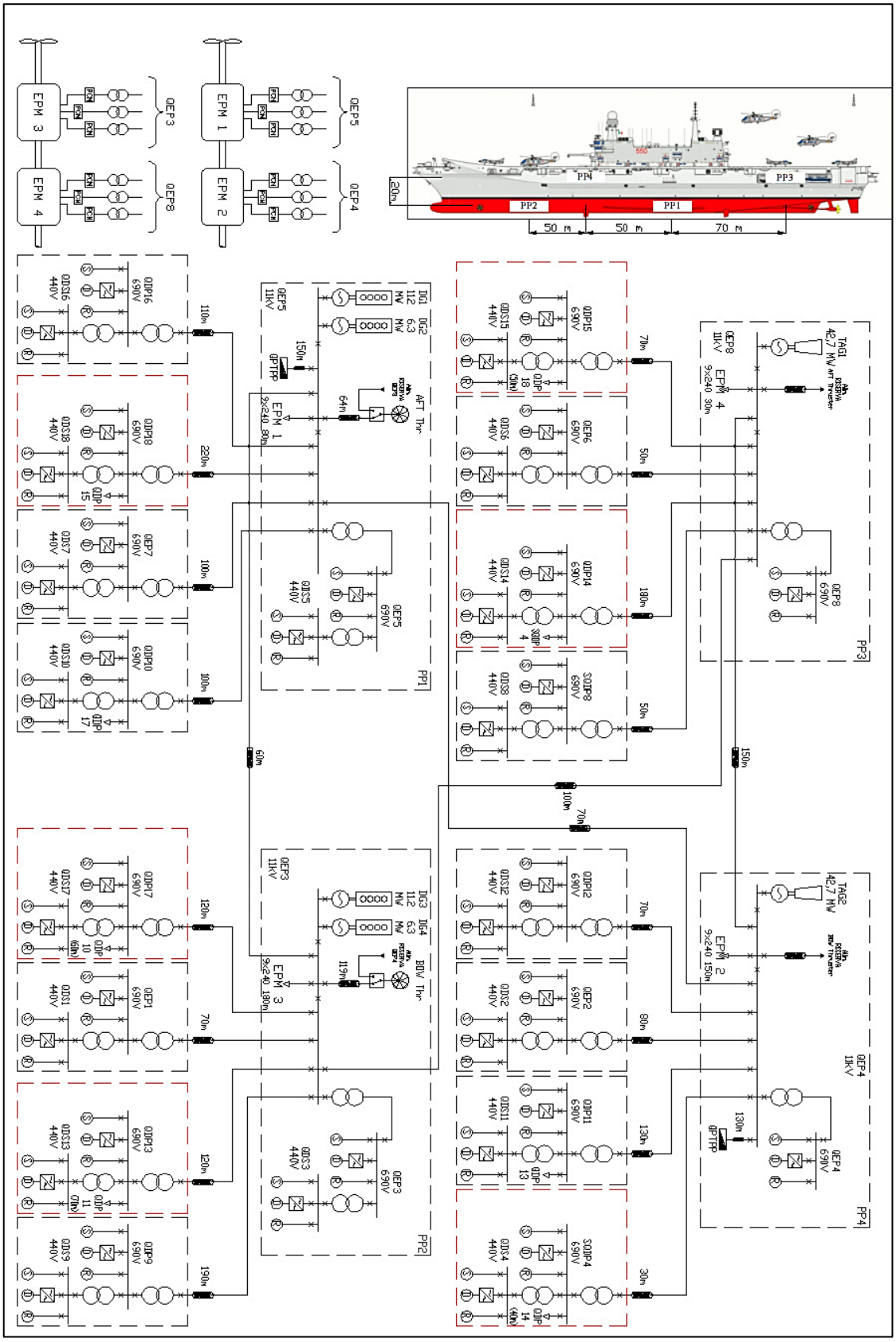

Figure 76 - All Electric MVAC - Alternating Current MV System Layout

Table 21 reports loads distribution, subdivided by electrical panels, for the MVAC layout. The power consumption is reported in combat condition at 25 navigation kns, when engines require maximum power and the electric equipment needs the highest reliability.

Table 21 – Loads Distribution for Each Electrical Subpanel In Combat 25 Knot Operation For MVAC

	Static loads		**Converter**		**Rotating**		**Total**	**Combat Role**		
	P [kW]	Q [kVAr]	P [kW]	Q [kVAr]	P [kW]	Q [kVAr]	S [kVA]	P [kW]	Q [kVAr]	S [kVA]
QEP1	121	31	618	261	291	142	1118	256	116	281
QEP2	36	19	688	301	423	182	1252	293	143	326
QEP3	232	91	1106	548	494	269	2044	498	265	565
QEP4					153	83	174	18	11	21
QEP5	96	16	361	68	145	29	612	66	19	69
QEP6	108	28	327	135	110	62	590	53	21	57
QEP7	128	79	1059	583	505	274	1934	502	278	574
QEP8	46	25	465	262	264	150	890	106	59	122
SQDP8	101	62	630	355	308	169	1192	36	22	42
SQDP4	41	25	212	128	100	60	412	70	44	82
QDP9	31	19	205	121	106	62	397	35	17	39
QDP10	112	70	660	385	267	157	1205	190	117	224
QDP11	66	41	452	289	152	89	790	9	5	10
QDP12	233	144	836	473	181	101	1442	218	132	255
QDP13	274	164	1047	555	123	61	1641	201	116	232
QDP14	140	81	895	534	391	244	1665	136	79	157
QDP15	336	215	1221	763	291	162	2171	648	428	777
QDP16	281	174	687	390	0	0	1120	197	119	230
QDP17	120	63	432	95	0	0	574	230	63	239
QDP18	107	66	224	130	42	20	432	170	102	198
QDS1	35	17	173	101	59	40	310	51	27	58
QDS2	27	11	219	129	92	61	393	61	32	68
QDS3	53	17	315	153	139	77	563	100	49	111
QDS4	42	3	380	176	132	76	610	146	60	158
QDS5	21	6	186	105	80	53	331	43	26	50
QDS6	19	11	175	104	51	35	288	41	22	47
QDS7	25	6	246	139	106	71	435	103	54	116
QDS8	58	29	335	199	138	91	620	88	49	101
QDS9	19	11	155	95	67	44	283	59	36	69
QDS10	9	4	93	53	25	17	147	21	11	23
QDS11	11	0	148	86	70	49	266	63	35	73
QDS12	24	17	114	72	30	21	201	45	30	54
QDS13	45	18	281	174	123	89	529	106	61	123
QDS14	48	23	258	154	85	61	458	87	47	99
QDS15	81	36	406	237	165	110	756	143	76	162
QDS16	33	12	165	94	59	42	297	72	39	82
QDS17	50	26	162	89	35	24	283	77	41	87
QDS18	17	11	119	73	45	29	214	53	33	62
Total	**Static loads**		**Converter**		**Rotating**		**Total**	**Combat Role**		
	P [kW]	Q [kVAr]	P [kW]	Q [kVAr]	P [kW]	Q [kVAr]	S [kVA]	P [kW]	Q [kVAr]	S [kVA]
	3223	1671	16056	8608	5848	3304	28638	5290	2882	6039

6.3.1 Normal operation (full propulsion power)

The distribution is 50 Hz in radial configuration with three voltage levels (specified in 6.2). The loads related to electric propulsion are divided as follows:

- two 1 MW thruster tunnels each, powered respectively by the 11 kV busbars of the QEP5 and QEP3 main electrical panels;

- four "Electric propulsion engines" (MEP), each powered by MV QEP3, QEP4, QEP5, QEP8 main electrical panels. With MEP users we mean the set of three three-phase lines derived from the MV busbars that feed the three transformer-converters groups of each MEP.

Two electrical panels have been placed in MV dedicated to the shore connection [110], necessary for the ship to be powered from the shore side during mooring at port, positioned in the QEP5 (stern area) and in the QEP4 (forward area).
4 electrical panels are directly connected with the bus-bars of each MV power generation plant installed in different rooms of the ship, in addition to the LV section of the central unit's QEP.
Four interconnections between power plants have been planned:

- two connected power stations where different power sources are installed, i.e. DG and TAG, and they are the Cross Connection 1 (connection QEP8-QEP3) and the Cross Connection 2 (connection QEP5-QEP4);
- two connected central units with homogeneous sources, i.e. DG with DG and TAG with TAG, and are Tie Connection 1 (connection QEP8-QEP4) and Tie Connection 2 (connection QEP5-QEP3).

By managing the interconnection lines, it is possible to cope with a relevant number of fault modes, achieving almost a double system redundancy. The two elements for which it was deemed necessary to guarantee a higher degree of safety are the two maneuvering thrusters.
During a system failure, reconfigurations are envisaged such as to restore service continuity, but in the event of a breakdown in the power supply line of the maneuvering propulsions inevitably a loss of engines occurs. To increase the degree of reliability, the system was set up to receive power from two distinct sources, namely:

- normal: power supply from QEP5 (Aft Thruster) and QEP3 (Bow Thruster);
- reserve: power supply from QEP8 (Aft Thruster) and QEP4 (Bow Thruster).

Upstream of the thrusters transformer[15], a switch selects the line that feeds the motors by means of manual intervention or the automation system.

6.3.2 Emerging operation (half propulsion power)

During ship operations, the main busbars, where the drives are connected, are coupled for various reasons, including the goal of reaching the maximum propulsion power available. Therefore, under "normal" conditions the drive has a 24-pulse network side reaction. In the event of a mechanical, or electrical failure, or a failure that entails up to 2 contiguous compartments, the requirement is to use half of the propulsion power. Therefore, in the hypothesis of losing 2 propulsion drives, the other two must continue to operate.
In this case, the network side reaction becomes 12 pulses (if the drives are suitably arranged in the various zones). Finally, in the event of an electrical fault that makes only one branch of an engine drive unusable (failure of one of the transformers, of one of the converters, or an entire stator winding of an engine), the drive must continue to operate. In this case, the main side will always have a 24-pulse response, but with an unbalanced load (one of the engines can absorb up to 2/3 of the power of the others). It is possible to compensate this event with appropriate control strategies, for example by reducing the power absorbed by the other motors to return to a balanced load.

[15] The maneuvering thrusters are fed by LV distribution through a special transformer upstream of the electronic drive

6.4 All electric MVAC "hybrid" - MV system with alternating current with "islands" / electrical areas in direct current, in MV and/or Low Voltage (BT).

The second layout proposed, called "MVAC hybrid", is shown in Figure 77.

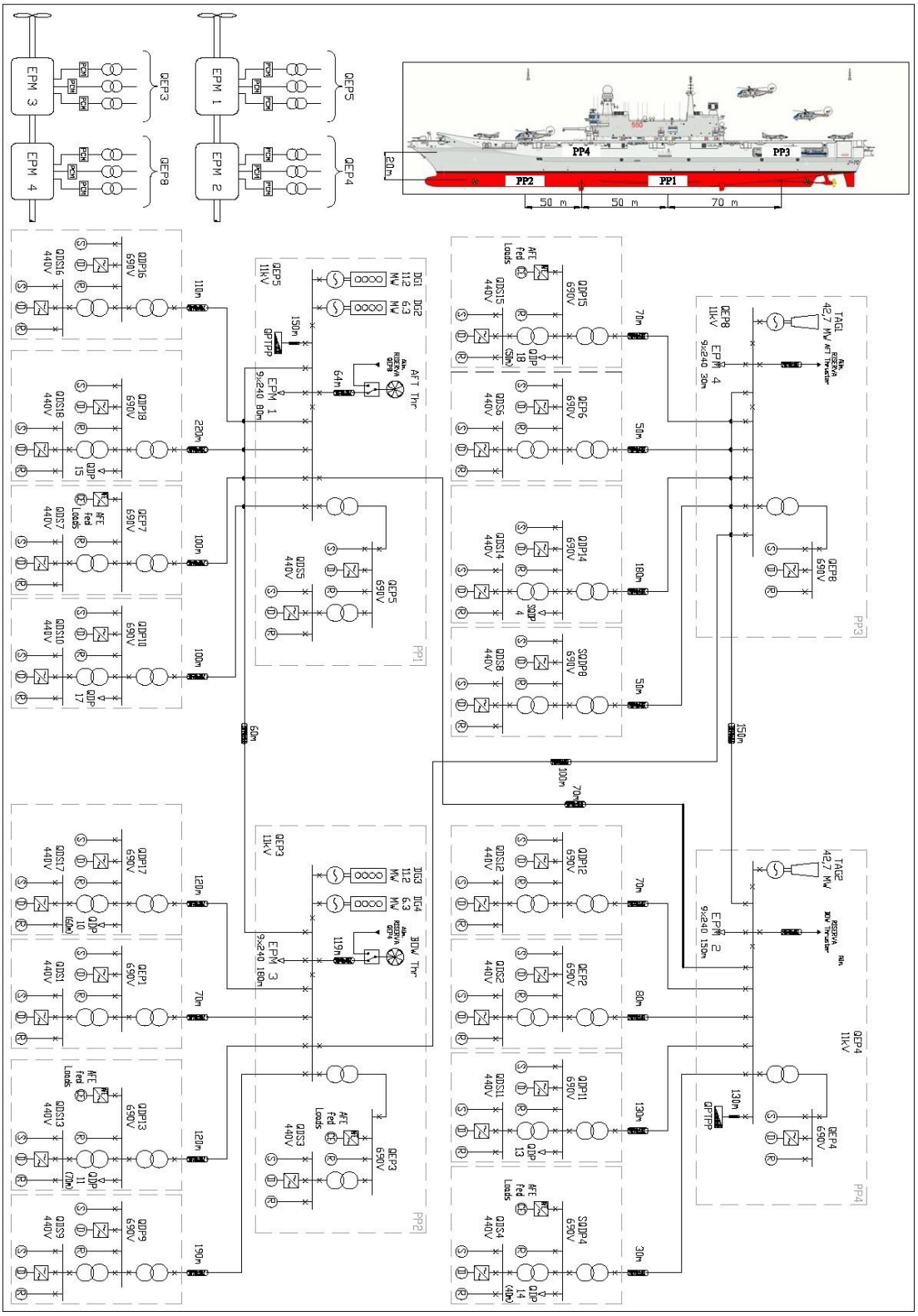

Figure 77 - All Electric MVAC "Hybrid" - MV System With Alternating Current With "Islands" / Electrical Areas In Direct Current, In MV and/or Low Voltage (BT).

Table 22 - Loads Distribution for Each Electrical Subpanel in Combat 25 Knot Operation For MVAC Hybrid

	Static loads		Converter		Rotating		Total	Combat Role		
	P [kW]	Q [kVAr]	P [kW]	Q [kVAr]	P [kW]	Q [kVAr]	S [kVA]	P [kW]	Q [kVAr]	S [kVA]
QEP1	121	31	618	261	291	142	1118	256	116	281
QEP2	36	19	688	301	423	182	1252	293	143	326
QEP3	1338	638	0	0	494	269	2044	498	265	565
QEP4					451	259	520	18	11	21
QEP5	96	16	361	68	145	29	612	66	19	69
QEP6	108	28	327	135	110	62	590	53	21	57
QEP7	1187	1642	0	0	505	274	2556	502	278	574
QEP8	46	25	714	410	430	249	1373	78	44	90
SQDP8	101	62	630	355	308	169	1192	36	22	42
SQDP4	658	404	0	0	77	46	862	70	44	82
QDP9	31	19	205	121	106	62	397	35	17	39
QDP10	112	70	660	385	267	157	1205	190	117	224
QDP11	66	41	452	289	152	89	790	9	5	10
QDP12	233	144	836	473	181	101	1442	218	132	255
QDP13	1321	719	0	0	123	61	1641	201	116	232
QDP14	320	180	787	474	319	204	1665	136	79	157
QDP15	1547	950	0	0	349	202	2218	648	428	777
QDP16	281	174	687	390	0	0	1120	197	119	230
QDP17	209	110	343	157	0	0	613	230	111	256
QDP18	327	189	46	28	0	0	432	170	102	198
QDS1	35	17	173	101	59	40	310	51	27	58
QDS2	27	11	219	129	92	61	393	61	32	68
QDS3	53	17	315	153	139	77	563	100	49	111
QDS4	42	3	380	176	132	76	610	146	60	158
QDS5	21	6	186	105	80	53	331	43	26	50
QDS6	19	11	175	104	51	35	288	41	22	47
QDS7	25	6	246	139	106	71	435	103	54	116
QDS8	58	29	335	199	138	91	620	88	49	101
QDS9	19	11	155	95	67	44	283	59	36	69
QDS10	9	4	93	53	25	17	147	21	11	23
QDS11	11	0	148	86	70	49	266	63	35	73
QDS12	24	17	114	72	30	21	201	45	30	54
QDS13	45	18	281	174	123	89	529	106	61	123
QDS14	48	23	258	154	85	61	458	87	47	99
QDS15	81	36	406	237	165	110	756	143	76	162
QDS16	33	12	165	94	59	42	297	72	39	82
QDS17	50	26	162	89	35	24	283	77	41	87
QDS18	17	11	119	73	45	29	214	53	33	62
Totale	**Static loads**		**Converter**		**Rotating**		**Total**	**Combat Role**		
	P [kW]	Q [kVAr]	P [kW]	Q [kVAr]	P [kW]	Q [kVAr]	S [kVA]	P [kW]	Q [kVAr]	S [kVA]
	8753	5719	11286	6081	6232	3544	30626	5262	2916	6024

6.4.1 Normal operation (full propulsion power)

Compared to the previous layout (MVAC), 5 electrical panels have been identified, they are characterized by high power absorption (QEP3, QEP5, QDP13, QDP15) and by sensitive/essential loads (SQDP4), which will be defined as DC islands. These network sections are interfaced with the alternating current network through active front ends converters, characterized by sinusoidal absorption which allows energy recovery in the network. The utilities contained in the grouping of the distorting loads were inserted into the static loads, making the disturbances produced by the six-phase converters disappear. The other part of the system remains unchanged, including voltage

values based on the module and phase of the voltage, since the power balance at the nodes of the network remains unchanged.

6.4.2 Emerging operation (half propulsion power)

Also in this case the system will be analysed in the hypothesis of loss of propulsion power equal to 50% of the total. In particular, since the propelling engines are directly connected to the axis line in a compound tandem configuration, the loss of one of the two engines on both shafts (for example the loss of EPM1 and EPM3, or alternatively EPM2 and EPM4) will be taken into consideration. The scenario in which both axis lines maintain 50 % of the propulsion power does not provide for any countermeasures to be taken to compensate for this situation, with the exception of the different distribution of power between the power plants to be taken into account. In the event of loss of two motors of the same shaft line, besides the need for changing power distribution on board, the asymmetric thrust on the ship must also be compensated (one of the two propellers is driven, while the other is blocked in a position of lower drag or drag drag) by means of corrective actions of the rudders, thus decreasing the overall efficiency.

6.4.3 DC island

The "traditional" low voltage DC island topology is shown in Figure 78 and includes: i) a FEC used to interface the AC grid, ii) two DC/DC converters to connect an Energy Storage System (ESS) and a Power Storage System (PSS) to the DC grid and iii) other DC/DC converters to adapt feeder voltages to DC loads. The presence of ESSs and PSSs ensures both energy and power performances and improves the continuity and quality of the supply to the DC network. In fact, they can to counteract the loss of the AC grid and/or DC grid power unbalances, due to load steps, i.e. pulsating or impulsive loads. In addition, they permit to decouple the AC grid from DC islands, as demonstrated by experimental tests [111].
DC loads and storage systems, whose operating voltage generally differs from that of the DC island, are interfaced to the DC micro-grid through DC/DC converters: due to the characteristics of storage devices, converters usually "boost" towards the grid. Depending on the type of FEC and DC/DC converters, faults occurring in the DC micro-grid might damage power semiconductors so they must be cleared in a short time. Since circuit breakers suitable for this application are not available on the market yet three main design solutions to avoid semiconductor damage in case of DC faults are (at least in theory) considered,: i) over-dimensioning of converter power semiconductors, ii) installation of static circuit breakers downstream of converters and iii) introduction of a new DC grid configuration, based on multi-port DC/DC converters (MPDCCs).
Systematic over-dimensioning of converters would involve a substantial increase in costs, whereas studies on static suitable circuit breakers are still in progress and their installation would decrease the efficiency of the DC island, because of breakers conduction losses.

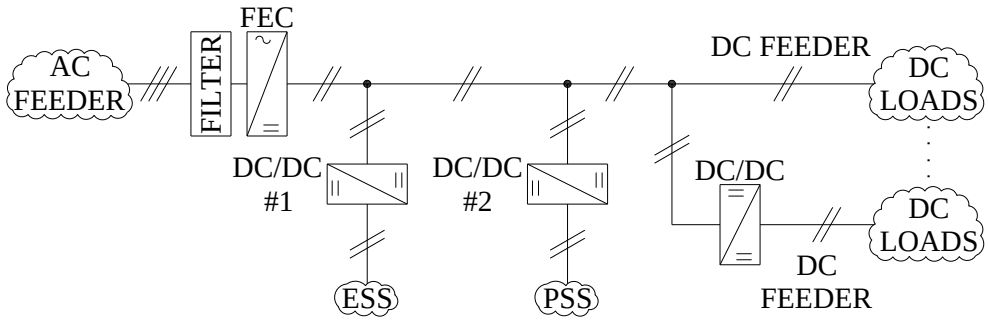

Figure 78- Traditional DC Island Topology.

The installation of multi-port DC/DC converters seems, however, very promising. The new system structure is shown in Figure 79 The FEC, storage systems and DC feeders are connected to the MPDCC, which acts as a power router and also protects the micro-grid: in [112] - [113] some of the Authors propose a topology of such converter. Its control strategy permits to manage power flows during normal working conditions as well as limit fault currents, avoiding damages. Ports connected to the storage systems and the FEC are controlled by means of voltage droop algorithms, while DC feeders ports are managed in order to regulate their voltages according to DC loads requirements. The MPDCC itself is bi-directional, so the installation of a four quadrant FEC would extend the benefits of the storage systems also to the AC system upstream.

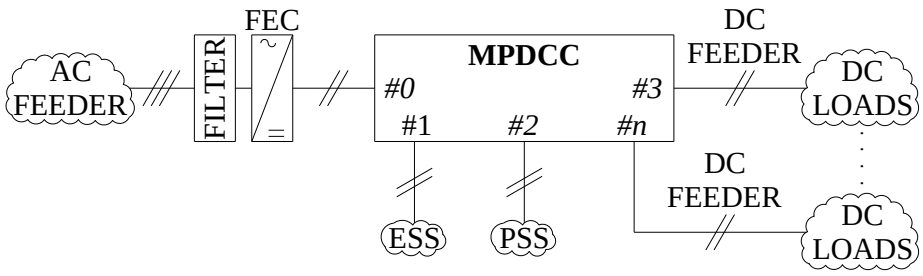

Figure 79- DC Island Topology Including The MPDCC.

High standards are required for supply continuity, especially for military applications. Consequently, the Zonal Electrical Distribution Systems (ZEDSs) can be adopted to supply DC islands and achieve quality, reliability and redundancy levels [114] - [115]. The distribution system can be compartmentalized, with different feeders supplying separate zones (each corresponding to a DC microgrid) of the ship (the first division between zones being e.g. port and starboard), to minimize the effects of faults and battle damages. If "Zones" (i.e. the relevant DC microgrids) are supplied by AC feeders, the AC/DC conversion is distributed; DC supply implies, in turn, centralized AC/DC conversion. The former trades off higher reliability with increased costs.

A potential AC/DC distributed conversion topology is shown in Figure 80. Each zone can be supplied by MV or LV AC feeders, depending on the DC island rated power. The AC MV to DC LV conversion must be achieved by means of AC/DC converters with isolating transformers, for security and MPDCC optimal functioning reasons. Otherwise, traditional FECs can be installed for LV AC/DC conversion. The latters require zero-sequence current control, in order to limit loop currents among different islands.

Within the DC microgrid, loads not requiring the highest level of the quality of service (QoS) are fed by only one MPDCC port. On the other hand, uninterruptible DC loads are connected to two MPDCCs through the auctioneering diodes D_{ik3} and D_{jk3} installed at the positive poles. It must be highlighted that this kind of utilities can be simultaneously supplied by both DC feeders with a different load factor. This operation modality is possible thanks to the implementation of a voltage droop control also for the MPDCC ports number 3 in Figure 80. At the steady-state, uninterruptible DC loads are operated at a voltage that depends on the intersection of these voltage droop curves. These mathematical functions can be changed by the DC island supervisor, in order to manage power flows. Auctioneering diodes are necessary to decouple the two DC feeders, improving the continuity of loads supply.

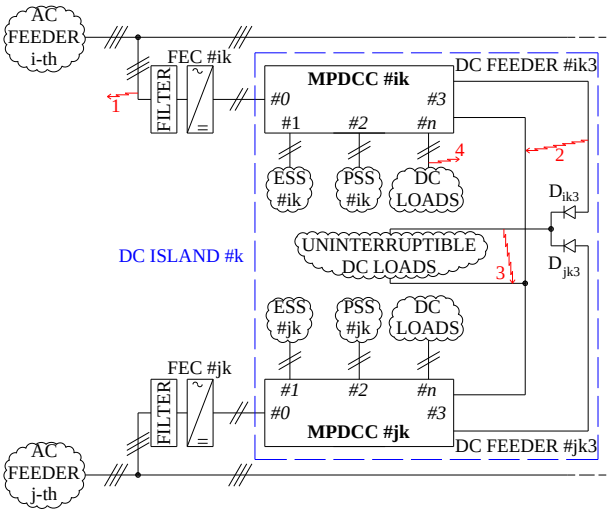

Figure 80 - Proposed K-Th DC Island Topology In A ZEDS And Including Mpdccs.

It is important to analyse system behaviour in case of line-to-line faults; Figure 80 shows some studied fault locations. Ground faults have not been taken into account, because the overall distribution system is usually operated with ungrounded or high-resistance grounded neutral, to improve the continuity of supply. The same practices are also adopted for DC islands, where they also help reducing corrosion phenomena.

Case 1 represents a fault that occurs at the AC feeder. This event would not interrupt the supply of any DC load, thanks to storage systems, and only affects the AC part of the plant.

Case 2 shows a fault at the DC feeder, upstream of auctioneering diodes. This fault would reduce the voltage of the affected feeder, making the relevant auctioneering diode inversely polarized. In this situation, uninterruptible DC loads would be supplied only by the other grid; the system must be properly designed in order to limit the ensuing voltage dip to acceptable values (usually, the maximum admissible voltage variation is ± 10 % of the rated voltage). The power exchange between all ports of the relevant MPDCC would not be possible until the tripping of the protection device installed downstream of port number 3. Communication between the MPDCC supervisor and all protection devices would lead to a faster fault clearance. This consideration is also valid for cases 3 and 4.

Case 3 represents a fault downstream of auctioneering diodes, which would have severe consequences, in that it would stop the supply to uninterruptible DC loads. As for case 2, the power exchange between all ports of both MPDCCs is not possible until the tripping of protection device(s) installed downstream of port number 3.

Finally, Case 4 shows a fault at a port supplying “standard” DC loads. Again, this event would stop the power exchange inside the MPDCC till relevant protection device would trip. During this period, uninterruptible DC loads would be supplied only by the other MPDCC.

6.5 Definition and characterization of a "hybrid" propulsion naval unit

A hybrid layout, different from the one presented before, is proposed; in particular, propulsion is entrusted to two aft propellers, which can be moved either by means of electric motors (electric navigation) or diesel and gas turbines (trims at maximum speed). In this case, the power consumption by propulsion drive is much lower than the MVAC and MVAC “hybrid” layouts presented in section 6.2.

Considering this new layout, a new electric balance and operational profile was delivered by the Italian Navy. Therefore, this chapter presents a completely different architecture as compared to the one outlined before.

Generation system

The ship is equipped with four diesel generators (DDGG) with a nominal power of 6.52 MVA each. The alternators feed the medium voltage network at 6 kV, 50 Hz via the main electrical panels located at stern and bow of the ship. The variability of the electric load, due to the different operating conditions, involves the partial use of the 4 generating units. In particular, we move from the connection of a single diesel generator group during "port" operation, to 3 diesel generators in the operational profiles in which the electric propulsion is fundamental. In all other settings, two DDGG groups are sufficient at the same time.

Distribution system

The distribution system is a 6 kV-50 Hz medium voltage network, the LV network has multiple voltage levels (690 V, 400 V, 230 V) and a 440 V grid, 115 V at 60 Hz (STANAG[16]), to power military equipment, such as weapon and command and surveillance systems. STANAG network is connected to the 6 kV network by means of two 50/60 Hz rotating converters. Table 23 shows the voltage levels for the various types of load areas.

Table 23 – Voltage Levels

Electric propulsion	6kV 50 Hz 3ph
Engines for propulsion	690V 3ph
Pumps/air conditioning	690V 50 Hz 3ph
Laundry, Hospital, Workshop	400V 50 Hz 3ph
Light and LV service	230V 50 Hz 1/3ph
Weapon equipment	440 V-3ph 60 Hz 115 V 3ph o 1ph 60 Hz 24 V DC
Communication, control and monitoring	230 V 50 Hz 115 V 60 Hz 24 V DC
Navigation systems	230 V 50 Hz 115 V 60 Hz 24 V DC
Aircraft support	200/115 V 400 Hz

The neutral distribution of the three-phase systems is differentiated according to the voltage level. In particular:

- 6kV, neutral point to ground via high resistance;
- 690, 440, 115 V, isolated neutral point;
- 400 - 230 V, neutral point directly to the ground. It is insulated for essential loads.

Propulsion and manoeuvring system

Two aft propellers ensure propulsion, they can be operated either by electric engines (from 0-10 knot), or by Diesel engines (10-18 knot) and gas turbines (18-25 knot maximum speed). Electric propulsion is driven by the action of two 2.25 MW asynchronous motors (one per shaft line). These are powered by static converters at 690 V and absorb 5 MW average power; the efficiency of these converters is 0.90. These engines can also operate in PTO (power take off) configuration with a generation capacity of 2,186 MW each one. Two Diesel engines (each of 11 MW per shaft line) provide the propulsion in a middle range speed, optimizing consumption. Two Gas turbines (each of 37 MW per shaft line) allow to rush to maximum speed.

[16] A Standardization Agreement (STANAG) is a NATO standardization document that specifies the agreement of member nations to implement a standard, in whole or in part, with or without reservation, in order to meet an interoperability requirement.

There are also three manoeuvring propellers, two at the bow (2.2 MW each) and one at the stern (1.35 MW). Considering yields and contemporaneity coefficients during tight manoeuvres, two engines absorb an average power of 3.83 MW and one engine 1.13 MW respectively.
Table 24 shows the main data concerning generation, propulsion, maneuver, converters and transformers.

Table 24 - Main Characteristics of Power Generation, Propulsion, Maneuvering, Rotary Converters and Transformers

4 DDGG	6520 kVA 6 kV 50 Hz Cosfi 0.8	Unit in operation: 1 in port 3 navigation totally electric (10knt) 2 other operation profiles
2 Asynchronous engines for propulsion / generation	2250 kW propulsion 2186 kW generation Converter 690V 50 Hz	Power consumption of 5 MW during navigation totally electric 1.46 MW maneuvering Efficiency of converter 0.90
2 Diesel for propulsion	11000 kW	Power consumption of 22 MW from 10 to 18 knot
2 Gas Turbines	37000 kW	Power consumption of 74 MW from 18 to 25 knot
2 Propeller engines for maneuvering	2200 kW	Power consumption 3.83 MW Efficiency = 0.92 Contemporary factor = 0.8
1 Stern maneuver propeller engine	1350 kW	Power consumption 1.13 MW Efficiency = 0.95 Contemporary factor= 0.8
2 Rotary converters 50/60 Hz	Power 1.5/2.8 MW (to define) Power factor 0.8	Efficiency fra 0.86-0.89
8 MV/LV transformers	2 Mvz1 2.1 MVA 2 Mvz2 4.1 MVA 2 Mvz3 4.6 MVA 2 Mvz4-5 1.5 MVA	Efficiency= 0.98 Vcc 7%

Main electric loads

Table 25 shows the main relevant electrical loads in terms of absorbed power.
The table shows the nominal power (NP), the power absorbed (AP), the units in operation and the respective coefficient of contemporaneity (fco).

Table 25 - The Main Relevant Electrical Loads In Terms Of Absorbed Power

	Rete 690v 50 Hz	**NP [kW]**	**AP [kW]**	**N**	**Note**
200 propulsion					
4	233 lubricating pump backup MMTTPP	107	118.89	2	Not present in any operational profile
5	223 water preheating	206	223.9	2	Fco 0.1
12	234 starter motor TG	96	96	2	2/2 maximum speed (fco 0.05)
17	234 cooling fan TG	200	215.05	2	2/2 maximum speed (fco 1)
23	241 stand-by pump lubricating gear reducer	63	70.79	2	Only during maneuvering (fco 0.5)
26	245 pump for propeller pitch	90	96.77	4	In navigation
30	264 engine oil heating	65	65	2	2/2 only in operational profile (fco 0.6)
33	Engine oil purifier heating	60	60	2	2/2
41	E/P diesel propulsion	90	97.83	6	4/6 only in operational profile
42	256 sea water pump DDGG bow and stern	55	60.44	6	3/6 when electrical propulsion is in operation 2/6 in other operational profile
	300 users				
16	330 light	252	252.32		Average Power 158kW
22	water preheater	81	88.04	4	2/4 with fco 0.10 1/4 in combat operational profile (fco 0.10)
400 command					
7	474 magnetic compensation system	350	402.33	1	Not for port operational profile (fco 0.7)
500 aux/maneuver					

1	E/P fire pump	200	212.77	6	
2	524 sea water pump aux	35	38.89	2	2/2 for each operational profile fco 1 (0.5 port)
3	524 sea water pump aux	35	38.89	2	2/2 for each operational profile fco 1 (0.5 port)
17	531 reverse osmosis desalinator	21	22.83	5	4/5 Not for port operational profile (fco 1)
33	551 compressor 350bar D/G	55	60.4	4	2/4 (fco 0.8 in combat operational profile)
42	593 waste treatment	75	82.42	2	1/2 with fco 0.25
49	561 rudder	100	106.38	4	4/4 (fco 0.6 in combat and maneuvering operational profile)
50	565 stabilizer fins	110	120.88	2	2/2 in navigation (fco 0.4)
56	572 crane 20 t	75	81.52	2	Fco 0.2 in port otherwise 0.1
58	575 stern ramp	200	224.72	1	Only in port
59	581 hydraulic units –bow	95	103.26	2	1/2 in maneuver
60	581 hydraulic unit CN	55	60.4	2	1/2 in maneuver
61	581 hydraulic units –stern	80	87.91	2	1/2 in maneuver
62	Crane boats 15m	65	70.65	2	2/2 only in port
69	589 elevator - bow	400	425.53	1	Fco 0.2 in combat operational profile, 0.1 otherwise Switch off during maneuver
70	589 elevator -stern	400	425.53	1	Fco 0.2 in combat operational profile, 0.1 otherwise Switch off during maneuver
73	589 elevator for food	80	87.91	1	Not in combat operational profile
74	589 elevator garage/hangar	120	131.87	1	Only at port
75	Munitions elevator - bow and stern	150	166.67	2	Only at port
500 air conditioning (summer)					
6	513 garage puller	55	64.71	4	2/4 in operation
7	513 garage puller reversible	55	64.71	2	2/2 in operation
8	513 hangar puller	37	43.53	4	4/4 in operation
9	513 hangar puller	44	51.76	4	4/4 in operation
10	514 fridge groups	390	402.06	8	During the summer 4/8 (5/8 humanitarian mission) (fco 0.76/0.82)
11	514 sea water pump	32	33.56	8	During the summer 4/8 (5/8 humanitarian mission)
12	514 pump refrigerator water	80	88.89	8	During the summer 4/8 (5/8 humanitarian mission)
13	514 air handling units	470	552.94	1	
14	514 extractor	131	154.12	1	
15	514 fan coils	171	213.75	1	
18	514 room ventilation	494	581.18	1	
500 air conditioning (winter)					
6	513 puller garage	55	64.71	4	2/4 in operation
7	513 garage puller reversible	55	64.71	2	2/2 in operation
8	513 puller hangar	37	43.53	4	4/4 in operation
9	513 puller hangar	44	51.76	4	4/4 in operation
10	514 fridge groups	390	402.06	8	During the winter 2 (fco 0.4 in combat operational profile)
11	514 sea water pump	32	33.56	8	During the winter 2/8
12	514 pump refrigerator water	80	88.89	8	During the winter 2/8
13	514 air handling units	470	552.94	1	in maneuver
14	514 extractor	131	154.12	1	
15	514 fan coils	171	213.75	1	in maneuver
18	514 room ventilation	494	581.18	1	Fco 0.9
19	514 humidificator system	799	799	1	Only in winter (fco 0.95) 683kW Average power
20	514 electric heater	163	163	1	Only in winter (fco 0.85)
29	517 hot water pump	25	27.78	4	During the winter 3 - 83.33kW Average power
600 mounting					
8	651 kitchens	190.6		1	Reserve
9	651 kitchens	380.9		1	137kW Average power
19	652 hospital 400v	-	100.6	1	54 kW Average power
20	655 laundry	263.4	280.21	1	100kW Average power 126kW di Average power in humanitarian mission
Rete 440v 60 Hz					Rotating converters supply STANAG network they start in 3steps, with absorption steps of 545 kVA spaced 10-15 s or 30 sec The minimum power factor is 0.8 It is possible for guns and firearms to operate at the same time, while all other loads are fully operational
400 communication and security					
1	411 CMS CSS		74.2		always in operation
5	441 commununication		354		always in operation (fco 0.5 in combat operational profile)

8	453 radar dbr x		228		fco 0.7 5 in combat operational profile 228 kVA not in emission 250 kVA in emission (200usec) T= 1.34ms Minimum power factor = 0.8
9	453 radar dbr c		448		fco 0.7 in combat operational profile 448 kVA not in emission 518 kVA in emission (200usec) T= 1.34ms Minimum power factor = 0.8
10	453 radar early - AESA L		250	1	fco 0.7 in combat operational profile 250 kVA not in emission 450 kVA in emission (200usec) T= 1.34msec Minimum power factor = 0.8
21	400 GFE item		67	-	fco 0.4 in combat operational profile e fco 0.5 in amphibious operations) power absorbtion step: 10 kVA every 10 s Minimum power factor = 0.8
700 weapons system					
2	711 MCG guns		80	3	fco 0.8 in combat operational profile 50 kVA DC motor for per handling load: 135 kVA inrush; 20-25kVA basic; 42 kVA pressure restoring 10 second for the start of two successive guns
4	721 anti-missile defense		50	1	fco 0.8 in combat operational profile

6.5.1 Network architecture

Figure 81 shows the network layout with diesel generator, main electrical panels, propulsion engines, manoeuvring thruster, rotary converter and main 50-60 Hz distribution systems.

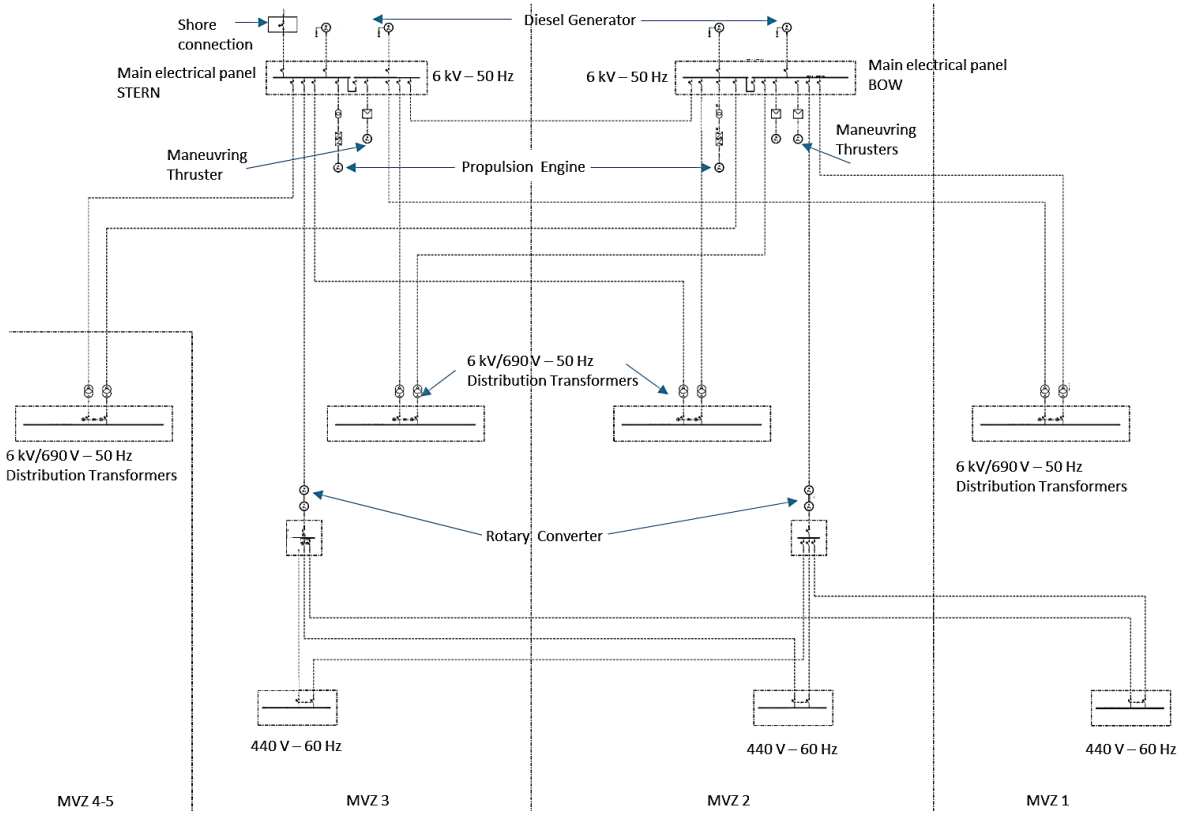

Figure 81 – Network Layout

6.5.2 50 Hz network - load conditions

The paragraph shows the classification and characterization of ship loads, for different voltage and frequency levels. In relation to the electric balance of the various operational profiles of the ship, the power absorptions of the various loads installed on board are specified. Operational profiles taken into account are referred to the summer season electrical balance. Table 26 shows the operational profiles the ship.

Table 26 – Operational Profiles

Operational Profiles	Number
Port	1
Port Operational Role / Training	2
Humanitarian Mission	3
Maneuver	4
Navigation (10 knots) Operational Role / Training with Electric Propulsion	5
Navigation (16 nodes) Operational Role / Training	6
Navigation (18 knots) Operational Role / Training	7
Navigation (Maximum Speed) Operational Role / Training	8
Anchor Ship Operational Role / Training	9
Navigation (10 knots) Role Combat with Electric Propulsion	10
Navigation (Maximum Speed) Combat Role	11
Amphibious Operations Combat Role with Electric Propulsion	12

Figure 82 shows the total power absorbed at 6 kV - 50 Hz bus-bars, Bow and Stern, including losses, project margins (10%) and growth (5%). It ranges from a minimum of 4.382 kW for the first operational profile, “Port”, to a maximum of 14.032 kW for the Navigation (10 knots) Combating Role with Electric Propulsion.

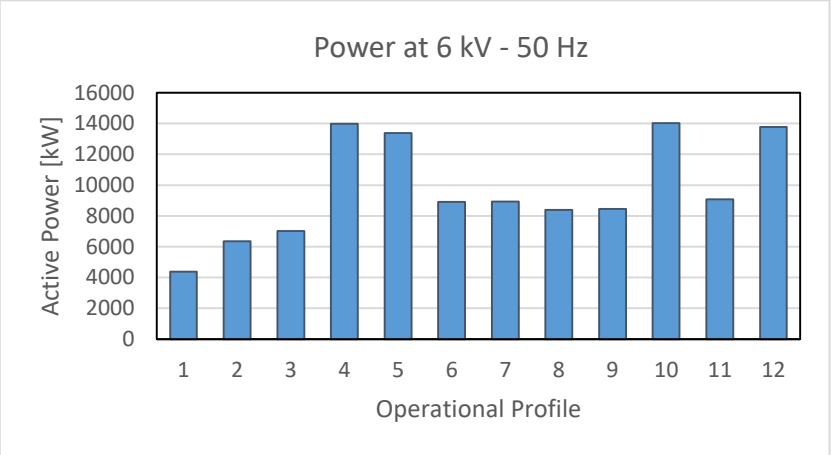

Figure 82 – Active Power Consumption

It is possible to highlight how the absorption for some operational profile is similar to others. It was therefore decided to group the operational profiles of the ship based on similar power absorption. Table 27 shows the five operational profiles of the ship, grouped as follows:

- Operational profile A1: Port (4.382 kW);
- Operational profile A2: Port Operational Role/Training (6.351 kW), Humanitarian Mission in Port (7.010 kW);
- Operational profile A3: Navigation (16 knots) Operational Role/Training (8.919 kW), Navigation (18 knots) Operational Role/Training (8.925 kW), Navigation (Maximum

Speed) Operational Role/Training (8.397 kW), Anchor Ship Operating Role/Training (8.459 kW), Navigation (Maximum Speed) Combat Role (9.081 kW);

- Operational profile A4: Navigation (10 knots) Operational Role/Training with Electric Propulsion (13.383 kW), Navigation (10 knots) Combating Role with Electric Propulsion (14.032 kW);
- Operational Structure A5: Maneuverer (13.993 kW), Amphibious Operations Combat Role with electric propulsion (13.785 kW).

The operational profiles A4 and A5 show similar power absorption but different load features, in particular, the use of the bow and stern thrusters in A5, led to the following further division.

Table 27- Operationl Profile Grouped

Operational profile subdivided for power consumption	Number
A1	1
A2	2 – 3
A3	6 – 7 – 8 – 9 – 11
A4	5 – 10
A5	4 – 12

Figure 83 shows the total power absorbed at 6 kV - 50 Hz for grouped operational profile.

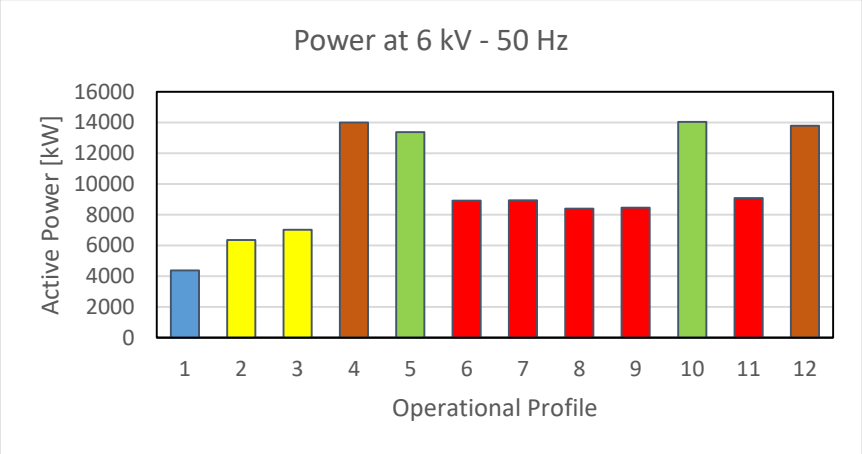

Figure 83 - Power Absorbed At 6 kV - 50 Hz for Grouped Operational Profile.

Figure 84 shows the power absorbed by Ventilation and Conditioning.

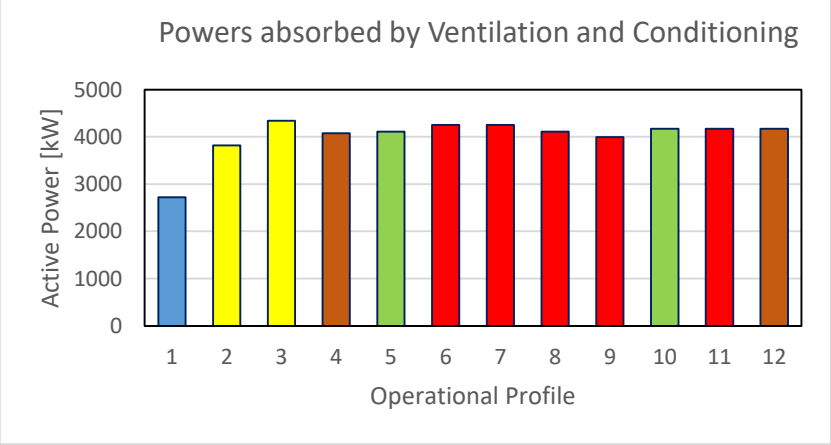

Figure 84 - Power Absorbed By Ventilation and Conditioning

Figure 85 shows the powers absorbed by the Ship equipment: the power absorbed by the electrical systems, command, surveillance, auxiliary systems, fittings and furniture.

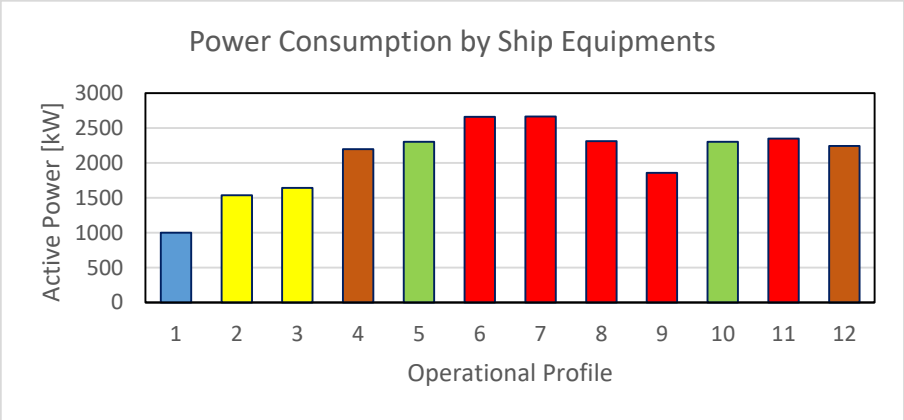

Figure 85 - The Power Absorbed by The Electrical Systems, Command, Surveillance, Auxiliary Systems, Fittings and Furniture

Figure 86 shows the powers absorbed by the STANAG network, 440 V- 60 Hz.

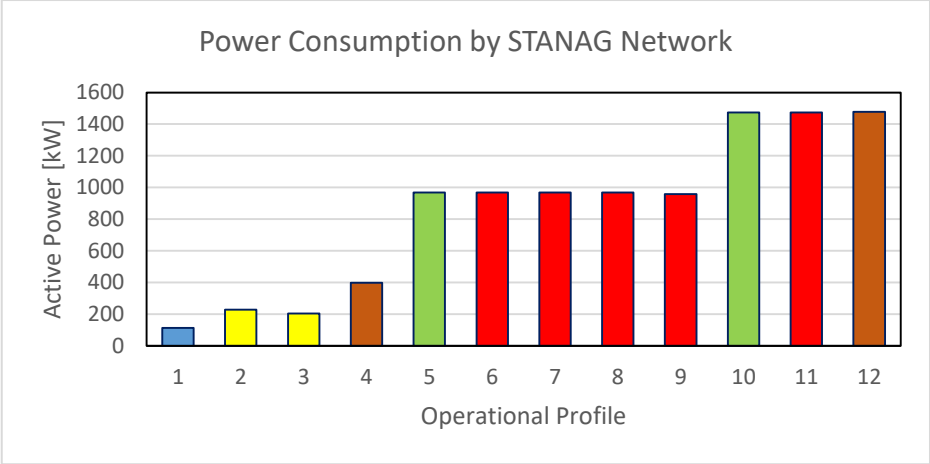

Figure 86 - STANAG Power Absorbed Power 440 V - 60 Hz

Figure 87 shows the power absorbed by the electric propulsion engines, active only in the A4 and A5 operational profiles

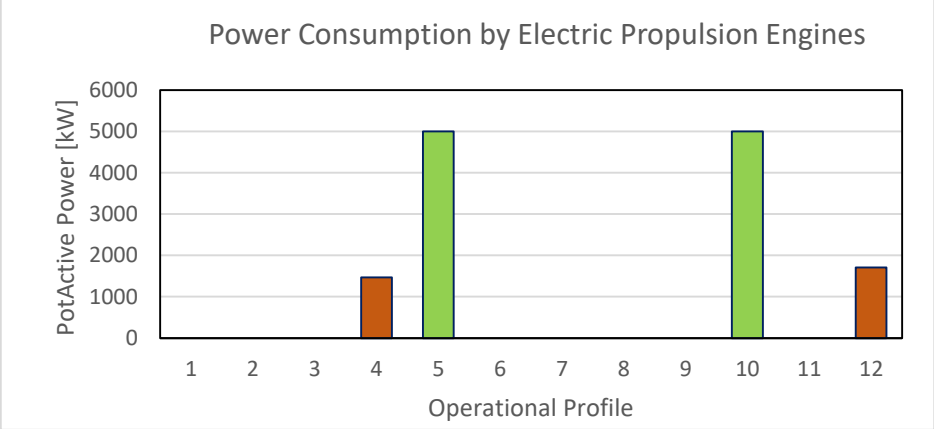

Figure 87- Power Absorbed by Electric Propulsion Engines

Figure 88 and Figure 89 show the power absorbed in A5 and A3 operational profiles, for stern and bow maneuvering propellers.

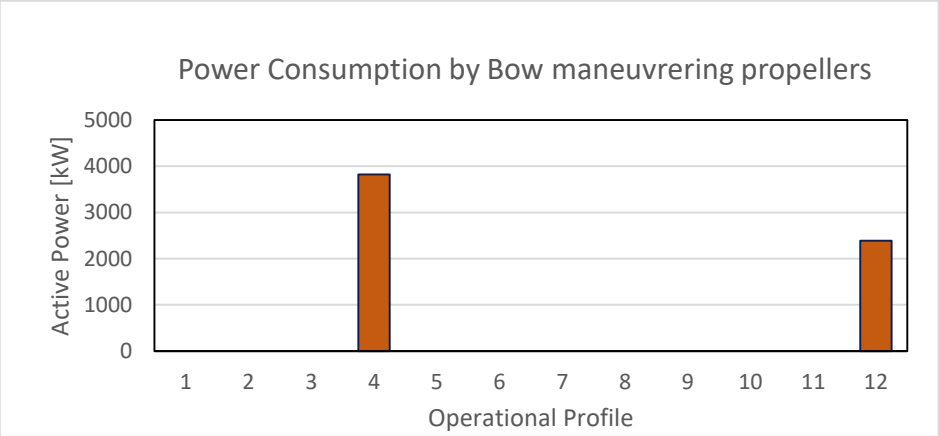

Figure 88 – Power Consumption by Bow Maneuvering Propellers

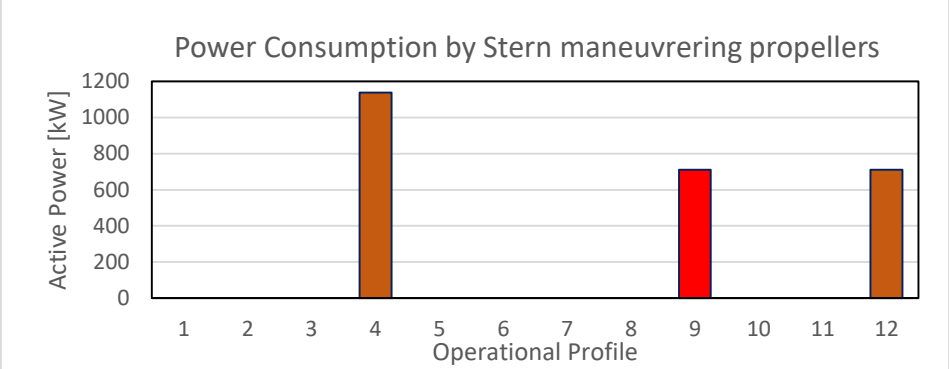

Figure 89 - Power Consumption by Stern Maneuvering Propellers

Figure 90 shows the percentage of static and rotating load for each operational profile.

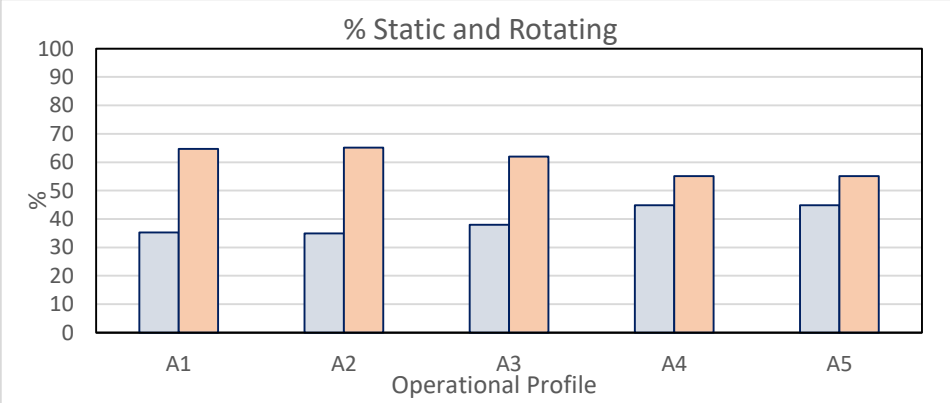

Figure 90 - Percentage of Static And Rotating Load For Each Operational Profile.

Figure 91 shows the total power absorbed, at 6 kV - 50 Hz, bus bars (bow and stern) for each operational profile, highlighting the power absorbed by each group of utilities.

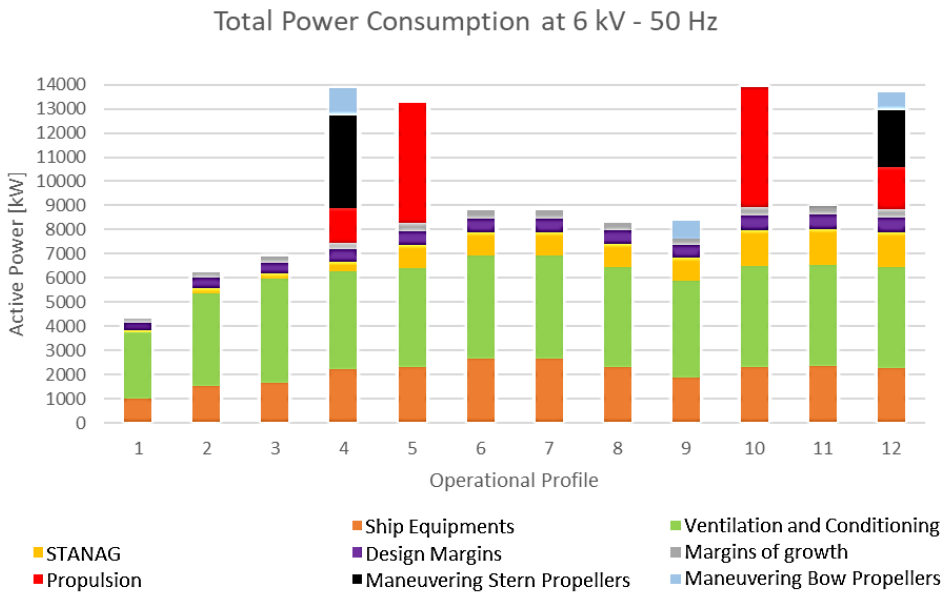

Figure 91 - Total Powers Detail by Each Group of Utilities

It is possible to highlight that ventilation and air conditioning are a fundamental and continuous load, with a power value which stands at 4 MW of power, as compared to small deviations depending on different operational profiles.

6.5.3 60 Hz network -load conditions

The STANAG network supply at 60 Hz 440 V and 115 V military equipment, such as weapon systems, command and surveillance.
Figure 92 shows the power absorbed by the STANAG network in the various operational profiles.

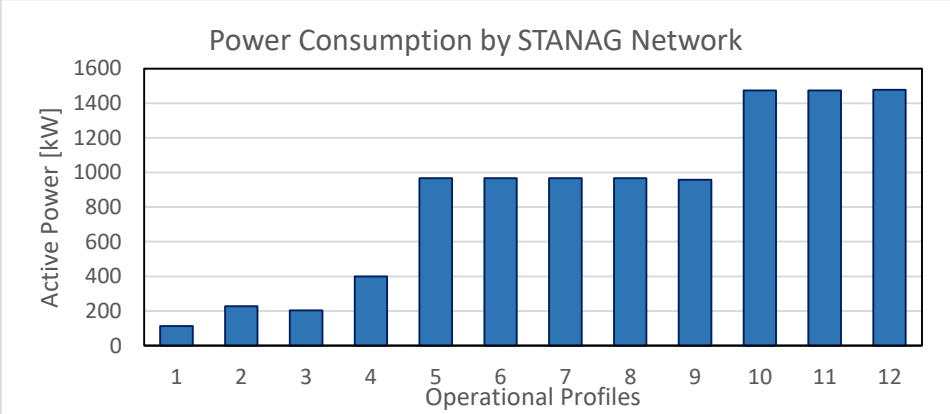

Figure 92- Power Absorbed By The STANAG Network

Table 28 shows the three operational profiles of the ship grouped, they are divided as follows:

- Operational Profile B1: Port (111 kW), Port Operative Role/Training (227 kW), Port Humanitarian Mission (203 kW), Maneuver (398 kW);
- Operational Profile B2: Navigation (10 nodes) Operational Role/Electric Propulsion Training (967 kW), Navigation (16 nodes) Operational Role/Training (967 kW), Navigation (18 nodes) Operational Role/Training (967 kW), Navigation (Maximum Speed) Operational Role/Training (967 kW), Anchor Ship Operational Role/Training (958 kW);

- Operational Profile B3: Navigation (10 knots) Combat Role with Electric Propulsion (1.473 kW), Navigation (Maximum Speed) Combat Role (1.473 kW), Amphibious Operations Combat Role with Electric Propulsion (1.477 kW).

Table 28 – Operational Profiles Grouped

Operational Profile subdivided for Power Consumption	*Number*
B1	1 – 2 – 3 – 4
B2	5 – 6 – 7 – 8 – 9
B3	10 – 11 – 12

Figure 93 shows the total power absorbed by rotary converters for operational profiles, considering the rotary converter efficiency and losses.

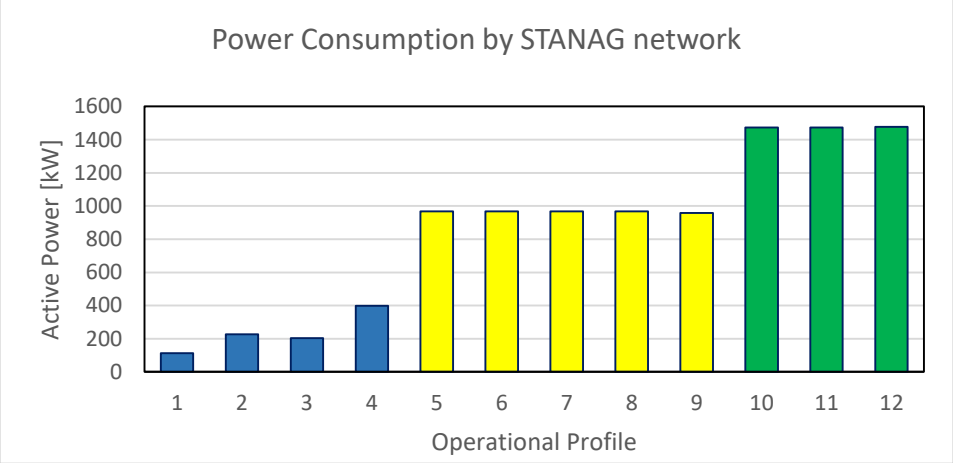

Figure 93 - Total Power Absorbed By Rotary Converters Considering Efficiency and Losses.

It is also useful specify the different power absorptions by command, surveillance and weapon systems. Figure 94 shows the power absorbed by the command and surveillance system.

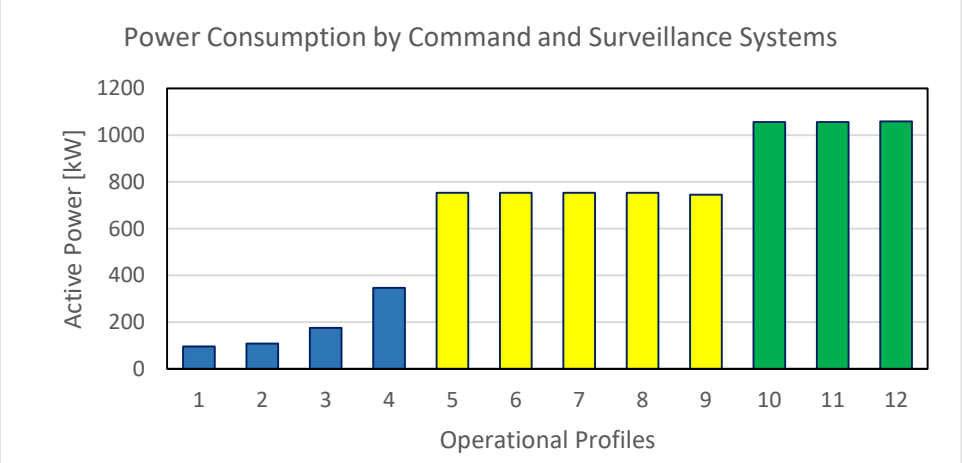

Figure 94 - Power Absorbed By The Command And Surveillance System.

Figure 95 shows the power absorbed by the weapon system. The weapon system is not in operation in operational profiles 1, 3, and 4.

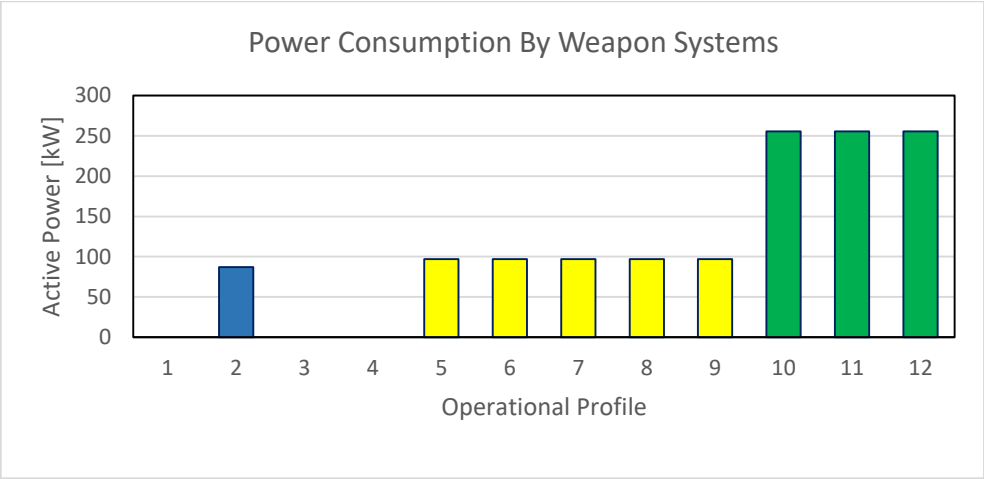

Figure 95 - Power Absorbed By The Weapon System

Figure 96 shows the total power absorbed by the STANAG network in relation to the power required by the command and surveillance systems as well as the weapon system.

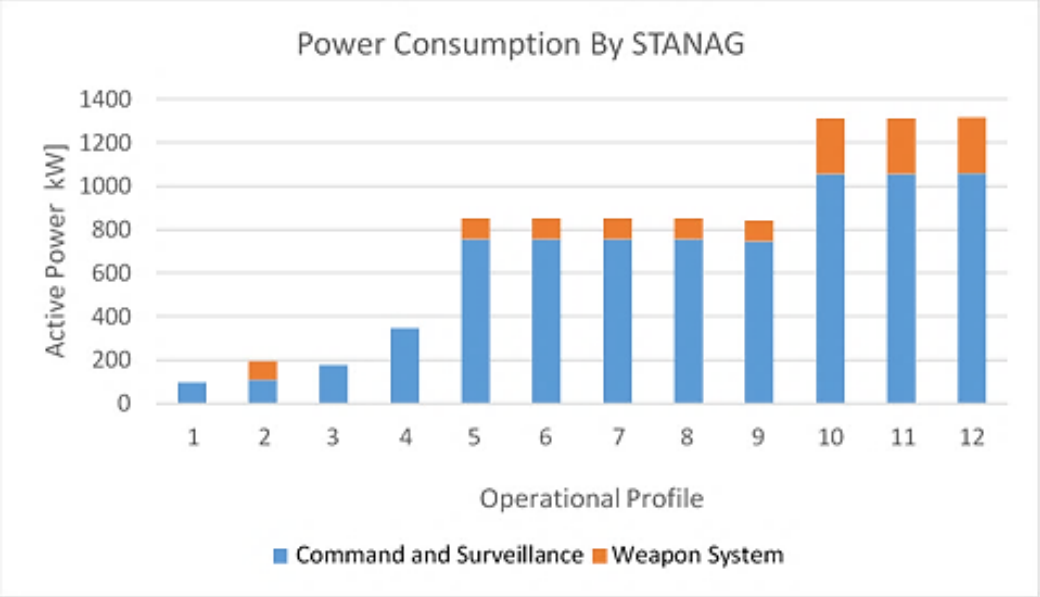

Figure 96 - Total power absorbed by the STANAG network

It is also possible to classify and highlight all the devices connected to the individual rotary converters. Radar, Local VLS Apparatus, Shooting Direction Equipment, Radio equipment, Local Gyro, and Weapon system are connected to the Stern converter.
Local SDC, SR2, Celd, Radio Operator, Local Backup COC, Helmsman, SR3, MAOC 28, Shooting Control Room, REA – METOC, SDC, COC Nave 1, COC Nave 2, VLS devices, Local Electrical Devices, and Weapon system are connected to the Bow converter.

Chapter VII: Network Equivalents in Frequency Domain

This chapter reports the methodology to carry out a simplification of the network and maintain results accuracy based on network impedance analysis. The aim of this methodology is to find the best solutions to represent the network and aggregating loads, in order to reach the closest accuracy to the real representation with each simulated load. It was verified how the network equivalents have an impact on the calculated values.
To perform the analysis of the two electrical systems (Chapter VI) in the frequency domain, the calculation codes and models presented in Chapter V were used. The code was developed by researchers of the Department of Astronautics, Electrical and Energy Engineering (DIAEE) and was calibrated on measurements carried out on the Cavour aircraft [99] [97] [116].
An area of the 50 Hz distribution network of the Hybrid Electric/Diesel/Gas Turbines propulsion MVAC – alternating current MV system 50-60 Hz (6.5.1 Figure 81) was chosen and 5 layouts were derived, each characterized by different loads aggregation. The results achieved with the layout characterized by maximum adherence of the simulated scheme with the real one were compared with those obtained with the layouts where some equivalents replace some parts of the network. A further sensitivity analysis was carried out on the cables in order to assess the impact of some possible uncertainties on their actual lengths.
Moreover, since the presence of rotary converters is an obstacle to the mutual influence of the disturbances generated by the distorting loads supplied at 50 Hz and 60 Hz respectively, the two network sections were simulated separately.

7.1. Electrical network case study

The chosen network section is shown in Figure 97. The Area includes the following features:

- 6 kV generation board (stern main panel);
- 6.5 MVA generator;
- 95 m cable length between 6 kV panel and 6kV/690 V transformer for the MVZ4-5 panel;
- 110 m; cable length between the secondary of the 6kV/690V transformer and the MVZ 4-5 sub-panel;
- 50 m cable length between 6 kV panel and the rotating converter;
- 30 m cable length between 6 kV switchboard and the 6kV/690 V transformer of the propulsion;
- 18 power supplies connected to the MVZ4-5 690 V panel (represent the loads in operation);
- 1/2 of the total load of the 60 Hz network portion downstream of the rotary converter;
- no connections between the electrical panels;
- 1600 kW transformer 6 kV/690 V for MVZ4-5 panel;
- 2800 kW transformer 6 kV /690 V for the propulsion engine;
- 2.5 MW propulsion engine.

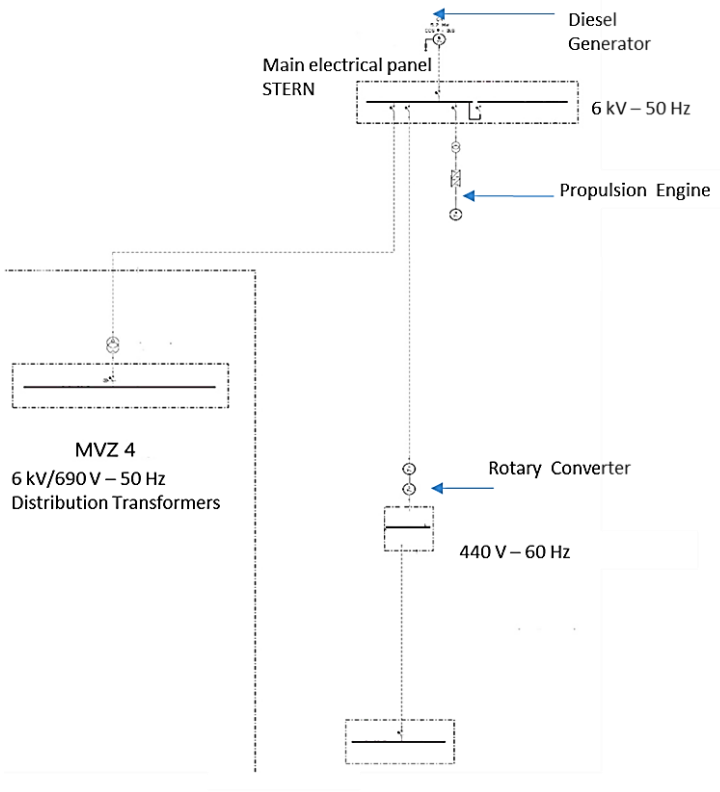

Figure 97 - Area of The 50 Hz Distribution Network of Hybrid Electric/Diesel/Gas Turbines propulsion MVAC – Alternating Current MV System 50-60 Hz

To perform the study of a model of the electrical distribution network, five layouts were analyzed, characterized by different equivalents of both loads and cables. In all schemes the 220 V distribution was incorporated in the equivalent load and it remained unchanged across the five layouts. The values used in the simulation are:

- electric propulsion consumption equal to 2.5 MW;
- equivalent load downstream of the rotary converter equal to 0.74 MW and 0.55 MVAr;
- 6.5 MVA generator;
- 95 m cable length between 6 kV panel and 6kV/690 V transformer for the MVZ4-5 panel with *R = 0.308 [Ω/km] X = 0.123 [Ω/km] C = 199.2 [nF/km];*
- 50 m cable length between 6 kV electrical panel and rotary converter with R = 0.058 [Ω/km] *X = 0.032 [Ω/km] C = 750.0 [nF/km];*
- 30 m cable length between 6 kV and 6kV/690 V propulsion engine transformer with *R = 0.154 [Ω/km] X = 0.059 [Ω/km] C = 399.8 [nF/km];*
- 6 kV/690 V 1600 kW transformer for MVZ4-5 panel;
- 6 kV/690 V transformer of 2800 kW for the propulsion engine.

The cables lengths used for aggregation of loads, were obtained by calculating the electrical moment (equation (35)), cables sections were determined based on the value of the total load fed.

$$L_{equivalent} = \sum_0^n (Po * Lo) + \cdots (Pn * Ln) / \sum_0^n Po + \cdots Pn \quad (35)$$

The specific features of the five layouts are presented and analyzed. The nodes where impedance is calculated (alphanumeric abbreviation, Z (f), followed by a number), were identified for each representation.

Case-1

Figure 98 shows the equivalent network model for Case-1.

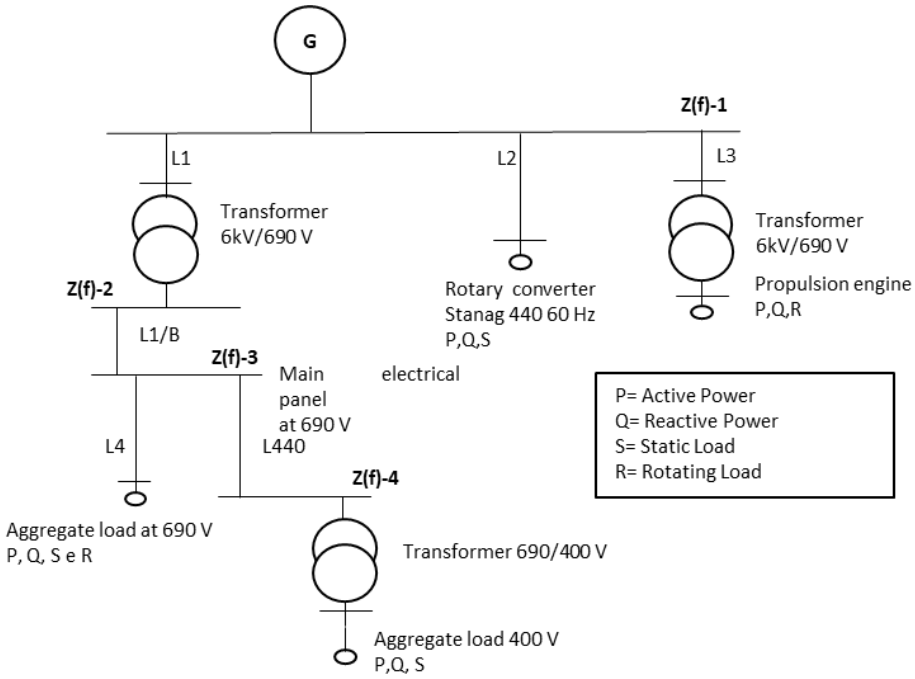

Figure 98 – Case 1

Table 29 and Table 30 report the power absorbed by the loads, the lengths and the sections of the cables. In particular, L4 cable was obtained with the electrical moment formula (equation (1)) and the section was determined thanks to the value of the total load it feeds.

Table 29 – Loads Features

Aggregated Load	Active power [MW]	Reactive power [MVAr]	% Static	% Rotating
690 V	0.82	0.62	6	94
400 V	0.06	0.04	100	0

Table 30- Cables Features

Line Name	Length [m]	R [Ω/km]	L [Ω/km]	C [nF/km]
L1/b	110	0.017	0.011	5118.0
L4	90	0.044	0.029	1919.0
L440	20	0.172	0.090	639.0

Case-2

Figure 99 shows the network model equivalent to Case-2. The loads supplied by the 690 V were grouped according the length of their power cables. In particular, three groups were identified: 0-50 m (group 1), 50-100 m (group 2), 100-150 m (group 3).

Each load was assigned to a group based on the length of its power cable. As a result, it was possible to subdivide all aggregate loads into three equivalent loads.

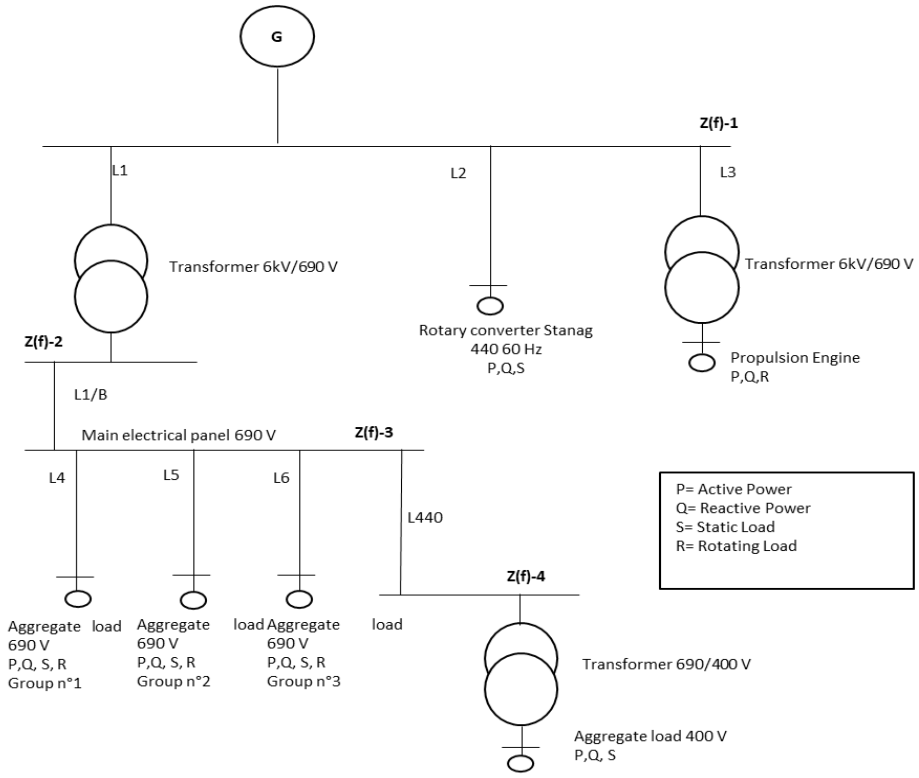

Figure 99- Case 2

Table 31 and Table 32 report the power absorbed by loads, lengths and sections of the cables. In particular, cables L4, L5, L6 were obtained by means of the electrical moment formula (equation (1)) and the section was determined thanks to the value of the total load it feeds.

Table 31 - Loads Features

Aggregated Load	Active power [MW]	Reactive power [MVAr]	% Static	% Rotating
Group 1	0.325	0.244	5	95
Group 2	0.156	0.117	1	99
Group 3	0.338	0.124	1	99
400 V	0.06	0.04	100	0

Table 32 - Cables Features

Line Name	Length [m]	R [Ω/km]	L [Ω/km]	C [nF/km]
L1/b	110	0.017	0.011	5118.0
L4	50	0.104	0.088	650.0
L5	70	0.433	0.101	535.0
L6	110	0.044	0.029	1919.0
L440	20	0.172	0.090	639.0

Case -3

Figure 100 shows the real network model for Case-3.

All feeders starting from the node Z (f)-3 have been considered; this case therefore, represents the network with the highest level of detail. A single equivalent load has been aggregated on the STANAG network (690/400 V).

Case-3 was taken as a reference for determining the approximations of the results obtained with the other 4 equivalent network representations.Table 33 and Table 34 report the power absorbed by the loads, the lengths and the sections of the cables. Cables from L4, up to L18, were taken from the official report; in this case all loads were represented.

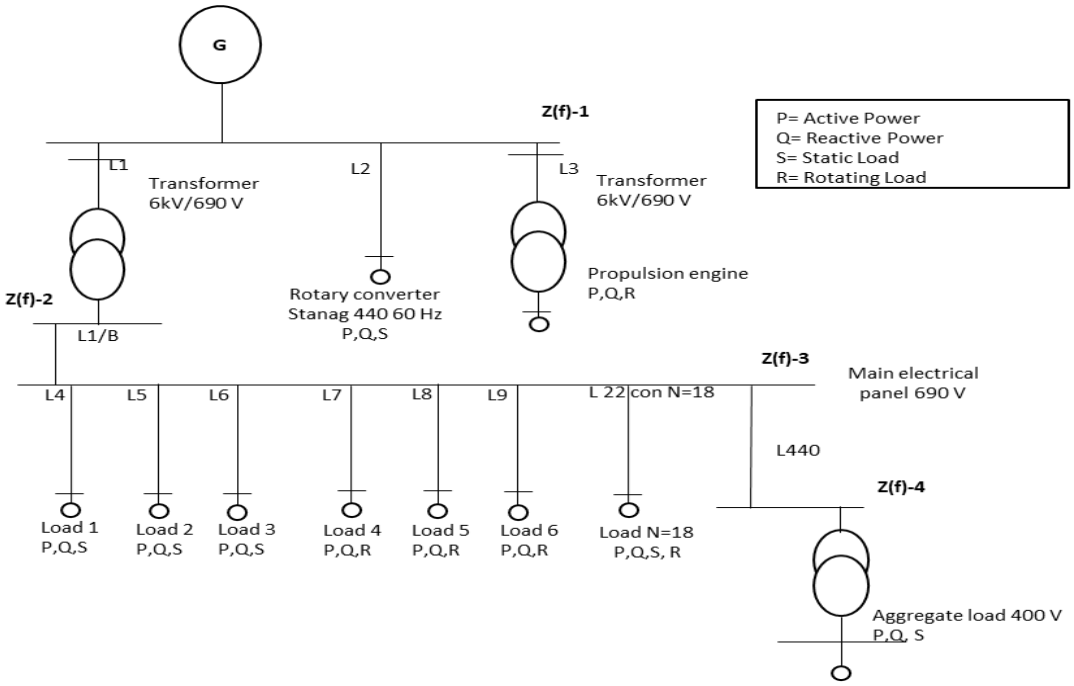

Figure 100 – Case 3

Table 33 - Loads Features

Aggregated Load	Active power [MW]	Reactive power [MVAr]	% Static	% Rotating
Load 1	0.003	0.005	100	0
Load 2	0.003	0.005	100	0
Load 3	0.013	0.010	1	99
Load 4	0.065	0.048	1	99
Load 5	0.065	0.048	1	99
Load 6	0.044	0.033	1	99
Load 7	0.044	0.033	1	99
Load 8	0.044	0.033	1	99
Load 9	0.044	0.033	1	99
Load 10	0.065	0.048	1	99
Load 11	0.065	0.048	1	99
Load 12	0.052	0.039	1	99
Load 13	0.052	0.039	1	99
Load 14	0.052	0.039	1	99
Load 15	0.052	0.039	1	99
Load 16	0.004	0.003	1	99
Load 17	0.076	0.057	1	99
Load 18	0.076	0.057	1	99
400 V	0.06	0.04	100	0

Table 34 - Cables Features

Line Name	Length [m]	R [Ω/km]	L [Ω/km]	C [nF/km]
L1/b	110	0.017	0.011	5118.0
L4	90	1.311	0.095	410
L5	60	1.311	0.095	410
L6	60	1.311	0.095	410
L7	60	0.821	0.087	430
L8	40	0.821	0.087	430
L9	60	1.311	0.095	410
L10	60	1.311	0.095	410
L11	20	1.311	0.095	410
L12	35	1.311	0.095	410
L13	150	0.821	0.087	430
L14	130	0.821	0.087	430
L15	130	0.821	0.087	430
L16	140	0.821	0.087	430
L17	100	0.821	0.087	430
L18	110	0.821	0.087	430
L19	110	0.433	0.101	534
L20	50	0.099	0.032	1680
L21	50	0.099	0.032	1680
L22	90	0.104	0.088	410
L440	20	0.172	0.090	410

Case - 4

Figure 101 shows the network model for Case-4.

It is equivalent to case 1 except for the representation of the L1/b and the L4 cable (Figure 98). The total load was concentrated directly after the transformer on the 690 V main electrical panel. This simplification was proposed to quantify the effect of the slight extension of cables present on board in network impedance values. For load power values and cables features, reference should be made to Table 29 and Table 30.

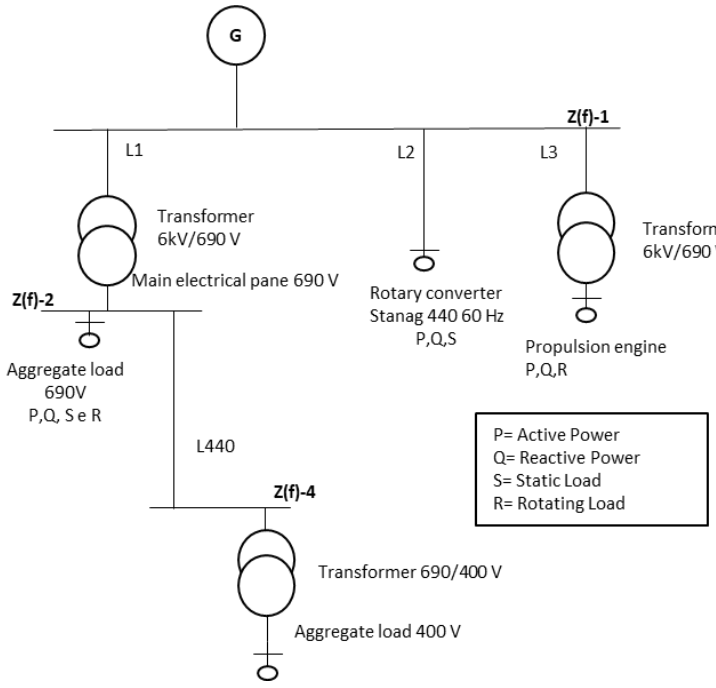

Figure 101- Case 4

Case – 5

Figure 102 shows the equivalent network model for Case-5.

This is the most simplified case, through a unique representation of aggregate load (690/400 V). Only the L1 connection from the 6 kV panel to the 6 kV/690 V transformer was taken into account on the 690 V main electrical panel. This configuration reports the smallest detail of the network elements.

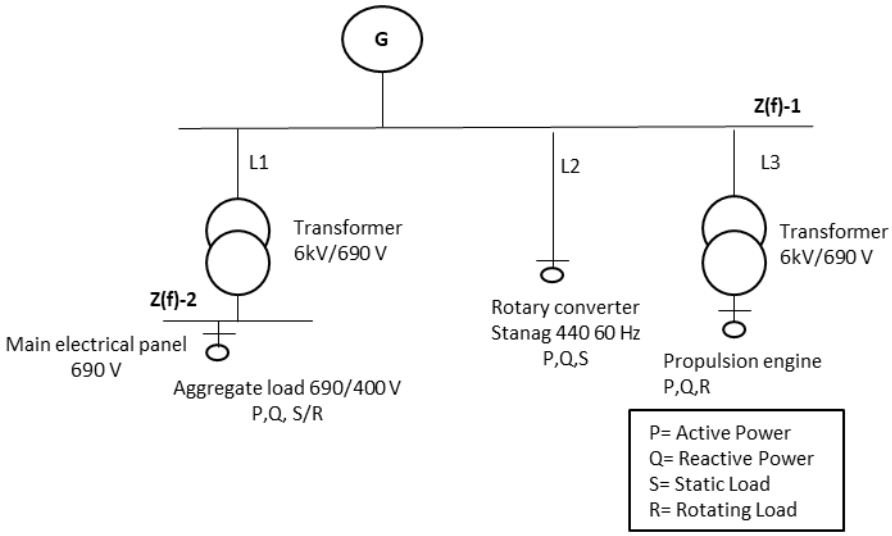

Figure 102- Case 5

Features of aggregated load (690/400 V) are shown in Table 35.

Table 35 – Load features

Aggregated Load	Active power [MW]	Reactive power [MVAr]	% Static	% Rotating
690/400 V	0.88	0.66	7	93

7.3 Network impedance

7.3.1 Network impedance evaluation for each equivalent network model

For each equivalent network model (Case 1-5 in Chapter 7.2), the network impedances Z(f) were calculated at the nodes. Figure 103 reports the results achieved**.**

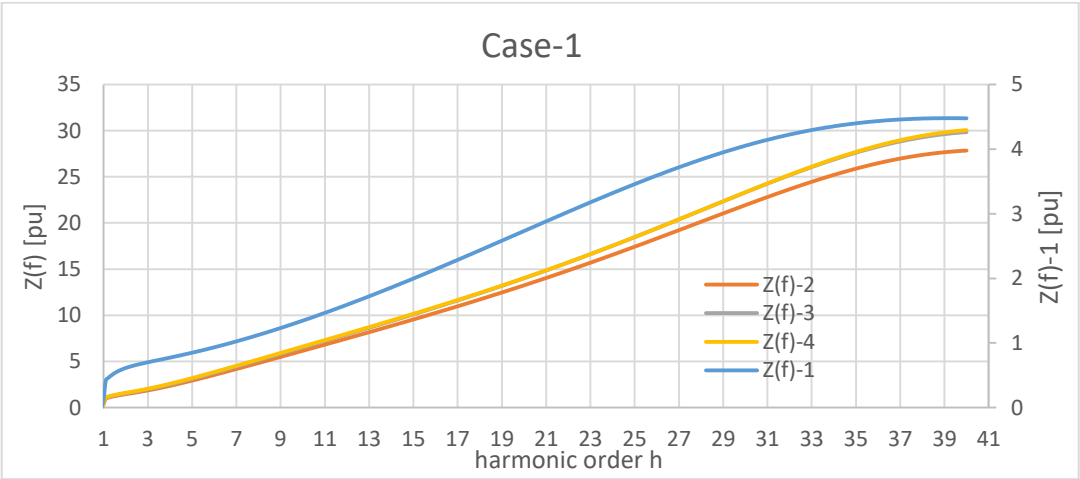

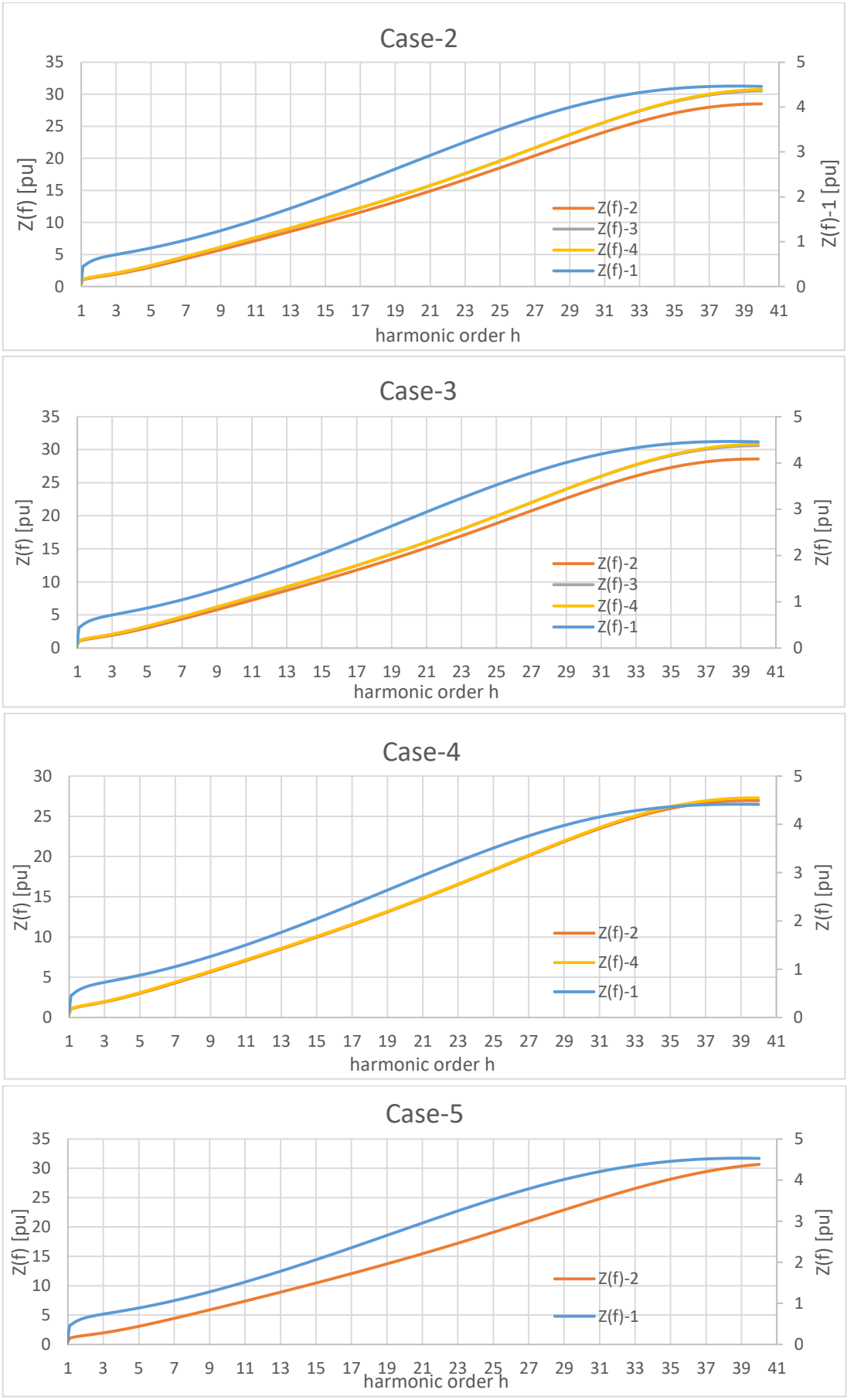

Figure 103 - Network Impedance for Each Case

The analysis of the Figures shows that the trend of Z (f) is increasing and without resonances.
This last aspect is due to a limited effect of the transversal capacitances of the cables (a consequence from the moderate extension of the cables themselves) and from the absence of power factor correction like in capacitors or filters.
In order to better quantify the differences between the values of the Z (f) calculated using different network schemes, Figure 104 gathers the calculated impedance trends for each node.

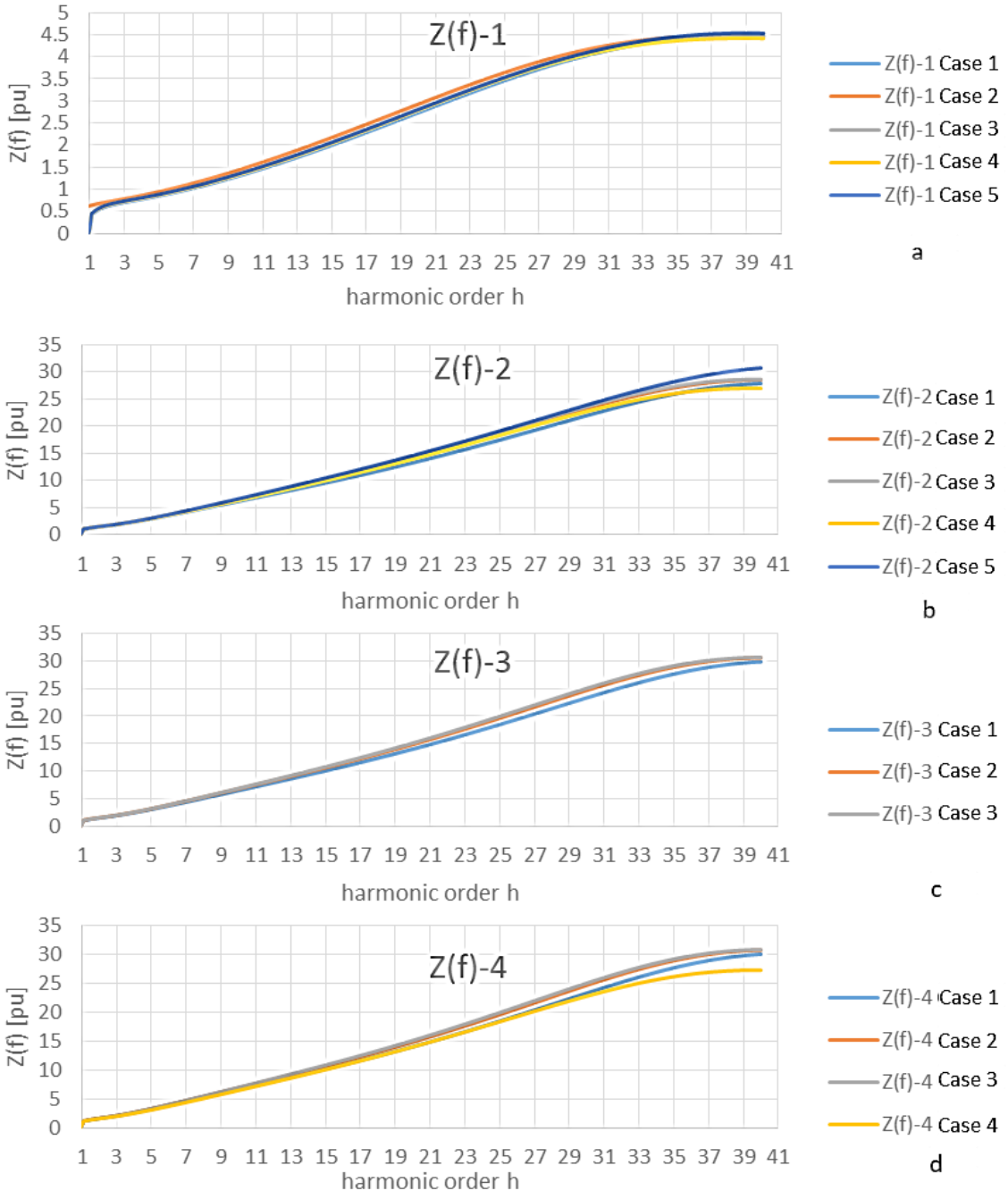

Figure 104 – Network Impedance Trend VS Equivalent Network Model

Figure 104a clearly shows that the values of Z (f) at 6 kV (Point of common coupling) are not influenced by the representation (greater or lesser detail) of the 690 V distribution network. This is justified by the predominant role of the 6 kV distribution compared to the 690 V and 400 V networks, which is not relevant thanks to the transformers.
Some differences are found in the values calculated on the 690 V busbar, at the output of the transformer (Figure 104b and d) or at the Z (f) - 3 node (Figure 104c). In these cases, obviously, the

role assumed by the equivalent (cables and load) is more important therefore, the final choice of the optimal equivalent model to use for the analysis of harmonic penetration cannot be separated from a detailed analysis of the position of sensitive loads and non-linear loads.
The values of the approximations obtained in Cases 1, 2, 4 and 5, in percent, compared to Case 3, are described in the following paragraph.

7.3.2 – The Network Equivalent Accuracy

7.3.2.1 Comparison among network equivalents

In order to evaluate the network equivalent for the results obtained, the difference of the Z (f) values using network models Case - 1, 2, 4 and 5 was calculated. Z (f)-1 and Z (f)-2 values (PCC of the test network) have been compared to those obtained with the adoption of Case-3 network model, which represents the most detailed network taken into consideration.
Figure 105 and Figure 106 show the values of approximation achieved using different network equivalent models. In particular, Figure 105 refers to the results achieved up to the 40th harmonic and Figure 106 summarizes the comparison up to the 19th harmonic; the latter being a limit for networks whose non-linear loads are mainly interfaced with converter bridges.

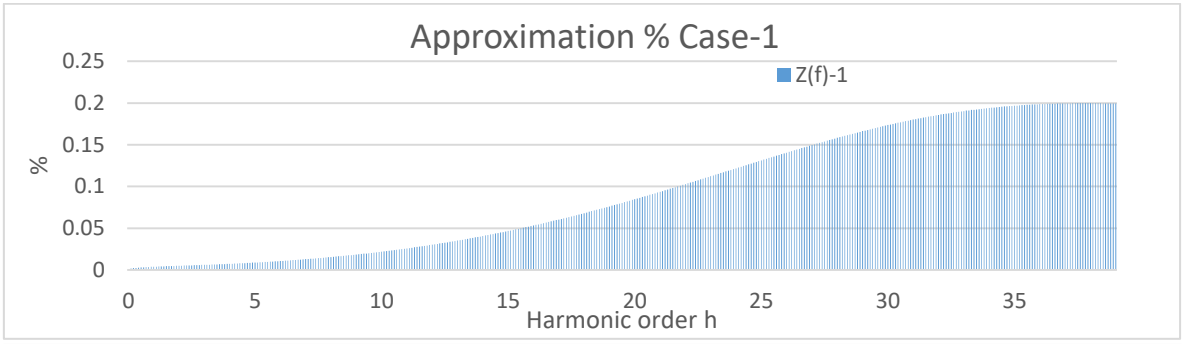

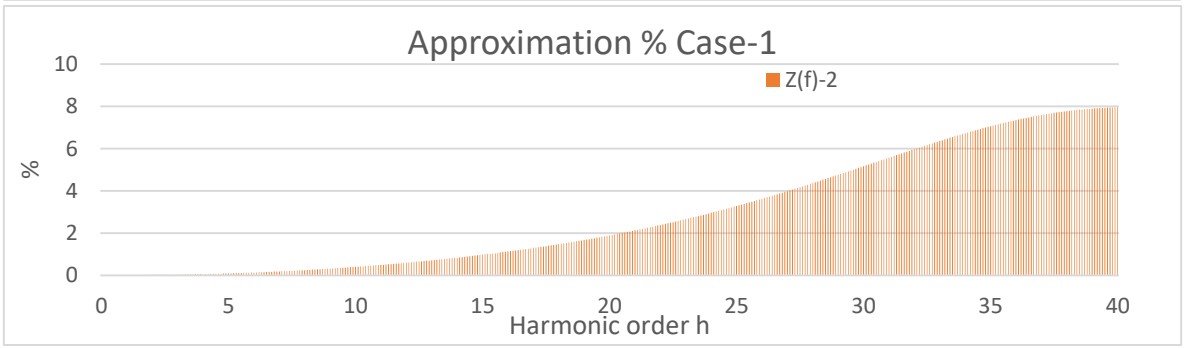

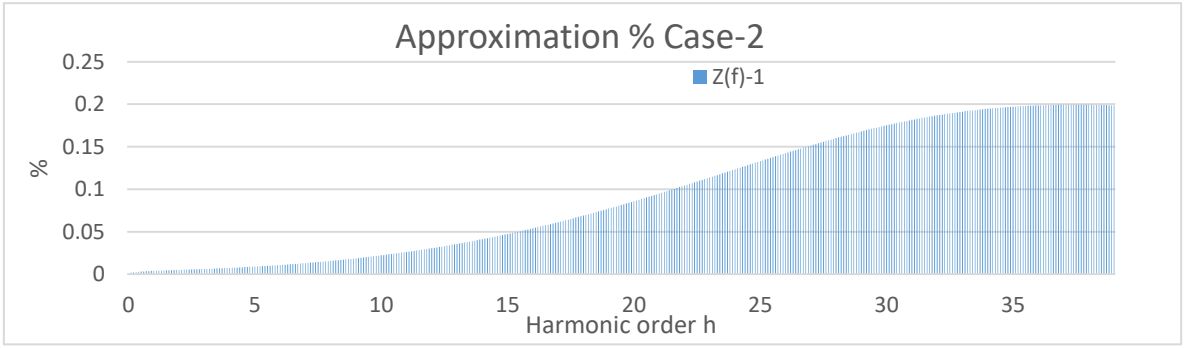

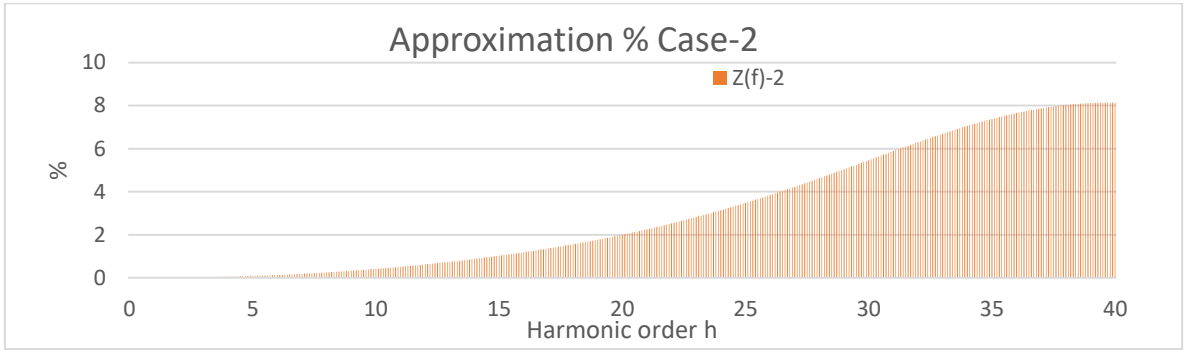

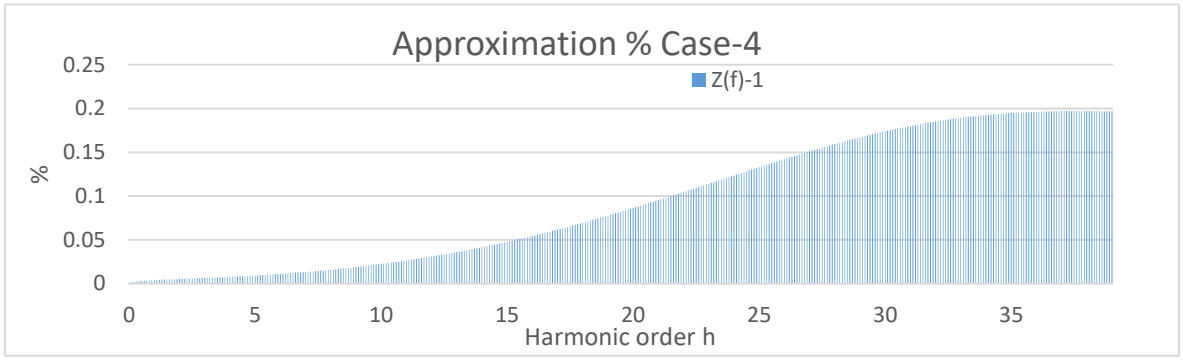

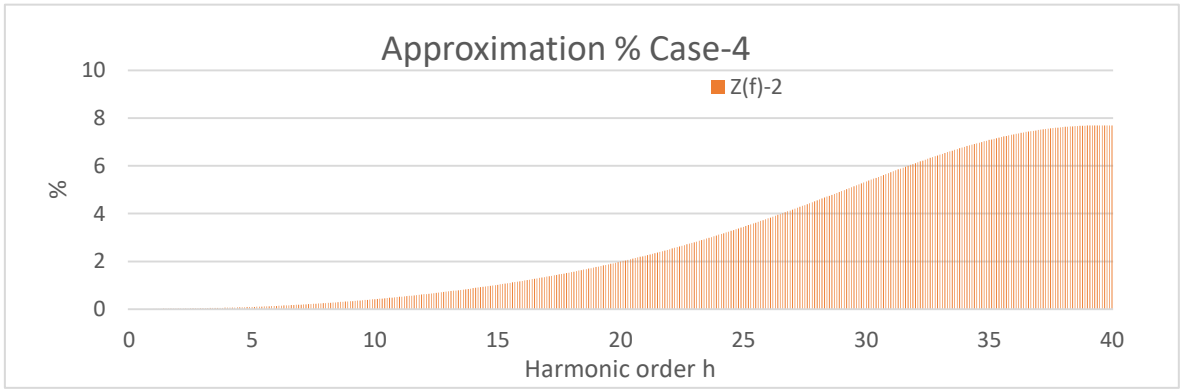

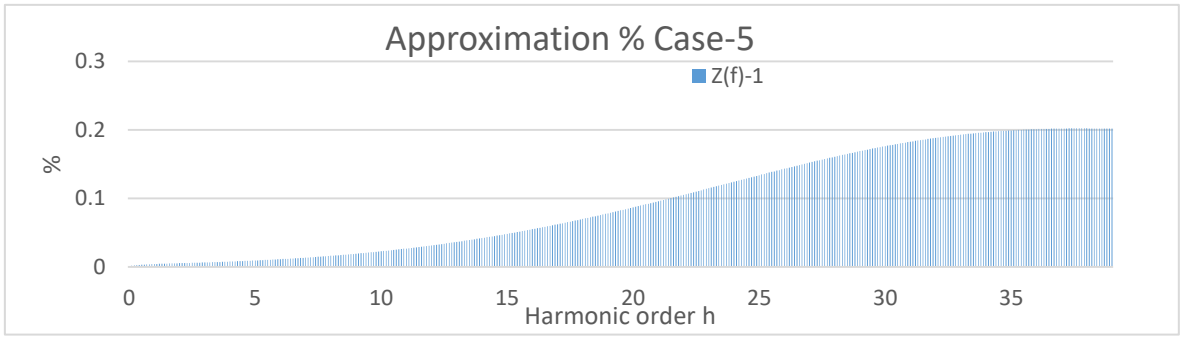

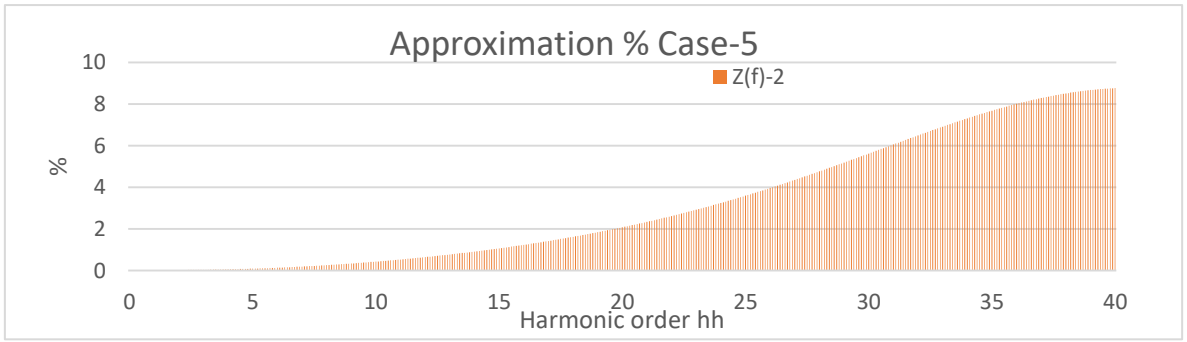

Figure 105 - Values of Approximation Achieved By Varying The Network Equivalents

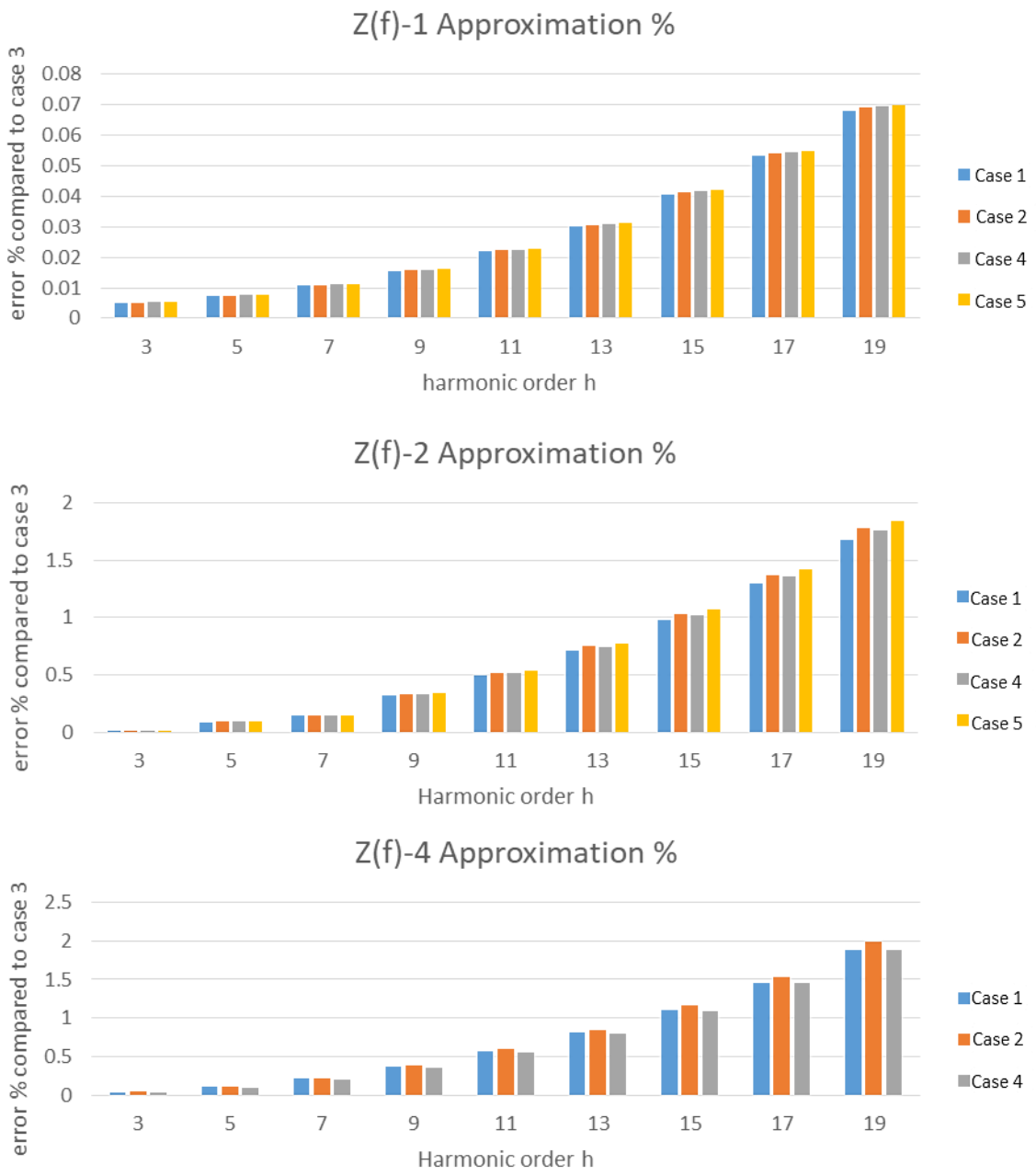

Figure 106 – Approximation % for Each Harmonic on Network's Impedance According Equivalent Network Cases

The approximations calculated at the point of common coupling (PCC) are extremely limited up to the 19th harmonic, therefore, in presence of conducted disturbances generated by converter bridges, it is certainly possible to adopt a simplified equivalent network. The presence of non-linear loads with higher frequencies content, requires higher harmonic orders as compared to what is described above. Percentage variations obtained in Cases 4 and 5 with the calculation of the impedances for the node Z (f)-2 appear significant (up to over 8% with Case-5) and therefore an excessive simplification of the network does not appear suitable.

7.3.2.2 - Influence of cables length on network impedance calculation

In order to take into account some uncertainties related the real length of network cables, a further analysis was carried out to evaluate if it has an impact on results accuracy.
The test was carried out by referring to Case-1 (Figure 98). The length of the cable that reaches the MVZ4 main panel at 690 V (L1/B) originating from the secondary of the 6 kV/690 V transformer and that reaches the 440 V electrical panel (L440) from the secondary of the 690/400 V transformer was varied.
Three simulations have been carried out, choosing the values of the minimum and maximum lengths according to the design documentation. Three cases were identified:

- Case-1_{min} - minimum lengths for both cables (L1/B = L440 = 15 m);
- Case-1_{max} - maximum lengths for both cables (L1/B = L440 = 120 m);
- Case-1 - effective lengths (L1/B = 110 m; L440 = 20 m).

Figure 107 shows the trend of network impedance at one of the common coupling points (Z(f)-2).

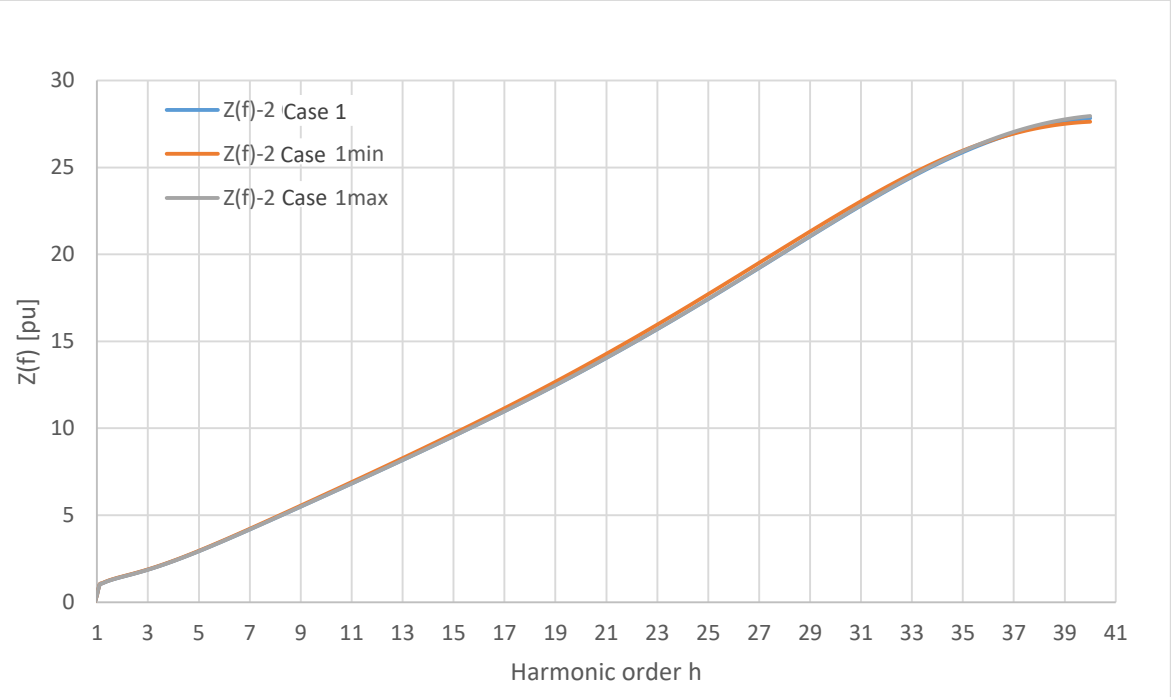

Figure 107 - Trend of The Network Impedance According To The Length Of The Cables

Figure 107 confirms that for networks with a limited cables extension, the uncertainties of their values have no impact on the accuracy of the results.

Chapter VIII: Harmonic Analysis

8.1 Network impedance

The best equivalent network model, described in chapter 7, was used to analyze harmonics on the three electrical system architectures proposed (chapter 6), according to the requirements for the new naval unit, taking into account different operational profiles.

The architectures proposed are:

- Hybrid Electric/Diesel/Gas Turbines propulsion MVAC – alternating current 50-60 Hz MV systems;
- All electric MVAC - alternating current MV system;
- All electric MVAC "hybrid"- MV system with alternating current and "islands"/electrical areas in direct current, both in MV and/or Low Voltage (BT);

8.2 layout “Hybrid Electric/Diesel/Gas Turbines propulsion MVAC – alternating current MV system”

8.2.1 - 50 Hz network

Taking into account the absorption deriving from the specific operational profile, 5 load scenarios were identified for the 50 Hz network. Loads supplied at 220 V were not highlighted, but aggregated in the total load supplied at 690 V. Table 36 show the aggregated operational profiles for the *Hybrid Electric/Diesel/Gas Turbines propulsion MVAC – alternating current MV system – 50 Hz network*

Table 36 – 50 Hz Network Aggregated Operational Profile For The Hybrid Electric/Diesel/ Gas Turbines propulsion MVAC – Alternating Current MV System – 50 Hz Network

Operational profile group	Operational profile	Power Consumption (MW)
A1 - I	Port (stern generator)	4.5
A1 - II	Port (bow generator)	4.5
A2	1) Port Operational Role / Training 2) Humanitarian Mission	6-7
A3	1) Navigation (16 nodes) Operational Role/Training 2) Navigation (18 knots) Operational Role/Training 3) Navigation (Maximum Speed) Operational Role/Training 4) Anchor Ship Operational Role/Training 5) Navigation (Maximum Speed) Combat Role	8-9
A4	1) Navigation (10 knots) Role Combat with Electric Propulsion 2) Navigation (10 knots) Operational Role/Training with Electric Propulsion	13
A5	1) Amphibious Operations Combat Role with Electric Propulsion 2) Maneuver	13

Figure 108 ÷ Figure 113 show the single-line diagrams with the aggregate loads, the lengths and the characteristic parameters of the entire 50 Hz network for each group of operational profiles.
Network impedances were evaluated as a function of frequency at the nodes highlighted in red.
Figure 114 ÷ Figure 119 show the trends of the network impedances as a function of the frequency in the nodes identified in red (Figure 108 ÷ Figure 113) with a number ranging from 1 to 7.

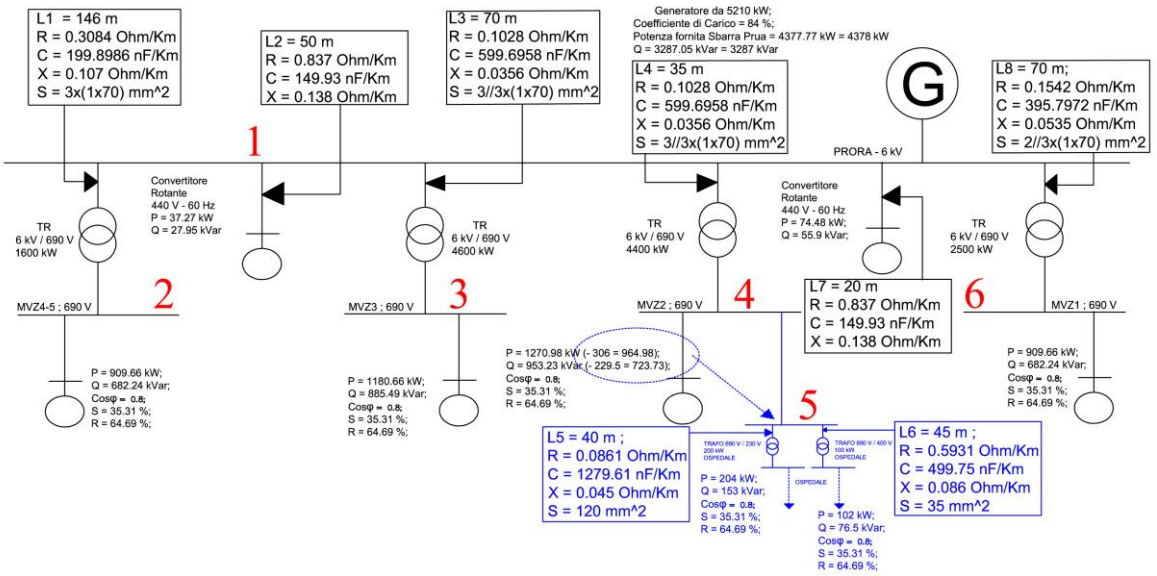

Figure 108 - A1-I

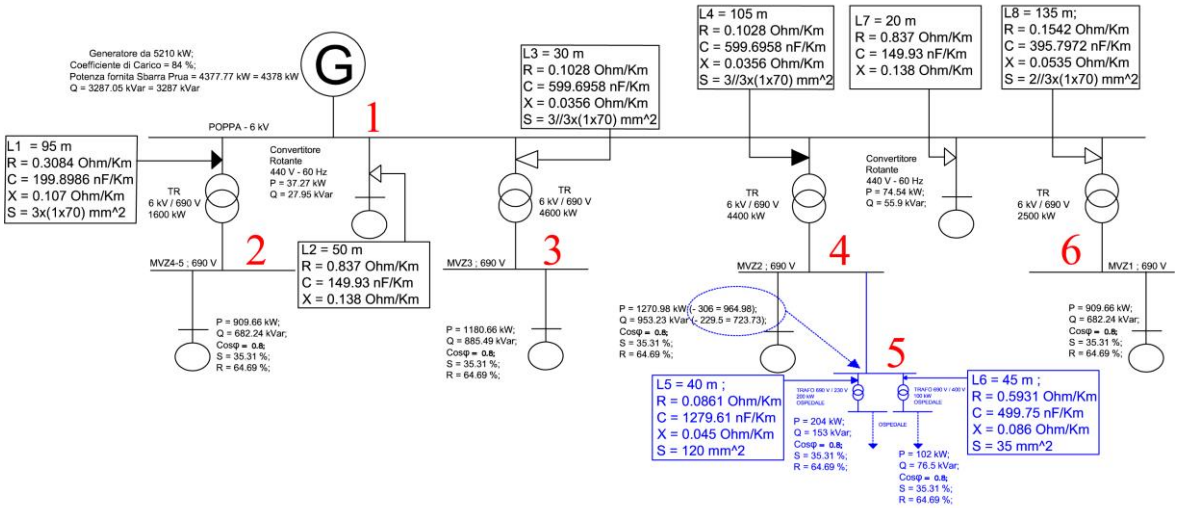

Figure 109 - A1–II

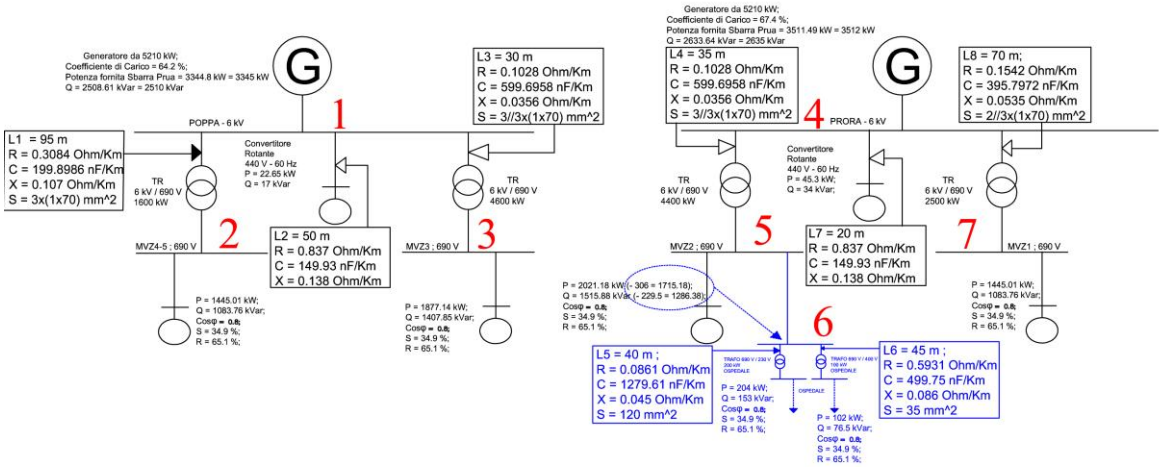

Figure 110 - A2

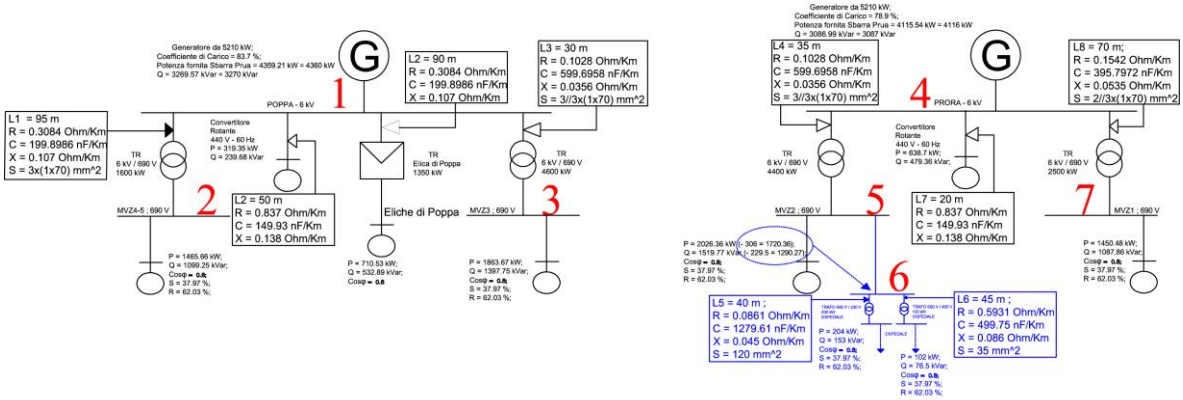

Figure 111 - A3

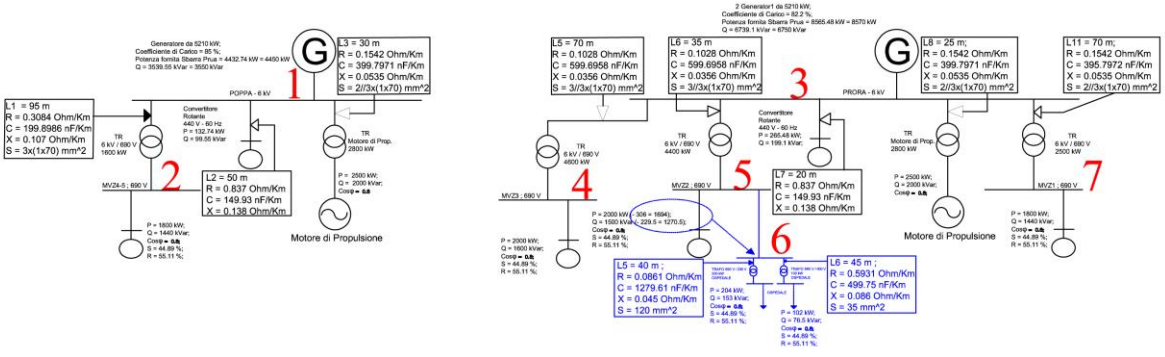

Figure 112 - A4

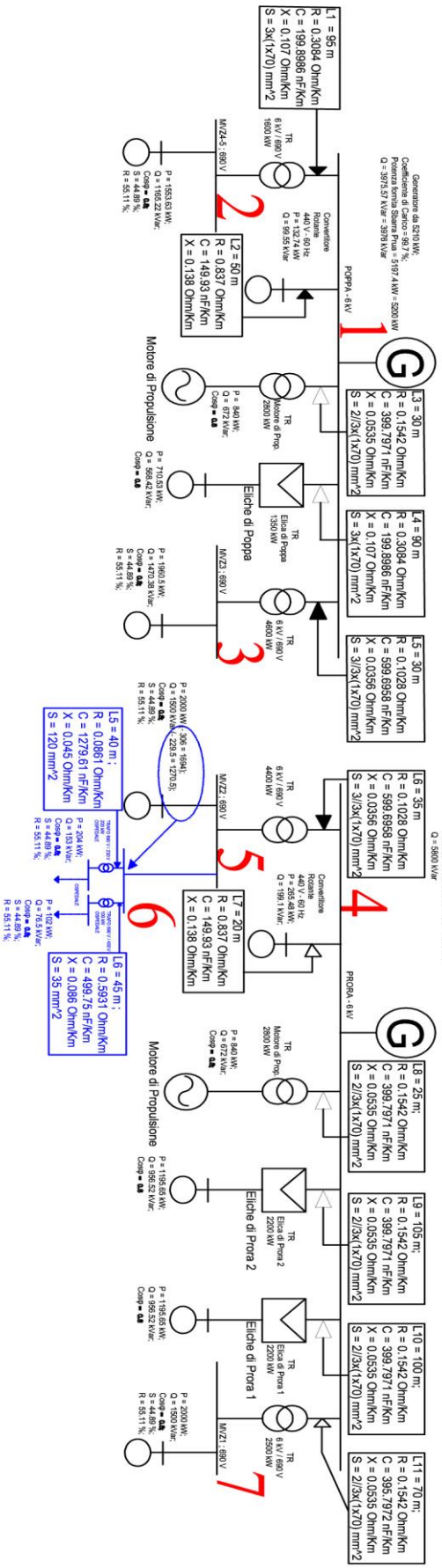

Figure 113 - A5

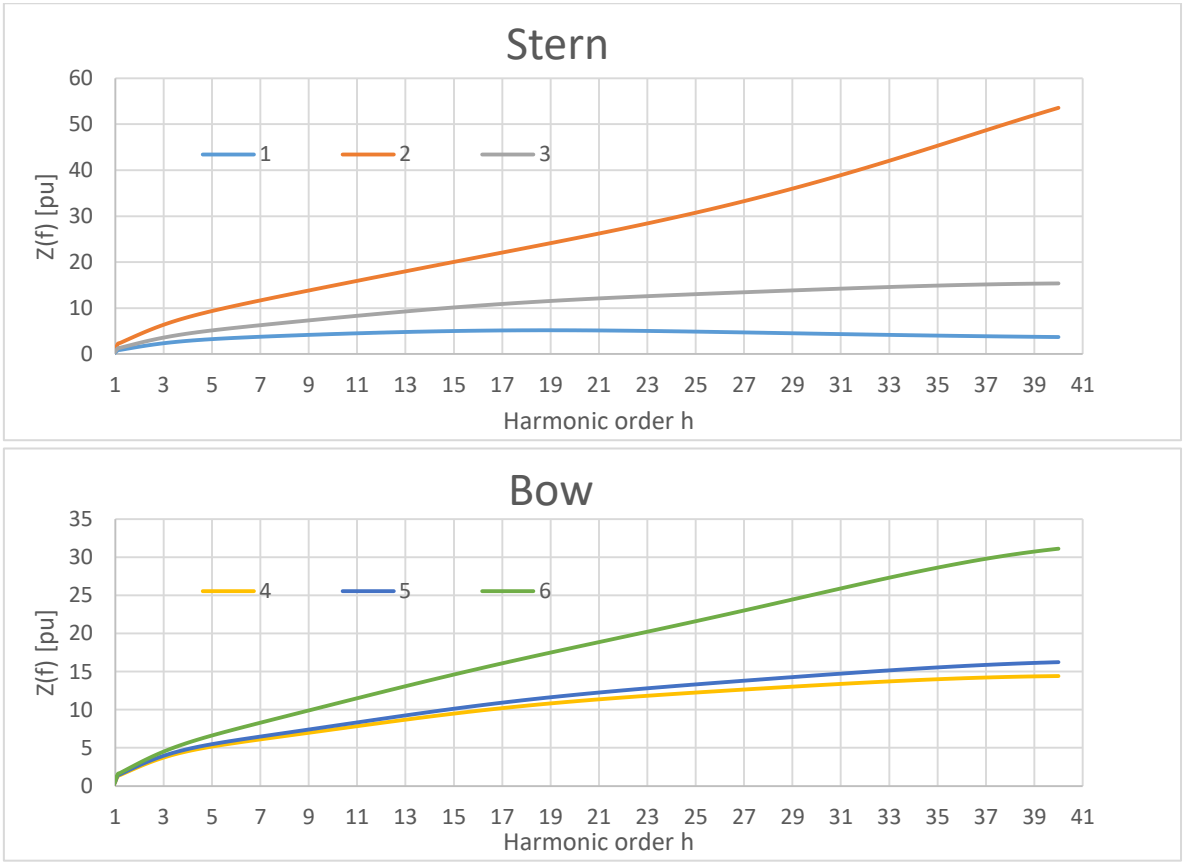

Figure 114 - Network Impedances for A1 Operational Profile Group

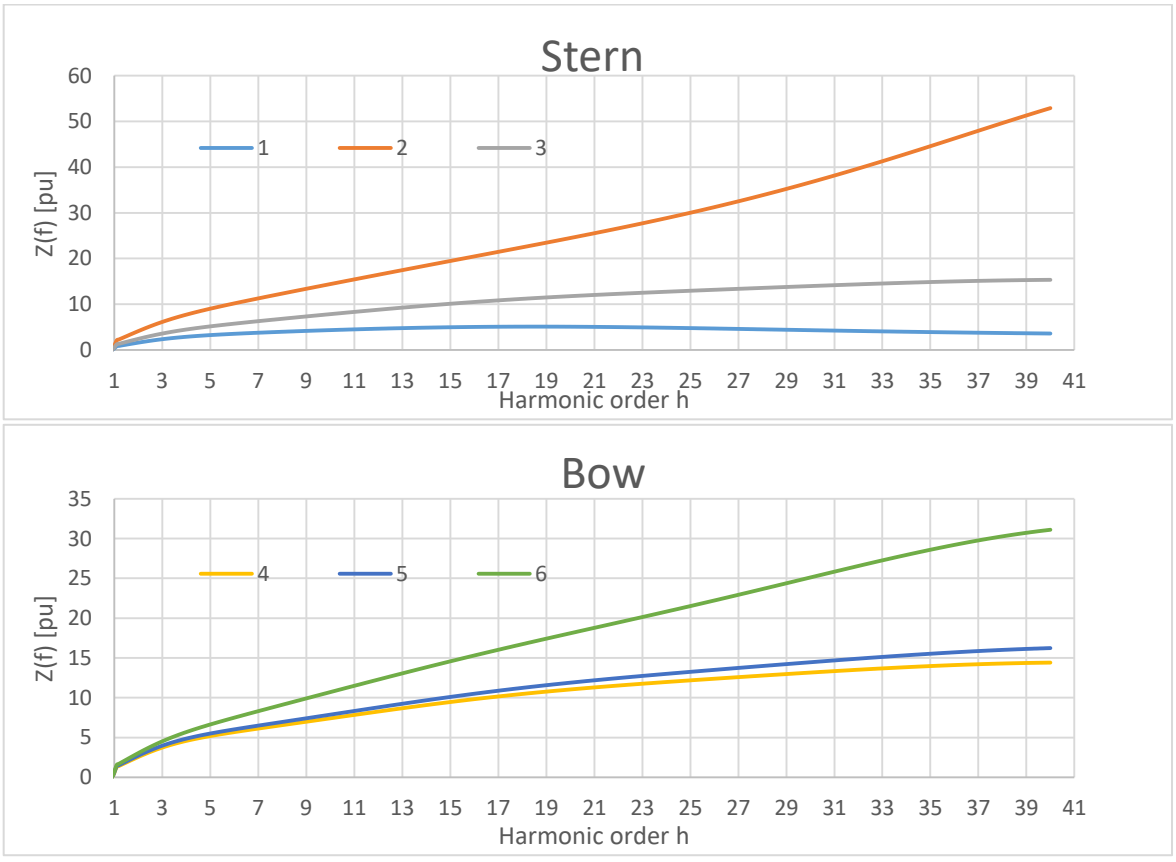

Figure 115 - Network Impedances for A1- II Operational Profile Group

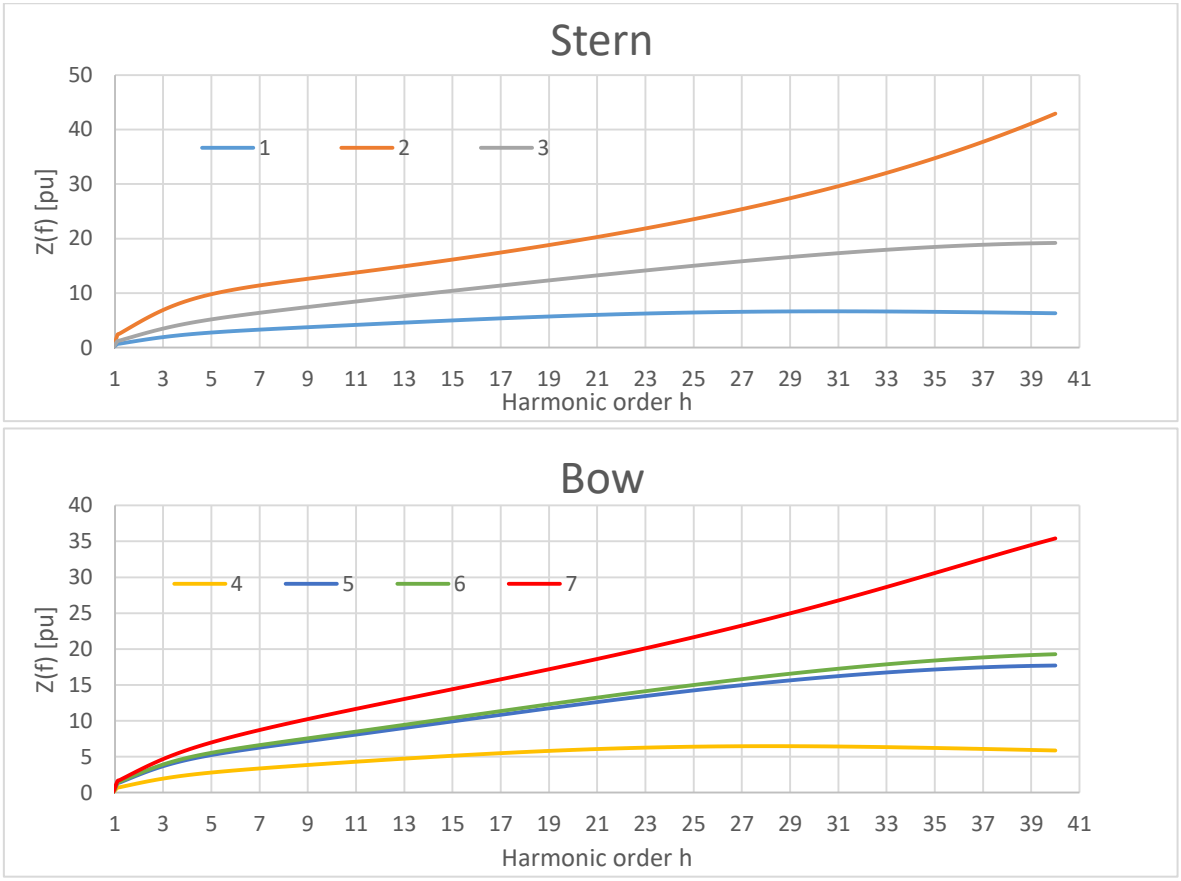

Figure 116 - Network Impedances for A2 Operational Profile Group

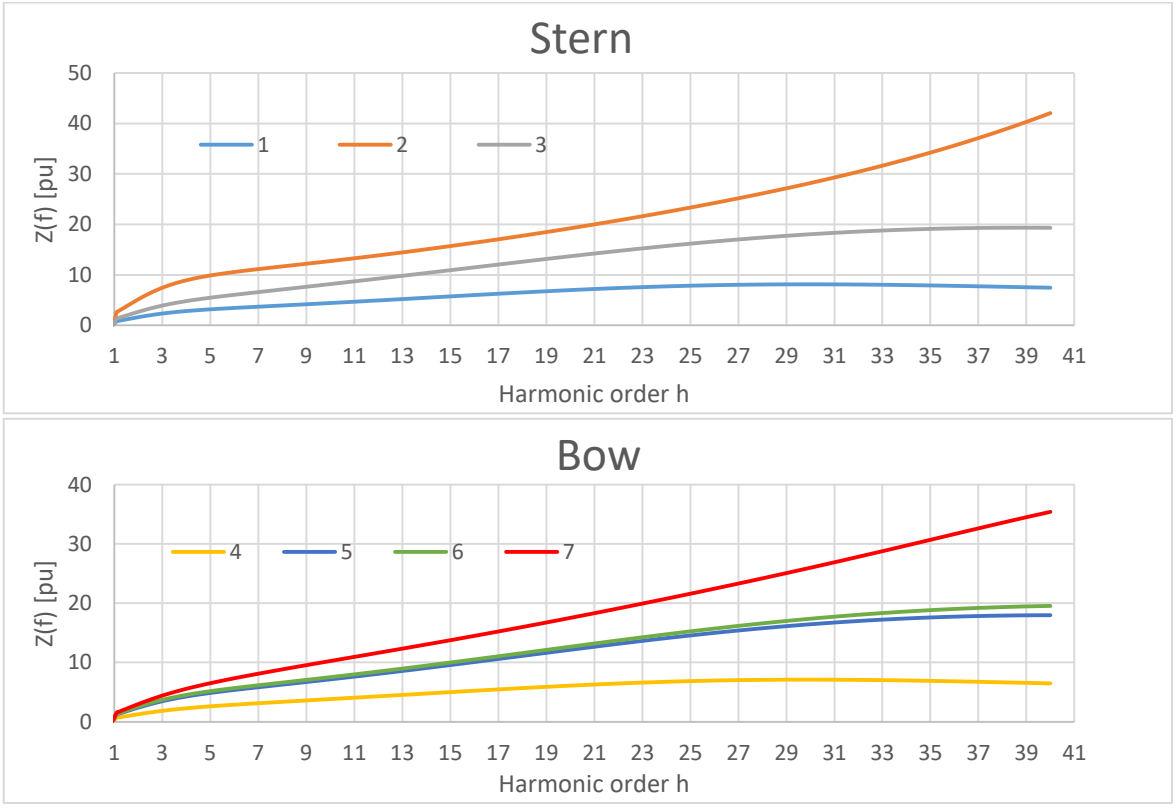

Figure 117- Network impedances for operational profile group A3

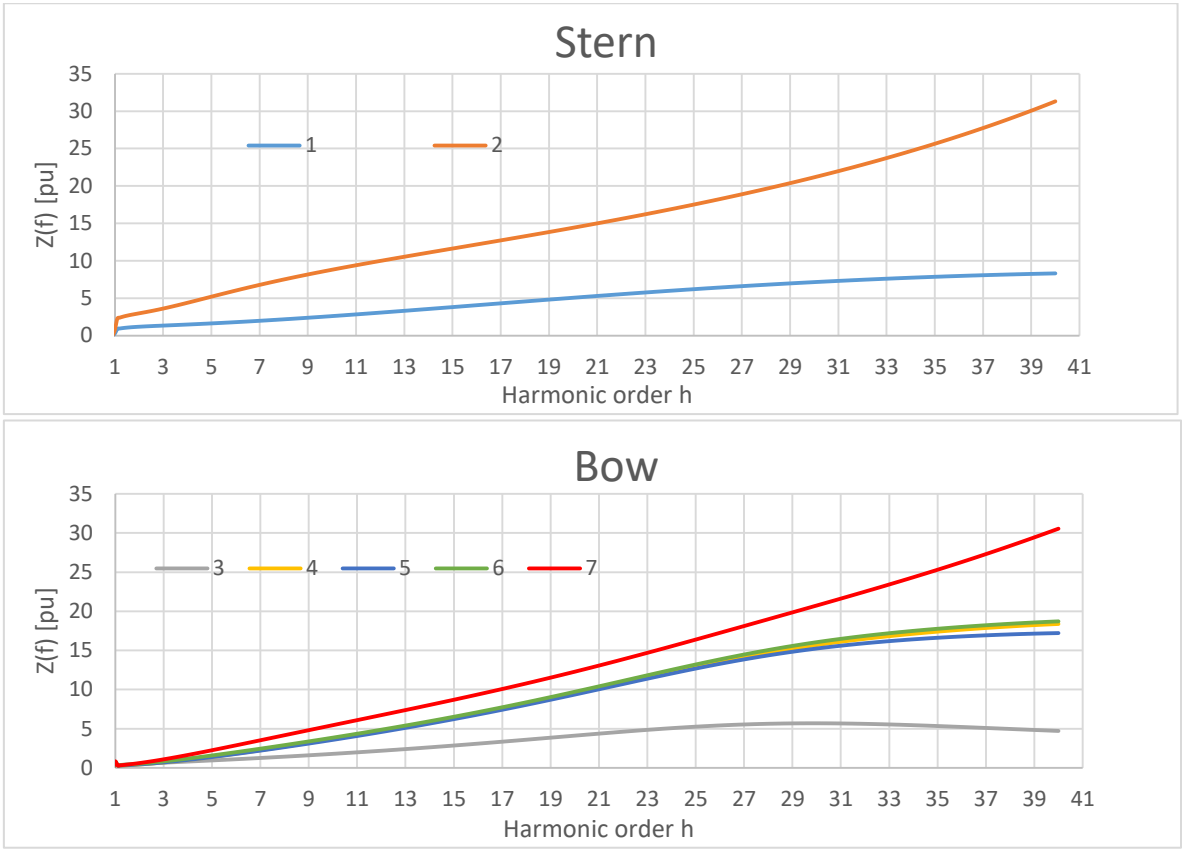

Figure 118 - Network impedances for operational profile group A4

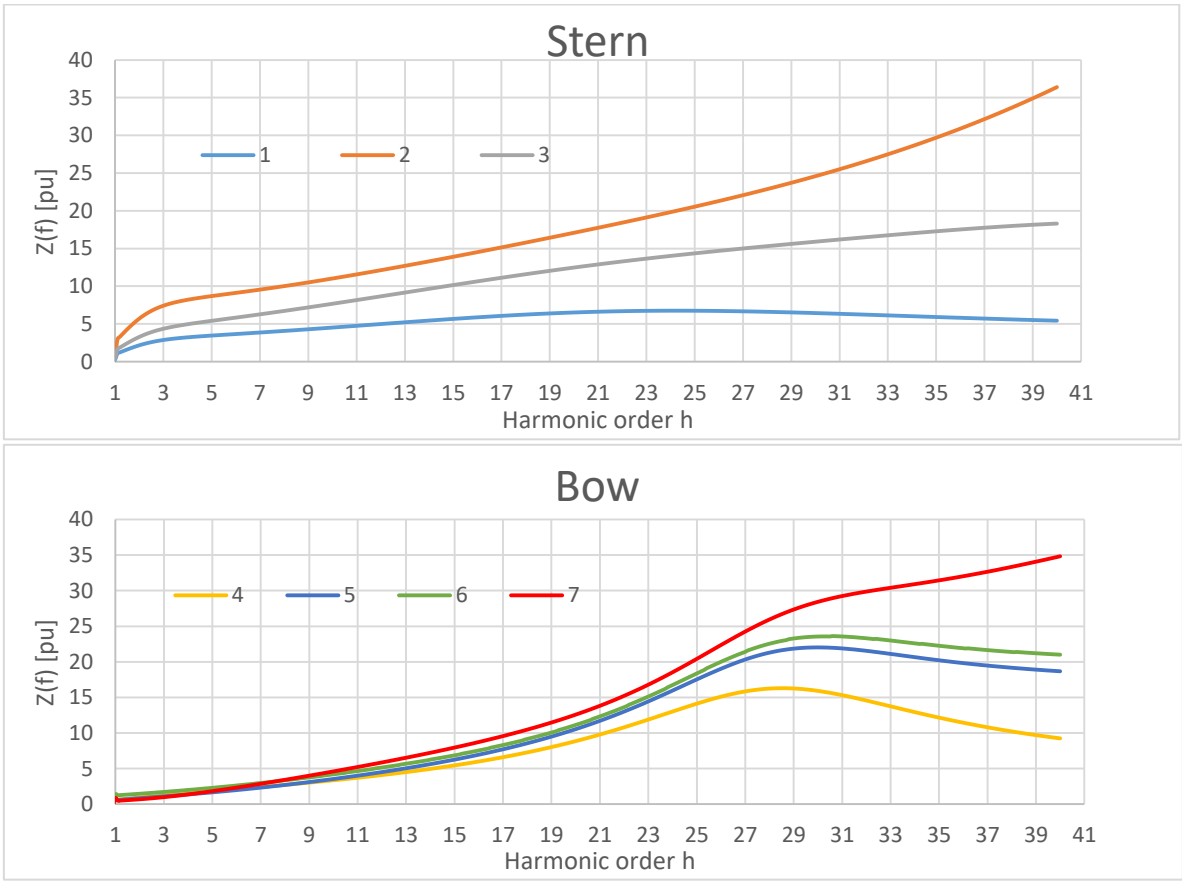

Figure 119 - Network impedances for operational profile group A5

Analyzing the network impedance it is possible affirm that there are no particular criticalities in the Groups A1 to A4. On the contrary, for the A5 operational profile group, a resonance between the 25th and the 31th harmonic was noticed. This aspect can be influenced by the predominantly rotating load and by the considerable power supplied through the main 6 kV electrical panel. In particular, a propulsion engine and two thrusters with a power consumption of about 900 kW, 1200 kW and 1200 kW respectively are located in the main electrical panel of the bow.

8.2.2 –60 Hz network

Taking into account the absorption deriving from the specific operational profile 6 load scenarios (three under normal conditions and 3 under load conditions on a single converter) for the STANAG - 60 Hz network were identified (Chapter 6).
Only the 440 V network was simulated, including the load of the 115 V network. Table 36 shows the aggregated operational profiles for the 60 Hz network.
Figure 120 ÷ Figure 122 show the 60 Hz network single-line diagrams with the aggregate loads, the lengths and the characteristic parameters of the entire 60 Hz network for each group of operational profile. The network impedances were evaluated as a function of frequency at the nodes highlighted in red.

Table 37 –Aggregated Operational Profile for Hybrid Electric/Diesel/Gas Turbines propulsion MVAC – Alternating Current MV System" - 60 Hz Network

Operational profile group	Operational profile	Power Consumption (kW)
B1	1) Port Operational Role / Training 2) Humanitarian Mission 3) Port 4) Maneuver	400
B2	1) Navigation (16 nodes) Operational Role / Training 2) Navigation (18 knots) Operational Role / Training 3) Navigation (Maximum Speed) Operational Role / Training 4) Anchor Ship Operational Role / Training 5) Navigation (Maximum Speed) Combat Role 6) Navigation (10 knots) Operational Role / Training with Electric Propulsion	1000
B3	1) Navigation (10 knots) Role Combat with Electric Propulsion 2) Navigation (Maximum Speed) Combat Role 3) Amphibious Operations Combat Role with Electric Propulsion	1500

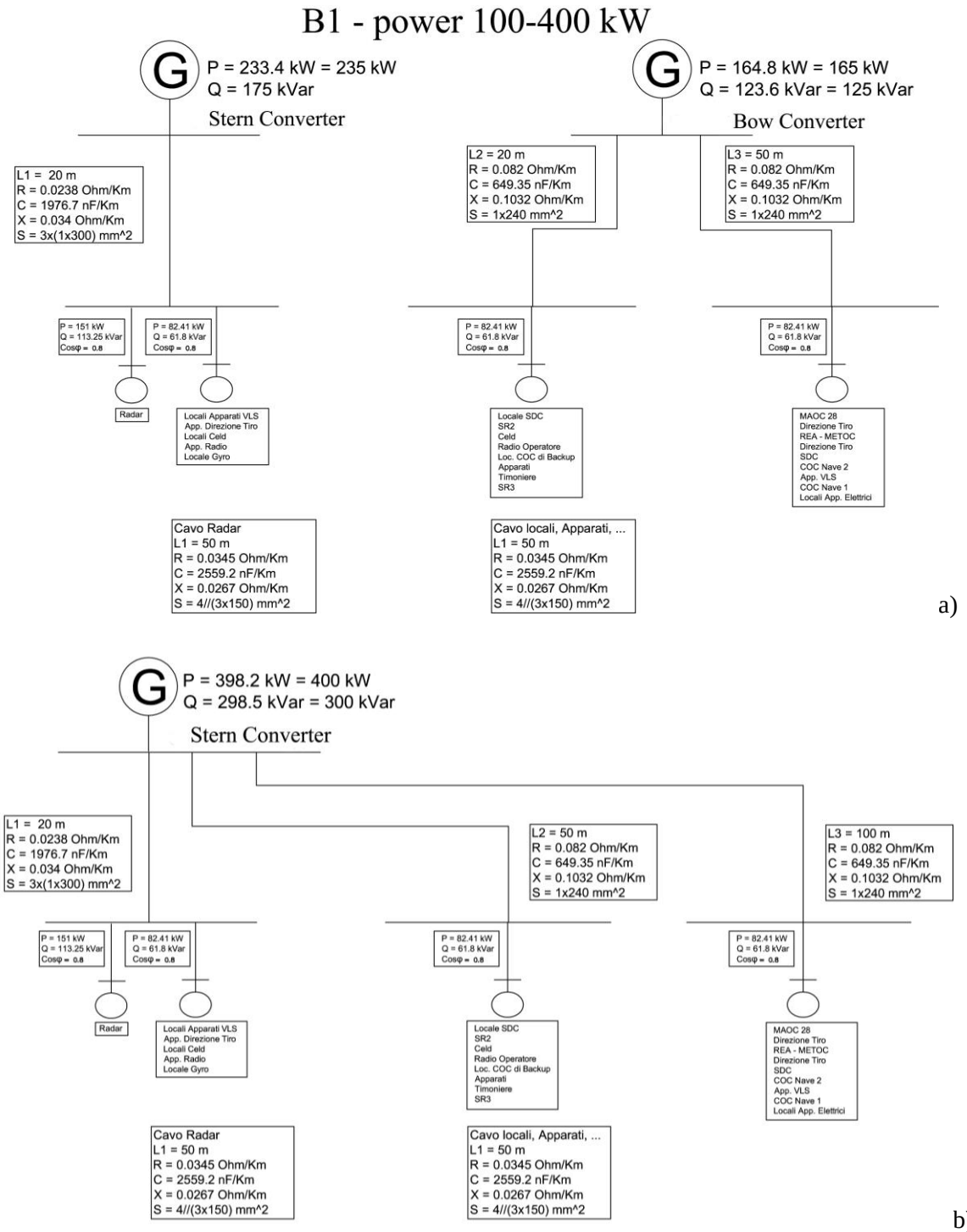

Figure 120 – B1 60 Hz a) Normal b) Supplied By Stern Rotary Converter

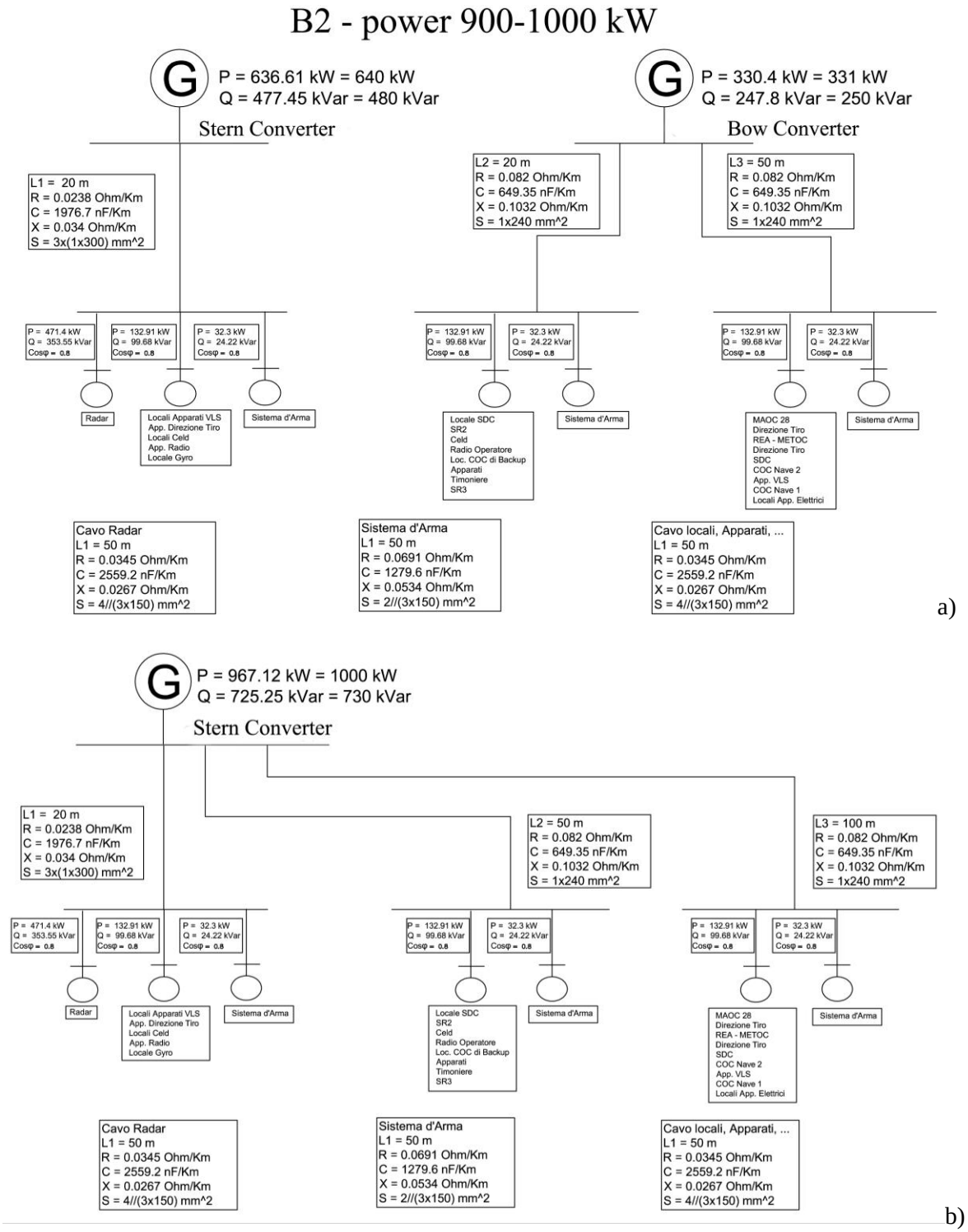

Figure 121 – B2 60 Hz a) Normal b) Supplied By Stern Rotary Converter

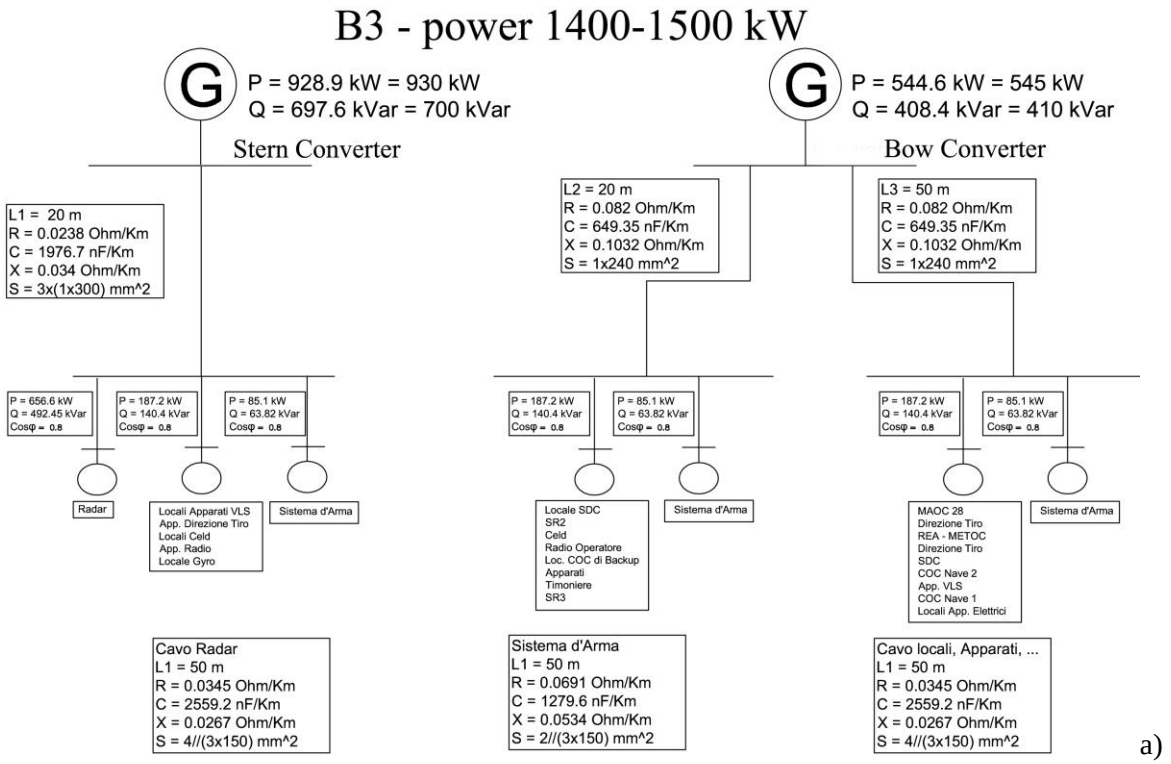

Figure 122 - B3 – 60 Hz a) Normal b) Supplied By Stern Rotary Converter

For the 60 Hz network, every aggregated operational profile group has been simulated either in normal conditions (two converters in operation), or in emergency conditions where a converter supplies the entire STANAG network.

Since the lengths of each power supply cable are not reported on the circuit documents, hypotheses were developed for this network as a function of the maximum length of the cables found on circuit documents.

Figure 123 ÷ Figure 125 show the trends of the network impedances as a function of the frequency of the nodes identified in red (Figure 113) with a value ranging from 1 to 7.

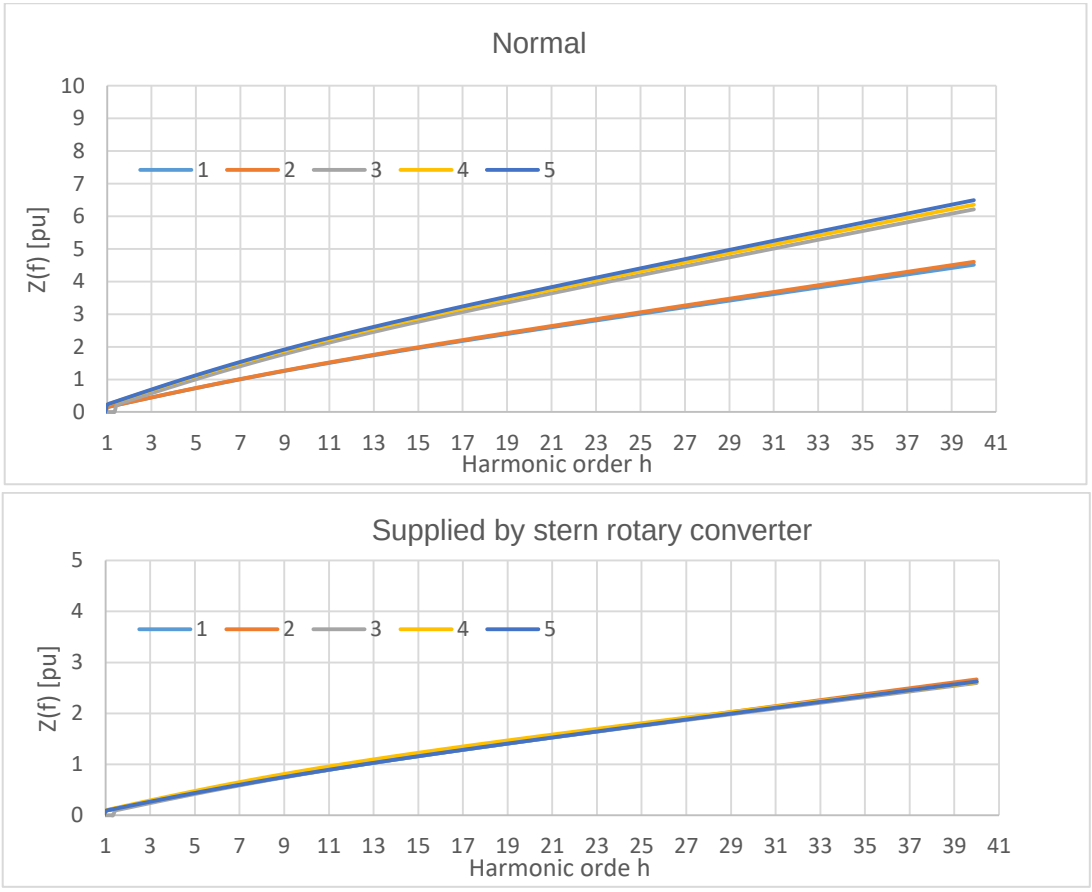

Figure 123 - Network Impedances for Operational Profile Group B1

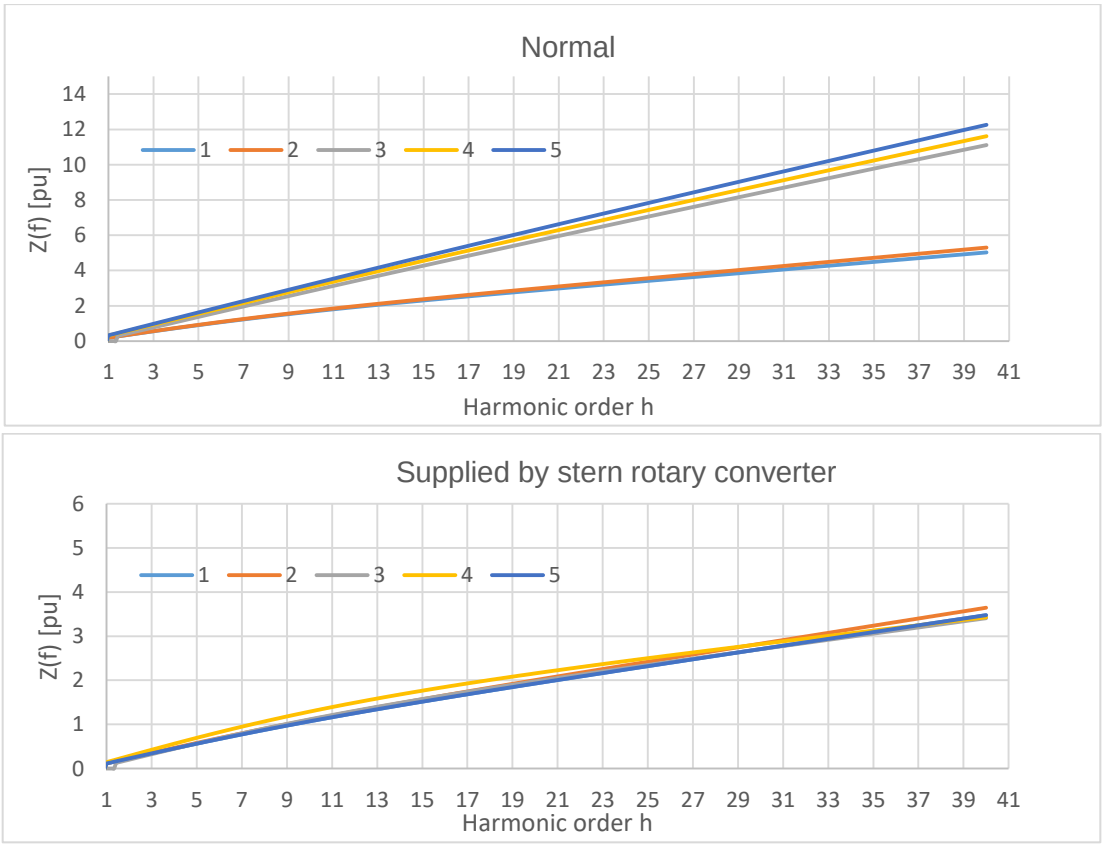

Figure 124 - Network Impedances for Operational Profile Group B2

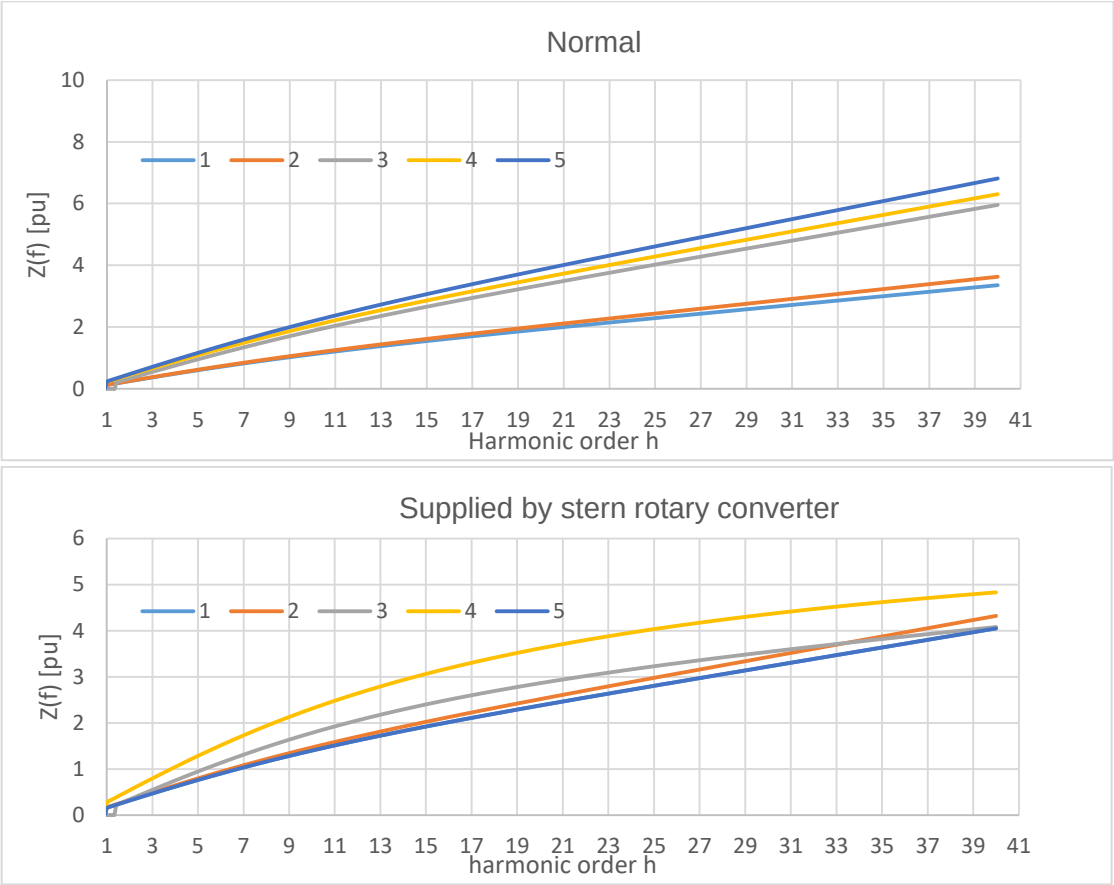

Figure 125 - Network Impedances for Operational Profile Group B

8.3 All electric MVAC/MVAC "hybrid"

This section describes the analyzes related to the MVAC and MVAC "hybrid" electrical network in the frequency domain. In particular, the values of network impedances were analyzed on the generation nodes and on those identified by the busbars of the electrical panels that supply the essential utilities. In this case, the equivalent network referred to the operational profile “Combat condition at 25 navigation kns” (Chapter 6.2 -Table 18) was reported. This operational profile takes into account the highest propulsion consumption. As shown in Figure 119 for Hybrid Electric/Diesel/Gas Turbines propulsion MVAC – by alternating current MV system architecture, a high amount of rotating load could cause resonance.

The investigation of this particular case could be the most critical, where the maximum reliability operation for electric equipment is also required.

Figure 126 shows the single-line diagrams of equivalent networks carried out. Electrical generation stations are distributed on interconnected 11 kV busbars. Each busbar is linked to two others, by means of a tie connection for busbars interfaced to power stations with the same kind of generators (2-4 and 1-3), or, otherwise through a cross connection (1-4 and 2-3). Through this approach, at least a double redundancy is performed and it is possible to react to a large number of failure modes by system reconfiguration. It is important to note that at least one connection must be open to achieve a radial distribution; in this case study, the tie connection 2-4 was analyzed.

The network impedances were evaluated as a function of frequency at the nodes highlighted in red. In particular, the evaluations refer to the following nodes:

- generation nodes: QEP3, QEP4, QEP5, QEP8;
- essential user nodes: QDP13, QDP14, QDP15, QDP17, QDP18, SQDP4.

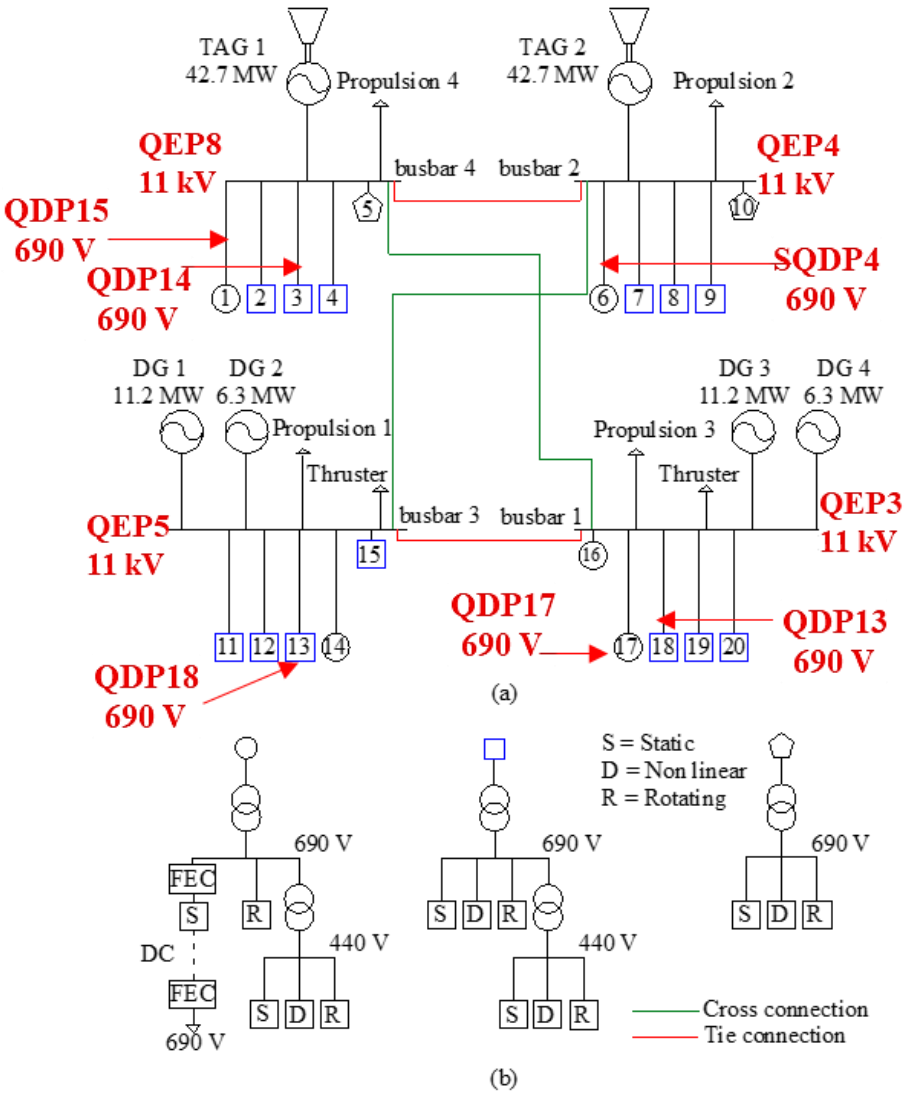

Figure 126 - (A) Equivalent Distribution Network Scheme. (B) Aggregate Loads in The Distribution Network.

Table 38 ÷ Table 41 show: i) the total power absorbed by electrical loads, ii) static and rotating electrical power iii) non-linear power distribution on each feeder and iiii) feeder lengths in distribution network. The tables also show the total power demand subdivided between two BT distribution levels.

Table 38 - Total Power Absorbed by Electrical Loads in Combat Role.

P [kW]	Q [kVAr]
5250	2900

Table 39 - Static and Rotating Power Absorbed, Sort by Distribution Level.

Combat Role		690 V	440 V
Static	P [kW]	720	126
	Q [kVAr]	430	40
Rotating	P [kW]	730	270
	Q [kVAr]	380	180

Table 40 - Non-Linear Power Distribution on Each Feeder (% of Total Power S [kVA])

	MVAC		Hybrid-MVAC			MVAC		Hybrid-MVAC	
	(%)		(%)			(%)		(%)	
Feeder	660 V	440 V	660 V	440 V	Feeder	660 V	440 V	660 V	440 V
1	9	2	0	2	11	2	0	2	0
2	1	1	1	1	12	2	1	2	1
3	2	1	1	1	13	2	1	0	1
4	0	1	0	1	14	6	1	0	1
5	1	0	1	0	15	1	1	1	1
6	0	2	0	2	16	6	1	0	1
7	3	1	3	1	17	2	1	0	1
8	3	1	3	1	18	3	1	2	1
9	0	1	0	1	19	3	1	3	1
10	0	0	0	0	20	0	1	0	1

Table 41 - Feeder Lengths

Feeder	Length (m)	Feeder	Length (m)
1	70	11	100
2	50	12	110
3	180	13	220
4	50	14	100
5	10	15	10
6	30	16	10
7	70	17	120
8	80	18	120
9	130	19	70
10	10	20	190

In the MVAC case, the total power generated by non-linear loads is 65 %, and it is distributed as follows: 47 % at 690 V and 18 % at 440 V.
In Hybrid-MVAC case, the total power of non-linear load is 38 %; at 690 V the percentage of non-linear load decreases from 47 % to 20 %. The difference (27 %) was distributed on network at 690 V level and added in static load family.
In this operating condition, total active and reactive generated powers are equal to 103 MW and 76 MVAr respectively. Only TAG 1 & 2 and DG 1 & 3 are functioning.
Harmonic analyses were carried out at the generation MV busbars, considering three different filter configurations, namely: uncompensated, high pass filters and tuned filters plus high pass filter Filters sizing was obtained using the expressions shown in Chapter 6.2 - Table 20.
The filters types used for different network configurations are:

- High pass filter, with 12^{th} harmonic cut-off frequency (HP);
- 11^{th} and 13^{th} harmonics single tuned filters (ST), plus high pass filter with a 24^{th} harmonic cut-off frequency (HP+ST).

Filtering around the 12^{th} harmonics is meant to cope with the loss of half the propulsion power, entailing 12-pulse operation of front end converters.
Figure 127 ÷ Figure 130 show network impedances at harmonic frequencies evaluated at 11 kV/690 busbars (Figure 126) as a function of frequency, in the (0 ÷ 2000) Hz range for Hybrid-MVAC case. Figure 127 shows the response of the uncompensated system. Figure 128 shows the response of the power factor correction. Figure 129 and Figure 130 show the effect of high pass filters and the effects of a combination of tuned (11^{th} /13^{th}) and high pass filters, respectively.

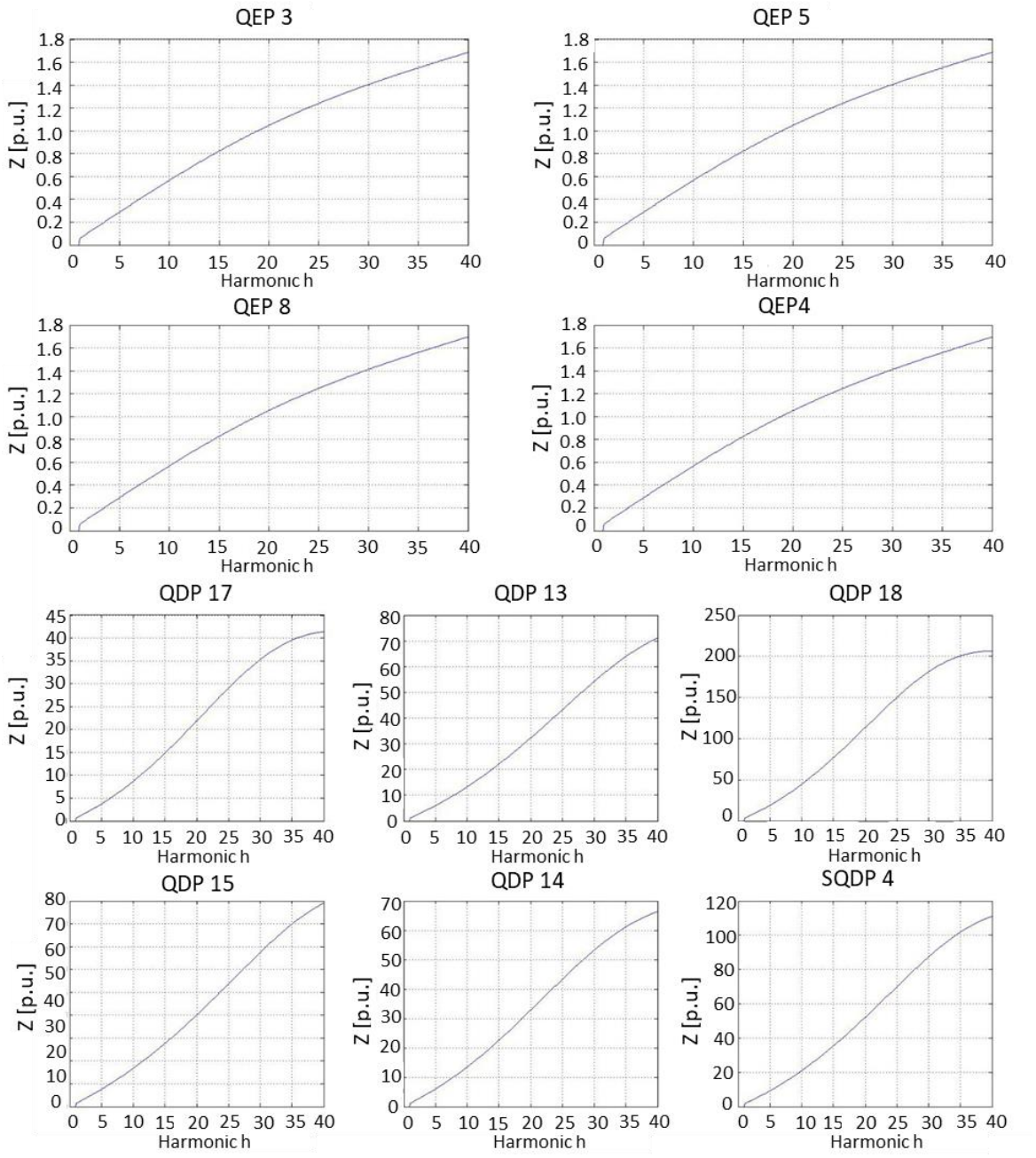

Figure 127 - Network Impedances at Harmonic Frequencies: Uncompensated

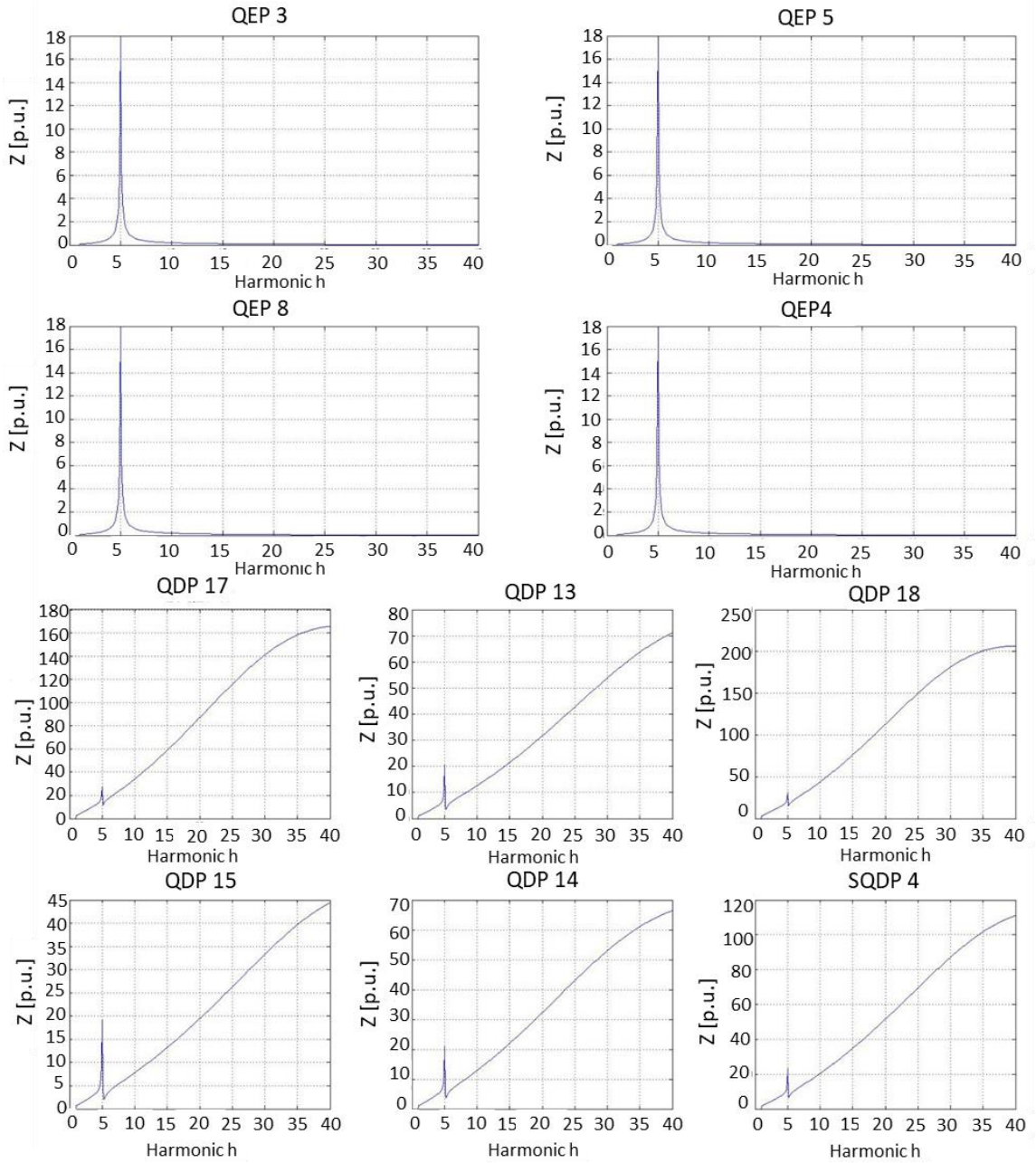

Figure 128 - Network Impedances at Harmonic Frequencies: Power Factor Correction

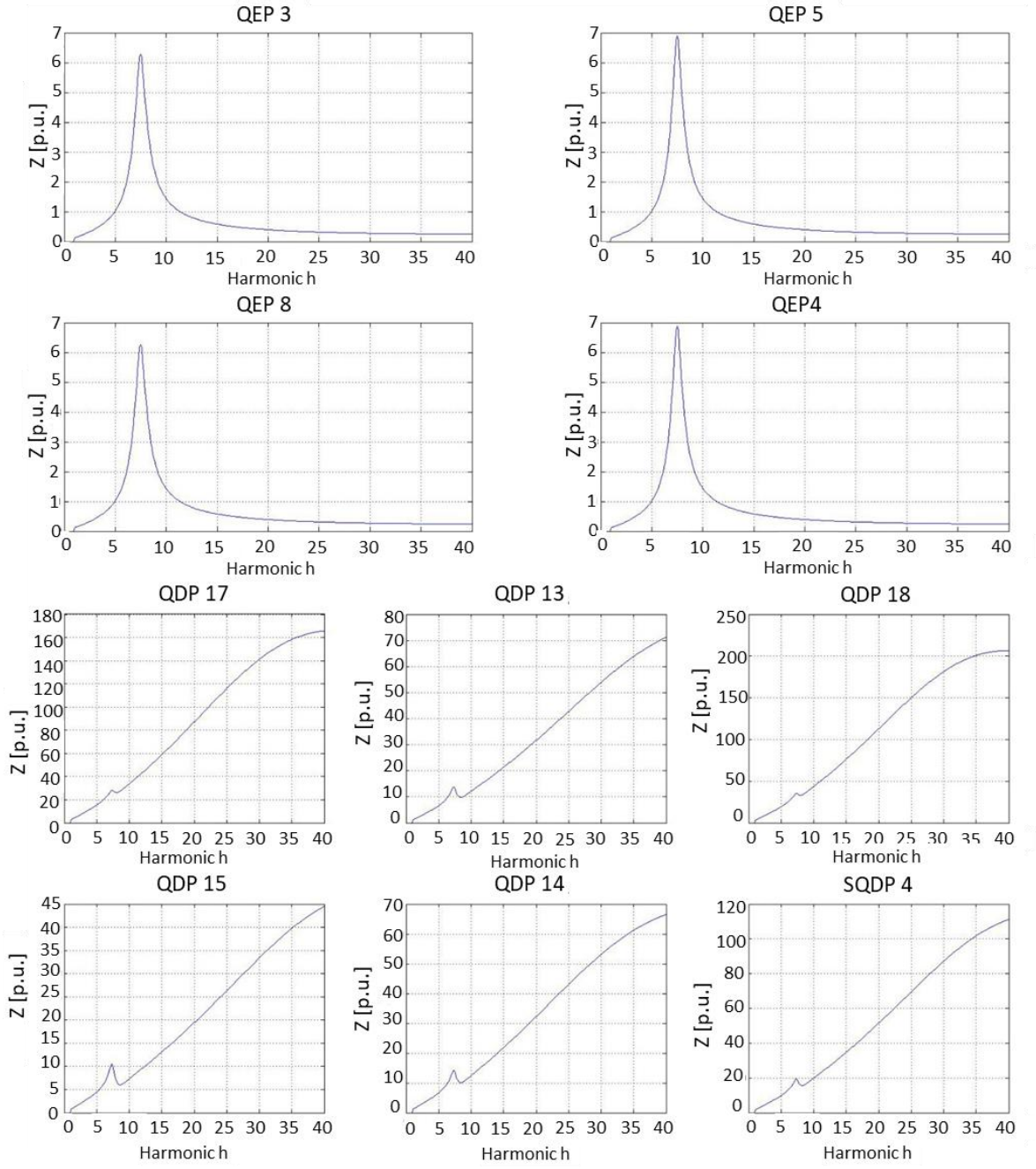

Figure 129 - Network Impedances at Harmonic Frequencies: High Pass Filter

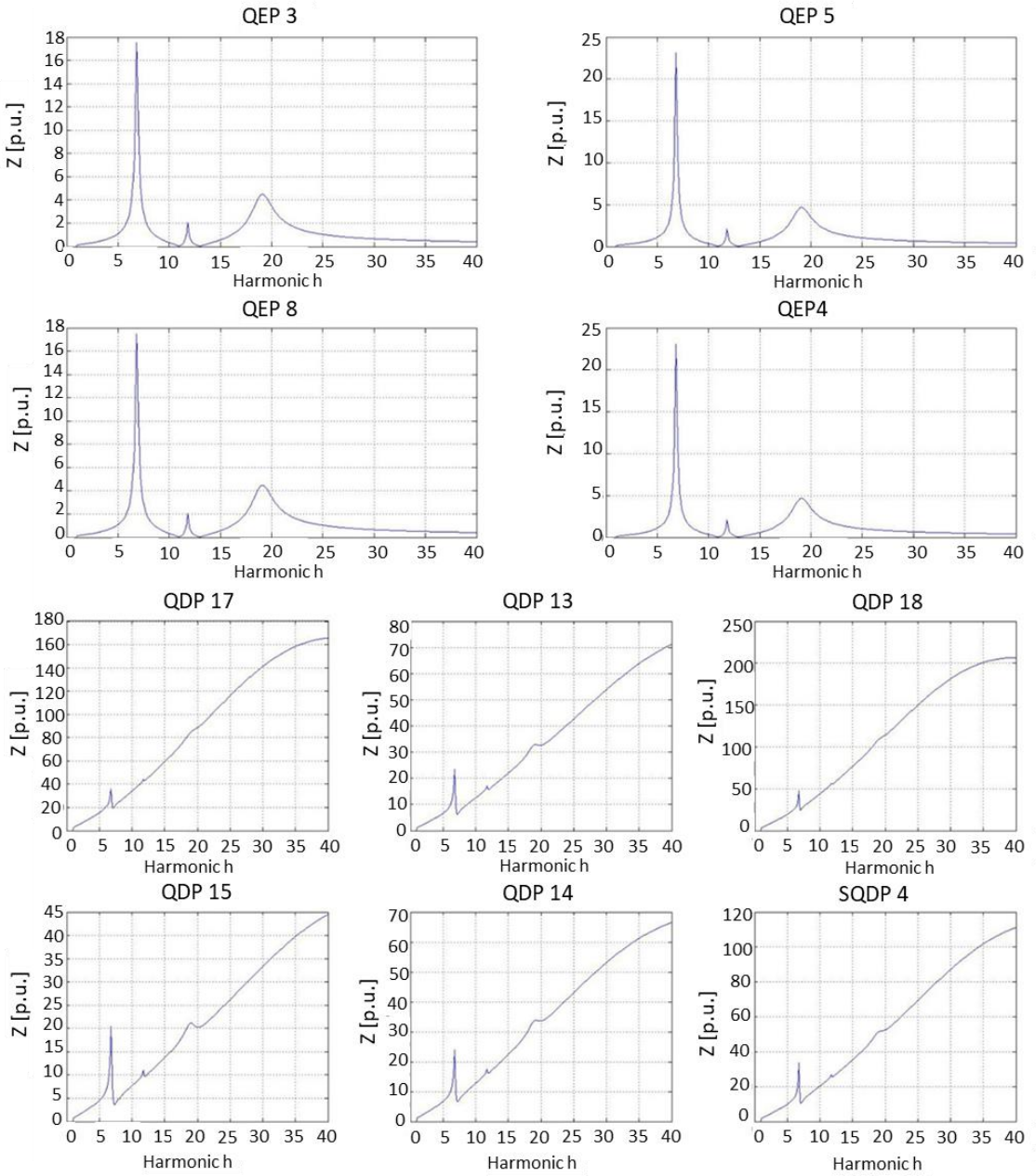

Figure 130 - Network Impedances At Harmonic Frequencies: Tuned Filters And High Pass Filter (HP+ST).

In generation busbars without filters or capacitors, no resonances are found (Figure 127). With power factor correction a resonance on the 5th is detected (Figure 128), with the HPF filter (Figure 129) the resonance is between the 5th and 10th harmonic (375 Hz), meanwhile with ST and HP filters, three resonant frequencies are located at 340 Hz, 590 Hz and 955 Hz (Figure 130).

Resonances are detected in all electrical panels that supply essential loads (QDP 17, QDP 13, QDP18, QDP15, QDP14, SQDP4), apart from QDP18 and QDP17.

A resonance on the 5th harmonic with power factor correction is found (Figure 128), with the HPF filter the resonance is between the 5th and 10th harmonic (Figure 129). With the STF + HPF filters three resonances were discovered, namely between the 5th and the 10th harmonic, the 10th and the 15th harmonic and between the 15th and the 20th harmonic (Figure 130). For QDP18 and QDP17 electrical panels the resonances indicated show a negligible magnitude with the exception of the 5th harmonic.

Network impedances for MVAC systems

The results relating MVAC network were not reported since they were substantially similar to those relating to the "hybrid" MVAC network.
The results of network impedance for MVAC network show difference respect MVAC "hybrid":

- in the generation busbars Z (f) has the same resonance on the 5th harmonic, however the amplitude increases, passing from 18 p. u. to 50 p. u.;
- in electrical panels supplying essential loads, Z (f) presents resonance on the 5th harmonic, and its amplitude increases from 20 ÷ 25 p. u. to 50 ÷ 60 p. u.;
- with the HPF filters tuned to the 12th harmonic, Z (f) is the same;
- with the STF + HPF filters the resonances identified are the same (340 Hz, 590 Hz, 955 Hz) and there is a difference in amplitudes limited to the resonance found at 340 Hz. In particular, the amplitude is greater than 5 p.u. in generation nodes and 10 p. u. on electrical panels that supply essential loads.

8.3.1 Total Harmonic Distortion evaluation "all electric"

Harmonic distortion was evaluated on the extremely simplified equivalent network of Figure 126.
DC islands in the "Hybrid"- MVAC system were represented with the scheme of Figure 80. For each electrical switchboard, loads have been grouped into three main categories: Static loads; Non-linear loads-converters and Rotating loads (Chapter 4). Five switchboard/feeders (Figure 126 No. 1, 6, 14, 16, 17) are characterizes by either large power absorption or by supplying essential loads (e.g. ship hospital, communications and navigation support), possibly via DC islands. The latter are interfaced with AC grid by active FECs, characterized by a sinusoidal current input waveform.
Simulations have been carried out considering passive front-end converters, i.e. 6-pulse diode bridges with the harmonic magnitude spectrum reported in Table 42.

Table 42 - Harmonic Disturbances Used in Harmonic Evaluation

Harmonic order	**1**	**5**	**7**	**11**	**13**	**17**	**19**	**23**	**25**
% $I_{Nominal}$	100	17.5	11.1	4.5	2.9	2.0	1.0	0.9	0.8

In practice, since the front-end propulsion system ensures 24-pulse operation, only the 23^{th} and 25^{th} harmonics were considered in unfaulted scenarios; 12-pulse operation was assumed in case of loss of 50 % of propulsion power, thus adding the 11^{th} and 13^{th} harmonics.
Table 43 and Table 44 show THD_V % evaluated at the 11kV generation busbar for the different filter configuration, along with values of IHD % for significant harmonics. Two sets of THD_V % values are reported: the first is calculated assuming a uniform distribution of harmonic voltage phases (Case A); the second is the worst condition (in-phase harmonic voltages, Case B).
As shown in Table 43 and in Figure 127 ÷ Figure 130, the large harmonic emission of the high-power propulsion system results in significantly high THD_V % values in the absence of filters.
Table 43 shows the effectiveness of filters in reducing the MVAC system THD_V %, especially the HP+ST configuration. However, such filters also introduced new resonances (Figure 130) which actually increase the 7^{th} harmonic distortion; as a result, the 8 % maximum THD_V %, allowed by the Standard at the MV point of common coupling is complied with only in Case A, reaching instead a value of 10.9 % in Case B.
Simulation results reported in Table 44 for the H-MVAC system evidence how the THD_V % could be reduced with DC islands, and represents a valid solution in terms of continuity of supply on board.

Table 43 - THD_V % In MVAC Configuration

	MVAC			
	A	B		
	THD_V [%]	THD_V [%]	h	IHD [%]
Uncompensated	9.8	20	23	14
Power Factor correction	24.8	87	5	85
HP	8.4	9.6	11	7.6
ST+HP	6.5	10.9	7	9.2

Table 44 - THD_V % In Hybrid MVAC Configuration

	Hybrid-MVAC			
	A	B		
	THD_V [%]	THD_V [%]	h	IHD [%]
Uncompensated	9.8	20	23	14
Power Factor correction	5.1	17	5	10
HP	8.2	8.6	11	7.2
ST+HP	5.4	6.2	23	4.2

The large harmonic emission of the high-power propulsion system results in significantly high THD_V %. So, it is necessary to install filters, in order to reduce harmonic disturbances. The HP+ST configuration represents the best solution for filters effectiveness in reducing the MVAC system THD_V %.

Filters introduce benefits regarding THD_V, but, at the same time, create resonances, consequently, harmonic disturbances generated by onboard non-linear loads can be excited by system resonances and, thus, increase THD_V % values.

For this reason, the supply of such loads by means of DC islands is preferable, thanks to the harmonic disturbances immunity at the DC side and the installation of AC/DC converters with sinusoidal absorption at the AC side. In the case study, the introduction of only five DC islands in the “Hybrid” MVAC system reduces THD_V %. In addition, the installation of storage systems and four-quadrant FECs would also improve AC network stability and continuity of supply, thanks to active and reactive power controls. High quality and continuity of supply are also provided to DC loads.

Chapter IX – Reliability Analysis

In this chapter a preliminary analysis on the availability, reconfigurability and reliability of the naval integrated power system is reported. In order to consider fault events, which may cause main failures such as partial collapse of the network, the use of the connections between the busbar (cross connection) and the redundancy in the power supply systems was considered. Through system reconfiguration operations, this design solution allows to limit the number of disconnected loads due to a fault. In order to make this operation more efficient, a double power supply for essential loads was also envisaged through interconnections between different electrical panels, placed in different compartments, and powered by separate sources. This chapter reports the preliminary assessments relating to the reliability of the system, starting from some important failures related to the loss of power to essential users. The investigations carried out are directly connected with the reliability of the systems (in par 3.3 Electrical System Dependability). However, because we intended to advance some preliminary observations on the correlation between the system's architecture and its reliability features, some basic concepts such as Fault detection, Fault tolerance, System reconfiguration and top event analysis were employed.

9.1 Reliability of the electrical system for "all electric" layouts

Preliminary evaluations on the system reliability are limited; in particular, the study was conducted on:

- all the main components and electrical panels supplied by 11 kV medium voltage (QEP5, QEP8, QEP4, QEP3);
- for the low voltage (690 V all the main components and electrical panels that supply essential loads/islands in DC (QDP14, QDP15, QDP18, SQDP4, QDP13, QDP17, QEP3 LV, QEP7 LV).

Table 45 shows all the components referred to MVAC and Hybrid MVAC shown in Figure 76 and in Figure 77 (such as busbars, switches, generators, motors, cables, etc.), identified by a code, with the respective functions within the system.

Table 45 - Components of The Electrical System

Component	Description	Function
$Busbar_{mv}$ 1	Busbar QEP5 MT 11kV	Busbar MT 11 kV
$Busbar_{mv}$ 2	Busbar QEP4 MT 11kV	Busbar MT 11 kV
$Busbar_{mv}$ 4	Busbar QEP8 MT 11kV	Busbar MT 11 kV
$Busbar_{mv}$ 3	Busbar QEP3 MT 11kV	Busbar MT 11 kV
Cable $_{Rth}$1	Power supply connection cable from QEP8 to TOft thruster	Cable power supply reserve
Cable $_{Rth}$2	Power supply connection cable from QEP4 to Bow thruster	Cable power supply reserve
Cable $_{Th}$1	power cable from QEP5 to Aft thruster	Power cable th
Cable $_{Th}$2	Power cable connection from QEP3 to Bow Thruster	Power cable th
Cable $_{Tie}$2	Power cable connection tie QEP3-QEP5	Power cable tie
Cable $_{Tie}$1	Power cable connection tie QEP8-QEP4	Power cable tie
$Cable_{c}$1	Power cable connection for cross connection QEP8-QEP3	Power cable cross connection
$Cable_{c}$2	Power cable connection for cross connection QEP5-QEP4	Power cable cross connection
$Cable_{mv}$3	Power cable QEP3-QDP13	Power cable to LV
$Cable_{mv}$3-1	Power cable QEP3-QDP17	Power cable to LV
$Cable_{mv}$3-2	Power cable QEP3-QEP3bt	Power cable to LV
$Cable_{mv}$2	Power cable QEP4-SQDP4	Power cable to LV
$Cable_{mv}$1	Power cable QEP5-QDP18	Power cable to LV
$Cable_{mv}$1-1	Power cable QEP5-QEP7LV	Power cable to LV
$Cable_{mv}$4	Power cable QEP8-QDP14	Power cable to LV
$Cable_{mv}$4-1	Power cable QEP8-QDP15	Power cable to LV
Cable $_{EMP}$1	Power cable from QEP5 to propulsion engine EPM1	Power cable for propulsion
Cable $_{EMP}$2	Power cable from QEP4 to propulsion engine EPM2	Power cable for propulsion

Cable $_{EMP}3$	Power cable from QEP3 to propulsion engine EPM3	Power cable for propulsion
Cable $_{EMP}4$	Power cable from QEP8 to propulsion engine EPM4	Power cable for propulsion
DG1	Diesel generation (16V38) on QEP5	Diesel generation
DG2	Diesel generation (9l38) on QEP5	Diesel generation
DG3	Diesel generation (16V38) on QEP3	Diesel generation
DG4	Diesel generation (9l38) on QEP3	Diesel generation
TAG1	Gas turbine on QEP8 (LM6000-Pf)	Gas turbine generation
TAG2	Gas turbine on QEP4 (LM6000-Pf)	Gas turbine generation
I_C1	Circuit breaker switch QEP8 side of cross connection QEP8 and QEP3	Circuit breaker switch cross connection
I_C2	Circuit breaker switch QEP3 side of cross connection QEP8 and QEP3	Circuit breaker switch cross connection
I_C3	Circuit breaker switch QEP5 side of cross connection QEP5 and QEP4	Circuit breaker switch cross connection
I_C4	Circuit breaker switch QEP4 side of cross connection QEP5 and QEP4	Circuit breaker switch cross connection
$I_{DG}1$	Circuit breaker switch DG1 on QEP5 (16V38)	Circuit breaker switch Diesel generator
$I_{DG}2$	Circuit breaker switch DG2 on QEP5 (9L38)	Circuit breaker switch Diesel generator
$I_{DG}3$	Circuit breaker switch DG3 on QEP3 (16V38)	Circuit breaker switch Diesel generator
$I_{DG}4$	Circuit breaker switch DG4 on QEP3 (9L38)	Circuit breaker switch Diesel generator
I_p1	Circuit breaker switch on engine line EMP1 connected to QEP5	Circuit breaker switch propulsion engine
I_p2	Circuit breaker switch on engine line EMP2 connected to QEP4	Circuit breaker switch propulsion engine
I_p3	Circuit breaker switch on engine line EMP3 connected to QEP3	Circuit breaker switch propulsion engine
I_p4	Circuit breaker switch on engine line EMP4 connected to QEP8	Circuit breaker switch propulsion engine
$I_{rTH}1$	Circuit breaker switch reserve power supply Aft Thruster on QEP8	Reserve circuit breaker switch Th
$I_{rTH}2$	Circuit breaker switch reserve power supply Bow Thruster on QEP4	Reserve circuit breaker switch Th
I_T1	Circuit breaker switch TAG QEP8 (LM6000-PF)	Circuit breaker switch Gas turbine
I_T2	Circuit breaker switch TAG QEP4 (LM6000-PF)	Circuit breaker switch Gas turbine
$I_{TH}1$	Circuit breaker switch Aft Thruster on QEP5	Circuit breaker switch Th
$I_{TH}2$	Circuit breaker switch Bow Thruster on QEP3	Circuit breaker switchT h
$I_{tie}1$	Circuit breaker switch QEP8 side of tie QEP8 and QEP4	Circuit breaker switch tie
$I_{tie}2$	Circuit breaker switch QP4 side of tie QEP8 and QEP4	Circuit breaker switch tie
$I_{tie}3$	Circuit breaker switch QEP5 side of tie QEP5 and QEP3	Circuit breaker switch tie
$I_{tie}4$	Circuit breaker switch QEP3 side of tie QEP5 and QEP3	Circuit breaker switch tie
K1	Generation joint - Propulsion of TAG1 on QEP8	Joint busbar circuit breaker switch MV
K2	Generation joint - Propulsion of TAG2 on QEP4	Joint busbar circuit breaker switch MV
K3	Generation joint - Propulsion of DG1-DG2 on QEP5	Joint busbar circuit breaker switch MV
K4	Generation joint - Propulsion of DG3-DG4 on QEP3	Joint busbar circuit breaker switch MV
K5	Joint distribution - Propulsion on QEP8	Joint busbar circuit breaker switch MV
K6	Joint distribution - Propulsion on QEP4	Joint busbar circuit breaker switch MV
K7	Joint distribution - Propulsion on QEP5	Joint busbar circuit breaker switch MV
K8	Joint distribution - Propulsion on QEP3	Joint busbar circuit breaker switch MV
$I_{LV}4$	Circuit breaker switch QDP14 side for power cable connection to QEP8-QDP14	Circuit breaker switch LV
$I_{LV}3$	Circuit breaker switch QDP13 side for power cable connection to QEP3-QDP13	Circuit breaker switch LV
$I_{LV}4$-1	Circuit breaker switch QDP15 side for power cable connection to QEP8-QDP15	Circuit breaker switch LV
I_{LV} 3-1	Circuit breaker switch QDP17 side for power cable connection to QEP3-QDP17	Circuit breaker switch LV
I_{LV} 3-2	Circuit breaker switch QEP3 side for power cable connection to QEP3-QEP3LV	Circuit breaker switch LV
$I_{LV}1$	Circuit breaker switch QDP18 side for power cable connection to QEP5-QDP18	Circuit breaker switch LV
$I_{LV}1$-1	Circuit breaker switch QEP7 side for power cable connection to QEP5-QEP7LV	Circuit breaker switch LV
$I_{LV}2$	Circuit breaker switch SQDP4 side for power cable connection to QEP4-SQDP4	Circuit breaker switch LV
$I_{MV}3$	Circuit breaker switch QEP3 side for power cable connection to QEP3-QDP13	Circuit breaker switch MV
$I_{MV}3$-1	Circuit breaker switch QEP3 side for power cable connection to QEP3-QDP17	Circuit breaker switch MV
$I_{MV}3$-2	Circuit breaker switch QEP3 side for power cable connection to QEP3-QEP3LV	Circuit breaker switch MV
$I_{MV}2$	Circuit breaker switch QEP4 side for power cable connection to QEP4-Sqdp4	Circuit breaker switch MV

$I_{MV}1$	Circuit breaker switch QEP5 side for power cable connection to QEP5-QDP18	Circuit breaker switch MV
$I_{MV}1$-1	Circuit breaker switch QEP5 side for power cable connection to QEP5-QEP7LV	Circuit breaker switch MV
$I_{MV}4$	Circuit breaker switch QEP8 side for power cable connection to QEP8-QDP14	Circuit breaker switch MV
$I_{MV}4$-1	Circuit breaker switch QEP8 side for power cable connection to QEP8-QDP15	Circuit breaker switch MV
Th1	Maneuvering AftThruster	Thruster
Th2	Maneuvering Bow Thruster	Thruster
EPM1	Propulsion engine	Propulsion engine
EPM2	Propulsion engine	Propulsion engine
EPM3	Propulsion engine	Propulsion engine
EPM4	Propulsion engine	Propulsion engine
$Busbar_{LV}4$	Busbar QDP14 to 690 V essential loads	Busbar LV 690 V
$Busbar_{LV}4$-1	Busbar QDP15 to 690 V essential loads /Island DC.	Busbar LV 690 V
$Busbar_{LV}1$	Busbar QDP18 to 690V essential loads	Busbar LV 690 V
$Busbar_{LV}1$-1	Busbar QEP7LV to 690 V Island DC.	Busbar LV 690 V
$Busbar_{LV}2$	Busbar SQDP4 to 690 V essential loads /Island DC.	Busbar LV 690 V
$Busbar_{LV}3$	Busbar QDP13 to 690V essential loads /Island DC.	Busbar LV 690 V
$Busbar_{LV}3$-1	Busbar QDP17 to 690 V essential loads	Busbar LV 690 V
$Busbar_{LV}3$-2	Busbar QEP3LV to 690 V Island DC.	Busbar LV 690 V
$S_{Trafo}3$	Transformer switch QEP3-QDP13	Transformer switch
S_{Trafo} 3-2	Transformer switch QEP3-QEP3bt	Transformer switch
$S_{Trafo}3$-1	Transformer switch QEP3-QDP17	Transformer switch
$S_{Trafo}2$	Transformer switch QEP4-SQDP4	Transformer switch
$S_{Trafo}1$	Transformer switch QEP5-QDP18	Transformer switch
$S_{Trafo}1$-1	Transformer switch QEP5-QEP7bt	Transformer switch
$S_{Trafo}4$	Transformer switch QEP8-QDP14	Transformer switch
$S_{Trafo}4$-1	Transformer switch QEP8-QDP15	Transformer switch
Trafo3	Transformer QEP3-QDP13	Transformer MV-LV
Trafo 3-2	Transformer QEP3-QEP3bt	Transformer MV-LV
Trafo3-1	Transformer QEP3-QDP17	Transformer MV-LV
Trafo2	Transformer QEP4-SQDP4	Transformer MV-LV
Trafo1	Transformer QEP5-QDP18	Transformer MV-LV
Trafo1-1	Transformer QEP5-QEP7bt	Transformer MV-LV
Trafo4-1	Transformer QEP8-QDP15	Transformer MV-LV
Trafo4	Transformer QEP8-QDP14	Transformer MV-LV

9.2 System Reconfigurability

In order to ensure the continuity and reconfigurability requirements of some LV electrical panels, supplying essential loads, backup supplies were provided. Table 46 shows the connections provided for the backup supplies.

Table 46 – Backup Supplies for Electrical Panels That Supply Essential Loads

LV connections between electrical panels that supply essential loads
From QDP18 to QDP15
From QDP10 to QDP17
From QDP11 to QDP13
From QDP 14 to SQDP4

9.3 Impact of faults on the electrical system

For each possible failure of the electrical system components (Table 45), Table 47 shows the effects on the general system, both in terms of navigation and shutdown of the "essential" electrical panels and in the case of a reconfiguration following an event. In particular, the table shows how the failure

of a component cannot report consequences (in the table: "no effect") for the system, thanks to the network configuration.

Table 47 – Failure Component Effects and Reconfiguration

Component out of service	Effects	Reconfiguration
$Busbar_{MV}$ 1	QEP5 out of service (Unavailability EPM1 and QEP3 LV - QEP7 LV that power DC island)	Supply QDP18 from QDP15
$Busbar_{MV}$ 2	QEP4 out of service (unavailability EPM2)	Supply SQDP4 from QDP14
$Busbar_{MV}$ 4	QEP8 out of service (unavailability EPM4)	Supply QDP14 from SQDP4 and QDP15 from QDP18
$Busbar_{MV}$ 3	QEP3 out of service (unavailability EPM3)	Supply QDP13 from QDP11 and QDP17 from QDP10
Cable $_{rth}$1	No effect (unavailability redundancy from QEP8)	
Cable $_{rth}$2	No effect (unavailability redundancy from QEP4)	
Cable $_{th}$1	No effect	Supply from QEP8
Cable $_{th}$2	No effect	Supply from QEP4
Cable $_{tie}$2	No effect	
Cable $_{tie}$1	No effect	
Cable $_{c}$1	No effect	Close tie connection QEP8-QEP4
Cable $_{c}$2	No effect	Close tie connection QEP8-QEP4
Cable $_{MV}$3	No effect	Supply from QDP11
Cable $_{MV}$3-1	No effect	Supply from QDP10
Cable $_{MV}$3-2	QEP3 LV out of service (island DC loss)	
Cable $_{MV}$2	No effect	Supply from QDP14
Cable $_{MV}$1	No effect	Supply from QDP15
Cable $_{MV}$1-1	QEP7LV out of service (island DC loss)	
Cable $_{MV}$4	No effect	Supply from SQDP4
Cable $_{MV}$4-1	No effect	Supply from QDP18
Cable $_{EMP}$1	Unavailability propulsion engine EPM1	
Cable $_{EMP}$2	Unavailability propulsion engine EPM2	
Cable $_{EMP}$3	Unavailability propulsion engine EPM3	
Cable $_{EMP}$4	Unavailability propulsion engine EPM4	
DG1	Change ship configuration	Operational profile 3-4-5-6-7
DG2	Change ship configuration	OPerational profile 4-5-6-7-8-9
DG3	Change ship configuration	Operational profile 3-4-5-6-7
DG4	Change ship configuration	Operational profile 4-5-6-7-8-9
TAG1	Change ship configuration	Operational profile 3-4-5 or 6 at 22kn
TAG2	Change ship configuration	Operational profile 3-4-5 or 6 at 22kn
I_C1	No effect	Close tie connection QEP8-QEP4
I_C2	No effect	Close tie connection QEP8-QEP4
I_C3	No effect	Close tie connection QEP8-QEP4
I_C4	No effect	Close tie connection QEP8-QEP4

$I_{DG}1$	Change ship configuration	Operational profile 3-4-5-6-7
$I_{DG}2$	Change ship configuration	Operational profile 4-5-6-7-8-9
$I_{DG}3$	Change ship configuration	Operational profile 3-4-5-6-7
$I_{DG}4$	Change ship configuration	Operational profile 4-5-6-7-8-9
I_p1	Unavailability propulsion engine EPM1	
I_p2	Unavailability propulsion engine EPM2	
I_p3	Unavailability propulsion engine EPM3	
I_p4	Unavailability propulsion engine EPM4	
$I_{rTH}1$	No effect (unavailability of backup supply)	
$I_{rTH}2$	No effect (unavailability of backup supply)	
I_T1	Change ship configuration	Operational profile 3-4-5 or 6 at 22kn
I_T2	Change ship configuration	Operational profile 3-4-5 or 6 at 22kn
$I_{TH}1$	No effect	Supply from QEP8
$I_{TH}2$	No effect	Supply from QEP4
$I_{tie}1$	No effect	
$I_{tie}2$	No effect	
$I_{tie}3$	No effect	
$I_{tie}4$	No effect	
K1	Change ship configuration	Operational profile 3-4-5 or 6 at 22kn
K2	Change ship configuration	Operational profile 3-4-5 or 6 at 22kn
K3	Change ship configuration	Operational profile 4-5 or 6 at 24 kn
K4	Change ship configuration	Operational profile 4-5 or 6 at 24 kn
K5	No effect	Close tie connection QEP8-QEP4 to maintain operational profile 6
K6	No effect	Close tie connection QEP8-QEP4 to maintain operational profile 6
K7	No effect	Close tie connection QEP8-QEP4 to maintain operational profile 6
K8	No effect	Close tie connection QEP8-QEP4 to maintain operational profile 6
$I_{LV}4$	No effect	Supply from SQDP4
$I_{LV}3$	No effect	Supply from QDP11
$I_{LV}4$-1	No effect	Supply from QDP 18
I_{LV} 3-1	No effect	Supply from QDP10
I_{LV} 3-2	QEP3LV loss (supply DC island)	
$I_{LV}1$	No effect	Supply from QDP 15
$I_{LV}1$-1	QEP7LV loss (supply DC island)	
$I_{LV}2$	No effect	Supply from QDP14
$I_{MV}3$	No effect	Supply from QDP11
$I_{MV}3$-1	No effect	Supply from QDP10
$I_{MV}3$-2	QEP3LV loss (supply DC island)	
$I_{MV}2$	No effect	Supply from QDP14
$I_{MV}1$	No effect	Supply from QDP 15

$I_{MV}1$-1	QEP7LV loss (supply DC island)	
$I_{MV}4$	No effect	Supply from SQDP4
$I_{MV}4$-1	No effect	Supply from QDP 18
Th1	Unavailability Aft thruster	
Th2	Unavailability bow thruster	
EPM1	Unavailability propulsion engine EPM1	
EPM2	Unavailability propulsion engine EPM2	
EPM3	Unavailability propulsion engine EPM3	
EPM4	Unavailability propulsion engine EPM4	
$Busbar_{LV}4$	Out of service “essential” QDP 14 electrical panel	
$Busbar_{LV}4$-1	Out of service “essential” QDP15 electrical panel that supply DC island	
$Busbar_{LV}1$	Out of service “essential” QDP18 electrical panel	
$Busbar_{LV}1$-1	QEP7 out of service (supply DC island)	
$Busbar_{LV}2$	Out of service “essential” SQDP4 electrical panel that supply DC island	
$Busbar_{LV}3$	Out of service “essential” QDP13 that supply DC island	
$Busbar_{LV}3$-1	Out of service “essential” QDP17	
$Busbar_{LV}3$-2	Out of service “essential” QDP15 that supply DC island	
$S_{Trafo}3$	No effect	Supply from QDP11
S_{Trafo} 3-2	QEP3LV out of service (supply DC island)	
$S_{Trafo}3$-1	No effect	Supply from QDP10
$S_{Trafo}2$	No effect	Supply from QDP14
$S_{Trafo}1$	No effect	Supply from QDP 15
$S_{Trafo}1$-1	QEP7LV out of service (supply DC island)	
$S_{Trafo}4$	No effect	Supply from SQDP4
$S_{Trafo}4$-1	No effect	Supply from QDP 18
Trafo3	No effect	Supply from QDP11
Trafo 3-2	QEP3LV out of service (supply DC island)	
Trafo 3-1	No effect	Supply from QDP10
Trafo 2	No effect	Supply from QDP14
Trafo 1	No effect	Supply from QDP 15
Trafo1-1	QEP7LV out of service (supply DC island)	
Trafo4-1	No effect	Supply from QDP18
Trafo 4	No effect	Supply from SQDP4

Top event (main failures)

Main breakdown event were assessed for the naval unit. Two top events failures have been identified:

1. loss of a propulsion engine;
2. loss of an electrical panel that supplies essential users and/or DC islands.

The first, leads to a reduction of ship movements, while the latter causes service interruption of an essential load/area. Both these situations can be framed by the dependability theory as cases of incorrect service.

A brief evaluation about the failures leading to such unavailability was reported in order to apply the improvement techniques previously mentioned. This is a simplified application of fault forecasting techniques.
Table 48 shows the failures of components that, individually or simultaneously, produce the first top event (loss of a propulsion engine), while in Table 49 are reported those that cause the second top event (essential users and/or DC islands).

Table 48 - Top event 1: Failures That Cause The Out of Service of Propulsion Engine

Engine propulsion out of service (eg: EPM1)						
FAILURE	ENGINE	QEP5-EPM1 connection	Feeding of the three stator triples	Cross connection QEP8-QEP3 Cross connection QEP4-QEP5 Tie connection QEP5-QEP3 Generator-propulsion joint QEP5	Cross connection QEP4-QEP5 Tie connection QEP5-QEP3 Generator-propulsion joint QEP5	DG1 DG2 Cross connection QEP4-QEP5 Tie connection QEP5-QEP3

Table 49 - Top event 2: Failures That Cause The Out of Service of A Electrical Panel That Supply "Essential" Load or DC Island

Unavailability of "essential" electrical panel QDP15 (supply also DC island)					
FAILURE	Busbar QDP 15 690 V	QEP8-QDP15 connection QDP18-QDP15 backup supply connection	TAG1 Tie connection QEP4-QEP8 Cross connection QEP8-QEP3 QDP18-QDP15 backup supply connection	Propulsion-distribution joint QEP8 Generator-propulsion joint QEP8 Cross connection QEP8-QEP3 QDP18-QDP15 backup supply connection	Propulsion-distribution joint QEP8 Cross connection QEP8-QEP3 QDP18-QDP15 backup supply connection

Unavailability of "essential" electrical panel QDP14					
FAILURE	Busbar QDP 14 690 V	QEP8-QDP14 connection SQDP4-QDP14 backup supply connection	TAG1 tie connection QEP4-QEP8 cross connection QEP8-QEP3 SQDP4-QDP14 backup supply connection	Propulsion-distribution joint QEP8 Generator-propulsion joint QEP8 Cross connection QEP8-QEP3 SQDP4-QDP14 backup supply connection	Propulsion-distribution joint QEP8 Cross connection QEP8-QEP3 SQDP4-QDP14 backup supply connection

Unavailabilityof "essential" electrical panel QDP18					
FAILUR	Busbar QDP 18 690 V	QEP5-QDP18 connection	DG1	Propulsion-distribution joint QEP5	Propulsion-distribution joint QEP5

		QDP15-QDP18 backup supply connection	DG2 Tie connectionQEP3-QEP5 Cross connection QEP4-QEP5 QDP15-QDP18 backup supply connection	Generator-propulsion joint QEP5 Cross connection QEP4-QEP5 QDP15-QDP18 backup supply connection	Cross connection QEP4-QEP5 QDP15-QDP18 backup supply connection

			Unavailability of QEP3LV (supply DC island)		
FAILURE	Busbar QEP3LV 690 V	QEP5-QEP3LV connection	DG3 DG4 Tie connection QEP3-QEP5 Cross connection QEP8-QEP3	Propulsion-distribution joint QEP3 Generator-propulsion joint QEP3 Cross connection QEP8-QEP3	Propulsion-distribution joint QEP3 Cross connection QEP8-QEP3

			Unavailability of QEP7LV (supply DC island)		
FAILURE	Busbar QEP7LV 690 V	QEP5-QEP7LV connection	DG1 DG2 Tie connection QEP3-QEP5 Cross connection QEP4-QEP5	Propulsion-distribution joint QEP5 Generator-propulsion joint QEP5 Cross connection QEP5-QEP4	Propulsion-distribution joint QEP5 Cross connection QEP5-QEP4

			Unavailability of "essential" electrical panel SQDP4 (supply also DC island)		
FAILURE	Busbar SQDP4 690 V	QEP4-SQDP4 connection QDP14-SQDP4 backup supply connection	TAG2 Tie connection QEP4-QEP8 Cross connection QEP4-QEP5 QDP14-SQDP4 backup supply connection	Propulsion-distribution joint QEP4 Generator-propulsion joint QEP4 Cross connection QEP5-QEP4 QDP14-SQDP4 backup supply connection	Propulsion-distribution joint QEP4 Cross connection QEP5-QEP4 QDP14-SQDP4 backup supply connection

			Unavailability of "essential" electrical panel QDP13 (supply also DC island)		
FAILUR	Busbar QDP13 690 V	QEP3-QDP13 connection	DG3	Propulsion-distribution joint QEP3	Propulsion-distribution joint QEP3

		QDP11-QDP13 backup supply connection	DG4 Tie connection QEP3-QEP5 Cross connection QEP8-QEP3 QDP13-QDP11 backup supply connection	Generator-propulsion joint QEP3 Cross connection QEP8-QEP3 QDP13-QDP11 backup supply connection	Cross connection QEP8-QEP3 QDP13-QDP11 backup supply connection

Unavailability of "essential" electrical panel QDP17					
FAILURE	Busbar QDP17 690 V	QEP3-QDP17 connection QDP17-QDP10 backup supply connection	DG3 DG4 Tie connection QEP3-QEP5 Cross connection QEP8-QEP3 QDP17-QDP10 backup supply connection	Propulsion-distribution joint QEP3 Generator-propulsion joint QEP3 Cross connection QEP8-QEP3 QDP17-QDP10 backup supply connection	Propulsion-distribution joint QEP3 Cross connection QEP8-QEP3 QDP17-QDP10 backup supply connection

The analysis conducted showed that the use of backup supply, provided in the MVAC and MVAC "hybrid" network, make it possible to ensure power supply for the electrical panels that supply essential loads and/or DC islands.
The main critical events are those related to propulsion engines, therefore it can be concluded that, from the preliminary analysis, the two network architectures have equivalent reliability features.

Chapter X: Three-Phase Short Circuit Analysis For MVAC 50-60 Hz Layout

Preliminary evaluations were carried out to analyze the behavior of the system when certain faulty events occur.
To perform system analyzes in steady-state and short circuit, the PSAF-Cyme simulation software was used. The calculation program allows to study the steady-state domain, i.e. load flow, optimal power flow, short circuits, voltage stability, harmonic analysis, electromechanical transients and motor starting. This software provides graphical results and numerical results [117].
The main features of the system (reported in chapter 6.5 “Definition and characterization of a "hybrid" propulsion naval unit”**)** are summarized below.
Summary of the main equipment of the electrical system:

- four diesel generators (DDGG), 6.52 MVA each;
- 6 kV-50 Hz medium voltage network with two main electrical panels positioned at bow and stern;
- different operating conditions involves the partial use of the four generating units (at "port" setting, the connection of a single DDGG group is represented. In operational profile where the electric propulsion is expected, the simultaneous operation of three DDGG groups is needed, and in the remaining operational profiles only two generators are connected);
- the distribution system consists of a 6 kV-50 Hz medium-voltage network, and a low voltage distribution network at 690 V, 400 V, 230 V. A 60 Hz STANAG network at 440 V and 115 V is specifically devoted to the military equipment, such as weapon systems and command and surveillance). The STANAG network is connected to the medium voltage network by means of two 50-60 Hz rotating converters;
- the neutral distribution of the three-phase systems is differentiated according to the voltage level. In particular:

  - 6 kV, neutral to ground with high resistance;
  - 690, 440, 115 V, isolated;
  - 400-230 V, neutral directly on the ground and insulated only for essential loads.

The propulsion of the ship is guaranteed by two aft propellers, which can be moved either by electric motors, for an "electric navigation", or by gas turbines for the sets at maximum speed. With electric propulsion, the ship is able to navigate at a speed of 10 knots, driven by the action of two 2.25 MW asynchronous motors, one per shaft line. These motors are powered by static converters at a voltage of 690 V and absorb a total of about 5 MW of power, the efficiency of these converters being 90%. There are three maneuvering thrusters, two are located at the bow (each of 2.2 MW) and one at the stern which is operated by a 1.35 MW motor.

10.1 Assumptions

Taking into account the subdivision into zones of the electrical network, the normal steady-state and three-phase short-circuit regimes were studied in different absorption conditions by analysing a singular zone.
Such considerations are obviously extendable to other areas.
We considered only one transformer in operation, and therefore an exercise of the network through a double radial scheme. The analyses carried out in steady-state domain refer to a global coefficient of use, given by the product of the coefficients of contemporaneity and utilization, equal to 0.4. Further simulations were carried out with a global coefficient of use equal to 1 to evaluate the existence of potentially dangerous overload conditions of the transformer.

Under the same conditions, the three-phase short-circuit currents were evaluated at all nodes of the network.
The portion of the plant being simulated is the zone MVZ2, is highlighted in green in Figure 131.
MVZ2 Zone was chosen because it includes the main MV bow electrical panel with diesel generators, the main MV loads installed on board (propulsion engine, two manoeuvring thruster) and the main LV electrical panel with relevant loads like Hospital, pumps, conditioning, lighting, gas turbine starting system, refrigerators and so on.)
In order to consider the contributions to the short-circuit coming from the transom, the two generators in the MVZ3 area were also considered (highlighted in yellow in Figure 131).

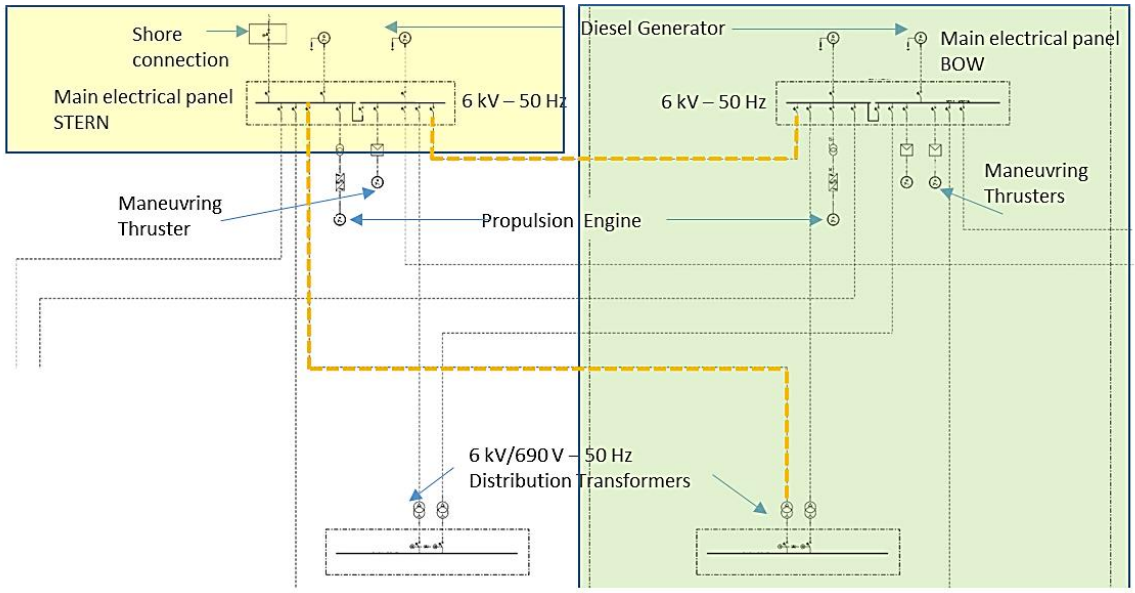

Figure 131 - The portion of the plant being simulated

The 690 V low voltage electrical panel (MVZ2) supplies a large number of static and rotating loads. Figure 132 illustrates the structure of the main low voltage panel.

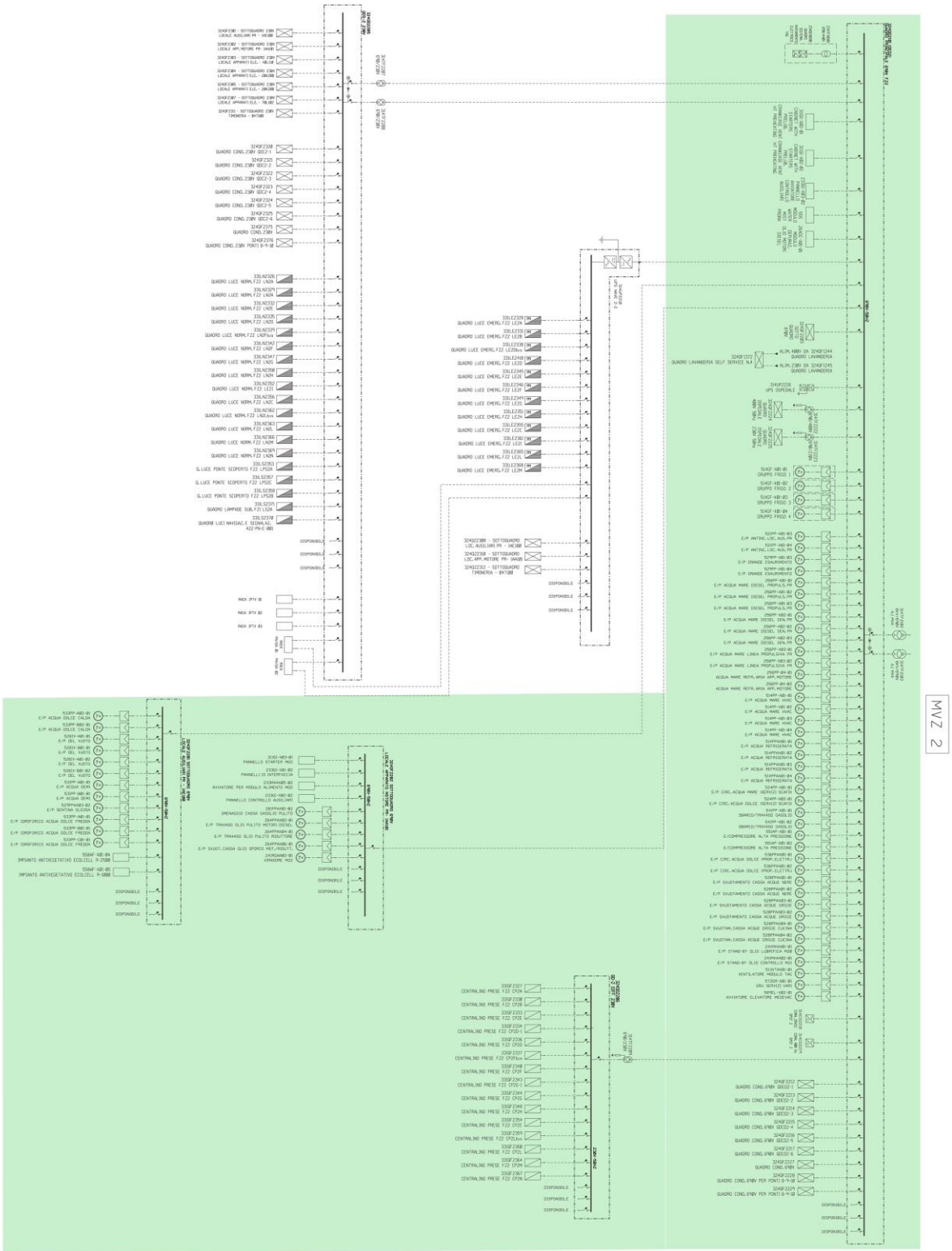

Figure 132 – Main Electrical Panel 690 V

The complete layout for the analysed area is shown in Figure 133.

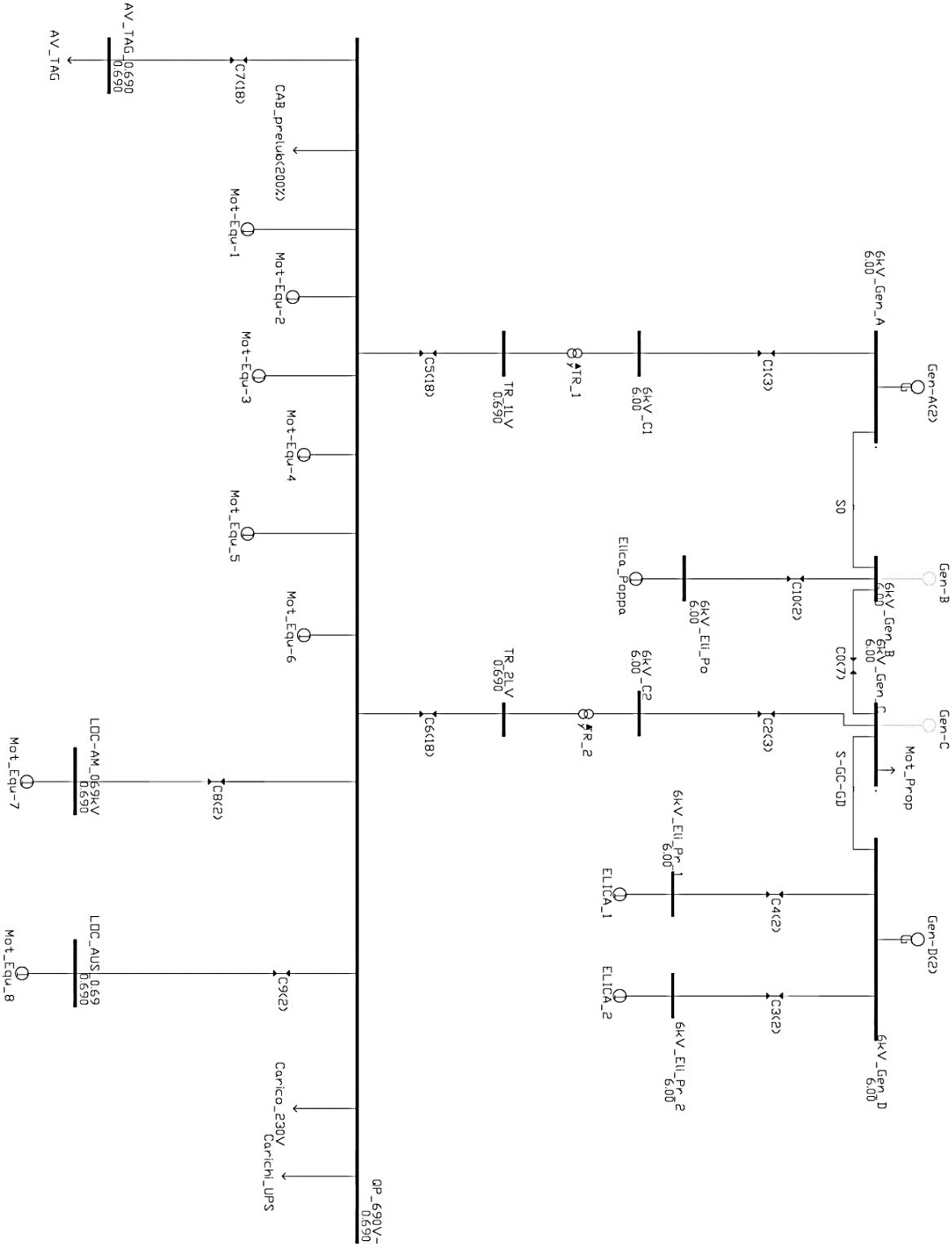

Figure 133 – Simulated Layout

The hypotheses for modelling the components used in the simulation are explained below:

- The synchronous generators have been simulated, in steady-state mode, as ideal voltage generators, characterized by the active and reactive power fed into the network. During a fault they were simulated with the sub-transitory impedance. The values are shown in Table 51 in the paragraph "Report of the simulations" and were taken from the data sheets provided by Fincantieri S.p.A.;

- The cables were simulated with the pi equivalent circuit from the series impedances and derived from the direct sequence. The values shown in Table 54 in the "Report of the simulations" paragraph were obtained from the General Catalogue “HFX Prysmian Naval Cables”;
- Asynchronous motors were simulated through the equivalent circuit, present in the PSAF-Cyme, software for electromechanical transients simulations, shown in Figure 134.

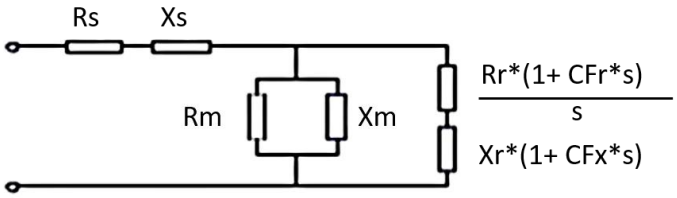

Figure 134 – Equivalent Circuit of Asynchronous Motor

The impedance values of the equivalent circuit were obtained from the motor nameplate data: V_n, P_n, η_n, $\cos\varphi_n$, C_{avv}, C_{max}, S_n, p, Cage factor (CF_r and CF_x). Only the first four were inferred from the data reported in the documents of Fincantieri, while the others were hypothesized using typical values of similar commercial asynchronous motors. The impedances of the equivalent circuit in Figure 134 were obtained by solving a system of non-linear equations. In calculating the short-circuit currents, the software routine simulate the asynchronous motor through their sub-transitory reactance, inferable from the equivalent circuit in the Figure 134. IEC 60092-202:2016 suggests that the contribution of induction motors for determining the maximum peak value attainable by the short-circuit current (i.e. the value of the current to be added to the maximum peak value of the short-circuit due to the generators) can be taken as equal to 8 I_n where I_n is the sum of the rated currents of the motors estimated normally when simultaneously in service (I_n is an RMS value). The sub-transient reactance values have been imposed equal to 0.125 p.u.

- The transformers were simulated through the equivalent circuit shown in Figure 135, in which only the Z_{cc} is present:

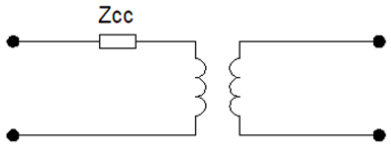

Figure 135 - Equivalent Circuit of The Transformer

The value of the Z_{cc} was obtained from the transformer datasheet, through the percentage short-circuit voltage.

- The nominal power of the loads were taken from the documents provided by Fincantieri.

In the study of the steady-state network, the four generators were modelled with two equivalent generators, placed both the stern and bow busbars. The stern bar generation node was placed as a balance node; having imposed the module and the phase of the node voltage, the phases of voltages and currents are therefore referred to it.
The node that represents the bus-bar was considered as a "generation node" and therefore the active and reactive power was fixed as external constraints. Within the calculation program, the load flow resolution is performed by the Newton-Raphson method.

10.2 Simulation Results

Steady-state domain

Figure 136 reports load flow results considering a global coefficient equal to 0.4.

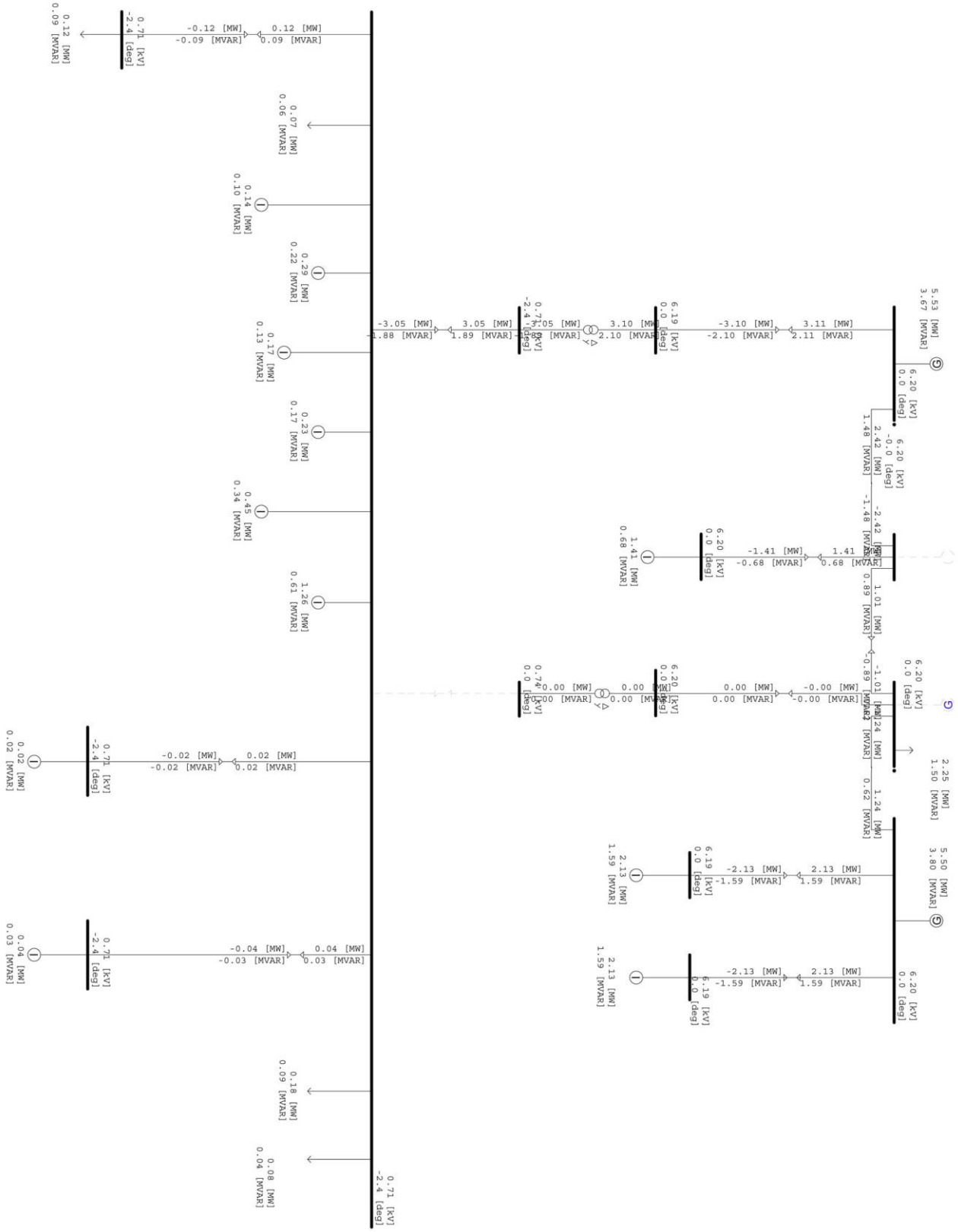

Figure 136 – Load Flow Results

Three-phase Short circuit directly to the ground

Figure 137 reports results to three-phase short circuit at the busbars having applied a global coefficient equal to 0.4

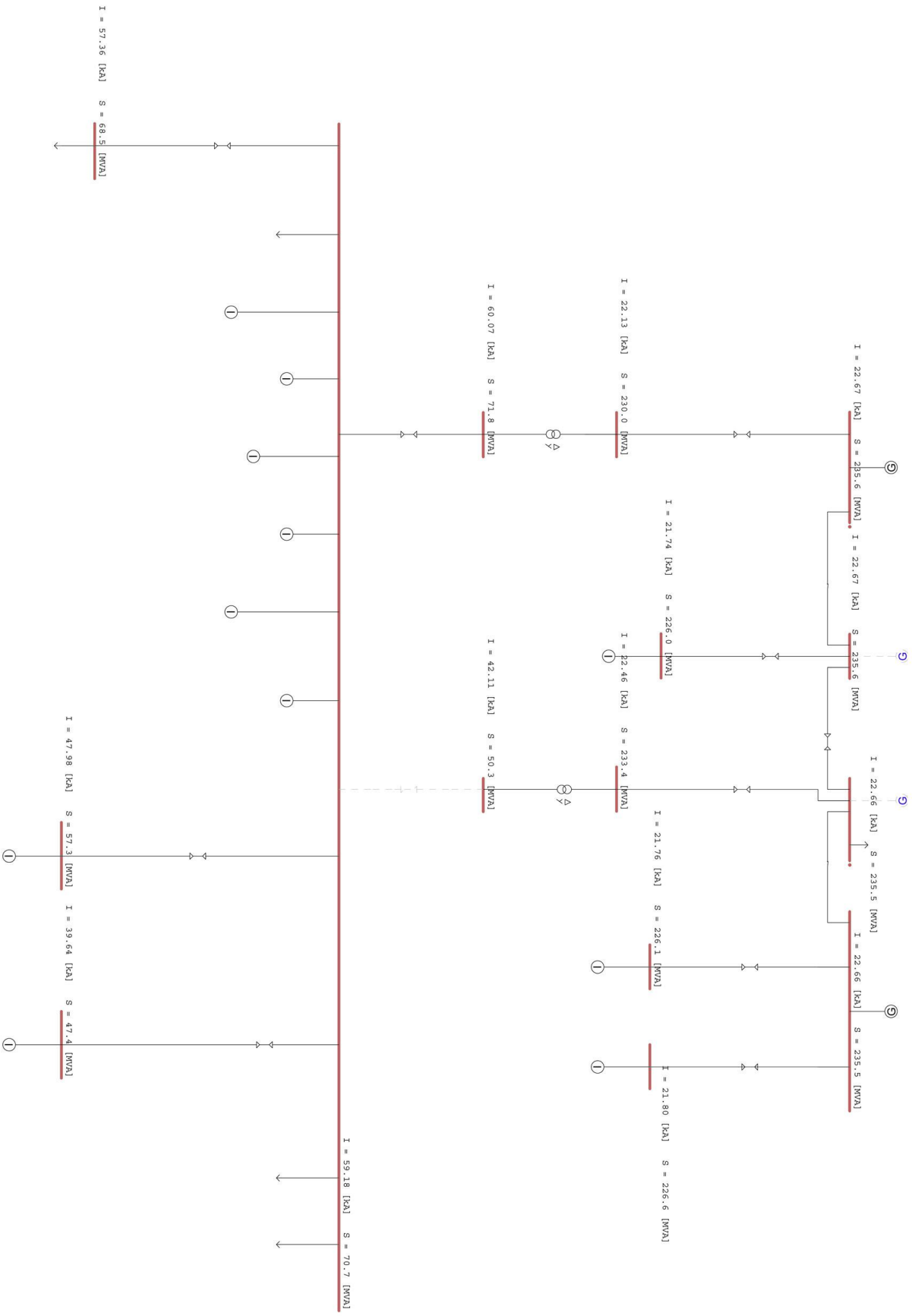

Figure 137 – Three-Phase Short Circuit on Each Busbar

A sensitivity analysis was carried out in order to evaluate the network even in conditions of transformer overload. The results of the three-phase short circuit at the bus bars are reported with a global coefficient value equal to 1.

Three-phase Short circuit directly to the ground with global coefficient equal to 1

Figure 138 reports results to three-phase short circuit at the busbars having applied a global coefficient equal to 1.

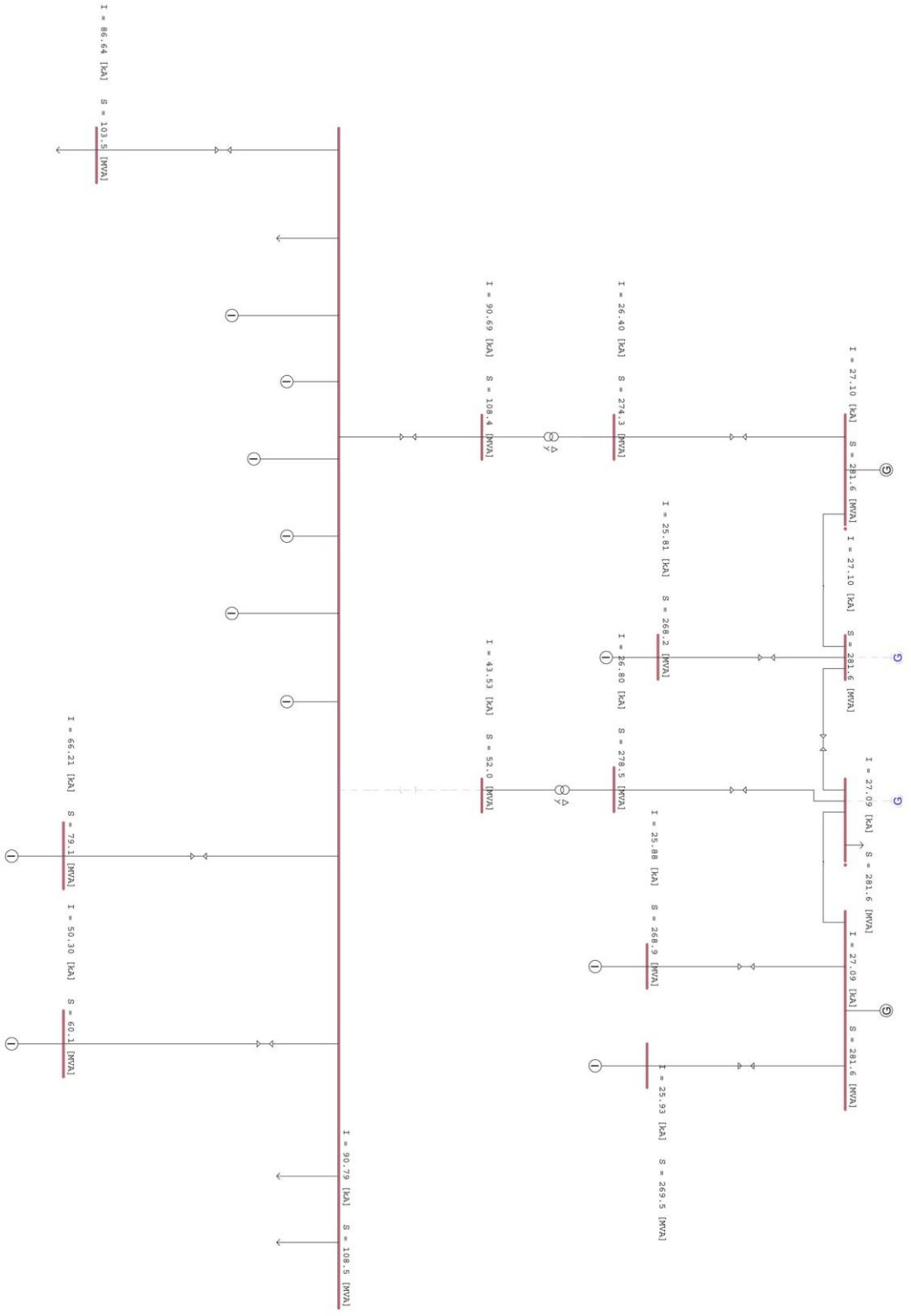

Figure 138 – Three-Phase Short Circuit on Each Busbar With Global Coefficient Equal To 1

The results of three-phase short circuit with a global coefficient equal to 0.4 for the busbar are reported from Figure 139 to Figure 144:

- for stern thruster;
- for bow thruster 1;
- for bow thruster 2;
- for main 690 V low voltage electrical panel;
- for auxiliary;
- for motor.

Three-phase Short circuit directly to the ground on the stern thruster busbar with a global coefficient equal to 0.4

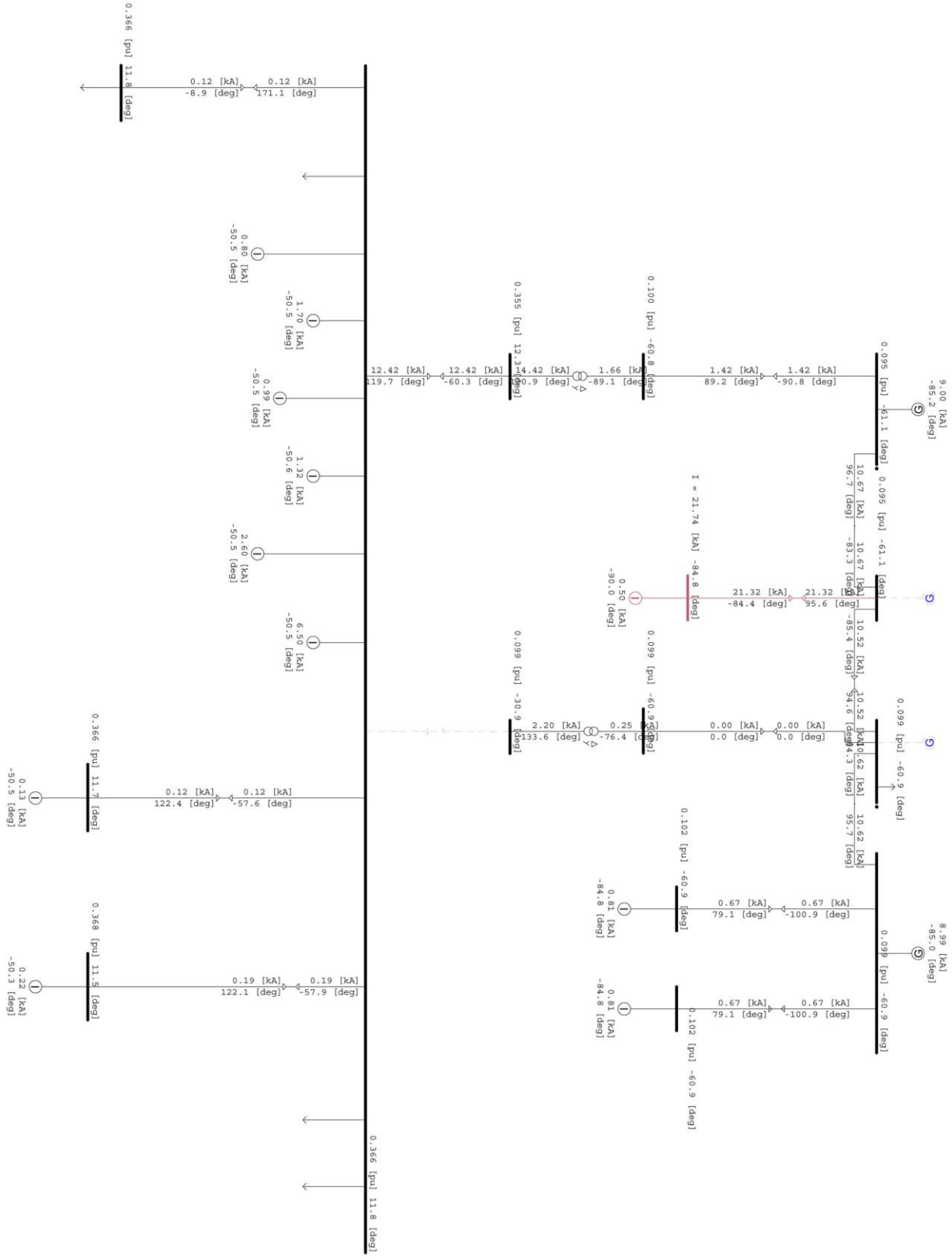

Figure 139 - Three-Phase Short Circuit Directly To The Ground On The Stern Thruster Busbar With A Global Coefficient Equal To 0.4

Three-phase Short circuit directly to the ground on the bow thruster 1 busbar with a global coefficient equal to 0.4

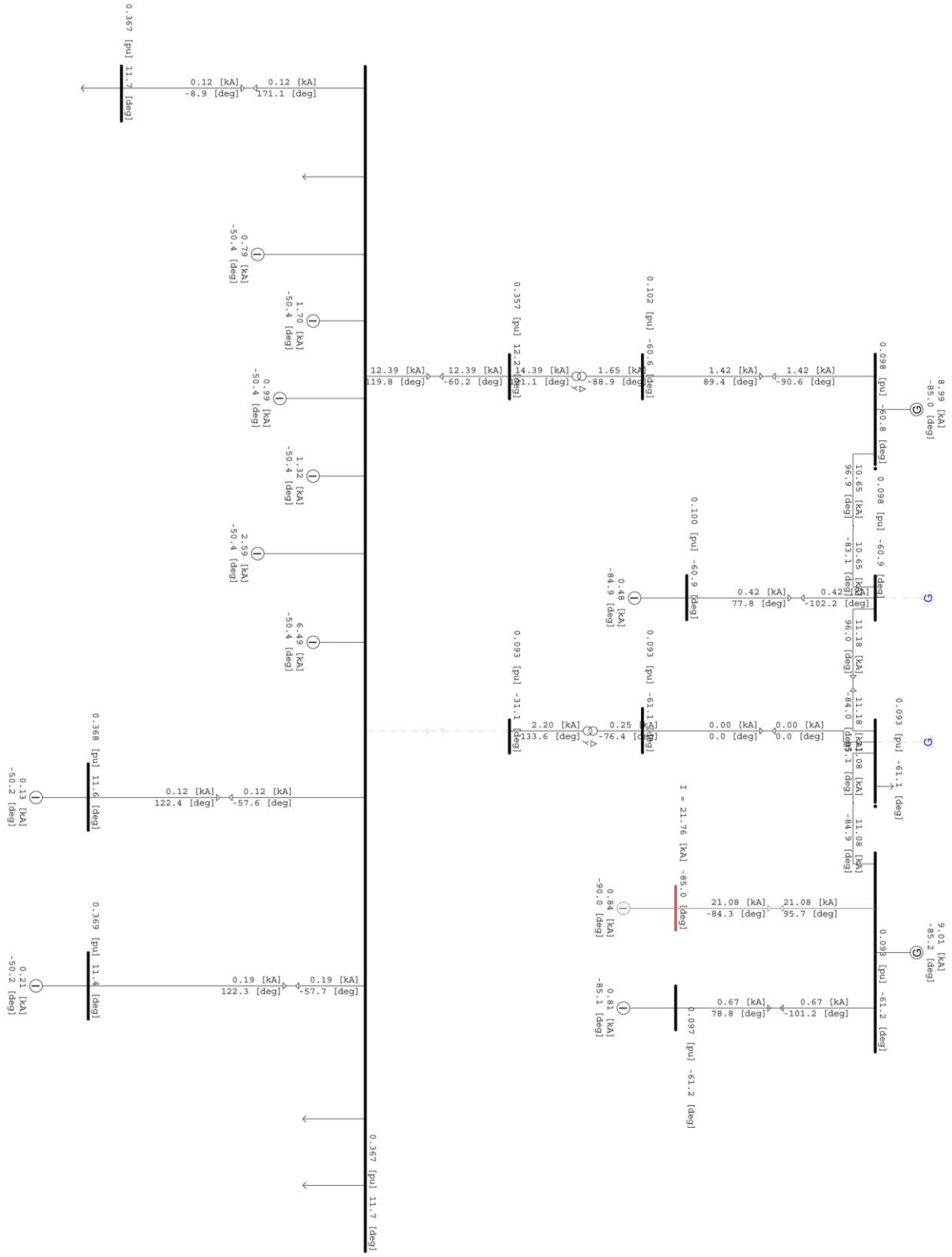

Figure 140 - Three-Phase Short Circuit Directly To The Ground On The Bow Thruster 1 Busbar With A Global Coefficient Equal To 0.4

Three-phase Short circuit directly to the ground on the bow thruster 2 busbar with a global coefficient equal to 0.4

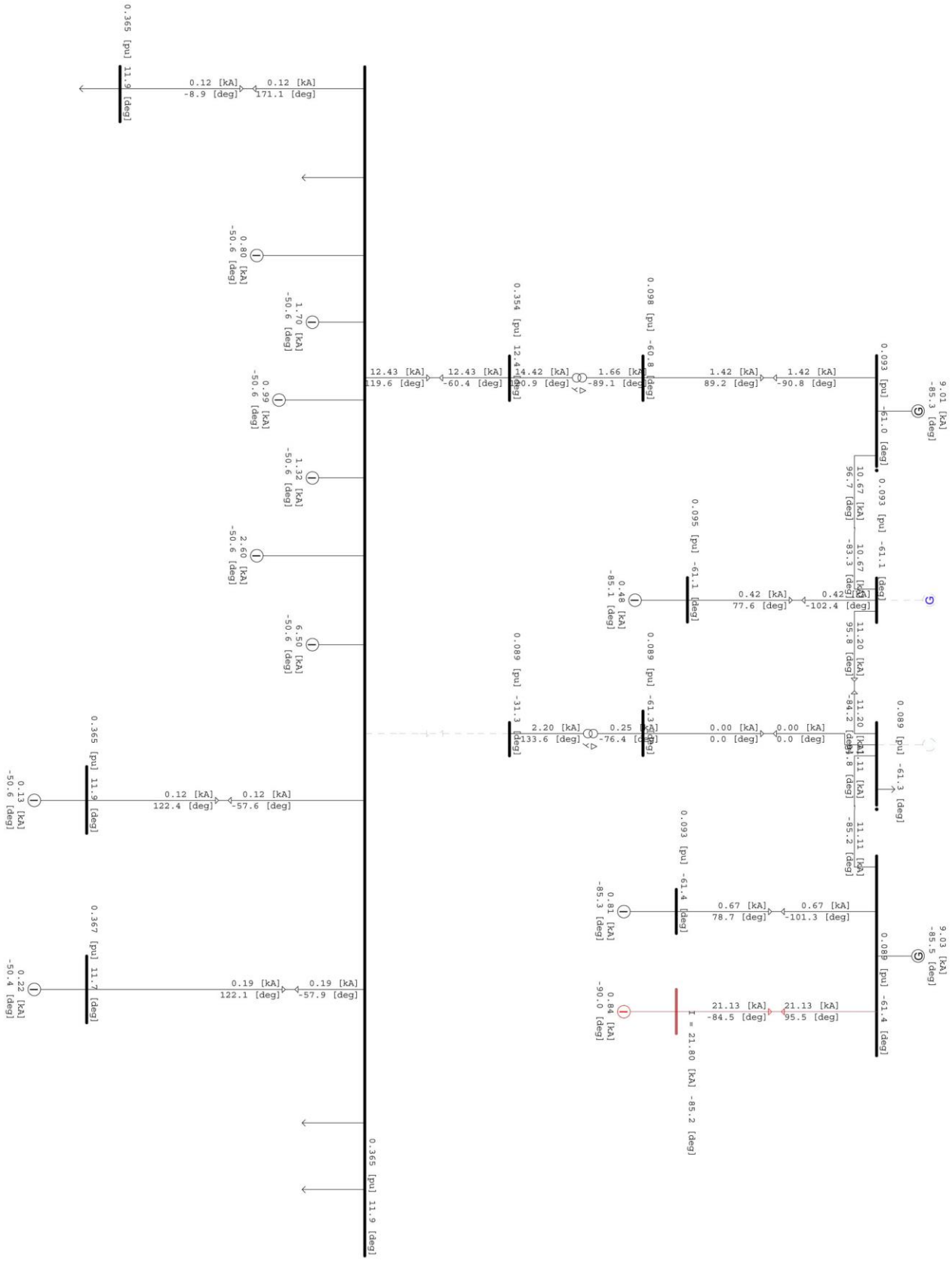

Figure 141- Three-Phase Short Circuit Directly To The Ground On The Bow Thruster 2 Busbar With A Global Coefficient Equal To 0.4

Three-phase Short circuit directly to the ground on the 690 V main electrical panel with a global coefficient equal to 0.4

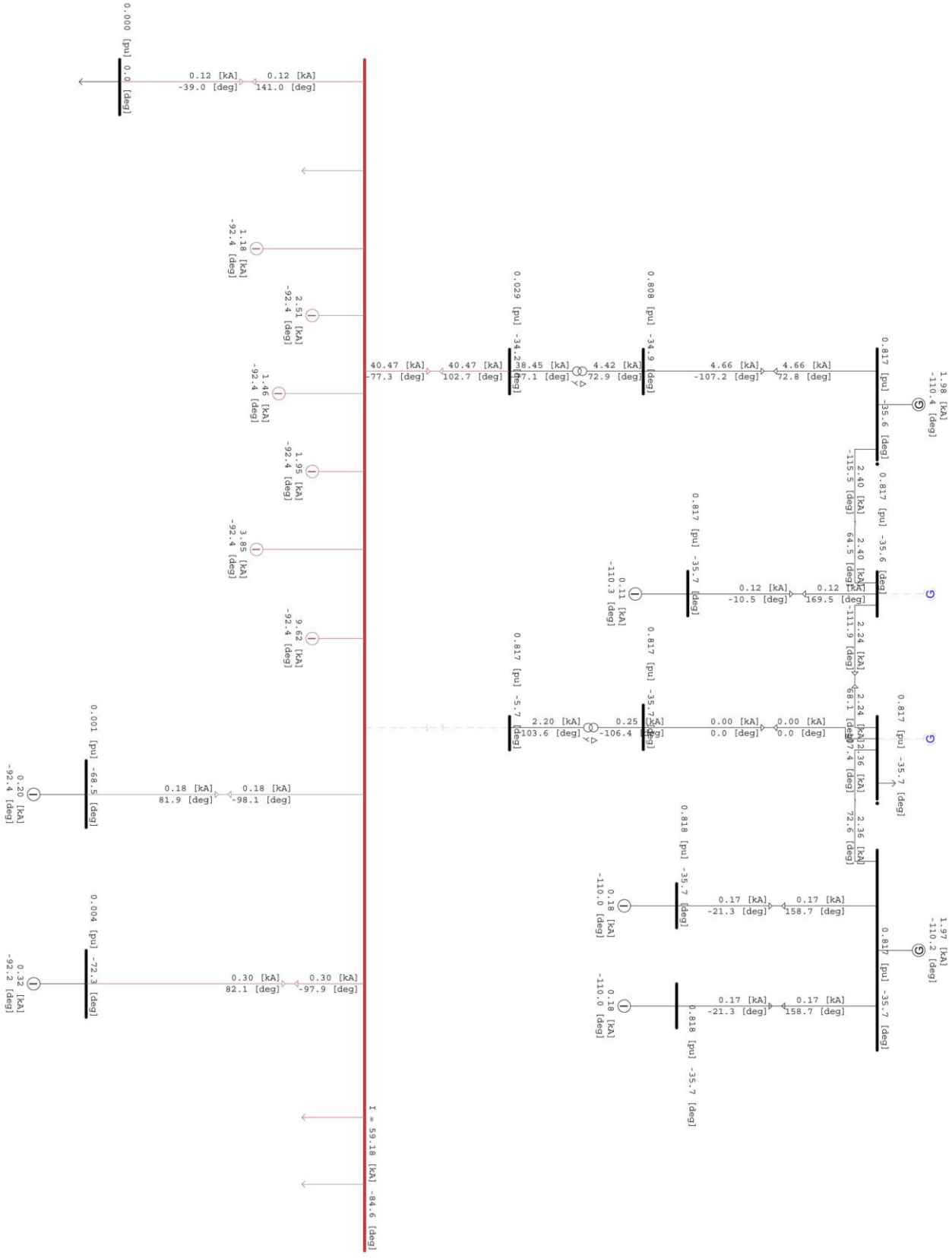

Figure 142 - Three-Phase Short Circuit Directly To The Ground On The 690 V Main Electrical Panel With A Global Coefficient Equal To 0.4

Three-phase Short circuit directly to the ground on the auxiliary busbar with a global coefficient equal to 0.4

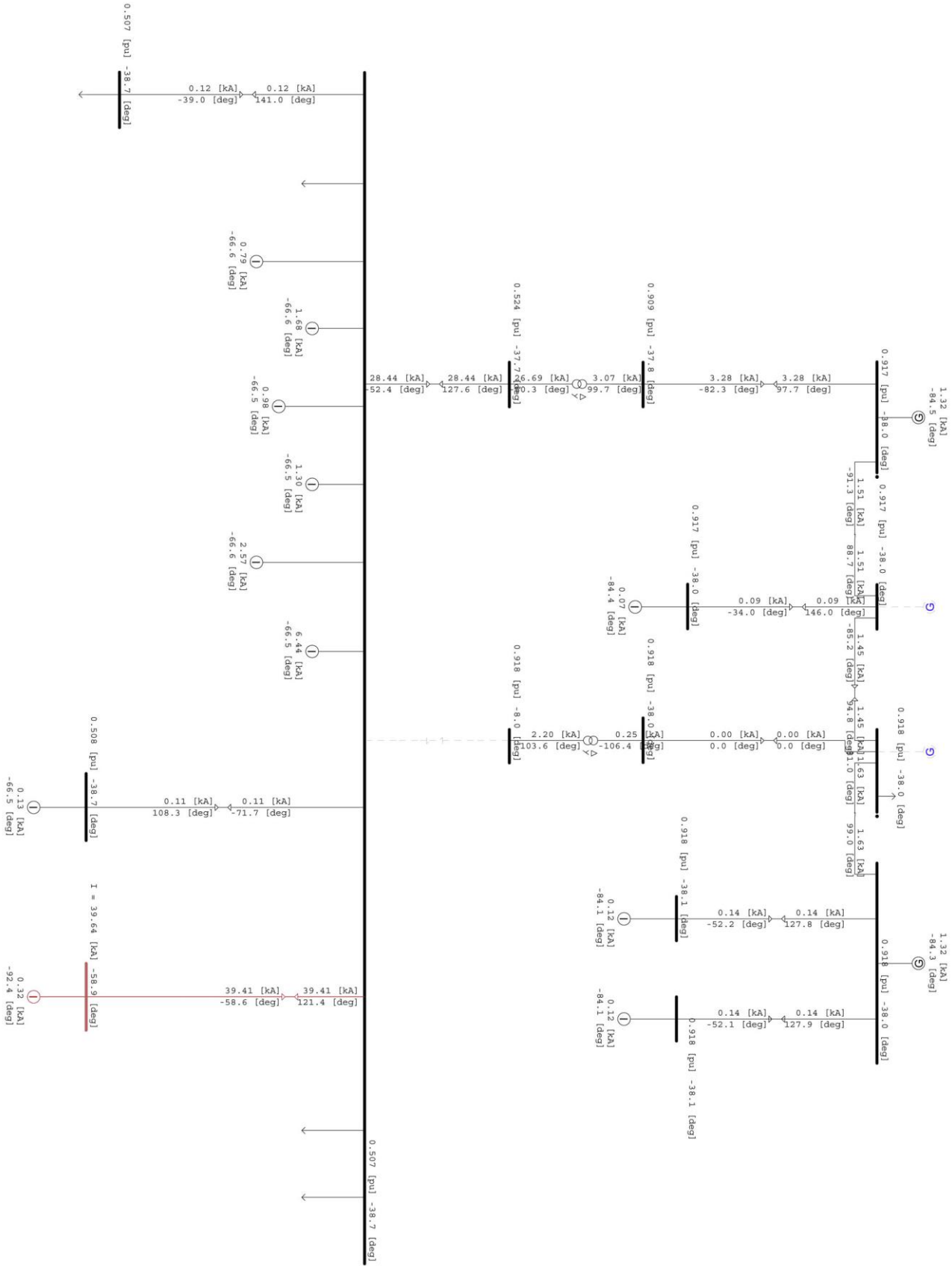

Figure 143 - Three-Phase Short Circuit Directly To The Ground On The Auxiliary Busbar With A Global Coefficient Equal To 0.4

Three-phase Short circuit directly to the ground on the engines busbar with a global coefficient equal to 0.4

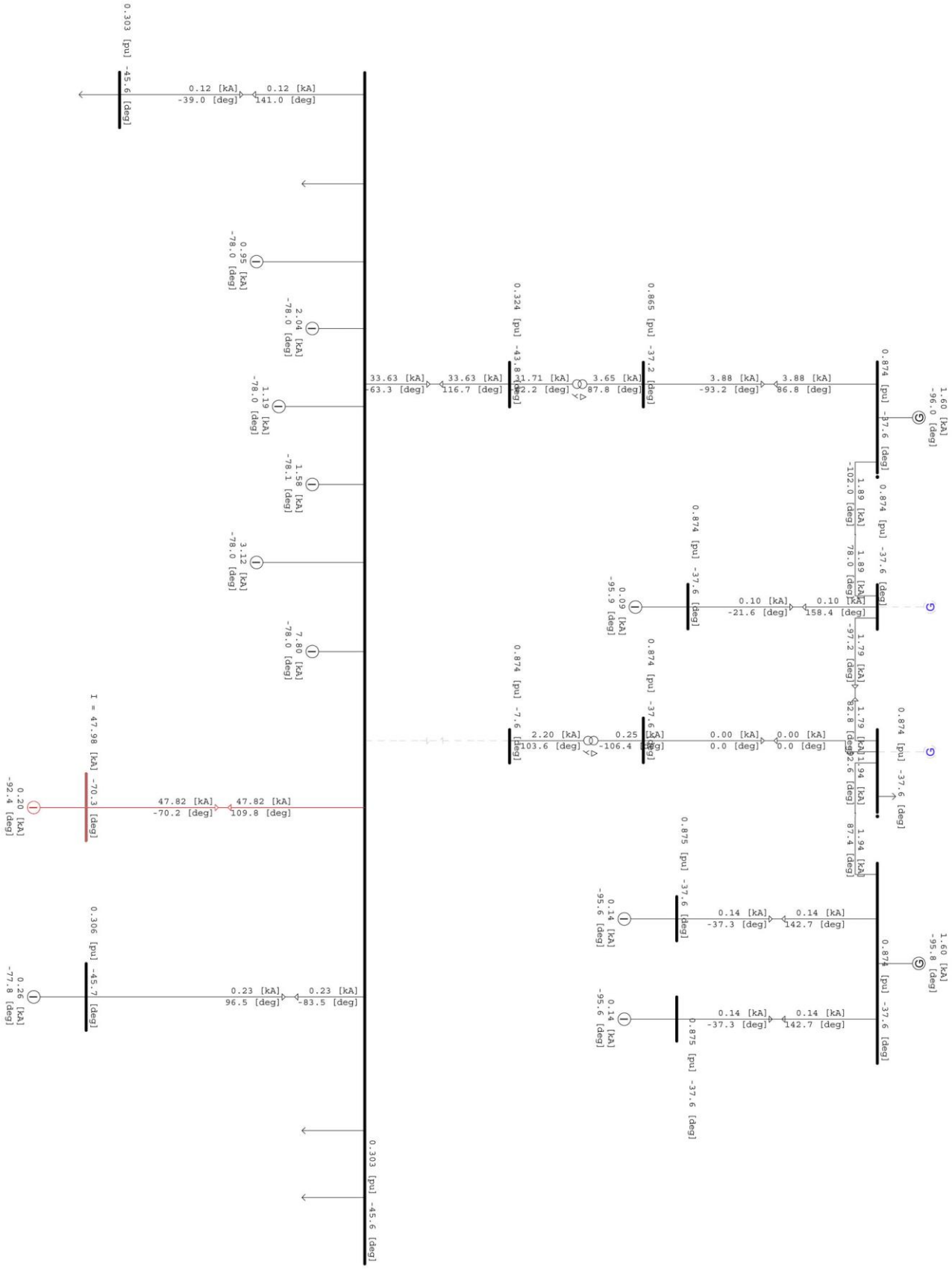

Figure 144 - Three-Phase Short Circuit Directly To The Ground On The Engines Busbar With A Global Coefficient Equal To 0.4

I/O Report

The input data used for the simulations and the results of the short-circuit currents in the individual nodes are shown. In particular, input data on nodes, generators, engines, static loads, cables and the transformers used, are reported from Table 50 to Table 55.
Table 56 and Table 57 show the values of the short-circuit currents for each nodes of the network, with the global coefficient respectively equal to 0.4 and 1.

Table 50 – Input Bus Data

ID	Status	kV Base	kV Oper	Zone	Vmin [p.u.]	Vmax [p.u.]	RQQ1 [p.u]	XQQ1 [p.u]
6kV_Eli_Pr_1	ON	6	6	0	0,9	1,1	0,1083	0,703
6kV_Eli_Pr_2	ON	6	6	0	0,9	1,1	0,1068	0,7024
TR_1LV	ON	0,69	0,69	0	0,9	1,1	0,2641	1,2792
TR_2LV	ON	0,69	0,69	0	0,9	1,1	0,2635	1,2793
6kV_Gen_D	ON	6	6	0	0,9	1,1	0,0769	0,6895
6kV_Gen_B	ON	6	6	0	0,9	1,1	0	0
6kV_Gen_C	ON	6	6	0	0,9	1,1	0	0
6kV_Gen_A	ON	6	6,2	0	0,9	1,1	0,1092	0,8391
AV_TAG_0.690	ON	0,69	0,69	0	0,9	1,1	0,3585	1,3103
QP_690V-	ON	0,69	0,69	0	0,9	1,1	0,2646	1,2795
LOC-AM_069kV	ON	0,69	0,69	0	0,9	1,1	0,7467	1,5001
LOC_AUS_0.69	ON	0,69	0,69	0	0,9	1,1	1,2781	1,6471
6kV_C2	ON	6	6	0	0,9	1,1	0,0831	0,6919
6kV_Eli_Po	ON	6	6	0	0,9	1,1	0,1428	0,8539
6kV_C1	ON	6	6	0	0,9	1,1	0,1253	0,845

Table 51 – Generators Input Data

ID	Status	Duplic	kV Nominal	Rated S [MVA]	Generator Type	P Gen [MW]	Q Gen [MVAR]	Power Factor [p.u.]	Number of Poles	Q Max [MVAR]	Q Min [MVAR]	Winding Connection	X'' [ohm]	X' [ohm]	Internal R [ohm]	Internal X [ohm]	R0 [ohm]	X0 [ohm]	Rground [ohm]	Xground [ohm]
Gen-A	ON	2	6	13,04	Swing	2,61	0	0,8	2	7,824	-4	YG	0,381	0,5135	**0,018**	4,61043	0,005	0,127	365	0,05
Gen-B	OFF	1	6	6,52	Voltage Controlled	0,2	0	0,8	2	3,912	-2	YG	0,762	1,027	**0,036**	9,22086	0,01	0,254	730	0,1
Gen-C	OFF	1	6	6,52	Voltage Controlled	0,2	0	0,8	2	3,912	-2	YG	0,762	1,027	**0,036**	9,22086	0,01	0,254	730	0,1
Gen-D	ON	2	6	13,04	Fixed Gener	8	6	0,8	2	7,824	-4	YG	0,381	0,5135	**0,018**	4,61043	0,005	0,127	365	0,05

Table 52 – Engines Input Data

ID	kV Nominal	Rated S [MVA]	Speed [RPM]	HP	kW	Efficiency [%]	R'' [ohm]	X'' [ohm]	Loading Factor [%]	Power Factor [p.u.]	Stator R	Stator X	Rotor R	Rotor X	Mag. RL	Mag. XM
ELICA_1	6	2,657	375	2949,5	2200	92	0,92405	2,28343	75	0,9	0,3113	1,2965	0,2675	1,2965	**1,3283**	24,0898
ELICA_2	6	2,657	375	2949,5	2200	92	0,92405	2,28343	75	0,9	0,3113	1,2965	0,2675	1,2965	**1,3283**	24,0898
Elica_Poppa	6	1,57	375	1742,8	1299,96	92	1,56382	3,86438	75	0,9	0,3113	1,2965	0,2675	1,2965	**1,3283**	24,0898
Mot-Equ-1	690	0,4278	750	412,95	308,02	90	81086,13	177608,2	100	0,9	0,05	1	0,1	1	**1000**	50
Mot-Equ-2	690	0,9132	750	881,49	657,5	90	40926,25	85496,76	100	0,9	0,05	1	0,1	1	**1000**	50
Mot-Equ-3	690	0,5319	750	513,43	382,97	90	71929,68	159962,1	100	0,9	0,05	1	0,1	1	**1000**	50
Mot-Equ-4	690	0,7083	750	683,71	509,98	90	59231,87	120681,9	100	0,9	0,05	1	0,1	1	**1000**	50
Mot_Equ-6	690	3,4959	1000	3412	2545,02	91	11076,18	24884,29	100	0,9	0,05	1	0,1	1	**1000**	50
Mot_Equ-7	690	0,0717	1000	70,75	52,77	92	500203,8	1230224	100	0,9	0,05	1	0,1	1	**1000**	50
Mot_Equ_5	690	1,3976	1000	1454	1084,54	97	18187,59	65657,92	100	0,9	0,05	1	0,1	1	**1000**	50
Mot_Equ_8	690	0,1158	1000	103,09	76,89	83	309711,7	761718,9	100	0,9	0,05	1	0,1	1	**1000**	50

Table 53 – Static Load Input Data

ID	P Load [MW]	Q Load [MVAR]
AV_TAG	0,3	0,225
CAB_prelub	0,184	0,138
Carichi_UPS	0,2	0,0968
Carico_230V	0,45	0,2178
Mot_Prop	2,25	1,394

Table 54 – Cables Input Data

ID	To Bus	KVLEVEL	Length [km]	R1 [ohm]	X1 [ohm]	B1 [uS]	R1' [ohm]	R0 [ohm]	X0 [ohm]	B0 [uS]	R0' [ohm]	Loading Limit [A]	Emergency Loading Limit [A]
C0	6kV_Gen_C	6	0,04	0,00111	0,00062	20,143	0,0011	0,01676	0,00084	43,496	0,01676	2030	2450
C1	6kV_C1	6	0,105	0,00945	0,00413	19,53	0,00674	0,10265	0,00515	48,933	0,10265	714	855
C10	6kV_Eli_Po	6	0,105	0,01417	0,00619	13,02	0,01011	0,15398	0,00773	32,622	0,15398	476	570
C2	6kV_C2	6	0,035	0,00315	0,00138	6,51	0,00225	0,03422	0,00172	16,311	0,03422	714	855
C3	6kV_Eli_Pr_2	6	0,1	0,0135	0,0059	12,4	0,00963	0,14664	0,00736	31,069	0,14664	476	570
C4	6kV_Eli_Pr_1	6	0,105	0,01417	0,00619	13,02	0,01011	0,15398	0,00773	32,622	0,15398	476	570
C5	QP_690V-	0,6	0,045	0,00021	0,00022	89,019	0,00048	0,00733	0,00037	125,83	0,00733	4284	5130
C6	QP_690V-	0,6	0,035	0,00016	0,00017	69,237	0,00037	0,0057	0,00029	97,866	0,0057	4284	5130
C7	AV_TAG_0.690	0,6	0,03	0,00045	0,00015	59,346	0,00032	0,00489	0,00025	83,885	0,00489	4284	5130
C8	LOC-AM_069kV	0,6	0,03	0,0023	0,00105	12,059	0,00289	0,04399	0,00221	9,3206	0,04399	476	570
C9	LOC_AUS_0.69	0,6	0,05	0,00483	0,00175	17,9	0,00482	0,07332	0,00368	15,534	0,07332	476	570

Table 55 – Transformers Input Data

ID	Rated S [MVA]	Primary [kV]	Secondary [kV]	Primary Winding	Secondary Winding	Phase Shift	Z1 [ohm]	Z0 [ohm]	X/R Positive	X/R Zero	Type	Loading Limit [MVA]
TR_1	4,1	6	0,72	D	Y	30	0,6146	0,1686	4,14	36	Shell type	4,1
TR_2	4,1	6	0,72	D	Y	30	0,6146	0,1686	4,14	36	Shell type	4,1

Table 56 – Report on Short-Circuit Current (global coefficient 0.4)

Bus Id	Prefault kV	C fact	LLL I [kA]	LLL S [MVA]
6kV_Eli_Pr_1	6	1,1	22,48	233,6
6kV_Eli_Pr_2	6	1,1	22,52	234,1
TR_1LV	0,69	1,05	67261	80,4
6kV_Gen_D	6	1,1	23,45	243,7
6kV_Gen_B	6	1,1	23,45	243,7
6kV_Gen_C	6	1,1	23,45	243,7
6kV_Gen_A	6	1,1	23,45	243,7
AV_TAG_0.690	0,69	1,05	50,08	59,8
QP_690V-	0,69	1,05	51,81	61,9
LOC-AM_069kV	0,69	1,05	42,11	50,3
LOC_AUS_0.69	0,69	1,05	35,16	42
6kV_Eli_Po	6	1,1	22,4	232,8
6kV_C1	6	1,1	22,77	236,7

Table 57 - Report on Short-Circuit Current (global coefficient 1)

Bus Id	Prefault kV	C fact	LLL I [kA]	LLL S [MVA]
6kV_Eli_Pr_1	6	1,1	25,88	268,9
6kV_Eli_Pr_2	6	1,1	25,93	269,5
TR_1LV	0,69	1,05	90,69	108,4
6kV_Gen_D	6	1,1	27,10	235,6
6kV_Gen_B	6	1,1	27,10	281,6
6kV_Gen_C	6	1,1	27,10	281,6
6kV_Gen_A	6	1,1	27,10	281,6
AV_TAG_0.690	0,69	1,05	86,64	103,5
QP_690V-	0,69	1,05	90,79	108,5
LOC-AM_069kV	0,69	1,05	66,21	79,1
LOC_AUS_0.69	0,69	1,05	50,30	60,1
6kV_Eli_Po	6	1,1	25,81	268,2
6kV_C1	6	1,1	26,40	274,30

The simulations carried out using a global coefficient equal to 0.4, show a correct operation of the system without overload of the transformer placed between the two electrical panels. In particular, in parallel operation of the generators, an appropriate adjustment was made to the active and reactive power supplied by the bow generation node, thanks to which it was possible to equally distribute the power supply.
The simulations carried out with global coefficients equal to 1, on the contrary, showed a practically unachievable exercise because of the systematic overload of the transformer. The hypothesis of having all the active loads at the same time, appears very unlikely despite being possible, because of the different nature of the static and rotating electrical loads. It can therefore be assumed that the data obtained in the hypothesis of a global coefficient of 0.4 are realistic.
For the simulations concerning the three-phase short-circuit, several calculations were carried out which allowed to estimate the short-circuit currents in each node of the network. Through this approach it was possible to calculate the short-circuit currents from the generation busbars to the low-voltage distribution boards.
This constitutes the basis for a first sizing of the breaking switches and therefore of the electrical panels inside the naval unit. The correct evaluation of the short-circuit currents plays a very important role in the protection devices to be installed, especially in relation to the respective dimensions. It should be noted that high short-circuit currents would lead to physically larger circuit breakers and, consequently, to the installation of bulkier electrical panels. Therefore, especially on board, where the space available is limited, the quantification of short-circuit currents is of fundamental importance.
Figure 137 to Figure 144 show the values of the short-circuit currents evaluated in different electrical panels of the ship.
From the results obtained, it can be observed that, considering a global coefficient equal to 0.4 (Figure 137), there are short-circuit currents values up to 60 kA, vice-versa, when using a global coefficient equal to 1 these values increase, even reaching 90 kA (Figure 138); these are unacceptable value for the transformer. As a consequence, for a more in-depth analysis several short-circuit simulations were carried out on the power supply busbars taken individually (Figure 139 to Figure 144) using the global coefficient equal to 0.4. This made it possible to visualize the single contributions coming both from the medium voltage loads and from the motors connected to the low voltage distribution board.
The results of the simulations illustrated in this report, using data derived from the documents provided by Fincantieri and hypothesized by drawing them from other sources, has allowed to conduct a pre-analysis of the modules and phases of the short-circuit currents on each branch and constitutes the premise to carry out a correct calibration of the protections.

Detection of DC faults

DC zones requires significant changes in the management of fault conditions, determining the need for new protection and control approaches. A distribution with MVDC architecture, as shown in Figure 145, or the simple presence of DC islands in a naval electrical system, entails the presence of electronic converters necessary to interface the areas in alternating current with DC link. These devices limit fault current values, making it more difficult to detect them because the amplitude and rate of current increase may not be significantly different from the values expected during normal system operations. Therefore, while offering great advantages in terms of flexibility and reliability, direct current networks make fault localization difficult.

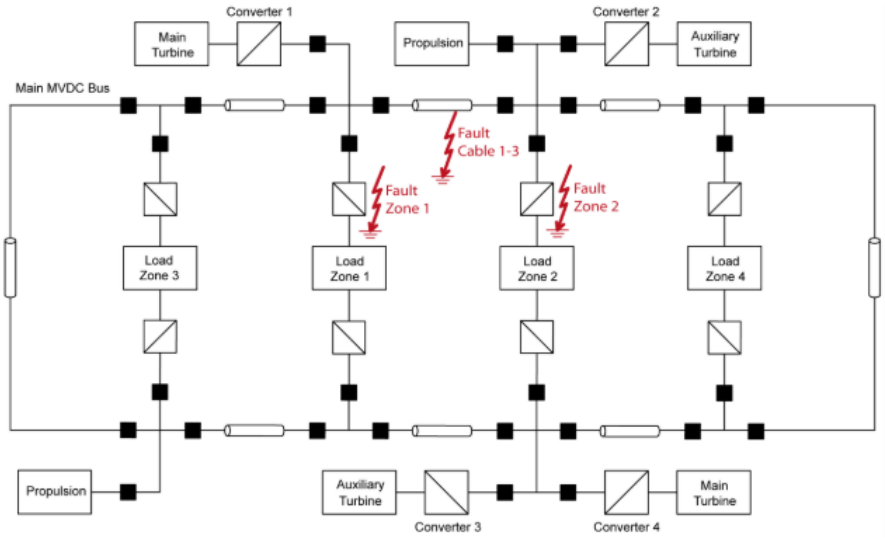

Figure 145- Example of MVDC Configuration for A High Performance Naval System

In this architecture, load zones are connected to the various sources and to the energy storage systems through a medium voltage ring bus, where the power can flow in every direction.
Each power supply and energy storage system is connected to the distribution bus via controllable (and often bidirectional) electronic power converters. If the main bus were armed as in a conventional AC system, the switches placed between the ring segments would open in the event of a fault in order to isolate it. The power converters are able to actively limit the current fed into the bus during a fault event, making it possible to reconfigure the system without having to interrupt high currents.
For naval plants, characterized by small direct current zone, fed by sources interfaced to a distribution bus via converters, some of the conventional detection methods used in alternating current are not easily applicable due to the limited current values, which are not much higher than the normal operating currents.
Methods based on current thresholds and current transients cannot be effective because of the similarity between nominal operating currents (referred for example to load steps, connections of several loads at the same time, capacitor connections) and short-circuit currents, due to the active limitation that the power converters make on the fault inputs from the generation busbars.
An example is the detection procedure of the instantaneous "Z-source" circuit-breakers which are able to detect high di/dt: the limiting action of the converters can then cause such devices to fail.
The detection method based on the estimation of the line inductance between protection devices through the measurement of the current gradient is similar: the high sensitivity to noise of the di/dt measurement makes it very difficult to implement a reliable detection circuit, in particular for DC networks in which the short-circuit currents are characterized by very fast transients.

However, there are methods based on detection of overcurrents, current gradients and differential currents; in these cases, however, the protection devices used must necessarily be solid state switches able to communicate with each other in order to provide adequate coordination.
Through the measurement of the differential current and the use of centralized measurement systems, information concerning the measured current between the sections of the system can be obtained, thus allowing a rapid and highly selective coordination of the protection system; the disadvantage of these methods, however, lies in the absolute integrity and reliability required by the communication network.
Some emerging methods then propose to measure the frequency spectrum of the bus impedance by injecting a broad-spectrum current and then measuring the resulting voltage perturbation, subsequently extracting the amplitude and phase of the associated impedance. However, the response times are necessarily dilated since the entire frequency spectrum must be scanned. Although the estimate of the impedance can then collect valuable information about the system, such a method requires high bandwidth and intensive computational capacity and is therefore more suitable for identifying the location of the fault after the system has been protected.
The measurement in the time domain of the voltage-current ratio, requires low computational requirements and is therefore suitable for the rapid detection of faults through the use of very economical filters and sensors.
Considering a MVDC network section where there are different load zones and converters for the interface with the generation systems R_L is the resistances associated to the various loads, R_{cable} and L_{cable} are the parameters related to the sections of the cables constituting the bus and R_F is the resistance of any failure that may occur anywhere on the network.
Thus, it is possible to measure voltage and current at the output terminals of each contactor and converter. The equivalent impedance Z_{eq} (s) can be defined in the frequency domain as the parallel between the branch failure and the different loads connected to the same converter:

$$Z_{eq}(s) = \frac{1}{\frac{1}{R_{cable}+R_F+s\cdot L_{cable}}+\sum_{i=1}^{n}\frac{1}{Z_{Li}}} \quad (36)$$

Z_{Li} is the sum of the equivalent resistance of the load i with the impedance of the cable placed between the converter and the generic load i.
Assuming that the impedance correlated to the fault resistance and the cable resistance is much smaller than the low frequency impedance of the parallel between the branches without faults, the impedance referred to the fault path dominates in the definition of the equivalent impedance and therefore is it is possible to neglect the contribution provided by the branches that are not affected by fault.
Moreover, the inductance reported in the equation can be noticed only at high frequency, so the inductive contribution of the cable to the equivalent impedance is negligible.
When a low impedance short circuits occurs, the fault resistance is then much lower than the cable resistance and therefore it is possible to implement the algorithm illustrated in order to obtain a distinction between faults near/far from the converter.
Each converter is equipped with a device for current and voltage measurement at its output terminals; such device calculates the apparent instantaneous resistance value:

$$R_n(t) = \frac{V_n(t)}{I_n(t)} \quad (37)$$

Where V_n e I_n are respectively voltage and current measured and R_n is the equivalent resistance calculated at output terminal of a generic device n.

This resistance is then compared with the thresholds set inside the controller in order to detect any failure located downstream of this device. The system selectivity is obtained through the use of several resistive thresholds which determine the opening of the contactors with different times, according to their distance from the fault.

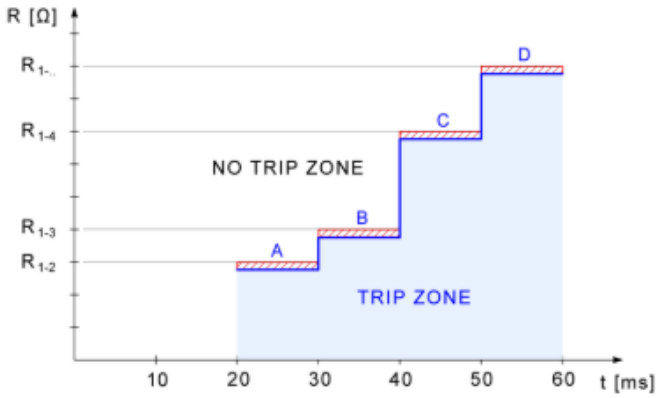

Figure 146 - Time-Resistance Characteristic for The Contactors Placed to Protect The Distribution Bus

Figure 146 shows an example of the time-resistance tripping characteristic for the contactors placed to protect the main distribution bus, in which the intervention levels marked A, B, C, D are examples of intervention thresholds.
Level A refers to the nearest section of the distribution bus that the contactor must protect; a minimum delay is associated. The intervention levels B, C and D are defined on the basis of progressively longer sections of dc bus to be protected.
In this case, also the delays associated with B, C and D intervention level progressively increase, in order to provide a coordination hierarchy.
Experimental studies have shown that is possible to limit the fault currents with intervention times of 10-20 minutes, allowing the system to be re-energized within 40-60 minutes.

Chapter XI: Conclusion

The electrical power system in naval application underwent impressive evolution during the years.
In the military field, the main innovations and technological transformations are due to the use of all electric or hybrid propulsion, the introduction of new equipment for ship's service, the massive adoption of electronic power converter coupled to the loads, new high power impulsive loads and advanced weapon systems. Moreover, thanks to the evolutionary development in power electronic technologies and the emergence of high-performance energy storage devices there is new interest in DC power distribution systems, already adopted in the early 1900s, which testify significant increase in research interest and industrial applications.
Nowadays the ship's electrical system design is focused on the concept of Integrated Power System (IPS) providing electric power to the propulsion and ship service constituting an integrated plant. The IPS requiring careful design and management in order to ensure Power Quality standard: achieve higher performance and reliability, cost reduction and reconfigurability.
Therefore, the electrical power architecture of new ships, that will be developed in the future, should consider these aspects and take into account several issues. It is necessary to develop guidelines and methodologies in order to investigate and analyze the several problems that may arise within the naval electrical systems.
This dissertation focuses on the Naval Smart Grid (NaSG) research project, completed in partnership with the University of Trieste and the Polytechnic University of Milan. The proposal of innovative and advanced solutions, capable of improving the IPS is considered as a novel contribution; the dissertation reports new methodologies to improve analysis techniques for studying the IPS and shows the results of several issues relating to on-board Power Quality (PQ). Moreover, smart solutions able to significantly improve the performance of the ship IPS are defined.
The research focuses on vessels endowed with electrical propulsion and either a full AC IPS or a hybrid AC/DC one, with particular attention to the integration of the best current technologies for on-board power systems with future technology.
The first part of the research activity concerned a measurement campaign on-board the Cavour ship, allowing to identify and characterize the most relevant loads.
The electrical loads installed on military ships are very diverse passing from common loads, that can be easily found also in commercial or industrial power plants such as lighting, fan coils, fridge groups to specific electric loads like radar, elevators, electric pumps, to impulsive loads such as weapon system that are specific of a warship. Moreover, aircraft carriers, like Cavour, incorporate hospital areas with relevant medical devices also having impulsive features, like TAC (Computerized Axial Tomography) that require high standards of power quality.
It is necessary to notice that some of the new electrical pulsed loads specific for military applications (e.g. radar, electromagnetic launchers, etc.) can cause severe disturbances to the system, thus causing the malfunctioning of other electric utilities. Some specific electrical loads presenting high distorted current absorption have been identified. Their characterization was considered particularly relevant, and was carried out in order to define their harmonic disturbance's contribution and their impact on the network.
The need to characterize specific loads on board military vessel allowed therefore the validation of the models of the system's components to be used.
Subsequently, different IPS's architectures have been defined in order to investigate possible and different solutions conceivable in the construction of new electric ships: a full all electric MVAC (Medium Voltage Alternate Current) power system, a hybrid all electric MVAC plus MVDC/LVDC islands (Medium/Low Voltage Direct Current) and a MVAC 50-60 Hz, with a hybrid (electric/diesel/gas turbine) propulsion.
The renewed interest in DC applications made it possible to evaluate the introduction of DC subnetworks in one of the proposed layouts. They interface with AC grid by active FECs,

characterized by a sinusoidal current input waveform; FECs have been evaluated for zone/switchboard constituted by either a large power absorption or by the supply of essential loads (e.g. ship hospital, communication and navigation support) to improve supply efficiency, quality and continuity to the overall shipboard electric power system.

Different and advanced solutions for the realization of the DC islands and for their interfaces with the AC network have been proposed, leading to a decoupling between AC and DC sections. The advantages of the adoption of storage systems and DC islands, that are useful to guarantee a high level of power quality and continuity of service to the loads, were highlighted.

The front-end converter decoupling action avoids disturbance propagation among the two power system sections, both in the steady state and during transients. Moreover, by introducing storage systems into the DC sections, a stable power supply can be obtained for a limited period, independently from the AC section state. Storage systems can also be used to manage either pulsed or periodical fast load variations, thus controlling transient power flows and performing peak-shaving functionality. By exploiting such functions, it is possible to reduce the whole distribution system sizing and limit the disturbances injected by the DC islands into the AC grid.

A methodology to represent an equivalent network was reported. Different equivalent network models have been proposed, and their accuracy was demonstrated in order to develop the best radial equivalent network to be used for simulations. It enhances the need to develop new approaches to be taken into account, also for the introduction of new technologies that very often require accurate analysis.

Once the loads were characterized and the most accurate network equivalent was identified, it was possible to carry out an exhaustive investigation on systems architecture in frequency domain with the aim to identifying resonances, non-linear loads, and detecting disturbances to frequencies by performing harmonic analysis.

The increase of electronically controlled loads and pulsed loads added to shipboard power systems led to an increase in harmonic distortions. Moreover, due to the increase in harmonic disturbances and the risk of incurring untimely tripping of the switches with a consequent disconnection of load areas, is an issue to be taken into account. Preliminary evaluations were carried out to analyze the behavior of the system when certain faulty events occur and the state of the art of new AC -DC protection equipment also in relation to the immunity to disturbances. Therefore, it is necessary for these systems to be properly evaluated based on a Standard in the perspective of harmonic limitation.

A complete study of the system's impedance and harmonic disturbances for the layout proposed was carried out showing how this kind of advanced evaluation is important and must be considered during the design process.

Moreover, for a complete Power Quality analysis the need to model time-varying non-linear load in power systems led to the development of a deterministic-probabilistic software. Depending on the ship operating role, in fact, the power consumption of various electrical loads can undergo significant variations, passing for example from the less energizing stages of parking and manoeuvring in port, up to special roles that require maximum electrical requirements such as in combat role. The main goal has been develop a complete analysis methodologies to assess harmonic disturbances.

The main results achieved for full MVAC (Medium Voltage Alternate Current) power system and hybrid MVAC plus MVDC/LVDC islands (Medium/Low Voltage Direct Current) showed that the large harmonic emission of the high-power propulsion system results in significantly high THDV %. The need to install filters, in order to reduce harmonic disturbances is thus highlighted. The study reports that the High Pass + Single Tuned filter configuration represents the best solution of effectiveness for them in reducing the MVAC system THDV %. Filters introduce benefits regarding THDV %, but, at the same time, they create resonances.

Consequently, these resonances excite harmonic disturbances generated by on board non-linear loads, amplifying singular harmonic disturbances order. These aspects, however, increase THDV % values due to the resonance that could occur on a specific harmonic.
For this reason, the supply of such loads by means of DC islands is preferable, thanks to the harmonic disturbances immunity at the DC side and the installation of AC/DC converters with sinusoidal absorption at the AC side. In the case study, the introduction of five DC islands in the H-MVAC system permits to reduce THDV %. In addition, the installation of storage systems and four-quadrants FECs would also improve AC network stability and continuity of supply, thanks to active and reactive power controls. High quality and continuity of supply is also provided to DC loads.
DC islands and storage systems help to improve efficiency, and quality and continuity of supply of the overall shipboard electric power system.
On the contrary, the MVAC 50-60 Hz layout, with a hybrid (electric/diesel/gas turbine) propulsion, shows a significant reduction of electric motors' power for propulsion.
In this case, no particular criticalities were found except for the case in which both propulsion engines and two maneuvering thruster were in operation, generating a resonance between the 25th and the 31th harmonic. This aspect can be influenced by the predominantly rotating load and by the considerable power present on the main panel. Particular care in techniques analysis was considered which permitted to carry out deep and accurate investigations for any type of network architecture.
Finally, in order to analyze the continuity of the service, preliminary studies about availability, reconfigurability, some top-events and short-circuit faults were performed by applying consolidate methodologies such as the dependability theory and the well know common criteria for protection, coordination calculation of short-circuit faults, introducing also the improvements and new research in DC protection.
The technology research activity carried out in the research project led to a relevant expertise improvement for the IT Navy, in terms of both analyses on the covered topics and evaluations about the commercial availability of the proposed solutions.
The exploitation of the research results and methodologies proposed will be useful for the design and requirements of new IT Navy vessels, equipped with better mission capabilities, mission power, and fuel efficiency, and integrating new high energy pulsed weapon systems. Moreover, developed models, calculation codes and advanced analysis methodologies are considered as novel contributions of the work. They could be adopted also to take into account very promising technology improvement such as the introduction of static converters in lieu of well consolidated rotating converters that are used for 50/60 Hz applications or the implementation of Front End Converters to limit harmonic distortion, as well as multi-port DC/DC converters coupled to storage systems to improve the efficiency, quality and continuity of the overall shipboard electric power system.

Acknowledgments

Thanks to the Italian Navy for the organization of measurement campaigns on the aircraft carrier Cavour and for the granting of the publication of data.
A Special Thanks to the engineer "*Comandante di Fregata*" Gennaro Lipardi.

References

[1] A. K. Ådnanes, «maritime electrical installations and diesel electric propolsion,» ABB AS Marine, April 2013.

[2] A. Vicenzutti, «Innovative integrated power system for all electric ships,» in *Tesi di dottorato Università degli studi di Padova*, 2017.

[3] G. Sulligoi , «All electric ships: present and future after 20 years of research and technical achievements,» in *Electrical Engineering Research Report.*, 2011.

[4] J. Hansen e F. Wendt, «History and State of the Art in Commercial Electric Ship Propulsion, Integrated Power Systems, and Future Trends,» in *Proceedings of the IEEE, vol.103, no. 12, pp. 2229-2242,*, Dec. 2015..

[5] M. Cupelli, F. Ponci, G. Sulligoi, A. Vicenzutti, C. Edrington, T. El-Mezyani e A. Monti, «Power Flow Control and Network Stability in an All-Electric Ship,» in *Proceedings of the IEEE, vol 103, no.12*, Dec 2015.

[6] E. Skjong, E. Rodskar, M. Molinas, T. Johansen e J. Cunningham, «The Marine Vessel's Electrical Power System: From its Birth to Present Day,» in *Proceedings of the IEEE vol 103, no.2*, Dec 2015.

[7] «http://www.marina.difesa.it/uominimezzi/navi/Pagine/Vespucci.aspx,» Marina Militare Italiana. [Online].

[8] «http://www.frenchlines.com/ship_en_355.php,» [Online].

[9] «http://www.qe2.org.uk/,» [Online].

[10] IEC, «International standard, "Electrical installations in ships - Part 201: System design – General". IEC 60092 – 201 ed4.0 1994-08-17».

[11] «International standard, "Guide for the Design and Application of Power Electronics in Electrical Power Systems on Ships". IEEE Std 1662-2008.».

[12] D. Zaninelli , «Sistemi elettrici a bordo delle navi,» Politecnico di MIlano, Milano, 2005.

[13] ABB, «Quaderni di applicazione tecnica N.12 Generalità sui sistemi navali e sulle installazioni di bordo,» 2011.

[14] Standard, «IEC 60038:2009,» IEC standard voltages.

[15] Standard, «IEC 60092-101:2018,» Electrical installations in ships - Part 101: Definitions and general requirements.

[16] Gatta e F. M. Gatta, Impianti elettrici, Società Editrice Esculapio, 2014.

[17] R. Poli, «Azionamenti elettrici di elevata potenza per applicazioni nella propulsione navale,» in *Tesi di laurea dell'Università di Padova*.

[18] N. Mohan, T. M. Undeland e W. P. Robbins, «Power Electronics: Converters, Applications, and Design,» 3rd Edition, 2002.

[19] M. Ceraolo, «Sistemi Elettrici Navali,» Accademia Navale di Livorno, volume A.N. 12-39..

[20] R. Hepburn, «Why a naval architect likes an electric ship,» in *Power Electronics, Electrical Drives, Automation and Motion, 2008. SPEEDAM 2008. International Symposium on*, Ischia, 2008.

[21] ABB, «Guida tecnica, criteri di protezione delle reti elettriche di media tensione,» 2016.

[22] ABB, «Quaderni di applicazione tecnica N.1,» 2015.

[23] A. Cavallaro e A. De Falco, Sistemi elettrici navali, 2009.

[24] R. M. Cuzner e V. Singh, «Future shipboard MVDC system protection requirements and solid state protective device topologiacl tradeoff,» in *IEEE Journal of emerging and selected topics in power electronics vol.5 n.1*, 2017.

[25] R. M. Cuzner, S. Vikas, R. Mohammed e N. Adel, «Converter topological and solid state protective device trafe offs for future shipboard MVDC system,» in *IEEE Electric ship technologies symposium (ESTS)*, Juky 2015.

[26] S. Electric, «Coordinamento delle protezioni BT - Guida tecnica».

[27] G. Lipardi, «Seminario Impianti Elettrici Navali,» Seminario per Corso di Sistemi Elettrici per la Mobilità, Università di Roma La Sapienza, 2013.

[28] «http://en.dcnsgroup.com/naval/products/best/,» [Online].

[29] M. . K. Saini e R. Kapoor, «Classification of power quality events – A review,» *International Journal of Electrical Power & Energy Systems*, vol. 43, n. 1, pp. 11-19, 2012.

[30] M. Bollen, «What is power quality?,» *Electric Power System Research*, vol. 66, n. 1, pp. 5-14, 2003.

[31] S. Chattopadhyay, M. Mitra e . S. Sengupt, «Electric Power Quality,» *Springer Netherlands*, pp. 5-21, 2011.

[32] P. Caramia, G. Carpinelli e P. Verde, Power quality indices in liberalized markets, John Wiley & Sons, 2009.

[33] A. Andreotti , A. Brancale, P. Caramia e et all, «Adaptive Prony method for the calculation of power-quality indices in the presence of nonstationary disturbance waveforms,» *IEEE Trans. Power Delivery*, vol. 24, n. 2, pp. 874-883, 2009.

[34] L. Qi, L. Qian, S. Woodruff e et all, «Prony analysis for power system transient harmonics,» *J. Appl. Signal Process*, pp. 170-182, 2007.

[35] C. Hsieh, . J. Lin e S. Huang, «Slant transform applied to electric power quality detection with field programmable gate array design enhanced,» *Electrical. Power Energy System*, vol. 32, n. 5, pp. 428-432, 2010.

[36] Z. Chen e P. Urwin, «Power quality detection and classification using digital filters,» in *Proc. IEEE Power Tech*, Porto, 2001.

[37] M. V. Ribeiro, C. A. Marques, C. A. Duque e et al, «Power quality disturbances detection using HOS,» in *IEEE Power Engineering Society General Meeting*, Montreal, Canada, 2006.

[38] T. Abdel-Galil, E. El-Saadany e . M. Salama, «Power quality event detection using Adaline,» *Electric Power Systems Research,*, vol. 64, n. 2, pp. 137-144, 2003.

[39] G. Hu, F. Zhu e Y. Tu, «'Power quality disturbance detection and classification using Chirplet transforms,» in *Proc. Springer Simulated Evolution and Learning*, Berlin, Germany, Oct. 2006.

[40] G. Heydt, P. Fjeld, C. Liu e et al, «Applications of the windowed FFT to electric power quality assessment,» *IEEE Transaction on Power Delivery*, vol. 14, n. 4, pp. 1411-1416, 1999.

[41] P. Wright, «Short-time Fourier transforms and Wigner–Ville distributions applied to the calibration of power frequency harmonic analyzers,» *IEEE Transaction. Instrument. Measurements*, vol. 48, n. 2, p. 475–478, 1999.

[42] Y. Gu e M. Bollen, «Time-frequency and time-scale domain analysis of voltage disturbances,» *IEEE Transaction on Power Delivery*, vol. 15, n. 4, pp. 1279-1284, 2000.

[43] S. Santoso, E. Powers e W. Grady, «'Power quality disturbance data compression using wavelet transform methods,» *IEEE Transaction on Power Delivery,*, vol. 12, n. 3, pp. 1250-1257, 1997.

[44] O. Poisson, P. Rioual e M. Meunier , «New signal processing tools applied to power quality analysis,» *IEEE Transaction on Power Delivery*, vol. 14, n. 2, pp. 561-566, 1999.

[45] H. Beides e . G. Heydt, «Dynamic state estimation of power system harmonics using Kalman filter methodology,» *IEEE Transaction on Power Delivery*, vol. 6, n. 4, pp. 1663-1670, 1991.

[46] H. Ma e A. Girgis, «Identification and tracking of harmonic sources in a power system using a Kalman filter,» *IEEE Transaction on Power Delivery,*, pp. 1659-1665., 1996.

[47] J. Barros e R. Diego, «Application of the wavelet-packet transform to the estimation of harmonic groups in current and voltage waveforms,» *IEEE Transaction on Power Delivery*, vol. 21, n. 1, pp. 533-535, 2006.

[48] S. Kaewarsa, K. Attakitmongcol e T. Kulworawani, «Recognition of power quality events by using multiwavelet-based neural networks,» *Electrical Power Energy System,*, vol. 30, n. 4, pp. 254-260, 2008.

[49] S. Upadhyaya, S. Mohanty e C. Bhende, «Hybrid Methods for Fast Detection and Characterization of Power Quality Disturbances,» *Control Automation Electrical System*, vol. 26, n. 5, pp. 556-566, 2015.

[50] J. Liu, . P. Ribeiro e P. Pillay, «Wavelet Analysis of Power Systems Transients Using Scalograms and Multi-Resolution Analysis,» *Electric Machines and Power Systems, Taylor and Francis*, pp. 1331-1341, 1999.

[51] P. Pillay, P. Ribeiro e Q. Pan, «Power Quality Modeling Using Wavelets,» in *International Conference on Harmonics and Power Quality*, Las Vegas, October 1996..

[52] P. Ribeiro, «Wavelet Transform: An Advanced Tool for Analyzing Non-Stationary Distortions In Power Systems,» in *ICHPS VI*, Italy, 1994.

[53] Y. Chen, «Passive filter design using genetic algorithms,» *IEEE Transaction Industrial Electronics*, vol. 50, n. 1, pp. 202-207, 2003.

[54] R. Pena-Alzola, M. Liserre, F. Blaabjerg e et al, «Analysis of the passive damping losses in LCL-filterbased grid converters,» *IEEE Transaction Power Electronics*, vol. 28, n. 6, pp. 2642-2646, 2013.

[55] W. Wu, Y. Sun, M. Huang e et al, «A robust passive damping method for LLCL-filter-based grid-tied inverters to minimize the effect of grid harmonic voltages,» *IEEE Transaction Power Electronics*, vol. 29, n. 7, pp. 3279-3289, 2014.

[56] A. Edris, «Proposed terms and definitions for flexible AC transmission system (FACTS),» *IEEE Transaction on Power Delivery*, vol. 12, n. 4, pp. 1848-1853, 1997.

[57] P. Roncero-Sanchez , E. Acha e J. Ortega-Calderon, «A versatile control scheme for a dynamic voltage restorer for power-quality improvement,» *IEEE Transaction on Power Delivery,*, vol. 24, n. 1, p. 277 284, 2009.

[58] S. Mohod e M. Aware, «A STATCOM-control scheme for grid connected wind energy system for power quality improvement,» *IEEE Syst. J*, vol. 4, n. 3, pp. 346-352, 2010.

[59] C. Gajanayake, D. Vilathgamuwa, P. Loh e et al, «Z-source-inverter-based flexible distributed generation system solution for grid power quality improvement,» *IEEE Transaction on Energy Conversion*, vol. 24, n. 3, pp. 695-704, 2009.

[60] M. Singh, V. Khadkikar, A. Chandra e et al, «Grid interconnection of renewable energy sources at the distribution level with power-quality improvement features,» *IEEE Transaction Power Delivery*, vol. 26, n. 1, pp. 307-315, 2011.

[61] M. Marei, E. El-Saadany e M. Salama, «A flexible DG interface based on a new RLS algorithm for power quality improvement,» *IEEE Syst. J*, vol. 6, n. 1, pp. 68-75, 2012.

[62] F. Beltran-Carbajal e G. Silva-Navarro, «A fast parametric estimation approach of signals with multiple frequency harmonics,» *Electric Power Systems Research*, vol. 144, pp. 157-162, 2017.

[63] N. Watson e J. Arrillaga, «Harmonics in large systems,» *Electric Power Systems Research*, vol. 66, n. 1, pp. 15-29, 2003.

[64] L. Feola,, R. Langella e A. Testa, «On the Effects of Unbalances, Harmonics and Interharmonics on PLL Systems,» *IEEE Transactions on Instrumentation and Measurement*, vol. 62, n. 9, pp. 2399-2409, 2013.

[65] G. Carpinelli, F. Gagliardi e P. Verde, «P. Probabilistic modelings for harmonic penetration studies in power systems,» in *Proceeding of conference on Harmonics in Power Systems (ICHPS)*, Budapest, 1992.

[66] A. Capasso, R. Lamedica, A. Prudenzi e P. Ribeiro, «Probabilistic assessment of harmonic distortion caused by residential load areas,» in *Proceeding of conference on Harmonics in Power Systems (ICHPS)*, Bologna, 1994.

[67] E. b. P. F. Ribeiro, Time-varying waveform distortions in power system, John Wiley & sons, LTD, 2009.

[68] A. Mansoor, W. M. Grady, A. H. Chowdhury e M. Samot, «An Investigation of Harmonics Attenuation and Diversity Among Distributed Single-Phase Power Electronic Loads,» *IEEE Trans. on Power Delivery*, vol. 10, pp. 467-473, 1995.

[69] A. Sharma, V. Moinuddin, M. N. Doja , I. Ibrahee e M. Khan, «Power Quality Assessment and Harmonic Comparison of Typical Non-linear Electronic Loads,» in *Proceeding of conference on Industrial Technology*, Goa, India, 2000.

[70] R. Langella e A. Testa, Chpater 6 "Summation of random harmonic currents" of book Time-varying waveform distortions in power system, Wiley, 2009.

[71] U. Grasselli, R. Lamedica e A. Prudenzi , «Time-varying harmonics of single-phase non-linear appliances, In Proceedings of the conference IEEE Power Engineering Society Transmission and Distribution,» New York, USA, January 2002.

[72] L. Alfieri, A. Bracale e A. Larsson, «New Power Quality Indices for the Assessment of Waveform Distortions from 0 to 150 kHz in Power Systems with Renewable Generation and Modern Non-Linear Loads,» *Energies*, vol. 10, p. 1633.

[73] V. Cuk, . J. F. Cobben, W. L. King e P. F. Ribeiro, «Analysis of harmonic current summation based on field measurements,» *IET Generation Transmission & Distribution,* vol. 7, n. 12, pp. 1391-1400, 2013.

[74] C. I. Chen, G. W. Chang , R. C. Hong e H. M. Li, «Extended Real Model of Kalman Filter for Time-Varying Harmonics Estimation,» *IEEE Transactions on Power Delivery,* vol. 25, n. 1, 2010.

[75] Cheng-I Chen e Yeong-Chin Chen,, «Comparative Study of Harmonic and Interharmonic Estimation Methods for Stationary and Time-Varying Signals,» *IEEE Transactions on Industrial Electronics,* vol. 61, n. 1, 2014.

[76] M. Lamich, J. Balcells, C. Montserrat e E. Griful, «Nonlinear Loads Model for Harmonics Flow Prediction, Using Multivariate Regression,» *IEEE Transactions on Industrial Electronics,* vol. 64, n. 6, 2017.

[77] M. Hermoso-Orzáez, A. Gago-Calderón e J. Rojas, «Power Quality and Energy Efficiency in the Pre-Evaluation of an Outdoor Lighting Renewal with Light-Emitting Diode Technology: Experimental Study and Amortization Analysis,» *Energies,* vol. 10, p. 836, 2017.

[78] X. Xiao, A. Testa e et al, «Analysis and Modelling of Power-Dependent Harmonic Characteristics of Modern PE Devices in LV Networks,» *IEEE Transactions on Power Delivery,* vol. 32, n. 2, pp. 1014-1023, April 2017.

[79] A. Collin , X. Xu, S. Djokic, R. Langella, A. Testa e J. Drapela, «Experimental evaluation and classification of LED lamps for typical residential applications,» in *IEEE PES Innovative Smart Grid Technologies Conference Europe (ISGT-Europe)*, Torino, 2017.

[80] R. Langella e A. Testa, Chpater 9 "probabilistic modeling of harmonic impedances" of Book "Time-Varying waveform distortions in power systems, Wiley, 2009.

[81] I. N. Santos, M. H. Bollen e P. F. Ribeiro, «Exploring the Concept of Hosting Capacity for Harmonic Distortions Assessment,,» in *Power & Energy Society General Meeting*, Denver, Colorado. Usa,, 2015.

[82] J. Jedrzejczak, G. Anders , M. Fotuhi-Firuzabad, H. Farzin e F. Aminifar, «Reliability Assessment of Protective Relays in Harmonic-Polluted Power Systems,» *IEEE Transactions on Power Delivery,* vol. 32, n. 1, 2017.

[83] M. M. Islam, Shipboard Power Systems Design and Verification Fundamentals, Wiley, July 2018.

[84] S. G. Jayasinghe , L. Meegahapola , N. Fernando e et al, «Review of Ship Microgrids: System Architectures, Storage Technologies and Power Quality Aspects,» *Inventions,* 2017.

[85] P. F. Ribeiro, M. Steurer e M. Islam, «Reevaluating electric power system harmonic distortion limits for shipboard systems,",» in *International Conference on Harmonics and Quality of Power*, Lake Placid, NY, USA, 2004.

[86] F. Iliceto, Impianti elettrici vol.1, 1984.

[87] G. Conte, Manuale di impianti elettrici, Hoepli, ed.2 , 2009.

[88] N. CEI-U, «Cavi elettrici isolati con materiale elastomerico o termoplastico per tensioni nominali non superiori a 1000 V in corrente alternata e a 1500 V in corrente continua - Portate di corrente in regime permanente per posa in aria».

[89] A. Capasso, R. Lamedica, R. Manigrasso, G. Sani, G. Superti Furga e E. Tironi, «Reference Power Network for Harmonic Propagation,» in *European Trans. On Electrical Power Engineering, vol.2, no.3, pp. 167-178*, May/Jun. 1992.

[90] R. Lamedica, A. Prudenzi, E. TIroni e E. Zaninelli, «A Model of Large Load Areas for Harmonic Studies in Distribution Networks,» in *IEEE trans on Power Delivery, vol. 12, no. 1, pp. 418-425*, , Jan. 1997..

[91] B. Gnedenko, Theory of Probability 6th Edition, Gordon and Breach Science Publishers, 1997.

[92] A. Vicenzutti, R. Menis e G. Sulligoi, «Dependable design of all electric ships integrated power system: New design process,» in *International Conference on Electrical Systems for Aircraft, Railway, Ship Propulsion and Road Vehicles & International Transportation Electrification Conference (ESARS-ITEC)*, Toulouse, 2016.

[93] R. Menis, A. da Rin, A. Vicenzutti e G. Sulligoi, «Dependable design of All Electric Ships Integrated Power System: Guidelines for system decomposition and analysis,» in *Electrical Systems for Aircraft, Railway and Ship Propulsion*, Bologna, 2012.

[94] E. O. S. Hansen, «DP Dependability,» in *Dynamic Positioning Conference*, 11-12 Oct. 2011..

[95] «http://www.fincantieri.it,» [Online].

[96] I. Mohammed M , «Annex H of A guide to electrical installations on shipboard,» IEEE Standard 45, 2004.

[97] G. Lipardi , L. Piva, L. Piegari, E. Tironi, R. Lamedica, A. Ruvio, G. Sulligoi e A. Vicenzutti, «Electric loads characterization in an aircraft carrier with ring-bus distribution system,» in *International Conference on Electrical Systems for Aircraft, Railway, Ship Propulsion and Road Vehicles (ESARS) pp. 1-6*, Aachen, 2015.

[98] «EC 60092 - 352 Ed. 2.0 Electrical installations in ships - part 352: Choice and installation of electrical cables,» 1997 - 2008..

[99] A. Capasso, R. Lamedica, S. Lauria, E. Tironi, A. Ruvio e M. Corti , «Voltage Quality Studies in Electric Power Systems: an AC/DC network for a Shipboard application,» in *IEEE EEEIC 2016 – 16th Conference on Environment and Electrical Engineering*, Florence, June 2016.

[100] M. R. Patel, «Shipboard Electrical Power Systems,» *CRC Press*, 2012.

[101] Z. Jin, G. Sulligoi, R. Cuzner, L. Meng e . J. Vasq, «Next-Generation Shipboard DC Power System: Introduction Smart Grid and dc Microgrid Technologies into Maritime Electrical Netowrks,» *IEEE Electrification Magazine*, vol. 4, n. 2, pp. 45-57, 2016.

[102] A. Smith, S. Williamson e C. Hodge, «High Torque Dense Naval Propulsion Motors,» in *IEEE International Electric Machines and Drive Conf., vol. 3, pp. 1421-1427*, 2003.

[103] T. Hoevenaars, I. Evans e A. Lawson, «New marine harmonic standards,» *IEEE Industry Applications Magazine*, vol. 16, n. 1, pp. 16-25, 2010.

[104] I. C. Evans, «Harmonic mitigation for AC thruster & small propulsion drive applications,» *Marine Propulsion International*, pp. 16-17, 2002.

[105] I. C. Evans e T. Hoevenaars, «Homing in on harmonics,» *Offshore Engineer*, pp. 55-57, 2006.

[106] X. Liang e O. IIocbonwu, «Passive harmonic filter design scheme for subsea cable applications with six-pulse variable frequency drives,» *IEEE Industry Applications Magazine*, vol. 7, n. 5, pp. 36-44, 2011.

[107] P. Guerin e L. Miegeville, «Optimal placement and sizing of harmonic filters aboard an electric propulsion ship,» *IET Gener. Trans. Distrib*, vol. 1, n. 4, pp. 612-618, 2007.

[108] Z. L. Liao, «Investigation of allocation of passive harmonic filters in a shipboard power system,» in *M. S. Thesis Submitted to National Cheng Kung University*, 2010.

[109] ". C. Su and C. Hong, C. Su e C. Hong, «Design of passive harmonic filters to enhance power quality and energy efficiency in ship power systems,» in *9th IEEE/IAS Industrial & Commercial Power Systems Technical Conference*, Stone Mountain, 2013.

[110] G. Parise, R. Lamedica, L. Martirano, A. Ruvio, L. Parise, B. Chavdarin e C. LIen, «TN-grounding system for the emerging cold ironing: multiple grounding system vs island system,» in *EEEIC 2018*, Palermo, 2018.

[111] S. Grillo, V. Musolino, L. Piegari e E. Tironi, «DC Islands in AC Smart Grids,» *IEEE Trans. On Power Electronics,* vol. vol. 29, n. no. 1, pp. pp. 89-98, Jan. 2014.

[112] E. Tironi, M. Corti e G. Ubezio, «DC Networks Including Multi-port DC/DC Converters: Fault Analysis,» in *Proc. 2015 15th IEEE Environment and Electrical Engineering International Conf, pp. 1109-1114.*, 2015.

[113] E. Tironi, M. Corti e G. Ubezio, «A Novel Approach in Multi-port DC/DC Converter Control,» in *Proc. 2015 5th International Conf. on Clean Electrical Power, pp. 54-60*, 2015.

[114] «IEEE Standard for Power Electronics Open System Interfaces in Zonal Electrical Distribution Systems Rated Above 100 kW, IEEE Standard 1826-2012,» IEEE, 2012.

[115] J. Shi, R. Amgai e S. Abdelwahed, «Modelling of Shipboard Medium-Voltage Direct Current System for System Level Dynamic Analysis,» *IET Electrical Systems in Transportation,* vol. vol.5, n. no. 4, pp. pp. 156-165, Dec. 2015.

[116] G. Sulligoi, A. Vicenzutti, E. Tironi, A. Ruvio, R. Lamedica, G. Lipardi e L. Piva, «Naval Smart Grid - Integrated Power System for All Electric Naval Vessels with control and reliability characteristics,» in *AEIT*, 2014.

[117] S. Cyme, «http://www.cyme.com/software/BR917001EN-CYME-software.pdf.,» [Online].

[118] «C.A 8335 (Qualistar +) technical datasheet and instrument equipment manual provided by Chauvin Arnoux group.».

[119] A. Capasso, R. Lamedica, S. Sangiovanni, A. Ruvio, C. Lazaroiu e G. A. Maranzano, «A measurement campaign in a metro trains deposit/maintenance and repair site for PV production optimal sizing,» in *EEEIC 2015*.

[120] S. Rios, R. Castaneda e Veas, «D. Harmonic distortion and power factor assessment in city street gas discharge lamps,» *IEEE Transactions on Power Delivery*, vol. 11, n. 2, pp. 1013-1018, 1996.

[121] «Z. Djurovic, B. Kovacevic and V. Barroso, "QQ-plot based probability density function estimation," Proceedings of the Tenth IEEE Workshop on Statistical Signal and Array Processing (Cat. No.00TH8496), Pocono Manor, PA, 2000, pp. 243-247. doi: 10.1109».

[122] I. 60038:2009, «IEC standard voltages».

ANNEX A - Measuring Instrument

The instrument used for the measurements was the Chauvin Arnoux CA 8335 network analyser (Figure A1). It measures 4 voltages and 4 currents, thus calculating all the relevant power quality parameters. It was then possible to record voltages, currents and power values for each measurement, and to perform harmonic disturbance analysis. The analyzer can measure, and log all parameters simultaneously, as well as transient waveforms and inrush currents. Its memory capacity allows recording all variables with a sampling period of 1 second. It can be used directly with voltages up to 1200 V and currents up to 6500 A, and it is also able to perform data analysis in accordance with EN50160. The intrinsic instrument error is equal to ± (0.5 % + 0.2 V) for RMS Voltage phase to phase and ± (0.5 % + 1 A) RMS current, not considering the current sensor.
For currents measure both calipers clamp (Figure A2 - MN93A - 100 A or 5 A with ± 0.7 % measurement error in RMS current) and Rogowsky coils (Figure A3 - AmpFLEXTM A 193 – 6500 A with ± 3 % measurement error in RMS current) were used. More details about measuring instrument are reported in [118]. The instrument uses FFT (16 bit) with 1024 points over four periods with a rectangular window (see IEC 61000-4-7).

Figure A1- Chauvin Arnoux CA 8335 Network Analyser

Figure A3- MN93A - 100 A or 5 A Calipers Clamp

Figure A3- AmpFLEXTM A 193 – 6500 A Calipers Clamp

ANNEX B – Simulink model validation

The Annex B reports the case study used to modelling time-varying non-linear loads in power systems, based on demand conditions. The model allows a pre-evaluation of harmonic disturbances under variable conditions using normal and uniform distribution to randomize the electrical values of the non-linear loads and the related harmonic spectra.
A measurement campaign conducted on an industrial area, a deposit/maintenance and repair site utilized for trains in operation on the metro line B of Rome, has been take into account to verify the model performance. The methodology allows estimating the voltage total harmonic distortion at the point of common coupling. Through a statistical analysis, the harmonic distortion distribution via common normality tests was evaluated.

Case study

Each underground line in Rome has large available areas where metro trains, deposits/maintenance, and a repair site are located. A measurement campaign was conducted on the deposit/maintenance and repair site utilized for trains in operation on the metro line B of Rome named Magliana [119].
In the areas of Magliana there are: Office, workplace canteen, Bar, dressing room, rolling stock maintenance, technological system, lighting towers and storehouses.
Figure B1 shows the total area of Magliana

Figure B1 - Buildings in Magliana's area

The main activity is the rolling stock maintenance that is performed in the maintenance building no.02 and has an area of 14000 m^2; this building shows the highest consumption of the entire area. The activities inside the building are mount and trolleys revision, tests, maintenance and faults repair. Others buildings, characterized by high power consumption, are:

- Building no.03: office, workplace canteen, bar, dressing room;
- Building no.5: a thermal power plant inside technological system;
- Lighting towers located on an external area.

The measurements were carried out first, for each of the above mentioned building connecting the instrument to the different lines and then on the main low voltage electrical panel located downstream of the transformer 20/0.4 kV to measure the global consumption of entire Magliana area.
The measurement of active and reactive power and harmonic profile during a weekday (24 hours), characterized by a high consumption, is reported in the following section. Unfortunately, there are

no measurements about harmonics phases therefore, in the simulation the phases were evaluated in all range for each phase (e.g. -20 +20 degree for the first phase, (-20 + 20) degree -/+ 120*pi/180, for the second and third phase) using a random process. For the other buildings located in the Magliana area a total load characterized mainly by the lighting was supposed with disturbances by harmonic injection referred to a measurement campaign reported in [120].

Building no.02 - Rolling Stock Maintenance

The main loads inside the maintenance building No.02 are: lighting, lathe in pit, miscellaneous tools used for maintenance work, small lathe and cranes. The three-phase feeding cable on the main electrical panel has a resistance of 0.022 Ω and an inductance of 42 μH.
Table B1 and B2 show the main values about Maximum and Minimum power consumption for the building No.02 and its current harmonic profile reported in percentage for each harmonic order.

Max Active Power [kW]	Min Active Power [kW]	Max PF	Min PF
120	80	0.9	0.8

Table B1 - Rolling stock maintenance Active Power and Power factor

Current Harmonic Order	Max Value %	Min Value %
3	12	10
5	1.5	0.7
7	5	1.5
9	2	0.5
11	3	0.9
13	0.1	0.1
15	0.5	0.5
17	0.4	0.4
19	0.1	0.1
21	0.9	0.3
23	0.4	0.4
25	0.4	0.4

Table B2 - Rolling stock maintenance Current Harmonic spectrum

Building no.03 - Office, Workplace Canteen, Bar, Dressing Room

The area includes: 13 offices, a meeting room, a bathroom, a service dining room, a phone room, a canteen, a bar and a dressing room. The three-phase feeding cable from the main electrical panel has a resistance of 0.013 Ω and an inductance of 13μH. Table B3 and B4 show the main values about Maximum and Minimum power consumption for the building no.03 and its current harmonic profile, reported in percentage for each harmonic order.

Max Active Power [kW]	Min Active Power [kW]	Max PF	Min PF
24	18	0.9	0.8

Table B3 - Office, Workplace Canteen, Bar, Dressing Room Active Power and power factor

Current Harmonic Order	Max Value %	Min Value %
3	11	2
5	12	8
7	10	3
9	8	3
11	11	3
13	3	0.2
15	1.5	0.2
17	1.5	0.2
19	1.5	0.2

21	2.3	0.2
23	1.8	0.2
25	1	0.2
27	6	0.2
29	0.8	0.2
31	2	0.2
33	2	0.2
35	2	0.2
37	2	0.2
39	2	0.2

Table B4 - Office, Workplace Canteen, Bar, Dressing Room Current Harmonic spectrum

Building n.05 Technological System

The technological system is installed inside the building No.8 and produces heating and hot water for the entire Magliana area. It is equipped with five generators with pumps, 20 distribution pumps (KSB), 4 generators of 1,250,000 Kcal, 1 generator of 500000 Kcal. The three phase feeding cable from the main electrical panel that supplies the Technological system has a resistance of 0.013 Ω and an inductance of 13 μH. Table B5 and B6 show the main values about Maximum and Minimum power consumption of the technological system and its current harmonic profile, reported in percentage for each harmonic order.

Max Active Power [kW]	Min Active Power [kW]	Max PF	Min PF
32	28	0.9	0.8

Table B5 - Technological system Active Power and Power factor

Current Harmonic Order	Max Value %	Min Value %
3	1	0.7
5	2	0.3
7	0.7	0.1
9	0.7	0.1
11	0.7	0.1

Table B6 - Technological system Current Harmonic spectrum

Lighting Towers

The lighting towers are located in the entire external area.
There are 3 lighting towers and 40 single lamps distributed on a large square. Table B7 reports the numbers and power of the lamps inside each lighting tower.
The feeding three-phase cable from the main electrical panel has a resistance of 0.013 Ω and an inductance of 13 μH.
Table B8 and B9 report the main values for lighting towers' Maximum and Minimum power consumption and current harmonic profile in percentage for each harmonic order. In this case no measure of the harmonic profile was carried out and so the Authors used the data reported in the literature [120].

Numbers of lamp	Lighting towers 1 [W]
2	40
4	1000
11	400
Numbers of lamp	**Lighting towers 2 [W]**
2	40
13	250
Numbers of lamp	**Lighting towers 2 [W]**
2	40

3	1000
12	400
Numbers of lamp	**Lamps on large square [W]**
40	70

Table B7- Lighting Towers and Lamps on External Area

Max Active Power [kW]	Min Active Power [kW]	Max PF	Min PF
22	0 (switch off)	0.9	0.88

Table B8- Lighting Towers and Lamps on External Area Active Power and Power Factor

Current Harmonic Order	Max values %	Min Value %
3	10	8
5	6	2.5
7	3	2
9	2	0.5
11	2	0.3
13	3	0.1
15	1.5	0.1
17	1.5	0.1
19	1.5	0.1

Table B9- Lighting Towers and Lamps on External Area Current Harmonic Content

Others Building

The others buildings located in Magliana area are:

- Recycling area - (white no.04);
- Storehouse - (brown no.05);
- Control tower - (green no.06 feeding by another substation);
- Coverage maintenance wagon - (pink no.07);
- Electrical component storehouse - (sky blue no.09);
- Washing - (violet no.10).

These buildings were not considered in the measurement but a total load of 80-120 kW can be considered in relation to the maximum power consumption recorded on the main busbar located downstream of the transformer 20/0.4 kV, where the lighting system is the main load.

Total Consumption

The measurements regarding active power and THD_V% at point of common coupling were carried out on the main busbar located downstream of the transformer 20/0.4 kV. The Maximum and Minimum total power consumption is ranging between 180 kW and 330 kW. THD_V% is ranging between 0.8 ÷ 2.4 % Table B10 show the Maximum values for voltage harmonic spectrum reported in percentage of each harmonic order.

Harmonic Order	Voltage Min Harmonic Value %	Voltage Max Harmonic Value %
3	0.3	0.8
5	0.6	1.4
7	0.1	1.2
9	0.1	0.5
11	0.1	0.8
13	0.1	0.3
15	0.01	0.1
17	0.01	0.1

19	0.01	0.1
21	0.01	0.1
23	0.1	0.4
25	0.01	0.1
27	0.01	0.1
29	0.01	0.1
31	0.01	0.1
33	0.01	0.1
35	0.01	0.1
37	0.01	0.1
39	0.01	0.1

Table B10 - Point Of Common Coupling Maximum Values for Voltage Harmonic Spectrum

Electric power system of case study

Figure B6 shows the case study represented and modelled by Simulink.

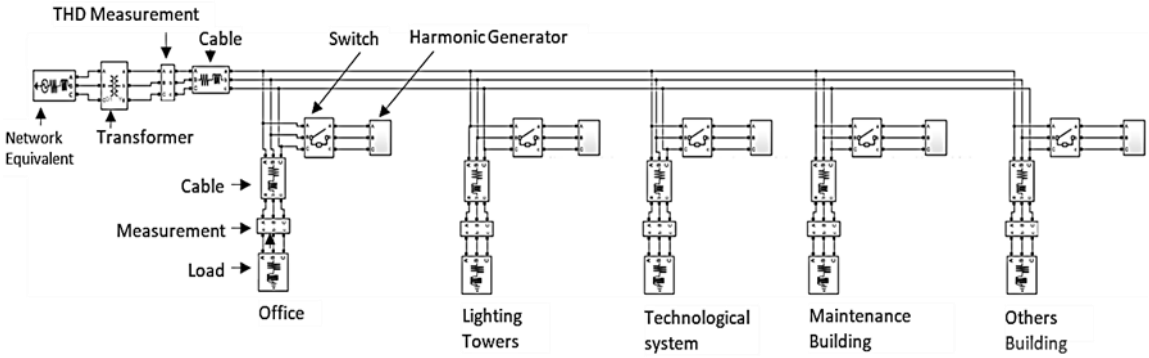

Figure B6-Case Study Modelled

SM is composed by a three-phase AC source, a three-phase distribution transformer, measurement blocks, three-phase LV feeder and loads represented by the sub-models presented previously.

Results

In figures B7 and B8 the results obtained through 500 simulations relevant to the total power absorbed by loads and the voltage total harmonic distortion (THD_V %) are illustrated.

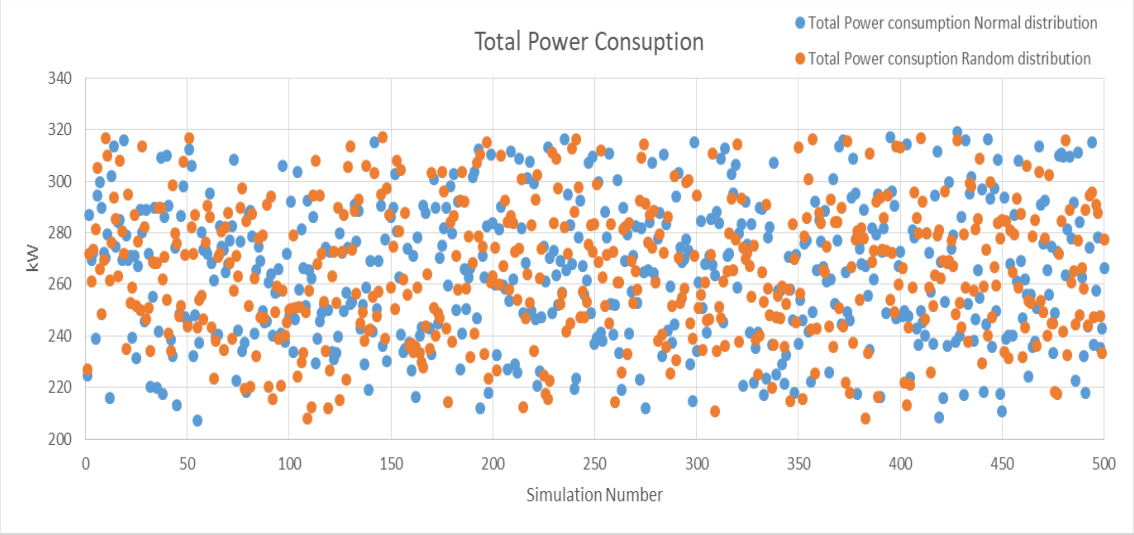

Figure B7- Total Power Consumption by Loads

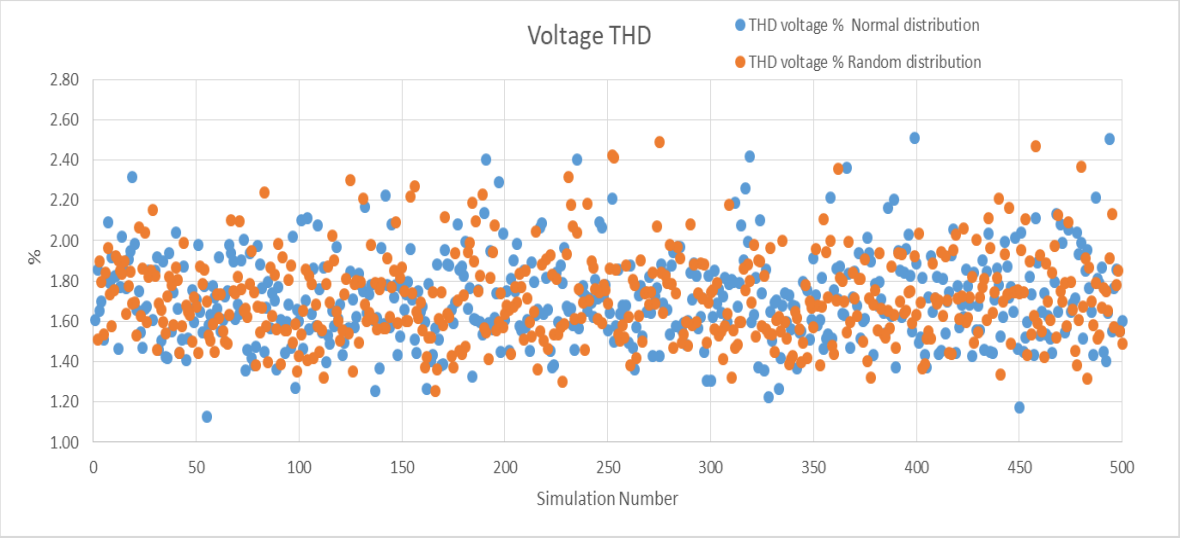

Figure B8 - THD_V % at Point of Common Coupling

Figures B7 and B8 show the simulation results using both uniform and normal distribution and they do not involve meaningful differences. The comparison demonstrated the possibility to use both the distributions to generate electrical load scenarios.

Table B11 reports the maximum and minimum values of voltage harmonic spectrum, in percentage of each harmonic order.

The number of simulations were chosen due to the computer's processing times.

Current Harmonic Order	Voltage Min Harmonic Value %	Voltage Max Harmonic Value %
3	0.6	1.6
5	0.3	0.9
7	0.4	1.1
9	0.2	0.7
11	0.3	1.1
13	0.1	0.7
15	0.1	0.5
17	0.1	0.5
19	0.1	0.5
21	0.1	0.4
23	0.1	0.7
25	0.2	0.6
27	0.0	0.1
29	0.0	0.2
31	0.0	0.2
33	0.0	0.2
35	0.0	0.5
37	0.0	0.3
39	0.0	0.1

Table B11- Maximum and Minimum Values for Voltage Harmonic Spectrum

Table B12 reports the comparison between simulation and measurements (Section 2 - G. Total Consumption) results. The Values are referred to maximum and minimum of Power consumption and THD_V.

	Value
Max THD_V Value % measured	2.5 %
Min THD_V Value % measured	1.1 %

Max THD_V Value % simulated	2.4 %
Min THD_V Value % simulated	0.8 %
Max Power consumption measured	330 kW
Min Power consumption measured	180 kW
Max Power consumption simulated	320 kW
Min Power consumption simulated	210 kW

Table B12- Comparison Between Simulation and Measurements Results

The comparison shows an agreement among the results. The maximum measured and calculated THD values are acceptable (2.4 % and 2.5%).
Further investigations is necessary to verify if the small differences encountered between measures and simulation are due to the background distortion which was not considered in the study because of lack of information by the DSO.
Some standard statistical tools were applied to analyse the simulation results that were compared both with a normal distribution and through a QQ-plot tool. The QQ-plot, or quantile-quantile plot, is a graphical tool that helps assessing if a set of data plausibly derives from some theoretical distribution such as a Normal or Exponential distribution [121].
As an example, the total power consumption and the THD_V % were compared with a normal distribution, as reported in Figures B10 and B12; Figures B11 and B13 show their QQ-plot.

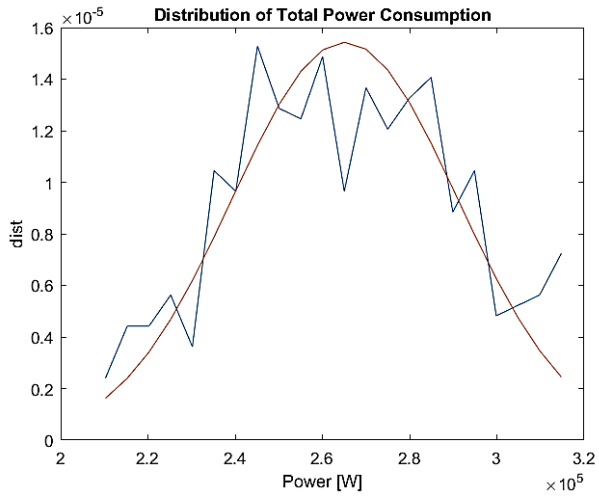

Figure B10 - Total Power Consumption Distribution. The Orange Line Represents The Normal Distribution With The Same Mean and Variance of The Blue Line Representing The Total Power Distribution.

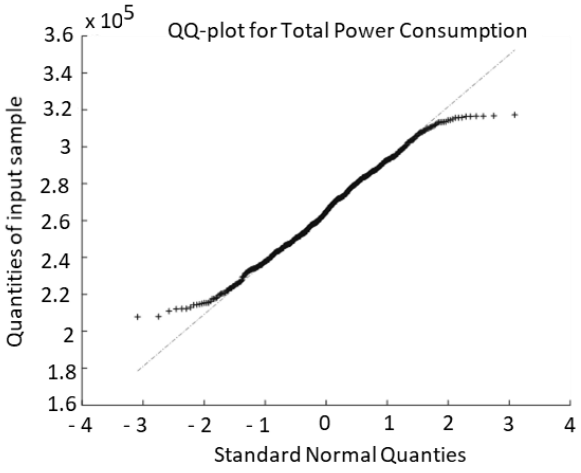

Figure B11- QQ-plot for Total Power Consumption

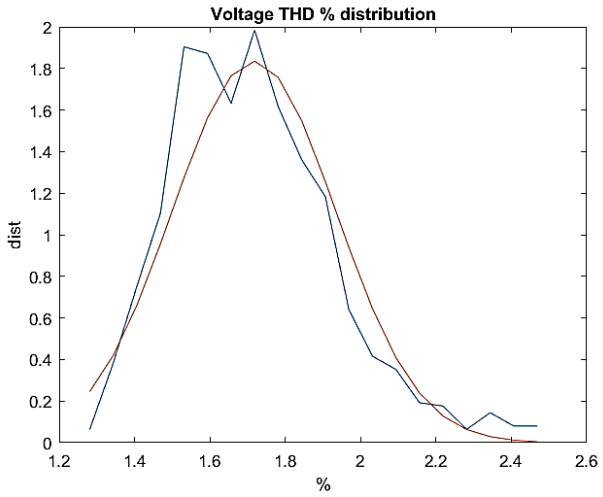

Figure B12 - THD$_V$ % Distribution. The Orange Line Represents The Normal Distribution With The Same Mean and Variance of The Blue Line Representing The THD$_V$ % Distribution..

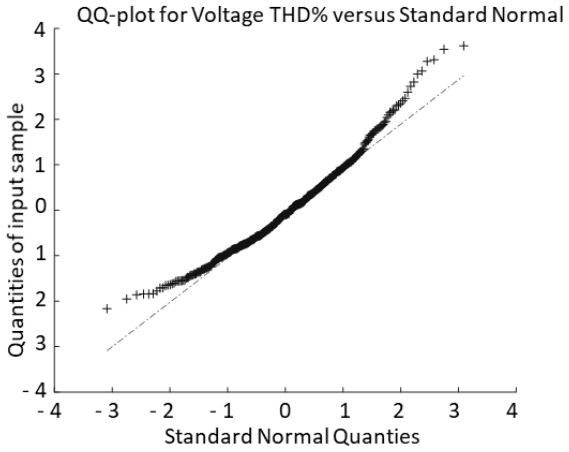

Figure B13- QQ-plot for THD$_V$ %

Analyzing the figures, it is possible to observe that the THD$_V$ % does not ensue a normal distribution (Figure B12), as confirmed by the QQ-plot analysis (Figure B13), instead, the total power consumption appears to better ensue normal distribution. Probably, the THD$_V$ % voltage value deviates from the normal distribution due to the process of extracting data in the range of the harmonic currents phases. The background harmonic distortion caused by other loads, which is always present and of a time-varying nature, may cause an imprecision on the results of the simulation.

Publications – Journals

[1] G. Graber, V. Calderaro, V. Galdi, A. Piccolo, R. Lamedica and A. Ruvio, "Techno-economic Sizing of Auxiliary-Battery-Based Substations in DC Railway Systems," in IEEE Transactions on Transportation Electrification, vol. 4, no. 2, pp. 616-625, June 2018. doi: 10.1109/TTE.2018.2825651

[2] Regina Lamedica, Ezio Santini, Alessandro Ruvio, Laura Palagi, Irene Rossetta "A MILP methodology to optimize PV - Wind renewable energy systems sizing" ENERGY journal Elsevier, Volume 165, Part B, 15 December 2018, Pages 385-398

[3] Regina Lamedica, Alessandro Ruvio, Paulo Fernando Ribeiro, Massimo Regoli "A Simulink model to assess harmonic distortion in MV/LV distribution networks with time-varying non linear loads" SIMPAT Elsevier journal, Volume 90, January 2019, Pages 64-80

[4] Regina Lamedica; Massimo Pompili; Silvia Sangiovanni; Luigi Calcara; Bruno Cauzillo; Alessandro Ruvio "Transient-State Analysis of MV Instrument Transformers" Power Systems Research EPSR Elsevier journal, Volume 168, March 2019, Pages 162-168.

[5] Lamedica, R., Muzi, F., Prudenzi, A., Elia, S., Podestà, L., Ruvio, A., Sangiovanni, S., Santini, E., Trentini, F. "Electrical and thermal integrated load management of tertiary buildings" International Review of Electrical Engineering, Volume 13, Issue 4, July-August 2018, Pages 276-289

[6] Cresta, M., Gatta, F.M., Geri, A., Lamedica, R., Lauria, S., Maccioni, M., Paulucci, M., Ruvio, A. " Operation of a medium voltage distribution network with a large penetration of distributed generation" International Review on Modelling and Simulations Volume 9, Issue 4, 2016, Pages 280-287.

[7] R. Lamedica, A. Geri, F.M. Gatta, M. Maccioni, S. Lauria, A. Ruvio "A methodologic approach to evaluate service dependability of a high speed railway line" International Review of Electrical Engineering (I.R.E.E.).

[8] F.M. Gatta, A. Geri, R. Lamedica, S. Lauria, M. Maccioni, F. Palone, M. Rebolini, A. Ruvio "Application of a LiFePO4 BESS to Primary Frequency Control: Simulations and Experimental Results" Energies — Open Access Energy Research, Engineering and Policy Journal

[9] Lamedica, R., Geri, A., Gatta, F.M., Maccioni, M., Lauria, S., Prudenzi, A., Regoli, M., Ruvio, A. "An optimization procedure to evaluate the service performances in high-speed railway lines under fault conditions" International Review on Modelling and Simulations Volume 9, Issue 4, 2016, Pages 288-294.

[10] G. Graditi, M.G. Ippolito, R. Lamedica, A. Piccolo, A. Ruvio, E. Santini, P. Siano, G. Zizzo, "Innovative control logics for a rational utilization of electric loads and air-conditioning systems in a residential building "Energy and Buildings102(2015) 1–17.

[11] Capasso, R. Lamedica, A. Ruvio, G. Giannini. "Sistemi di trasporto urbano ecosostenibili. Un confronto tra le richieste energetiche dei sistemi filoviario e tranviario" Rivista Ingegneria Ferroviaria – CIFI Aprile 2014.

Publications – Conference

[1] C. Spalvieri, R. Lamedica, A. Ruvio "A methodologic approach to define the railway junctions capacity" AEIT 2018 Bari 3-5 October 2018

[2] Regina Lamedica, Marco Maccioni, Alessandro Ruvio, Alberto Geri, Fabio Massimo Gatta "Harmonic Disturbance Control in Islanded Smart Grids" SPEEDAM 2018 Amalfi, June 2018

[3] G. Parise, R. Lamedica, L. Martirano, A. Ruvio, L. Parise, B. Chavdarian, Chun-lien Su "TN-Grounding Systems for the Emerging Cold Ironing: Multiple Grounded System Vs Island System" EEEIC 2018, Palermo, June 2018

[4] Regina Lamedica, Fabio Massimo Gatta, Alberto Geri, Silvia Sangiovanni, Alessandro Ruvio "A software validation for dc electrified transportation system: a tram line of Rome" EEEIC 2018, Palermo, June 2018

[5] A. Colavitto; G. Sulligoi, A, Vicenzutti, R. Lamedica; A. Ruvio, E. Tironi; S. Negri, G. Lipardi "Naval Smart Grid Research Program: Phase 2" ESARS 2018, November 2018 Nottingham, United Kingdom (Accepted).
[6] R. Lamedica, M. Maccioni, A. Ruvio and P. F. Ribeiro, "EVs recharging management to maintain high PQ levels in LV islanded networks," 2018 18th International Conference on Harmonics and Quality of Power (ICHQP), Ljubljana, 2018, pp. 1-6. doi: 10.1109/ICHQP.2018.8378923
[7] A. Capasso, R. Lamedica, A. Ruvio, M. Ceraolo and G. Lutzemberger, "New approaches to simulate AC electrified railway systems," 2017 AEIT International Annual Conference, Cagliari, 2017, pp. 1-6.
[8] C. Spalvieri, L. Pantalone, R. Lamedica, A. Ruvio, M. Maccioni and E. Bombelli, "A methodologic approach to define a new layout of 3 kV DC railway substation," 2017 AEIT International Annual Conference, Cagliari, 2017, pp. 1-5.
[9] L. Martirano et al., "An example of smart building with a km zero energy performance," 2017 IEEE Industry Applications Society Annual Meeting, Cincinnati, OH, 2017, pp. 1-8.
[10] L. Martirano, R. Araneo, A. Ruvio, Z. Leonowicz, J. Rezmer, "A microgrid with PV production and energy storage for an university building" Source of the Document Proceedings of the 2017 IEEE 14th International Conference on Networking, Sensing and Control, ICNSC 2017.
[11] A. Capasso, R. Lamedica, G. Aloisio, A. Ruvio, M. Ceraolo, G. Lutzemberger, L. Sani, P. Bolognesi "Modelling 2×25 kV-50 Hz traction systems for power frequency studies IEEE EEEIC 2017 – 17th Conference on Environment and Electrical Engineering, June 2017, Milan.
[12] Capasso, A. Lamedica, R. Ruvio, A. Ceraolo, M., Lutzemberger, G. "Modelling and simulation of electric urban transportation systems with energy storage" IEEE EEEIC 2016 – 16th Conference on Environment and Electrical Engineering, June 2016, Florence.
[13] Gatta, F.M., Geri, A., Lamedica, R. , Maccioni, M., Ruvio, A. "PQ and hosting capacity issues for EV charging systems penetration in real MV/LV networks " 19th Power Systems Computation Conference, PSCC 2016, 10 August 2016, Genova.
[14] Codino, A., Gatta, F.M., Geri, A., Lamedica, R., Lauria, S., Maccioni, M. , Ruvio, A., Calone, R. "Cross-country fault protection in ENEL Distribuzione's experimental MV loop lines" 19th Power Systems Computation Conference, PSCC 2016, 10 August 2016, Genova
[15] Capasso, A., Lamedica, R. , Gatta, F.M., Geri, A., Maccioni, M., Ruvio, A., Buffarini, G.G., Carones, N. "Individual driving style impact on traction energy consumption in railway lines: A simulation model" International Symposium on Power Electronics, Electrical Drives, Automation and Motion, SPEEDAM 2016, Capri; Italy; 22 June 2016.
[16] R. Lamedica, M. Pompili, B. A. Cauzillo, S. Sangiovanni, L. Calcara, A. Ruvio "Instrument Voltage Transformer Time-Response to Fast Impulse" International conference on harmonics and quality of power, ICHQP, Oct 2016, Belo Horizonte, Brazil
[17] R. Lamedica, F.M. Gatta, A. Ruvio, L. Pantalone, C. Spalvieri "A Simulation Model to Estimate Touch Voltage in DC Railway Systems" Convegno Annuale AEIT, Capri 2016.
[18] G. G. Buffarini, G. Trezza, R. Consalvi R. Lamedica, A. Ruvio, S. Muzi "Innovative Protection System for Separation Section between 15 kV a.c. and 3 kV d.c. Railway Networks" Convegno annuale AEIT, Capri 2016.
[19] Capasso, R. Lamedica, S. Lauria, A. Ruvio, E. Tironi, M.Corti. "Voltage Quality Studies in Electric Power Systems: an AC/DC network for a Shipboard application" IEEE EEEIC 2016 – 16th Conference on Environment and Electrical Engineering, June 2016, Florence.
[20] Calderaro, V , Galdi, V , Graber, G. , Piccolo, A , Capasso, A , Lamedica, R , Ruvio, A " Energy management of Auxiliary Battery Substation supporting high-speed train on 3 kV DC systems" 2015 International Conference on Renewable Energy Research and Applications, ICRERA 2015 23 February 2016, Article number 7418603, Pages 1224-1229 .
[21] Lamedica, R., Ruvio, A., Galdi, V., Graber, G., Sforza, P., Guidibuffarini, G., Spalvieri, C. "Application of battery auxiliary substations in 3kV railway systems" 2015 AEIT International Annual Conference, AEIT 2015 19 February 2016, Article number 7415249.
[22] Capasso, R. Lamedica, L. Podestà, A. Ruvio, S. Sangiovanni, G. C. Lazaroiu and G. A. Maranzano. "A measurement campaign in a metro-train deposit/maintenance and repair site for PV production optimal sizing" IEEE EEEIC 2015 – 15th Conference on Environment and Electrical Engineering.

[23] G. Lipardi, L. Piva, L. Piegari, E. Tironi R. Lamedica, A. Ruvio G. Sulligoi, A. Vicenzutti "Electric Loads Characterization in an Aircraft Carrier with Ring-Bus Distribution System" Proceedings IEEE ESARS 2015 – 3th International Conference on Electrical Systems for Aircraft, Railway and Ship Propulsion.

[24] U. Grasselli, R. Lamedica, S. Sangiovanni, A. Ruvio, MC. Cavaretta "Comportamento dei TV in presenza di transitori veloci di tensione per manovra degli interruttori MT in Sf6" Atti del XXXI Congresso Nazionale dell'associazione gruppo misure elettriche ed elettroniche 2014; (Not in Scopus).

[25] G.Sulligoi, A. Vicenzutti, E. Tironi, M. Corti, R. Lamedica, A. Ruvio, G. Lipardi, L. Piva "Naval Smart Grid - Integrated Power System for All Electric Naval Vessels with control and reliability characteristics", AEIT 2014.

[26] U.Grasselli, R.Lamedica, A.Ruvio, D. Novati "Management policies for residential and tertiary users: a measurement campaign" International Symposium on Power Electronics, Electrical Drives, Automation and Motion, SPEEDAM 2014; Ischia; Italy; 18 June 2014 through 20 June 2014;

[27] U.Grasselli, S. Sangiovanni, R.Lamedica, A.Ruvio, M.C. Cavarretta "IVTs Behavior in SF6 Switching Transients: Fast Front Voltage Impulse" ICHQP 2014.

[28] M.C. Falvo, R. Lamedica, A. Ruvio "Energy Storage Application in Trolley-Buses Lines for a Sustainable Urban Mobility" Proceedings IEEE ESARS 2012 - 2nd International Conference on Electrical Systems for Aircraft, Railway and Ship Propulsion.

[29] M.C. Falvo, R. Lamedica, A. Ruvio "An Environmental Sustainable Transport System: A Trolley-buses Line for Cosenza City" Proceedings IEEE SPEEDAM 2012.